Curry, W.B., Shackleton, N.J., Richter, C., et al., 1995
Proceedings of the Ocean Drilling Program, Initial Reports, Vol. 154

4. SITE 925[1]

Shipboard Scientific Party[2]

HOLE 925A

Date occupied: 4 February 1994

Date departed: 10 February 1994

Date reoccupied: 14 February 1994

Date departed: 19 February 1994

Time on hole: 8 days, 17 hr, 45 min

Position: 4°12.249′N, 43°29.334′W

Bottom felt (drill-pipe measurement from rig floor, m): 3053.0

Distance between rig floor and sea level (m): 10.8

Water depth (drill-pipe measurement from sea level, m): 3042.2

Total depth (from rig floor, m): 4033.4

Penetration (m): 930.4

Number of cores (including cores having no recovery): 69

Total length of cored section (m): 645.5

Total core recovered (m): 490.05

Core recovery (%): 75.9

Oldest sediment cored:
Depth (mbsf): 930.4
Nature: calcareous fragments limestone with clay
Age: middle Eocene
Measured velocity (km/s): 3.6–3.7

Comments: Hole 925A: 2015 hr, 4 February to 1300 hr, 8 February (3 days, 16 hr, 45 min); Hole 925A′: 0800 hr, 24 February to 0945 hr, 19 February (5 days, 1 hr, 45 min). Drilled 284.9 m (0.0–101.8, 111.0–197.9, and 207.5–303.7 mbsf)

HOLE 925B

Date occupied: 8 February 1994

Date departed: 10 February 1994

Time on hole: 1 day, 13 hr, 15 min

Position: 4°12.248′N, 43°29.349′W

Bottom felt (drill-pipe measurement from rig floor, m): 3052.0

Distance between rig floor and sea level (m): 10.9

Water depth (drill-pipe measurement from sea level, m): 3041.1

Total depth (from rig floor, m): 3370.0

Penetration (m): 318.0

Number of cores (including cores having no recovery): 34

Total length of cored section (m): 318.0

Total core recovered (m): 329.05

Core recovery (%): 103.5

Oldest sediment cored:
Depth (mbsf): 318.0
Nature: nannofossil chalk with foraminifers and foraminifer nannofossil chalk
Age: middle Miocene
Measured velocity (km/s): 1.8–2.2

HOLE 925C

Date occupied: 10 February 1994

Date departed: 12 February 1994

Time on hole: 1 day, 21 hr, 15 min

Position: 4°12.256′N, 43°29.349′W

Bottom felt (drill-pipe measurement from rig floor, m): 3051.5

Distance between rig floor and sea level (m): 10.9

Water depth (drill-pipe measurement from sea level, m): 3040.6

Total depth (from rig floor, m): 3411.6

Penetration (m): 360.1

Number of cores (including cores having no recovery): 38

Total length of cored section (m): 360.1

Total core recovered (m): 368.78

Core recovery (%): 102.4

Oldest sediment cored:
Depth (mbsf): 360.1
Nature: nannofossil chalk with foraminifers and clay
Age: early Miocene
Measured velocity (km/s): 2.01–2.06

HOLE 925D

Date occupied: 12 February 1994

Date departed: 13 February 1994

Time on hole: 1 day, 11 hr, 15 min

Position: 4°12.260′N, 43°29.363′W

Bottom felt (drill-pipe measurement from rig floor, m): 3051.5

Distance between rig floor and sea level (m): 11.0

Water depth (drill-pipe measurement from sea level, m): 3040.5

Total depth (from rig floor, m): 3405.5

Penetration (m): 354.0

Number of cores (including cores having no recovery): 37

Total length of cored section (m): 351.5

Total core recovered (m): 364.0

Core recovery (%): 103.6

Oldest sediment cored:
Depth (mbsf): 354.0

[1] Curry, W.B., Shackleton, N.J., Richter, C., et al., 1995. *Proc. ODP, Init. Repts.,* 154: College Station, TX (Ocean Drilling Program).

[2] The Shipboard Scientific Party is as given in the list of participants preceding the Table of Contents.

Nature: nannofossil chalk with foraminifers and clay
Age: early Miocene
Measured velocity (km/s): 2.06

Comments: Drilled from 0.0 to 2.5 mbsf.

HOLE 925E

Date occupied: 13 February 1994

Date departed: 14 February 1994

Time on hole: 11 hr, 15 min

Position: 4°12.257′N, 43°29.337′W

Bottom felt (drill-pipe measurement from rig floor, m): 3051.5

Distance between rig floor and sea level (m): 11.0

Water depth (drill-pipe measurement from sea level, m): 3040.5

Total depth (from rig floor, m): 3106.0

Penetration (m): 54.5

Number of cores (including cores having no recovery): 6

Total length of cored section (m): 54.5

Total core recovered (m): 55.65

Core recovery (%): 102.1

Oldest sediment cored:
Depth (mbsf): 54.50
Nature: clayey nannofossil ooze with foraminifers
Age: late Pliocene
Measured velocity (km/s): 1.6

Principal results: Site 925 is the shallowest of the depth transect of sites on the Ceara Rise. The site is located beneath warm surface waters that have a mean temperature around 27°C. The seafloor at a depth of 3040 m is bathed by North Atlantic Deep Water (NADW) well above the carbonate lysocline. The site was chosen to provide material for investigating the geological history of surface- and deep-water properties in the region.

Five holes were drilled at Site 925. Hole 925A was cored with the RCB from 303.7 to 930.4 mbsf, with spot cores between 101.8 and 110.0 mbsf and between 197.9 and 207.5 mbsf. The hole was logged from 300 to 907 mbsf. Hole 925B was cored with the APC from the mud line to 318.0 mbsf. Hole 925C was cored with the APC from the mud line to 321.5 mbsf and then with the XCB to 360.1 mbsf. Hole 925D was cored with the APC from 2.5 to 354.0 mbsf to ensure complete recovery of the section and to provide sufficient core material for high-resolution, shore-based investigations. Hole 925E was cored with the APC from the mud line to 54.5 mbsf, primarily to provide material for high-resolution interstitial-water sampling. Detailed comparisons between the magnetic susceptibility records generated on the MST track, and high-resolution color reflectance generated using a hand-held Minolta color analyzer, demonstrated that the sedimentary sequence to 370 mbsf had been completely recovered. In the composite section that was generated for the site, the deepest part (about 320–360 mbsf) was based on parallel cores recovered using three different drilling methods: APC, XCB, and RCB. The segments recovered by the RCB are so good that they make up a unique yardstick against which the distortions generated by APC and XCB coring may be evaluated. In addition, Holes 925D and 925E were cored using a new APC cutting shoe whereas Holes 925B and 925C were cored with the conventional APC cutting shoe. It is probable that the new shoe was responsible for our achieving 354 mbsf without excessive pullout.

The recovered sedimentary sequence at Site 925 spans the interval from the middle Eocene to the Holocene. Almost the entire sequence is characterized by rhythmic sedimentary cycles, and a preliminary evaluation suggests that these are chiefly related to the orbital precession cycle. These sedimentary cycles were well recorded by magnetic susceptibility and by color. In much of the section, we were also able to monitor cyclic variations in natural gamma-ray emission. All these three parameters were shown to record variations in the ratio of terrigenous material to biogenic carbonate in the sediments. Because of a pervasive magnetic overprint whose origin remains obscure, it proved impossible to obtain any magnetostratigraphic data for the site.

Biostratigraphic age control was provided by calcareous nannofossils and foraminifers throughout. In both these fossil groups, rich assemblages are preserved throughout the sequence, providing an outstanding biostratigraphic sequence and excellent opportunities for the investigation of evolutionary processes and ecological studies. Close sampling (generally 1.5 m or better, corresponding to 0.05–0.1 m.y.) in both fossil groups gives almost no suggestion of any breaks in the stratigraphic record; the prediction of hiatuses in the Miocene was not substantiated although there is indication of a minor hiatus in the latest Oligocene.

Sedimentation rates were highest in the early Oligocene (40 m/m.y.) and the Pleistocene (33 m/m.y.) and lowest in the late Miocene (15 m/m.y.). Since the Miocene, sedimentation rates have increased because of greater accumulation of terrigenous material, presumably derived from the nearby Amazon Fan. This increase has been most pronounced for the last 5 m.y. Carbonate accumulation has remained nearly constant since the Miocene, except that during the last 1 m.y. the rate of accumulation of carbonate has decreased by 50%.

BACKGROUND AND OBJECTIVES

Site 925 was the shallowest of a transect of sites drilled on the Ceara Rise (see fig. 2, "Introduction" chapter, this volume). The site is in an area of uniform relief; hydrosweep bathymetry coverage shows a range of only 20 m for several kilometers in all directions around the site (Fig. 1). The seismic section (Fig. 2) includes an upper layered sequence down to about 0.3 s (200 m); a middle more seismically incoherent unit between about 0.3 and 0.9 s (300–800 m); a unit with some parallel reflectors between 0.9 and 1.3 s (800–1300 m); and a fairly prominent reflector at around 1.3 s (1300 m) that appears to represent the base of the pelagic section. The deepest objective of drilling, time permitting, was to sample this reflector at 1300 m in the hope that it would provide constraints on the depth history of the rise. Drilling to this depth would also provide information on the nature of the rise soon after it was formed (e.g., whether it was subaerially exposed or covered by reefs). Above that reflector our aim was to recover the entire stratigraphic sequence so that we could obtain material useful for investigating the history of surface paleoceanography of the region as well as data from the shallowest member of a depth transect designed to record the detailed history of changes in deep-water physical and chemical properties in the western North Atlantic Ocean. We were particularly concerned about obtaining a truly complete section, with abundant material available for high-resolution sampling, of the uppermost part of the sediment column. We aimed to sample this upper section in triplicate with the APC to provide the means for high resolution investigation of the whole of the late Neogene. Oceanographic conditions in this region have probably been directly affected by the closure of the Panama Isthmus and uplift of the Andes during this time, in addition to having been affected by the globally pervasive effect of increased glaciation. The sediments were also expected to preserve a detailed history of the transport of terrigenous matter to the Atlantic Ocean by the Amazon River.

OPERATIONS

Transit from Barbados to Site 925

The *JOIDES Resolution* departed Bridgetown Harbor, Barbados, at 2145 hr (local time) on 28 January 1994. Outside the lee of the island, stiff trade winds from forward of the beam along with an opposing current were encountered. Transit speed was held below 10 kt for the first day. After a transit of 30 hr, the vessel reversed course and returned to Barbados to evacuate a crew member. The ship again departed Barbados for the Ceara Rise operating area at 0530 hr on 31 January. Speed was held to about 9 kt the first day out by opposing wind and currents. The wind held fairly constant at 25–30 kt for the entire transit, but variable currents caused the ship's speed to vary between 9 and 12 kt.

Approach to Site 925

On 4 February, the ship reached the Ceara Rise operating area and proceeded directly to the geographic coordinates of proposed Site CR-1. Speed was reduced for the final 8 nmi and the towed magnetometer was recovered. At 1615 hr the ship passed over the site and a positioning beacon was launched. Water depth per precision depth recorder (PDR) was 3040 m from sea level.

Hole 925A

For the first RCB hole, a prototype drag-type core bit was chosen in an attempt to optimize core recovery and quality. The bit featured a polycrystalline diamond compact (PDC) cutting structure and Amoco-designed anti-whirl construction.

In an attempt to determine the water depth by "feeling for bottom" and noting contact by a deflection of the rig's weight indicator, the top drive was deployed and the bit was lowered without circulation or rotation. The bit passed the PDR depth of 3051 m below driller's datum at 0330 hr on 5 February, but no positive weight indication was observed, even after the bit had been lowered to 26 m below the PDR depth. The mud pump was started and a momentary increase in pressure indicated that sediment had been plugging the bit nozzles. No definite indication of contact with the soft seafloor had been detected and a seafloor depth of 3042 m (2 m below PDR depth) was assigned on the basis of experience in similar areas.

Rotation and circulation then began and the 9⅞-in. hole was drilled to 102 mbsf, where the inner core barrel was exchanged for a clean one. Spot cores were taken at approximately 100, 200, and 300 mbsf. Sediment properties and core quality were suitable for the initiation of continuous RCB coring from 300 mbsf. The nannofossil chalk proved to be excellent material for coring and was well suited to penetration by the PDC bit. Coring continued with a high rate of penetration (ROP), excellent core quality, and a good recovery percentage. Core recovery statistics were held down only by a tendency for core to escape the core catchers occasionally, in lengths from 1 or 2 m to the full core length of 9.5 m.

"Drift shots" were taken with the multishot instrument each 100 m beginning at 300 mbsf. Hole deviation was less than 1½° to 700 mbsf, where a 2¼° reading was obtained.

Below about 690 mbsf, the ROP fell sharply from about 30 m/hr to about 6 m/hr. Core recovery remained essentially complete, but the core diameter was considerably reduced, especially in intervals that appeared to be richer in clay content. The sediment age was geologically correlative with a slow-penetration horizon in nearby DSDP Site 354 and faster penetration was expected at about 740 mbsf. Instead, the ROP dropped to less than 3 m/hr. Core 154-925A-49R was recovered after 8.5 m had been cut to check for jammed core or any signs of bit failure. An excellent 7.1-m core was recovered, which was not jammed and had an increased diameter over preceding cores. Circulating pressure and drill-string torque were normal, so another inner barrel was pumped into place. After 145 min of coring time on Core 154-925A-50R (Table 1), only 1 m had been cored despite all efforts to vary coring parameters and dislodge a possible clay ball from the bit. Coring operations were suspended in Hole 925A because of the unacceptable rate of progress.

The top drive was secured and the bit was tripped to 150 mbsf while a free-fall reentry funnel (FFF) was prepared for launch. A delay of 2¾ hr ensued while the FFF was installed around the drill string in the moonpool, dropped, and allowed to fall into place at the seafloor. The pipe trip then continued and the bit arrived on the drill floor at 0900 hr on 8 February. Suspicions of a balled bit were confirmed when about 30% of the bit's face area was found to be packed with clayey chalk to a depth that prevented the cutters from making contact with the formation. The buildup apparently was the result of the plugging of three circulation jets underlying the balled areas.

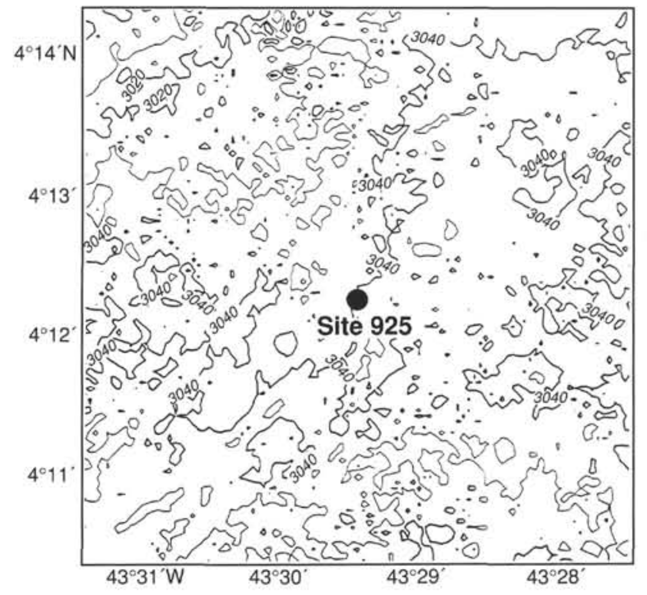

Figure 1. High-resolution swath bathymetry in the region of Site 925. The data were obtained during Ew9209 using the hydrosweep swath-mapping system. Regional bathymetric variability within several kilometers of Site 925 is less than 20 m of water depth.

Hole 925B

An APC/XCB BHA was assembled, with a 10⅛-in. PDC bit. At 1715 hr Hole 925B was spudded with a "mud-line" APC core. The seafloor interface was recovered and seafloor depth was established at 3041 m. Continuous APC coring then began with magnetic orientation from Core 154-925B-3H (Table 1). Coring conditions were excellent in the nannofossil ooze. Full stroke was achieved easily and pullout force was negligible to about 280 mbsf. Though pressure indications were questionable on the final three cores, full core barrels were recovered. Coring was terminated when an overpull of 140,000 lb was required to withdraw Core 154-925B-34H. The drill string then was pulled clear of the seafloor, ending Hole 925B.

Hole 925C

The ship was offset 20 m to the north and the APC system was deployed again and the first core "shot" from 3 m deeper than Core 154-925B-1H. The initial core measured depth to seafloor at 3051.5 m. Core orientation began on the first core, and the break between core intervals was offset 3 m downward to facilitate recovery of a complete section.

Coring performance and results were virtually identical to those of Hole 925B (Table 1). APC coring was suspended after Core 154-925C-34H (at 321.5 mbsf). The coring mode was switched to the XCB, and four additional cores were taken to drilling target at 360 mbsf. Coring results also were good with the XCB and over 94% average recovery was achieved.

A "wiper trip" was made to 73 mbsf and back to total depth. No drag or hole fill was encountered. The hole was swept with 30 bbl of mud, and a go-devil was pumped down to open the lockable float valve (LFV) before the bit was pulled to logging depth at 88 mbsf.

Logging operations began at 0900 hr on 11 February. The initial tool combination was the Quad combo, combining the seismic stratigraphy and lithoporosity suites. Multiple passes were made in the upper hole interval first to ensure both normal and high-resolution

Table 1. Coring summary, Site 925.

Core no.	Date (Feb. 1994)	Time (UTC)	Depth (mbsf)	Length cored (m)	Length recovered (m)	Recovery (%)
154-925A-						
		****Washed from 0.0 to 101.8 mbsf****				
1R	5	1100	101.8–111.0	9.2	4.82	52.4
		****Washed from 111.0 to 197.9 mbsf****				
2R	5	1330	197.9–207.5	9.6	5.93	61.8
		****Washed from 207.5 to 303.7 mbsf****				
3R	5	1730	303.7–313.7	10.0	4.29	42.9
4R	5	1830	313.7–323.4	9.7	9.90	102.0
5R	5	1930	323.4–333.1	9.7	9.88	102.0
6R	5	2015	333.1–342.7	9.6	4.65	48.4
7R	5	2100	342.7–352.4	9.7	8.88	91.5
8R	5	2145	352.4–362.0	9.6	8.92	92.9
9R	5	2230	362.0–371.7	9.7	9.90	102.0
10R	5	2315	371.7–381.3	9.6	2.98	31.0
11R	6	0010	381.3–390.8	9.5	8.03	84.5
12R	6	0105	390.8–400.4	9.6	4.51	47.0
13R	6	0245	400.4–410.0	9.6	1.81	18.8
14R	6	0330	410.0–419.7	9.7	7.52	77.5
15R	6	0420	419.7–429.3	9.6	9.88	103.0
16R	6	0500	429.3–438.9	9.6	9.58	99.8
17R	6	0540	438.9–448.6	9.7	9.34	96.3
18R	6	0615	448.6–458.2	9.6	9.85	102.0
19R	6	0655	458.2–467.8	9.6	4.81	50.1
20R	6	0740	467.8–477.4	9.6	9.87	103.0
21R	6	0830	477.4–487.1	9.7	0.00	0.0
22R	6	0915	487.1–496.7	9.6	9.86	103.0
23R	6	1010	496.7–506.3	9.6	6.15	64.0
24R	6	1100	506.3–516.0	9.7	9.50	97.9
25R	6	1145	516.0–525.6	9.6	0.00	0.0
26R	6	1220	525.6–535.3	9.7	10.02	103.3
27R	6	1300	535.3–544.9	9.6	9.34	97.3
28R	6	1345	544.9–554.6	9.7	0.24	2.5
29R	6	1430	554.6–564.2	9.6	1.99	20.7
30R	6	1515	564.2–573.8	9.6	9.97	104.0
31R	6	1600	573.8–583.5	9.7	2.92	30.1
32R	6	1650	583.5–593.1	9.6	9.83	102.0
33R	6	1745	593.1–602.8	9.7	9.93	102.0
34R	6	1840	602.8–612.4	9.6	8.26	86.0
35R	6	1940	612.4–622.1	9.7	6.13	63.2
36R	6	2030	622.1–631.7	9.6	9.89	103.0
37R	6	2105	631.7–641.4	9.7	0.00	0.0
38R	6	2210	641.4–651.1	9.7	9.88	102.0
39R	6	2305	651.1–660.8	9.7	9.20	94.8
40R	7	0005	660.8–670.4	9.6	9.59	99.9
41R	7	0125	670.4–680.1	9.7	3.38	34.8
42R	7	0230	680.1–683.1	3.0	2.66	88.6
43R	7	0345	683.1–689.7	6.6	6.05	91.6
44R	7	0620	689.7–699.3	9.6	6.62	68.9
45R	7	0920	699.3–709.0	9.7	9.89	102.0
46R	7	1300	709.0–718.3	9.3	9.93	107.0
47R	7	1530	718.3–727.9	9.6	7.89	82.2
48R	7	1800	727.9–737.6	9.7	9.84	101.0
49R	7	2240	737.6–746.1	8.5	7.10	83.5
50R	7	0015	746.1–747.1	1.0	2.13	213.0
51R	14	2330	747.1–757.0	9.9	6.18	62.4
52R	15	0215	757.0–766.6	9.6	9.86	103.0
53R	15	0430	766.6–776.3	9.7	9.09	93.7
54R	15	0620	776.3–786.0	9.7	9.97	103.0
55R	15	0820	786.0–795.6	9.6	8.74	91.0
56R	15	1100	795.6–805.2	9.6	8.69	90.5
57R	15	1330	805.2–814.8	9.6	9.92	103.0
58R	15	1615	814.8–824.5	9.7	9.90	102.0
59R	15	1900	824.5–834.2	9.7	9.79	101.0
60R	15	2110	834.2–843.8	9.6	6.83	71.1
61R	15	2325	843.8–853.5	9.7	7.09	73.1
62R	16	0225	853.5–863.1	9.6	9.93	103.0
63R	16	0525	863.1–872.8	9.7	6.66	68.6
64R	16	0825	872.8–882.5	9.7	9.43	97.2
65R	16	1115	882.5–891.8	9.3	3.77	40.5
66R	16	1400	891.8–901.4	9.6	1.46	15.2
67R	16	1730	901.4–911.1	9.7	9.94	102.0
68R	16	2130	911.1–920.7	9.6	0.02	0.2
69R	17	0245	920.7–930.4	9.7	9.24	95.2
Coring totals				645.5	490.05	75.9
Drilled				284.9		
Total				930.4		
154-925B-						
1H	8	2215	0.0–4.5	4.5	4.49	99.8
2H	8	2310	4.5–14.0	9.5	9.60	101.0
3H	9	0015	14.0–23.5	9.5	9.51	100.0
4H	9	0110	23.5–33.0	9.5	9.86	104.0
5H	9	0200	33.0–42.5	9.5	9.34	98.3
6H	9	0300	42.5–52.0	9.5	9.69	102.0
7H	9	0355	52.0–61.5	9.5	9.68	102.0
8H	9	0430	61.5–71.0	9.5	9.80	103.0
9H	9	0530	71.0–80.5	9.5	9.69	102.0
10H	9	0615	80.5–90.0	9.5	9.82	103.0
11H	9	0700	90.0–99.5	9.5	9.72	102.0
12H	9	0735	99.5–109.0	9.5	9.85	103.0
13H	9	0820	109.0–118.5	9.5	9.78	103.0
14H	9	0900	118.5–128.0	9.5	9.65	101.0
15H	9	0935	128.0–137.5	9.5	9.42	99.1
16H	9	1020	137.5–147.0	9.5	9.61	101.0
17H	9	1105	147.0–156.5	9.5	9.82	103.0
18H	9	1145	156.5–166.0	9.5	9.75	102.0
19H	9	1230	166.0–175.5	9.5	9.77	103.0
20H	9	1310	175.5–185.0	9.5	9.73	102.0
21H	9	1345	185.0–194.5	9.5	9.93	104.0
22H	9	1415	194.5–204.0	9.5	10.11	106.4
23H	9	1500	204.0–213.5	9.5	10.02	105.5
24H	9	1545	213.5–223.0	9.5	9.84	103.0
25H	9	1620	223.0–232.5	9.5	10.07	106.0
26H	9	1720	232.5–242.0	9.5	10.11	106.4
27H	9	1805	242.0–251.5	9.5	10.02	105.5
28H	9	1855	251.5–261.0	9.5	10.09	106.2
29H	9	1940	261.0–270.5	9.5	10.25	107.9
30H	9	2025	270.5–280.0	9.5	10.00	105.2
31H	9	2125	280.0–289.5	9.5	10.01	105.3
32H	9	2220	289.5–299.0	9.5	10.10	106.3
33H	9	2310	299.0–308.5	9.5	9.90	104.0
34H	10	0010	308.5–318.0	9.5	10.02	105.5
Coring totals				318.0	329.05	103.5
154-925C-						
1H	10	0425	0.0–8.0	8.0	8.13	101.0
2H	10	0515	8.0–17.5	9.5	9.62	101.0
3H	10	0555	17.5–27.0	9.5	9.73	102.0
4H	10	0640	27.0–36.5	9.5	9.76	103.0
5H	10	0715	36.5–46.0	9.5	9.50	100.0
6H	10	0750	46.0–55.5	9.5	9.65	101.0
7H	10	0830	55.5–65.0	9.5	9.84	103.0
8H	10	0910	65.0–74.5	9.5	9.69	102.0
9H	10	0950	74.5–84.0	9.5	9.63	101.0
10H	10	1030	84.0–93.5	9.5	9.55	100.0
11H	10	1110	93.5–103.0	9.5	9.25	97.3
12H	10	1145	103.0–112.5	9.5	9.56	100.0
13H	10	1215	112.5–122.0	9.5	8.96	94.3
14H	10	1300	122.0–131.5	9.5	9.86	104.0
15H	10	1330	131.5–141.0	9.5	9.45	99.5
16H	10	1405	141.0–150.5	9.5	10.01	105.3
17H	10	1440	150.5–160.0	9.5	9.59	101.0
18H	10	1510	160.0–169.5	9.5	9.94	104.0
19H	10	1545	169.5–179.0	9.5	9.82	103.0
20H	10	1645	179.0–188.5	9.5	9.89	104.0
21H	10	1740	188.5–198.0	9.5	10.10	106.3
22H	10	1825	198.0–207.5	9.5	10.20	107.3
23H	10	1905	207.5–217.0	9.5	10.13	106.6
24H	10	1945	217.0–226.5	9.5	10.01	105.3
25H	10	2030	226.5–236.0	9.5	10.19	107.2
26H	10	2115	236.0–245.5	9.5	10.08	106.1
27H	10	2200	245.5–255.0	9.5	10.12	106.5
28H	10	2255	255.0–264.5	9.5	9.92	104.0
29H	10	2345	264.5–274.0	9.5	10.10	106.3
30H	11	0025	274.0–283.5	9.5	10.10	106.3
31H	11	0145	283.5–293.0	9.5	10.06	105.9
32H	11	0240	293.0–302.5	9.5	10.01	105.3
33H	11	0350	302.5–312.0	9.5	9.98	105.0
34H	11	0445	312.0–321.5	9.5	9.97	105.0
35X	11	0635	321.5–331.2	9.7	8.07	83.2
36X	11	0725	331.2–340.8	9.6	9.04	94.1
37X	11	0805	340.8–350.4	9.6	9.41	98.0
38X	11	0900	350.4–360.1	9.7	9.86	101.0
Coring totals				360.1	368.78	102.4
154-925D-						
		****Drilled from 0.00 to 2.50 mbsf****				
1H	12	1150	2.5–12.0	9.5	9.98	105.0
2H	12	1315	12.0–21.5	9.5	9.96	105.0
3H	12	1415	21.5–31.0	9.5	9.81	103.0
4H	12	1500	31.0–40.5	9.5	9.71	102.0
5H	12	1545	40.5–50.0	9.5	9.74	102.0
6H	12	1625	50.0–59.5	9.5	10.00	105.2
7H	12	1700	59.5–69.0	9.5	9.79	103.0
8H	12	1750	69.0–78.5	9.5	9.12	96.0
9H	12	1850	78.5–88.0	9.5	10.08	106.1
10H	12	1945	88.0–97.5	9.5	10.13	106.6
11H	12	2030	97.5–107.0	9.5	9.77	103.0
12H	12	2115	107.0–116.5	9.5	9.82	103.0
13H	12	2200	116.5–126.0	9.5	10.12	106.5
14H	12	2250	126.0–135.5	9.5	9.84	103.0
15H	12	2340	135.5–145.0	9.5	9.91	104.0
16H	13	0030	145.0–154.5	9.5	9.97	105.0
17H	13	0145	154.5–164.0	9.5	10.15	106.8
18H	13	0240	164.0–173.5	9.5	9.89	104.0
19H	13	0345	173.5–183.0	9.5	10.21	107.5
20H	13	0430	183.0–192.5	9.5	9.35	98.4

Table 1 (continued).

Core no.	Date (Feb. 1994)	Time (UTC)	Depth (mbsf)	Length cored (m)	Length recovered (m)	Recovery (%)
21H	13	0515	192.5–202.0	9.5	10.11	106.4
22H	13	0600	202.0–211.5	9.5	9.45	99.5
23H	13	0650	211.5–221.0	9.5	9.84	103.0
24H	13	0740	221.0–230.5	9.5	10.16	106.9
25H	13	0830	230.5–240.0	9.5	10.14	106.7
26H	13	0905	240.0–249.5	9.5	10.15	106.8
27H	13	1000	249.5–259.0	9.5	9.23	97.1
28H	13	1040	259.0–268.5	9.5	10.00	105.2
29H	13	1115	268.5–278.0	9.5	9.11	95.9
30H	13	1145	278.0–287.5	9.5	9.97	105.0
31H	13	1245	287.5–297.0	9.5	10.17	107.0
32H	13	1335	297.0–306.5	9.5	10.02	105.5
33H	13	1500	306.5–316.0	9.5	10.10	106.3
34H	13	1550	316.0–325.5	9.5	8.84	93.0
35H	13	1700	325.5–335.0	9.5	9.45	99.5
36H	13	1800	335.0–344.5	9.5	9.87	104.0
37H	13	1900	344.5–354.0	9.5	10.07	106.0
Coring totals				351.5	364.03	103.6
Drilled				2.5		
Total				354.0		
154-925E-						
1H	13	2210	0.0–7.0	7.0	6.63	94.7
2H	13	2300	7.0–16.5	9.5	9.89	104.0
3H	14	0000	16.5–26.0	9.5	9.79	103.0
4H	14	0050	26.0–35.5	9.5	9.76	103.0
5H	14	0140	35.5–45.0	9.5	9.65	101.0
6H	14	0230	45.0–54.5	9.5	9.93	104.0
Coring totals				54.5	55.65	102.1

Note: UTC = Universal Time Coordinated.

coverage of that important section. When the tool was lowered to total depth, it encountered 9 m of hole fill. Upon completion of the log run from 351 to 58 mbsf, the tool string was recovered and replaced with the magnetic susceptibility tool. A susceptibility log was recorded from about 30 m off total depth to 88 mbsf. The final log was the Formation MicroScanner (FMS), which found fill at about the same depth and logged the interval from about 330 mbsf to the beginning of enlarged hole at about 108 mbsf. When all logging tools had been rigged down, the bit was pulled above the seafloor, ending Hole 925C at 0530 hr on 12 February.

Hole 925D

The vessel was offset 20 m to the west; the APC then was deployed, and preparations were made to spud the final hole of the triplicate APC effort. The first core was "shot" from 4 m deeper than Core 154-925C-1H for the purpose of obtaining overlapping core intervals. Cores were oriented from Core 154-925D-1H, and the experimental "slim-nose" catcher shoe was used for all cores. Plans included "pushing" the APC system beyond the depth reached by it in Holes 925B and 925C in an attempt to compare RCB, XCB, and APC cores over the same stratigraphic interval. The slim-nose catcher sub had been used on Cores 154-925C-32H and -34H. It was noted that overpull was considerably less on both of those cores than on the intervening Core 154-925C-33H. As coring in Hole 925D approached the depth of refusal for the earlier holes, it appeared that the new shoe did, indeed, reduce the force required to withdraw the corer. Overpull did not exceed 40,000 lb until Core 154-925D-37H, which reached the depth objective for the hole (354 mbsf) (Table 1). No further cores were attempted and the bit was pulled clear of the seafloor.

Hole 925E

The ship was moved 40 m east of Hole 925D and 20 m east of Hole 925B. Hole 925E was spudded with an oriented seafloor core at 1800 hr on 13 February that was "shot" at the same depth as Core 154-925C-1H. The recovered core length indicated the seafloor depth to be 3042 m. The primary objective of Hole 925E was to recover the uppermost 50 m of the section for geochemical whole-round sampling. Six oriented cores (Table 1) were taken to 54.5 mbsf in less than 5 hr to complete the shallow coring program at Site 925.

Return to Hole 925A

The ship was relocated to Hole 925A. A mechanical bit release (MBR) and a long-toothed roller-cone bit were installed on the BHA used earlier in Hole 925A. After 50 min of automatic station keeping (ASK) positioning, a successful reentry was made at 1220 hr on 14 February.

Minor drag was noted in the upper portion of the hole as the drill string was lowered. A fairly solid obstruction was met at about 190 mbsf. At that point, the trip was stopped for recovery of the camera and the circulating head was installed on the drill pipe. Upon resumption of the trip, the bit was circulated past the bridge without difficulty. The remainder of the pipe trip was accomplished without circulation and without encountering any resistance in the hole. About 35 m of fill was found in the hole and the top drive was picked up for completion of the trip. With circulation and rotation, the hole was cleaned easily to total depth. Continuous RCB coring resumed at 1545 hr.

From the outset, core quality was excellent and approached that produced by the PDC bit. Recovery was even better, apparently, because less core was being dropped through the core catchers. The ROP was disappointing, however, averaging around 8 m/hr. Below 855 mbsf, the ROP fell to about 5.5 m/hr and eventually to less than 4 m/hr. A bit deplugger was attached to an inner core barrel and pumped to the bit in an attempt to dislodge any obstruction in the throat of the core bit. All parameters appeared normal after the deplugger operation and another core was attempted. Core 154-925A-69R achieved 95% core recovery, but the ROP was only slightly faster than that of the previous core. Coring was terminated at 930.4 mbsf (Table 1) and preparations were made for logging. A wiper trip was made to about 200 mbsf, and 10 m of fill material was flushed from the hole with drilling mud.

When the bit and associated components had been released at total depth, the end of the pipe was pulled to logging depth at 212 mbsf. The Quad combo logging tool string was assembled and run into the hole. An obstruction at 438 mbsf stopped the tool, however, and the bridge could not be cleared. The upper portion of the hole was logged up to the end of the pipe and logging tools were recovered. The drill string was lowered past the obstruction in the hope that the hole would be open to total depth below it. Pump circulation was used on the final stand and no weight resistance was noted.

The second attempt with the Quad combo entered open hole but met another bridge at 497 mbsf. Again the hole was logged up to pipe and the tool string was recovered. It was decided that the side-entry sub (SES) could be used effectively to assist logging tools past the unstable hole intervals.

With the end of the drill string pulled back to 265 mbsf, the SES was made up into the string and again the Quad combo tool string was deployed. The drill string was lowered to 794 mbsf before the logging tool was run into open hole. The tool reached hole fill only 23 m off total depth and a good log was recorded from that depth. The caliper log revealed three short intervals between 450 and 507 mbsf, in which the hole diameter was several centimeters less than bit size. The Quad combo was exchanged for the FMS tool, and FMS data were recorded from 887 to 230 mbsf. The time allotted for logging had expired, so the logging tools were rigged down and the drill string was recovered.

One of the two positioning beacons was recovered routinely during the trip, but the other failed to surface after an indicated release. At 0545 hr on 19 February, *JOIDES Resolution* departed Site 925.

LITHOSTRATIGRAPHY

Introduction

The 930-m sequence of sediment recovered from five holes drilled at Site 925 are predominantly ooze, chalk, and limestone (Fig. 3) composed of calcareous nannofossils and foraminifers with significant but variable amounts of clay minerals. Minor, ubiquitous authigenic components include iron sulfide and oxides of iron (and possibly manganese). The main component of lithologic variability occurs at decimeter to meter scales throughout the section in the form of distinct cyclic changes in color that are related to changes in the relative proportions of biogenic carbonate, detrital clay minerals, and, to a lesser extent, authigenic oxides and sulfides. The uppermost part of the section is the only interval where, because of a steady downcore decrease in clay content, larger scale variability was observed.

The primary lithostratigraphic units for the Site 925 sedimentary sequence are defined on the basis of data obtained from eight sources: (1) smear-slide examination, (2) visual observation of color, (3) percentage of carbonate measurements, (4) degree of sediment lithification, (5) magnetic susceptibility measurements, (6) reflectance spectrophotometry measurements, (7) particle grain-size analysis, and (8) X-ray diffraction (XRD) analysis. Two gradational boundaries dividing three units were subsequently identified at levels where distinct changes in one or more of the above data are observed.

Unit I (0–135 mbsf) consists of early Pliocene to Holocene alternating nannofossil clay and clayey nannofossil ooze. Unit II (135–290 mbsf) consists of middle Miocene to early Pliocene nannofossil ooze with clay and foraminifers. Unit III (290–930 mbsf) consists of early Eocene to middle Miocene nannofossil limestone and chalk with foraminifers and clay. More subtle changes in lithologic character occur within the three lithostratigraphic units. These differences form the basis for dividing each unit into a series of subunits, which, along with the main units, are described below.

Description of Lithostratigraphic Units

Lithologic Unit I

Intervals: Core 154-925A-1R, Cores 154-925B-1H through -15H, Cores 154-925C-1H through -15H, Cores 154-925D-1H through -14H, and Cores 154-925E-1H through -6H
Age: Holocene to early Pliocene
Depth: 0–135 mbsf

Unit I sediments are dominated by variable amounts of calcareous nannofossils, clay, and foraminifers. The unit can be divided into two subunits: Subunit IA (0–30 mbsf) is a grayish brown (10YR 5/2) nannofossil clay with foraminifers alternating with light brownish gray (2.5Y 6/2) clayey nannofossil ooze with foraminifers. Subunit IB (30–135 mbsf) is a nannofossil ooze with varying amounts of foraminifers and a steadily increasing clay content toward the top of the subunit. The contact between the subunits is best observed as a shift in average carbonate content from 34% in the upper subunit to 61% in the lower subunit (Fig. 3). The change in carbonate content is associated with a downcore decrease in the average magnetic susceptibility of the sediments and an increase in the average percentage reflectance values of the sediments (Fig. 3).

Throughout Unit I, color reflectance varies as a function of relative clay content: darker sediments contain more clay. The XRD analysis of the clay fraction reveals kaolinite with lesser amounts of smectite. The decimeter- to meter-scale color changes seem to be more abrupt along downcore transitions from light to dark. Unit I contains no evidence of redeposition, reworking, or slumping. The disturbance caused by APC coring was minor and generally restricted to the topmost section of each core.

In addition to the main components mentioned above, Unit I contains minor concentrations of clay- to silt-size grains of iron and manganese oxides and pyrite which occur as distinct millimeter- to centimeter-size laminae, lenses, or blebs. Yellowish red oxide layers in Subunit IA tend to be concentrated in gradational intervals between brownish gray clay-rich layers and thinner light brownish gray more carbonate-rich layers. Iron oxide laminae show progressively increasing pyrite replacement in the deeper parts of Subunit IA. In Subunit IB (below 30 mbsf), iron oxide tends to be more disseminated, typically occurring as faint reddish yellow halos surrounding mottles, burrows, or pyrite layers. Microcrystalline pyrite is present throughout the lower subunit as specks within burrows, as millimeter-thick black laminations or bands, and as millimeter- to centimeter-size blebs. Pyrite laminae tend to be more abundant in the gradational intervals between lighter and darker beds (Fig. 4). Other sediment components detected in trace amounts (<1%) in smear slides and from X-ray diffraction analysis are sponge spicules, zeolites, dolomite, siderite, and detrital quartz.

Lithologic Unit II

Intervals: Core 154-925A-2R, Cores 154-925B-16H through -31H, Cores 154-925C-16H through -31H, and Cores 154-925D-15H through -31H
Age: early Pliocene to middle Miocene
Depth: 135–290 mbsf

Unit II (135–290 mbsf) consists of nannofossil ooze with varying amounts of clay and can be distinguished from Unit I by its nearly 20% higher average carbonate content (53% in Unit I to 72% in Unit II). The higher carbonate content is also reflected by an overall higher percentage of reflectance than in the overlying unit (Fig. 3). Unit II can be divided into three subunits separated by gradational boundaries on the basis of smaller but distinct changes in carbonate content, color, percentage reflectance patterns, and magnetic susceptibility patterns.

Subunit IIA (135–210 mbsf) consists of light gray (2.5Y 7/2) nannofossil ooze with clay alternating with grayish brown (10YR 6/2) clayey nannofossil ooze. The average carbonate content of this unit is 71%. The fainter and more gradational visual color changes are represented by the distinctly lower amplitude variability in percentage reflectance data observed for this subunit. Subunit IIB (210–260 mbsf) is a greenish gray (10Y 6/2) to light gray nannofossil ooze with the highest average carbonate content (77%) in the entire sequence. Its boundary with Subunit IIA is marked by a slump deposit (between 208 and 216 mbsf) and a short interval of low percentage reflectance values above. Its boundary with underlying Subunit IIC is marked by higher magnetic susceptibility values. Subunit IIC (260–290 mbsf) is composed of light greenish gray (7.5GY 7/1) nannofossil ooze with distinct bands of grayish brown (2.5Y 5/2) nannofossil ooze with clay. This subunit is characterized by high-amplitude variability in magnetic susceptibility and a comparatively low average carbonate content of 66%.

The relatively large biogenic component (60%–85% of total sediment) of Unit II is predominantly composed of discoasters and coccoliths with small amounts of foraminifers (5%–15% of total sediment). The remaining siliciclastic component is clay. Pyrite and iron and manganese oxides are present in trace quantities throughout the unit either as thin laminae or as bands. Iron oxide color banding is most common in Subunits IIB and IIC, particularly between 260 and 275 mbsf where many of the bands correspond to large-amplitude "spikes" in the magnetic susceptibility record and to spikes in the ratio of the red/blue (680/420 nm) reflectance channels (Fig. 5). Other minor trace minerals are siderite and dolomite.

Three distinct intervals of contorted bedding, irregular and wedge planar laminae, scoured contacts, and truncated burrows have been identified within Unit II (at the Subunit IIA/IIB boundary, 208–216 mbsf and at around 229 and 272 mbsf). These features, which tend to occur as 1- to 3-m-thick beds, indicate slumping.

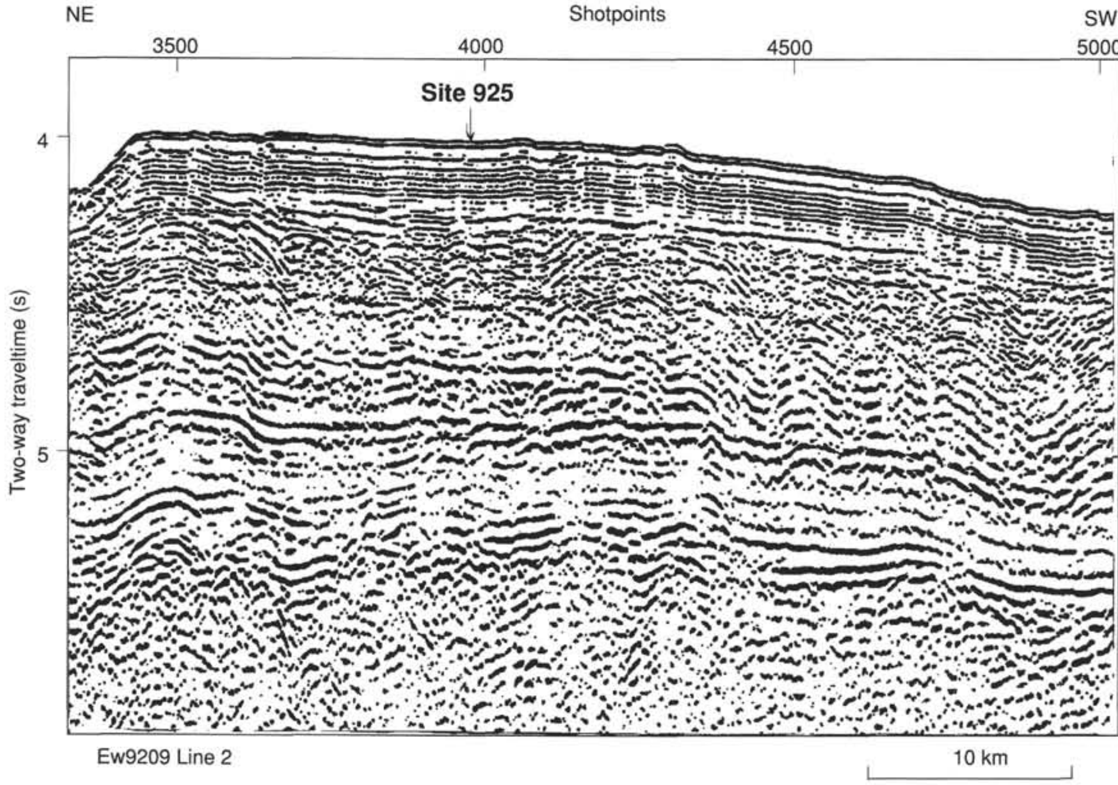

Figure 2. High-resolution, single-channel seismic record (Ew9209 Line 2) for Site 925. The data were obtained using an air-gun array (1350 cm^3, tuned to minimize the bubble pulse) during the Ew9209 site survey cruise (see Mountain and Curry, this volume).

Lithologic Unit III

Intervals: Cores 154-925A-3R through -69R, Cores 154-925B-32H through -34H, Cores 154-925C-31H through -34H, Cores 154-925C-35X through -38X, and Cores 154-925D-31H through -37H
Age: middle Miocene to early Eocene
Depth: 290–930 mbsf

Unit III is the thickest lithostratigraphic unit recognized at Site 925, extending from 290 mbsf to the bottom of the section at 930 mbsf. It consists of middle Eocene to middle Miocene light greenish gray (5GY 7/1) to greenish gray (10GY 6/2) nannofossil chalk and limestone with variable amounts of foraminifers and clay. The carbonate content is relatively high, averaging 68% over the entire interval. Most of the unit is characterized by meter-scale light to dark changes in color controlled by cyclic changes in carbonate content. The top of the unit is marked by a distinct increase in carbonate content (see Fig. 3), a reduction in both magnetic susceptibility and percentage reflectance variability (Fig. 3, 400–600 mbsf), and the apparent transition from ooze to chalk. Unit III is divided into two subunits on the basis of changes in percentage reflectance patterns and degree of lithification (chalk to limestone transition).

The upper section of Subunit IIIA (290–700 mbsf) exhibits pronounced meter-scale changes from nannofossil chalks with foraminifers and foraminifer nannofossil chalks to nannofossil chalks with clay and foraminifer nannofossil chalks with clay. The lower section exhibits similar meter-scale changes, but from nannofossil chalks and nannofossil chalks with clay and foraminifers to nannofossil chalks with clay and clayey nannofossil chalks. Lithologies with higher clay content tend to correspond to darker sediment colors throughout the subunit. The average carbonate content for this subunit is 70%. Fragments (<5%) of siliceous microfossils (sponge spicules, radiolarians, and silicoflagellates) are present in Hole 925C between 322 and 360 mbsf.

Subunit IIIB (700-930 mbsf) exhibits limestone lithologies that, in general, vary similarly on meter scales to the chalk lithologies of Subunit IIIA described above. The only exception occurs in the basal part of the sequence where the matrix material is predominantly micrite instead of nannofossils. Smear-slide, thin-section, and binocular microscope examination of Subunit IIIB limestones reveals evidence of significant calcite recrystallization ranging from spar-filled foraminifers to calcite cement. A distinct shift in average reflectance occurs at the top of Subunit IIIB; this marks the beginning of an interval of reduced amplitude in the meter-scale variability of reflectance values that continues to the bottom of the hole. In addition, carbonate content decreases at the top of the subunit and remains low down to 920 mbsf. The average of the entire subunit is 64%.

In contrast to the overlying units, trace fossils are relatively common in Unit III. *Chondrites, Zoophycos, Skolithos,* and *Planolites* traces occur throughout the section in all lithologies, although they are more conspicuous in the darker, clay-rich intervals.

Throughout Unit III, numerous intervals have been identified that exhibit contorted bedding, displaced blocks, wavy laminae, scoured contacts, microfaults, and graded beds (Figs. 6 and 7). These structures indicate that slump and turbidite deposits are scattered throughout this unit, particularly in Subunit IIIB where no less than three slump deposits and five turbidites have been identified (Fig. 3). The turbidites are characterized by relatively coarse, well-sorted sediment overlain by finer plane beds and ripple cross-laminated material (Fig. 7). In addition, the last 10 m (Core 154-925A-69R) of the sequence contains five distinct 10- to 30-cm-thick beds of grain-flow deposits that have sharp contacts with over- and underlying beds (Fig. 8). Thin sections reveal that these deposits are composed primarily of well-sorted foraminifers with grain-to-grain contacts. The high concentration of foraminifers and the lack of graded bedding or lamination/internal structure suggest that these deposits are foraminifer sands that were created

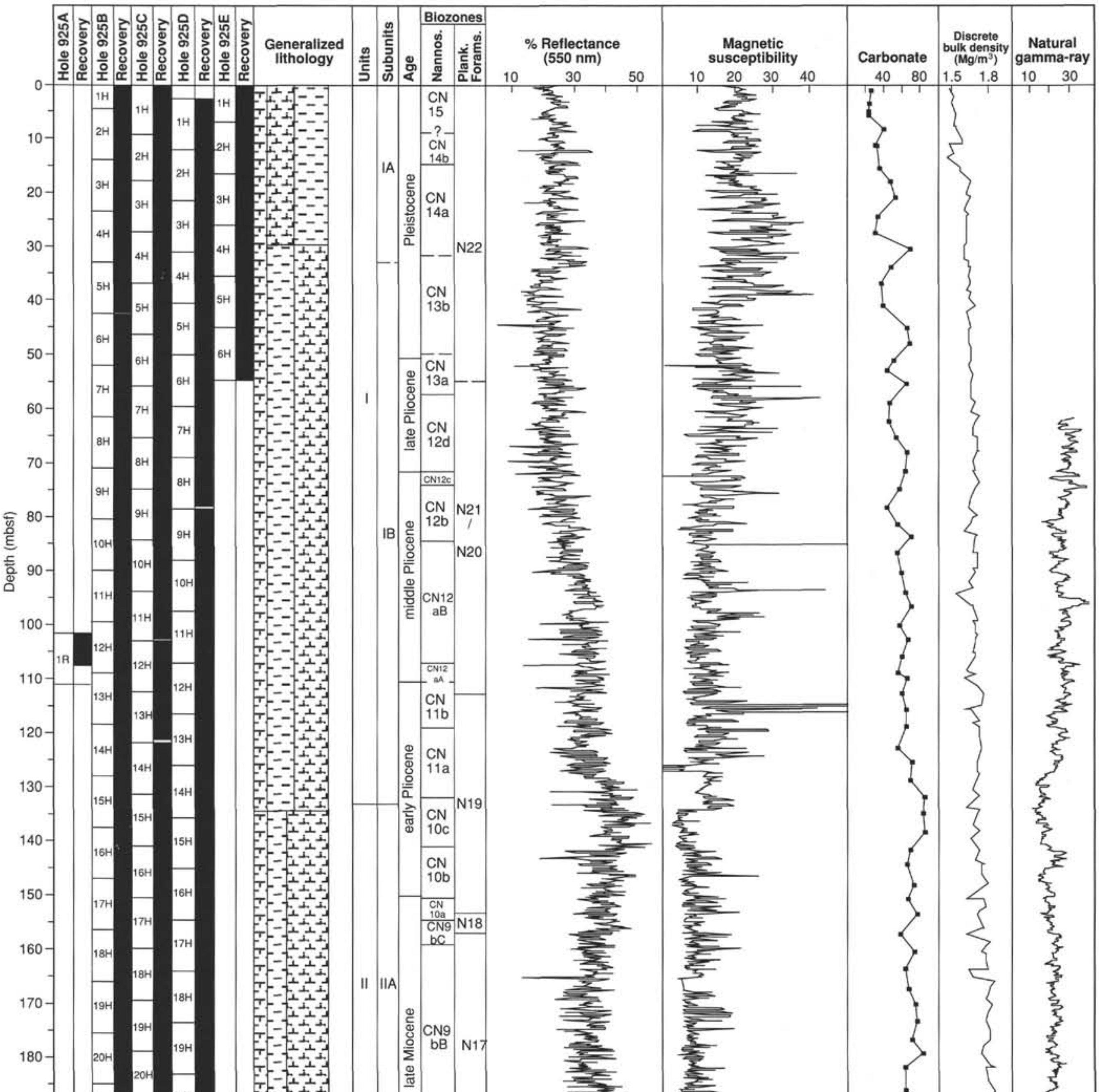

Figure 3. Core recovery, lithostratigraphy, age, biozones, percentage of reflectance (550 nm), magnetic susceptibility, carbonate content, bulk density, and natural gamma of sediments recovered at Holes 925A through 925E. Locations of slump (S), turbidite (T), and grain (G) deposits are shown in the column adjacent to the generalized lithostratigraphy. Percentage of reflectance and magnetic susceptibility values are from Hole 925B in the interval from 0 to 315 mbsf and from Hole 925A in the interval from 315 to 930 mbsf.

by winnowing. The sharp contacts indicate that these sands were created elsewhere and subsequently delivered to this location by grain flows.

Interpretation

The detailed description of the Site 925 lithostratigraphy presented in the last section has led to three observations that are important for understanding the depositional history of the Ceara Rise:

1. Decimeter- to meter-scale cyclic variability in percentages of reflectance and magnetic susceptibility occurs throughout the sediment sequence;
2. The clay mineral content of the sediments decreases with depth over the upper part of the sequence (Lithostratigraphic Unit I); and
3. Numerous sedimentary features occur within the basal part of the sequence (Subunit IIIB) that are associated with downslope transport and redeposition of sediment.

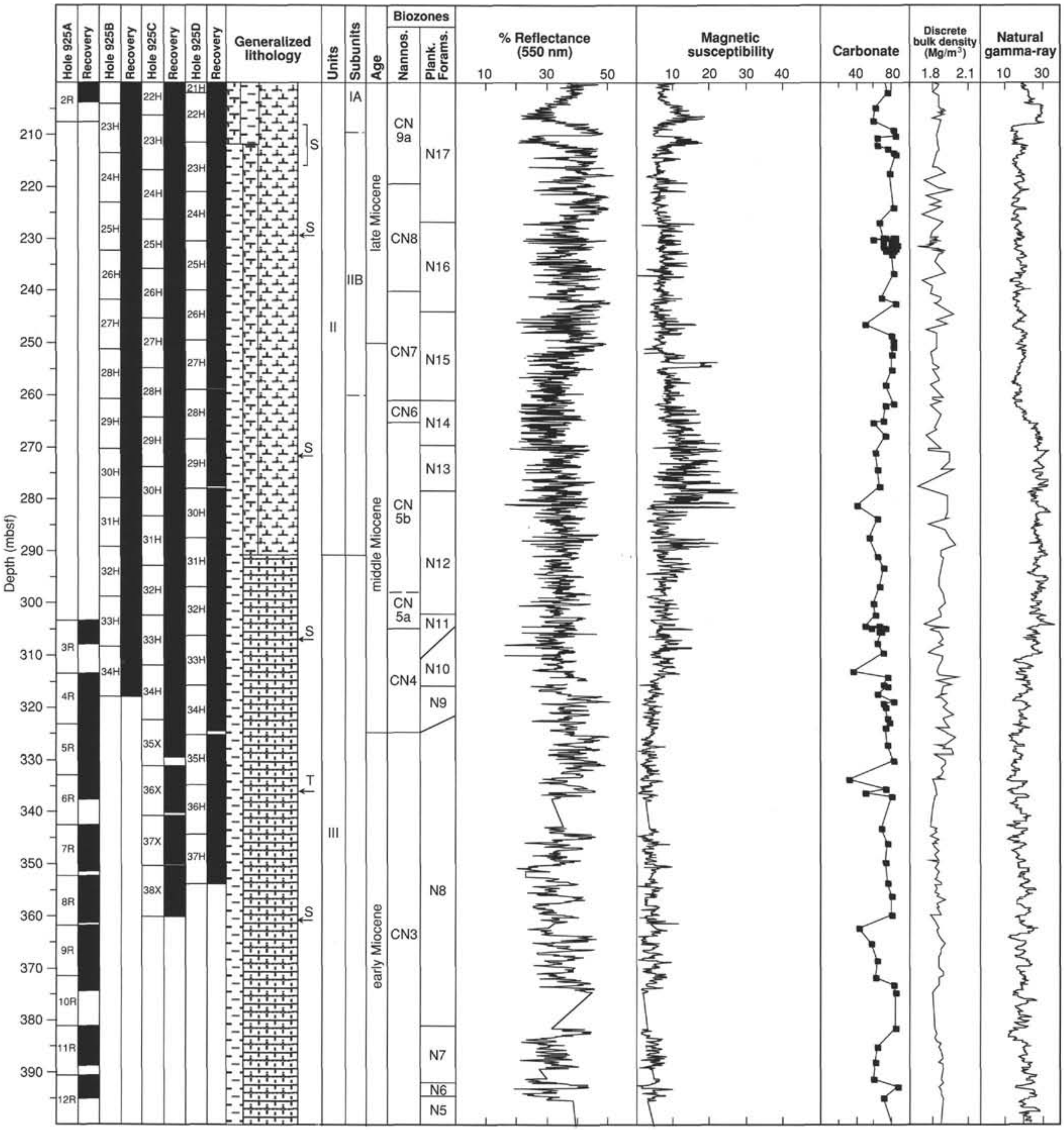

Figure 3 (continued).

One of the most prominent features of the Site 925 sediments is the persistent decimeter- to meter-scale changes in color. Although the color hues change at much larger scales, throughout the sequence there are always faint to very distinct alternations between darker and lighter colors (see previous section). These changes are precisely recorded by the percentage reflectance data collected at 5- to 10-cm intervals throughout the sequence (Fig. 3) and seem to be largely controlled by variations in the carbonate content of the sediment. In addition, the (high-resolution) magnetic susceptibility exhibits similar scale cyclic variability, particularly in the upper 700 m of the sequence (Fig. 3).

Percentage reflectance can be used as a first-order proxy for calcium carbonate content (Fig. 9). There appears to be a curvilinear relationship between the two parameters. The greater scatter at low carbonate contents may be related to variable quantities of oxides and sulfides of iron in the more clay-rich sediments. The ratio of "red" to "blue" (680/420 nm) reflectance values can be used to locate zones of increased abundances of iron oxides and oxyhydroxides (Fig. 5). In particular, beds with a high proportion of oxidized iron are readily detected by this ratio in Subunits IIA and IIB. In the top of Unit III, where the maximum reflectance in the visible range is about 550 nm ("green"), the red to blue ratio is centered at a value of 1.0, indicating reduced sediment.

At the bedding scale (0.1–1.5 m), reflectance at 550 nm oscillates between 15% and 45%. Spectral analysis of reflectance vs. depth

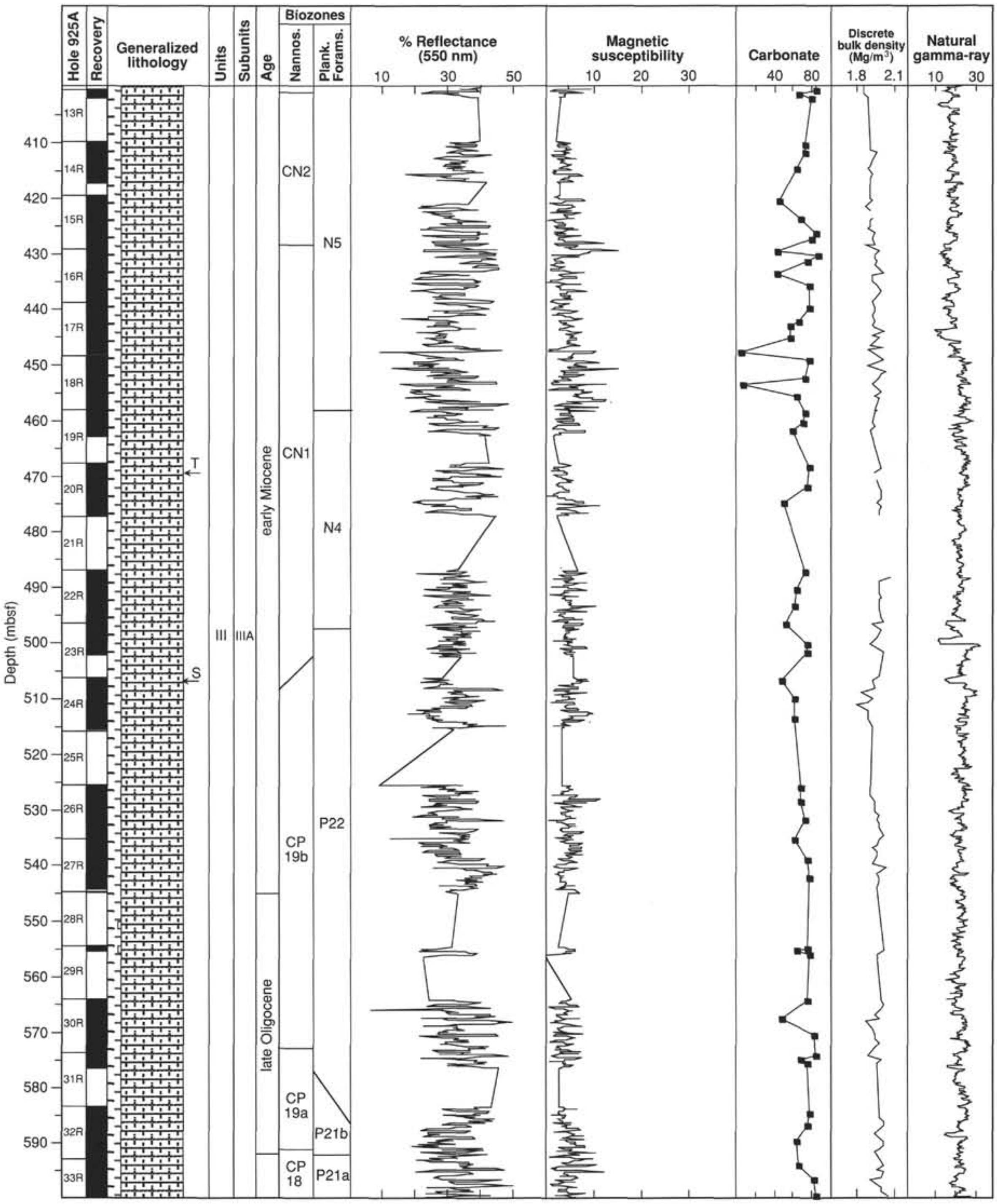

Figure 3 (continued).

demonstrates a regular sedimentary cyclicity at several wavelengths (Fig. 10). Biostratigraphic controls indicate an average sedimentation rate of 32.6 mcd/m.y. for 0 to 100 mcd (see "Composite Depth" section, this chapter). Based on this estimate, the shortest sedimentary cycles (wavelengths of 0.57, 0.69, and 1.24 m) correspond to periods of approximately 17.4, 21.2, and 38.1 k.y., respectively. This result suggests that the sedimentary cycles are connected to the orbital forcing of climate at periods of 19, 23, and 41 k.y. For comparison, time-series analysis of a late Oligocene interval (622–649 mcd) using the corresponding estimated sedimentation rate (23.3 mcd/m.y.) reveals a single regular cycle corresponding to a period of about 43 k.y. Thus, the change in wavelength of the sedimentary cycles recorded by reflectance is proportional to the variations in sedimentation rate.

The magnetic susceptibility covaries negatively with the reflectance (Fig. 11). The relationship is demonstrated in Figure 11 for Core 154-925A-38R, which shows an inverse correlation between the two high-resolution records. These observations are consistent with the hypothesis that the susceptibility magnitude is determined by the relative concentration of carbonate and clay minerals. This indicates that the magnetic susceptibility record of Site 925 can be considered a first-order proxy of the clay mineral content. Measurements of the particle grain size further support this hypothesis. A series of samples

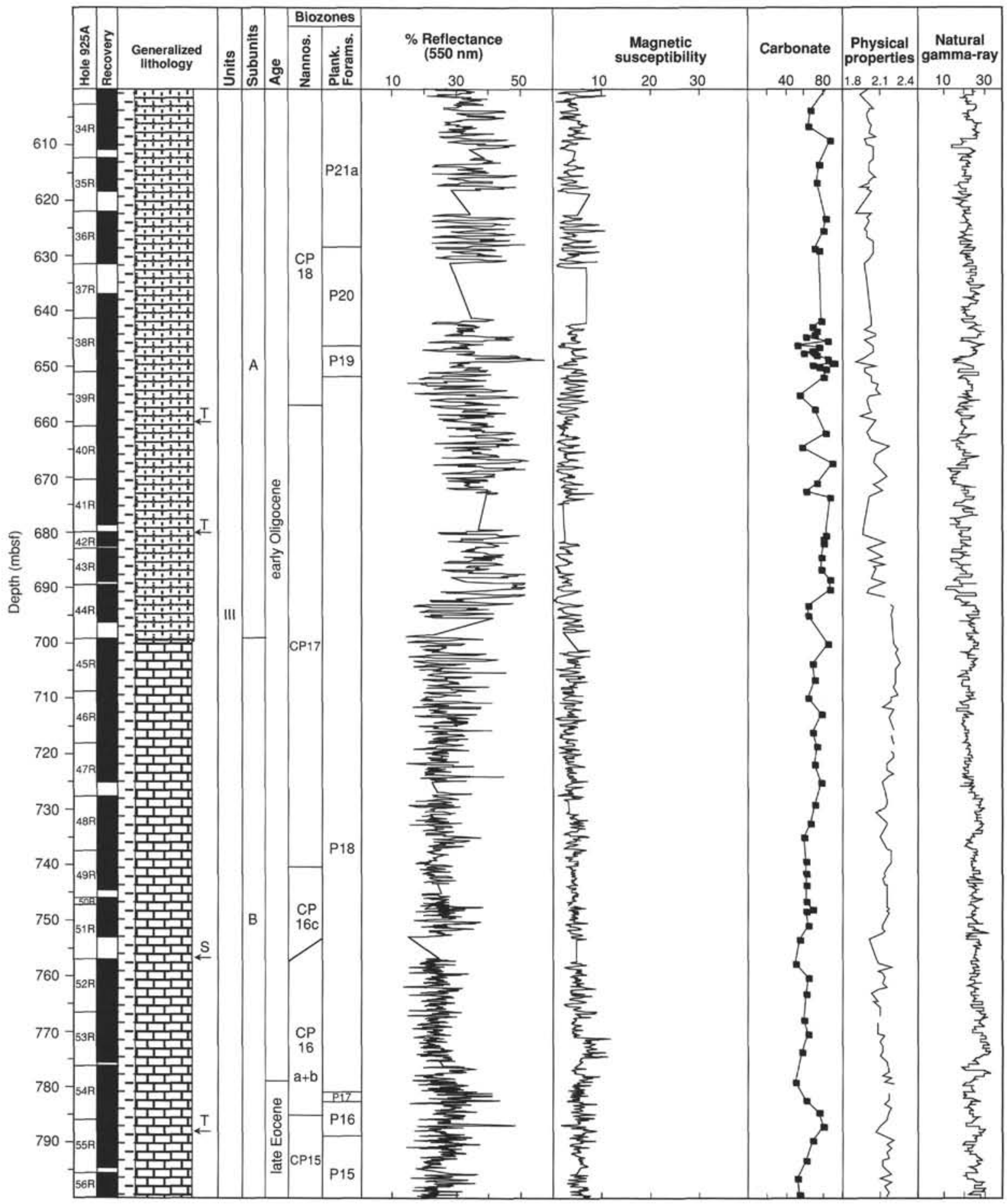

Figure 3 (continued).

at 5-cm intervals was analyzed in Core 154-925C-8H. Variations in the <4-μm clay-size fraction relative to all other size fractions appear to correspond with variations in the magnetic susceptibility record (Fig. 12). Also, on a longer time scale, variations in the clay-size fraction are similar to variations in the magnetic susceptibility record (Fig. 13).

Decimeter- to meter-scale cyclic changes in sediment carbonate content are caused by some combination of changes in carbonate production or dissolution, or the input rate of terrigenous clays. To fully resolve which of these processes was responsible for the Site 925 cycles will require detailed measurement of various dissolution and productivity proxies. Nevertheless, preliminary observation of microfossil preservation suggests that the higher clay intervals of the middle and late Miocene might be caused by dissolution (see "Biostratigraphy" section, this chapter). Pliocene and Pleistocene sediments, in contrast, show little, if any, change in preservation within cycles, indicating that they might reflect changes in the particle flux of carbonate or terrigenous clay minerals to this site. The latter would be more consistent with the late Neogene increase in clay content and sedimentation rates (see "Sedimentation Rates" section, this chapter).

Another prominent feature of Site 925 is the decrease in average carbonate content in the late Neogene (Unit I). This trend results from a steady increase in clay mineral content from the middle of the early

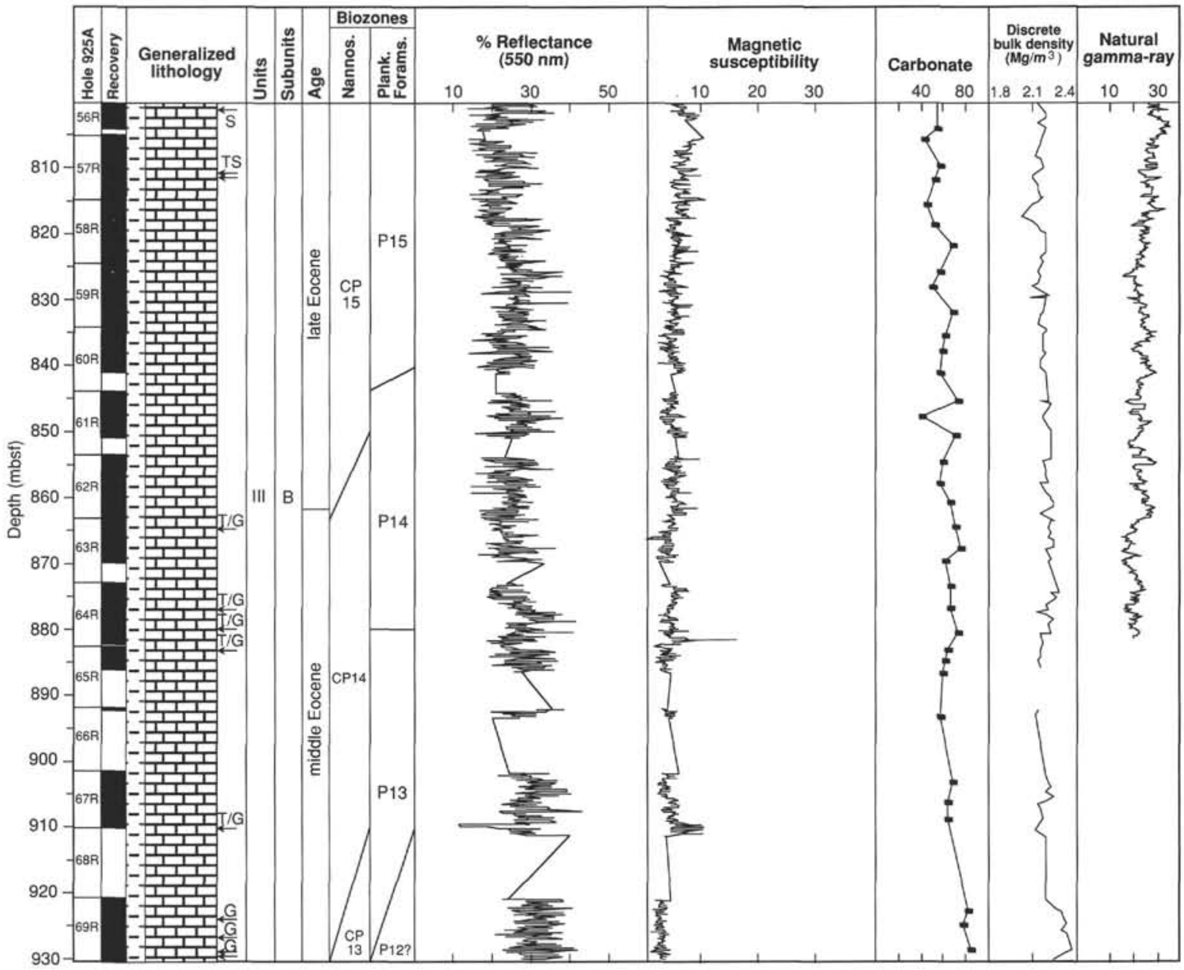

Figure 3 (continued).

Pliocene (around 4.5 m.y. ago) to the Holocene, a trend that is accompanied by increases in magnetic susceptibility (Fig. 3) and the clay-size (<4 μm) fraction (Fig. 13). Because sedimentation rates also increase over this interval, it is likely that the late Neogene increase in clay content reflects a progressive increase in the supply of suspended kaolinite-rich terrigenous clays from the Amazon River.

Although cyclic pelagic sedimentation is the norm at Site 925 since the middle Eocene, the basal part of the sequence in Subunit IIIB (710–930 mbsf) exhibits sedimentary structures suggestive of a period of more episodic deposition. Significant portions of the lower part of Subunit IIIB were clearly deposited by mass-transport processes such as slumps, turbidites, and debris flows. Between 860 and 930 mbsf, there are at least nine distinct intervals of rapidly deposited sediment. The abundance of these deposits suggests that this site was positioned either on or near the flank of a submarine high that was actively shedding sediment during the early middle Eocene. A prominent topographic high located several kilometers to the north of this site (Fig. 1) may have been the source. Seismic profiles indicate that the relief of this feature was greater in the past, having since been reduced by sediment accumulation along the flanks. Also, assuming subsidence rates over the last 45 m.y. were normal, it was probably shallower than at present. As a result, during the middle Eocene sediments may have been shed more frequently and/or transported farther than in the recent past. Moreover, the presence of isolated foraminifer sands lacking a significant clay or nannofossil component indicates that at least part of the source area was shallow enough for significant winnowing to occur. Although it is possible that the slumps and sands were derived locally, sediment redeposition from shallower depths is consistent with the sudden increase in carbonate content recorded over the lowermost portion of the sequence (see "Geochemistry" section, this chapter).

In summary, the variations in the lithology of Site 925 sediments are the result of the interaction between shorter term cyclic climatic changes (orbitally forced) superimposed upon longer term changes, which, to some extent, are produced by discrete climatic and depositional events. Given the lateral uniformity of seismic facies on the Ceara Rise, the variability observed at Site 925 should provide a reasonable framework for documenting and understanding the lithology of the sedimentary sequences recovered at subsequent sites.

BIOSTRATIGRAPHY

Introduction

Site 925 is located on the top of the Ceara Rise at 4°12.26′N, 43°29.35′W in 3041-m water depth. Five holes were drilled (Holes 925A through 925E), the deepest of which (Hole 925A) was penetrated by the RCB to a depth of 930.4 mbsf. Biostratigraphic control at Site 925 was provided by shipboard analyses of calcareous nannoplankton and planktonic foraminifers. Faunal assemblage changes in benthic foraminifers were also studied. No hiatuses were identified. Thus, the sequence is apparently complete from the middle Eocene to the Holocene.

One of the most promising aspects of Site 925 is that the sediments are characterized by cyclic variations in color and physical properties that appear to oscillate at the so-called Milankovitch band frequencies (see "Composite Section" and "Physical Properties" sections, this chap-

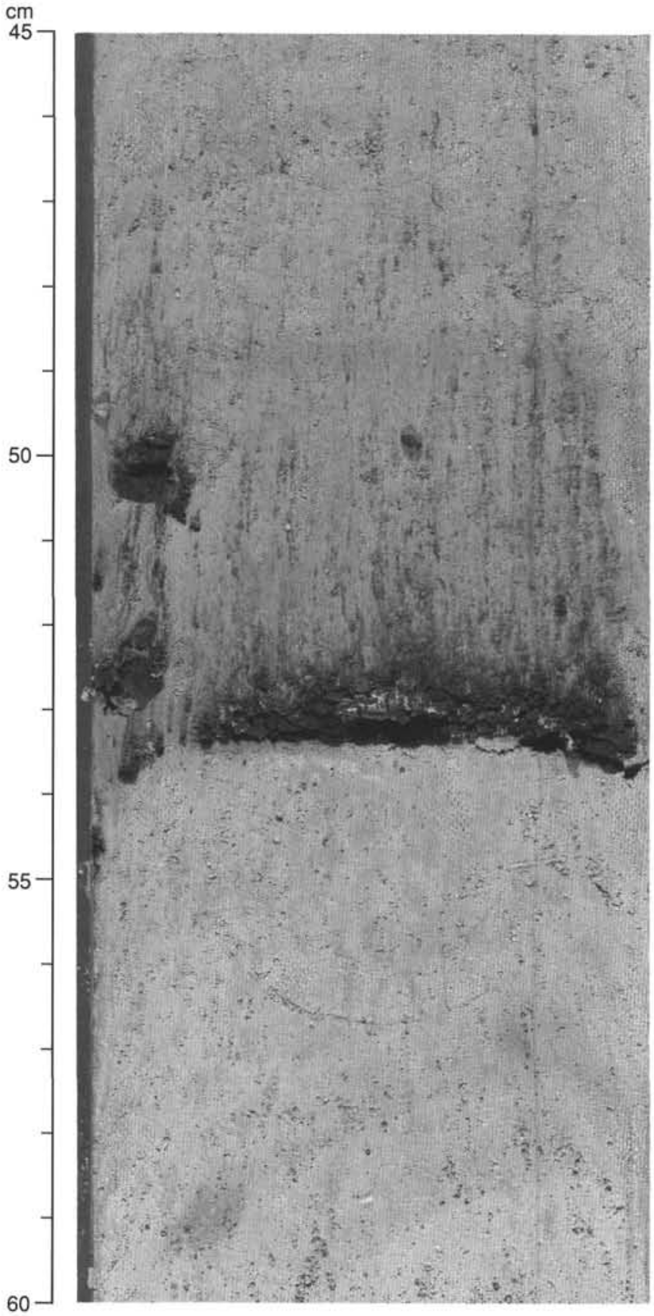

Figure 4. Photograph of a layer of microcrystalline pyrite at the contact between a dark and a light bed (interval 154-925B-6H-3, 45–60 cm).

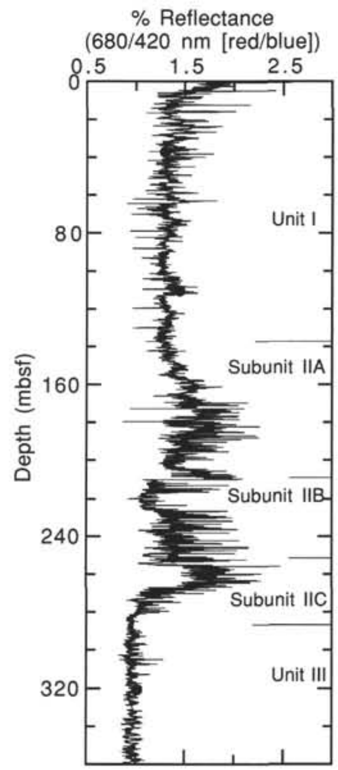

Figure 5. Ratio of percentage of reflectance at 680 nm (red) to 420 nm (blue) vs. depth in Hole 925C. Iron oxide and oxyhydroxide layers are emphasized by this ratio, particularly in Subunits IIB and IIC.

ter). These cycles allow the assembly of a complete composite stratigraphic section for much of the site. They also provide an unprecedented opportunity for precise determinations of the relative age spacing of biostratigraphic events from a low-latitude ocean paleoenvironment. The greatest potential for this work is in the ooze-chalk intervals; that is, in the Holocene to lower Oligocene interval. Preservation deteriorates at the chalk/limestone transition in the lower Oligocene.

Calcareous Nannofossils

The biostratigraphic information preserved in the calcareous nannofossil floras at Site 925 was investigated in nearly 1000 smear slides. The nannofossil biostratigraphy suggests that the sequences recovered represent an almost continuous stratigraphic record from the late Pleistocene–Holocene (Zone CN15) to the middle Eocene (at approximately the Zone CP13/CP14 boundary, at about 42 Ma).

The Neogene sediments in Holes 925B and 925D, ending in the lower middle Miocene (318.0 mbsf) and the upper lower Miocene (354.0 mbsf), respectively, were studied in greater detail than in the corresponding intervals in Holes 925A (washed to 303.7 mbsf), 925C (0–360.1 mbsf), and 925E (0–55.65 mbsf). Core-catcher samples from all holes, however, were investigated. The results from the biostratigraphic investigations are presented in Table 2 and Figure 14. Sample spacing varied from 0.05 to 9.5 m. Most of the conventionally adopted Eocene through Holocene nannofossil markers (Martini, 1971; Bukry, 1978) were determined to well within a core section in at least one of the five holes, giving an average depth uncertainty of between 0.50 and 0.75 m for each marker event in the integrated stratigraphic sequence. Several events were determined precisely in more than one hole, partly for the purpose of aiding the construction of the composite depth sections (see "Composite Section" section, this chapter). Note that we took most nannofossil samples as "tooth-pick" samples; where 1-cm^3 samples were taken, we have chosen to show the upper depth assignment (i.e., "40 cm" rather than "40–41 cm").

The nannofossil assemblages are generally diverse and well preserved. Short intervals in the Neogene–Oligocene interval exhibit varying degrees of dissolution, as indicated by increased fragmentation and increased abundances of disjointed discoaster rays. In some samples, dissolution pits are visible on the larger placoliths and helicosphaerids. Calcite overgrowth is most evident among the relatively low-diversity discoaster assemblages of the Oligocene and lower Miocene. Generally poor preservation, including both dissolution and secondary overgrowth, was encountered in some of the deepest buried middle Eocene cores in Hole 925A. In particular, Cores 154-925A-63R, -67R, -68R, and -69R are affected the worst. There is no evidence of severe sediment mixing, caused either through sedimentological processes or during the coring procedure. There are a few short intervals that appear affected by downslope transport processes (see "Lith-

Table 2. Calcareous nannoplankton events in Holes 925A, 925B, 925C, and 925D.

Event	Age (Ma)	Sample ID (top to bottom)	Depth (mbsf)	Mean depth (mbsf)	Depth (mcd)	Mean depth (mcd)
Hole 925A:						
T *Sphenolithus* spp.	3.62	1R-2, 30 to 1R-2, 105	103.60–104.35	103.98	111.91–112.66	112.29
T *Reticulofenestra pseudoumbilicus*	3.77	1R-3, 30 to 1R-3, 100	105.10–105.80	105.45	113.41–114.11	113.76
Bc *Discoaster surculus*	7.8	2R-2, 30 to 2R-CC	199.70–203.83	201.77	211.04–215.17	213.11
T *Helicosphaera ampliaperta*	15.8	5R-6, 110 to 5R-7, 30	332.00–332.70	332.35	370.34–371.04	370.69
B *Sphenolithus heteromorphus*	18.1	13R-1, 40 to 13R-1, 97	400.80–401.37	401.09	439.14–439.71	439.43
T *Sphenolithus belemnos*	18.4	14R-1, 17 to 14R-2, 40	410.17–410.66	410.42	448.51–449.00	448.76
T *Triquetrorhabdulus carinatus*	19.3	14R-4, 115 to 14R-5, 50	414.41–415.26	414.83	452.75–453.60	453.18
B *Sphenolithus belemnos*	19.7	15R-6, 140 to 15R-7, 20	428.60–428.90	428.75	466.94–467.24	467.09
T *Sphenolithus delphix*	23.3	23R-3, 121 to 23R-4, 125	500.91–502.45	501.68	539.25–540.79	540.02
T *Sphenolithus ciperoensis*	24.7	23R-CC to 24R-1, 120	502.85–507.50	505.18	541.19–545.84	543.52
T *Sphenolithus distentus*	26.5	30R-CC to 31R-1, 45	574.17–574.25	574.21	612.51–612.59	612.55
B *Sphenolithus ciperoensis*	28.1	32R-6, 120 to 32R-CC	592.20–593.33	592.77	630.54–631.67	631.11
B *Sphenolithus distentus*	30.4	39R-3, 50 to 39R-4, 140	654.60–657.00	655.80	692.94–695.34	694.14
T *Reticulofenestra umbilicus* >14 µm	32.1	49R-2, 71 to 49R-3, 61	739.81–741.21	740.51	778.15–779.55	778.85
T *Coccolithus formosus*	32.7	51R-CC to 52R-1, 1	753.66–757.01	755.34	792.00–795.35	793.68
T *Discoaster saipanensis*	34.2	54R-7, 61 to 54R-CC	785.91–786.27	786.09	824.25–824.61	824.43
T *Cribrocentrum reticulatum*	35.0	55R-5, 25 to 55R-5, 62	792.25–752.62	792.44	830.59–830.96	830.78
T *Calcidiscus protoannulus*	35.4	55R-CC to 56R-CC	794.72–804.29	799.51	833.08–842.63	837.85
T *Chiasmolithus grandis*	37.1	61R-CC to 62R-CC	850.89–863.43	857.16	889.23–901.78	895.50
B *Reticulofenestra umbilicus* >14 µm	42.2	67R-CC to 69R-CC	911.34–929.94	920.64	949.68–968.28	958.98
Hole 925B:						
B *Emiliania huxleyi*	0.26	1H-CC to 2H-CC	4.49–14.10	9.30	4.49–14.80	9.65
T *Pseudoemiliania lacunosa*	0.46	3H-1, 120 to 3H-2, 27	15.20–15.77	15.49	18.11–18.68	18.40
Reentrance medium *Gephyrocapsa* spp.	1.03	4H-5, 70 to 4H-6, 70	30.20–31.60	30.90	33.70–35.20	34.45
T large *Gephyrocapsa* spp.	1.24	5H-4, 30 to 5H-4, 100	37.80–38.50	38.15	41.74–42.44	42.09
B large *Gephyrocapsa* spp.	1.46	6H-3, 145 to 6H-4, 54	46.96–47.54	47.25	50.61–51.20	50.91
T *Calcidiscus macintyrei*	1.60	6H-4, 145 to 6H-5, 54	48.45–49.04	48.75	52.11–52.70	52.41
B medium *Gephyrocapsa* spp.	1.67	6H-5, 145 to 6H-6, 54	49.96–50.54	50.25	53.61–54.20	53.91
T *Discoaster brouweri*	1.95	7H-4, 125 to 7H-5, 45	57.75–58.45	58.10	62.00–62.79	62.44
B acme *Discoaster triradiatus*	2.15	8H-2, 115 to 8H-3, 40	64.15–64.90	64.53	68.26–69.01	68.64
T *Discoaster pentaradiatus*	2.44	9H-1, 90 to 9H-1, 115	71.90–72.15	72.03	77.23–77.48	77.36
T *Discoaster surculus*	2.61	9H-2, 115 to 9H-3, 140	73.65–75.4	74.03	78.98–80.73	79.86
T *Discoaster tamalis*	2.76	10H-2, 114 to 10H-3, 40	83.14–83.90	83.52	88.93–89.69	89.31
T *Sphenolithus* spp.	3.62	12H-5, 115 to 12H-6, 40	106.65–107.40	107.03	116.80–117.55	117.18
T *Reticulofenestra pseudoumbilicus*	3.77	13H-2, 20 to 13H-2, 42	110.70–110.92	110.81	122.77–122.99	122.88
B *Ceratolithus rugosus*	5.04	16H-4, 40 to 16H-4, 115	142.40–143.15	142.77	157.22–157.97	157.60
T *Ceratolithus acutus*	5.04	16H-4, 40 to 16H-4, 115	142.40–143.15	142.77	157.22–157.97	157.60
T *Triquetrorhabdulus rugosus*	5.34	16H-CC to 17H-1, 25	147.11–147.25	147.18	161.93–162.67	162.30
B *Ceratolithus acutus*	5.34	17H-1, 25 to 17H-2, 10	147.25–148.60	147.93	162.67–164.02	163.35
T *Discoaster quinqueramus*	5.6	17H-5, 80 to 17H-6, 10	153.80–154.60	154.20	169.22–170.02	169.62
T *Amaurolithus amplificus*	5.9	18H-4, 115 to 18H-5, 40	162.15–162.90	162.53	179.02–179.77	179.40
B *Amaurolithus amplificus*	6.5	21H-4, 115 to 21H-5, 40	190.65–191.40	191.03	211.94–212.69	212.32
B *Amaurolithus primus*	7.3	22H-3, 80 to 22H-3, 115	198.30–198.65	198.48	220.01–220.36	220.19
B *Discoaster berggrenii*	8.4	24H-4, 80 to 24H-4, 115	218.80–219.15	218.98	243.97–244.32	244.15
T *Catinaster calyculus*	9.36	26H-CC to 27H-1, 80	242.61–242.80	242.71	270.39–271.51	270.95
T *Discoaster hamatus*	9.4	27H-1, 100 to 27H-1, 108	243.00–243.08	243.04	271.71–271.78	271.75
B *Discoaster neohamatus*	9.6	27H-2, 80 to 28H-1, 20	244.30–251.70	248.00	273.01–280.05	276.53
B *Discoaster hamatus*	10.4	28H-CC to 29H-1, 20	261.59–261.20	261.40	289.94–292.57	291.26
B *Catinaster coalitus*	10.7	29H-4, 80 to 29H-5, 20	266.30–267.20	266.75	297.67–298.57	298.12
T *Coccolithus miopelagicus*	10.4	29H-6, 80 to 29H-7, 10	269.30–270.10	269.70	300.67–301.47	301.07
Tc *Discoaster kugleri*	11.3	30H-5, 121 to 30H-5, 126	277.71–277.76	277.74	310.55–310.60	310.58
Bc *Discoaster kugleri*	11.7	30H-CC to 31H-1, 38	280.50–280.38	280.44	313.34–314.80	314.07
T *Coronocyclus nitescens*	12.1	32H-7, 31 to 32H-7, 65	298.81–299.15	298.98	335.67–336.01	335.84
T *Cyclicargolithus floridanus*	13.2	33H-2, 80 to 33H-3, 70	301.30–302.70	302.00	339.25–340.65	339.95
T *Sphenolithus heteromorphus*	13.6	33H-7, 25 to 33H-7, 50	308.25–308.50	308.38	346.20–346.45	346.33
Hole 925C:						
B *Emiliania huxleyi*	0.26	1H-CC to 2H-CC	8.13–17.62	12.88	8.13–18.34	13.24
T *Pseudoemiliania lacunosa*	0.46	1H-CC to 2H-CC	8.13–17.62	12.88	8.13–18.34	13.24
Reentrance medium *Gephyrocapsa* spp.	1.03	3H-CC to 4H-CC	27.23–36.76	32.00	27.56–38.25	32.91
T large *Gephyrocapsa* spp.	1.24	4H-CC to 5H-CC	36.76–46.00	41.38	38.25–48.09	43.17
B large *Gephyrocapsa* spp.	1.46	5H-CC to 6H-CC	46.00–55.65	50.83	48.09–57.81	52.95
T *Calcidiscus macintyrei*	1.60	5H-CC to 6H-CC	46.00–55.65	50.83	48.09–57.81	52.95
B medium *Gephyrocapsa* spp.	1.67	5H-CC to 6H-CC	46.00–55.65	50.83	48.09–57.81	52.95
T *Discoaster brouweri*	1.95	6H-CC to 7H-CC	55.65–65.34	60.50	57.81–67.87	62.84
B acme *Discoaster triradiatus*	2.15	7H-CC to 8H-CC	65.34–74.69	70.02	67.87–79.51	73.69
T *Discoaster pentaradiatus*	2.44	7H-CC to 8H-CC	65.34–74.69	70.02	67.87–79.51	73.69
T *Discoaster surculus*	2.61	8H-CC to 9H-CC	74.69–84.13	79.41	79.51–89.20	84.36
T *Discoaster tamalis*	2.76	9H-CC to 10H-CC	84.13–93.55	88.84	89.20–99.71	94.46
T *Sphenolithus* spp.	3.62	11H-CC to 12H-CC	102.75–112.56	107.66	113.59–123.81	118.70
T *Reticulofenestra pseudoumbilicus*	3.77	11H-CC to 12H-CC	102.75–112.56	107.66	113.59–123.81	118.70
B *Ceratolithus rugosus*	5.04	14H-CC to 15H-1, 80	131.86–132.30	132.08	146.05–147.35	146.70
T *Triquetrorhabdulus rugosus*	5.34	16H-1, 100 to 16H-7, 50	142.00–150.50	146.25	157.39–165.89	161.34
B *Ceratolithus acutus*	5.34	16H-1, 100 to 16H-7, 50	142.00–150.50	146.25	157.39–165.89	161.34
T *Discoaster quinqueramus*	5.6	16H-CC to 17H-CC	151.01–160.09	155.55	166.40–176.56	171.48
T *Amaurolithus amplificus*	5.9	17H-CC to 18H-CC	160.09–169.94	165.02	176.56–187.16	181.86
B *Amaurolithus amplificus*	6.5	20H-CC to 21H-CC	188.89–198.60	193.75	208.43–219.35	213.89
B *Amaurolithus primus*	7.3	21H-CC to 22H-CC	198.60–208.20	203.40	219.35–229.87	224.61
B *Discoaster berggrenii*	8.4	23H-CC to 24H-CC	217.62–227.01	222.32	244.23–249.57	246.90
T *Catinaster calyculus*	9.36	26H-5, 115 to 26H-6, 40	243.15–243.90	243.53	269.98–270.73	270.36
T *Discoaster hamatus*	9.4	26H-6, 115 to 26H-7, 40	244.65–245.40	245.O3	271.48–272.23	271.86
B *Minylitha convallis*	9.4	26H-6, 115 to 26H-7, 40	244.65–245.40	245.O3	271.48–272.23	271.86
B *Discoaster hamatus*	10.4	28H-3, 40 to 28H-3, 114	258.40–259.14	258.77	288.23–288.97	288.60
B *Catinaster coalitus*	10.7	29H-1, 40 to 29H-1, 115	264.90–265.65	265.28	298.19–298.94	298.57
T *Coccolithus miopelagicus*	10.4	29H-3, 40 to 29H-3, 115	267.90–268.65	268.28	301.19–301.94	301.57
Tc *Discoaster kugleri*	11.3	29H-6, 50 to 29H-6, 63	272.50–272.63	272.57	305.79–305.92	305.86

Table 2 (continued).

Event	Age (Ma)	Sample ID (top to bottom)	Depth (mbsf)	Mean depth (mbsf)	Depth (mcd)	Mean depth (mcd)
Bc *Discoaster kugleri*	11.7	29H-6, 130 to 29H-7, 40	273.30–273.90	273.60	306.59–307.19	306.89
Tc *Cyclicargolithus floridanus*	13.2	31H-CC to 32H-CC	293.56–303.01	298.29	332.70–344.03	338.37
T *Sphenolithus heteromorphus*	13.6	33H-2, 80 to 33H-2, 100	304.80–305.00	304.90	346.90–347.10	347.00
T *Helicosphaera ampliaperta*	15.8	35X-CC to 36X-1, 40	329.57–331.60	330.59	366.76–368.19	367.48
T abundant *Discoaster deflandrei*	16.2	38X-1, 40 to 38X-1, 115	350.80–351.55	351.18	397.84–398.59	398.22
Hole 925D:						
T *Pseudoemiliania lacunosa*	0.46	2H-3, 80 to 2H-3, 140	15.72–16.32	16.02	18.31–18.91	18.61
Reentrance medium *Gephyrocapsa* spp.	1.03	4H-1, 40 to 4H-1, 80	31.40–31.80	31.60	35.17–35.57	35.37
T large *Gephyrocapsa* spp.	1.24	4H-5, 120 to 4H-6, 40	38.20–38.90	38.55	41.97–42.47	42.22
B large *Gephyrocapsa* spp.	1.46	5H-4, 80 to 5H-4, 120	45.80–46.20	46.00	50.34–50.74	50.54
T *Calcidiscus macintyrei*	1.60	5H-6, 40 to 5H-6, 80	48.40–48.80	48.60	52.94–53.34	53.14
B medium *Gephyrocapsa* spp.	1.67	6H-1, 80 to 6H-1, 120	50.80–51.20	51.00	55.38–55.78	55.58
T *Discoaster brouweri*	1.95	6H-5, 120 to 6H-6, 40	57.20–57.90	57.55	61.78–62.48	62.13
B acme *Discoaster triradiatus*	2.15	7H-2, 80 to 7H-2, 120	61.80–62.20	62.00	67.48–67.88	67.68
T *Discoaster pentaradiatus*	2.44	7H-CC to 8H-CC	69.29–78.12	73.71	74.97–84.59	79.78
T *Discoaster surculus*	2.61	7H-CC to 8H-CC	69.29–78.12	73.71	74.97–84.59	79.78
T *Discoaster tamalis*	2.76	8H-CC to 9H-CC	78.12–88.58	83.35	84.59–95.82	90.21
T *Sphenolithus* spp.	3.62	11H-CC to 12H-CC	107.27–116.82	112.05	117.52–127.73	122.63
T *Reticulofenestra pseudoumbilicus*	3.77	12H-4, 20 to 12H-4, 60	111.70–112.10	111.90	122.61–123.01	122.81
T *Triquetrorhabdulus rugosus*	5.34	16H-3, 40 to 16H-3, 115	148.40–149.15	148.78	162.93–163.68	163.31
B *Ceratolithus acutus*	5.34	16H-3, 115 to 16H-4, 40	149.15–149.90	149.53	163.68–164.43	164.06
B *Amaurolithus amplificus*	6.5	20H-6, 85 to 20H-7, 10	191.35–191.50	191.43	211.59–211.74	211.67
B *Amaurolithus primus*	7.3	21H-4, 40 to 21H-4, 115	197.40–197.15	196.77	219.81–220.56	220.18
B *Discoaster berggrenii*	8.4	23H-CC to 24H-1, 50	221.34–221.50	221.42	245.12–245.48	245.30
T *Catinaster calyculus*	9.36	26H-3, 115 to 26H-4, 40	244.15–244.90	244.53	270.12–270.87	270.49
T *Discoaster hamatus*	9.4	26H-4, 115 to 26H-5, 40	245.65–246.40	246.03	271.62–272.37	271.99
B *Minylitha convallis*	9.4	26H-5, 40 to 26H-5, 115	246.40–247.15	246.78	272.37–273.12	272.75
B *Discoaster hamatus*	10.4	28H-3, 40 to 28H-3, 115	262.40–263.15	262.78	291.86–292.61	292.24
B *Catinaster coalitus*	10.7	29H-1, 40 to 29H-1, 115	268.90–269.65	269.28	297.79–298.54	298.17
T *Coccolithus miopelagicus*	10.4	29H-3, 115 to 29H-4, 40	272.65–273.40	273.03	301.54–302.29	301.92
T *Coronocyclus nitescens*	12.1	30H-6, 115 to 31H-1, 40	286.65–287.90	287.28	317.55–319.72	318.643
Tc *Cyclicargolithus floridanus*	13.2	32H-6, 115 to 33H-1, 40	305.65–306.90	306.28	339.50–341.84	340.67
T *Sphenolithus heteromorphus*	13.6	33H-4, 115 to 33H-5, 40	312.15–312.90	312.53	347.09–347.84	347.47
T *Helicosphaera ampliaperta*	15.8	35H-2, 115 to 35H-3, 40	328.15–328.90	328.53	366.34–367.09	366.72
T abundant *Discoaster deflandrei*	16.2	37H-3, 40 to 37H-3, 115	347.90–348.65	348.28	396.29–397.04	396.67

Note: T = top, B = base, Tc = top common, and Bc = base common.

ostratigraphy" section, this chapter), which may help explain some of the few inconsistencies observed in the nannofossil record. For example, the anomalously short range of the lower Miocene species *Sphenolithus delphix* was observed only in a single sample.

The tropical location of Site 925 on the "warm" side of the Atlantic throughout the time interval under study has created assemblages that are exceptionally diverse, which makes this site ideal for investigations of rates of morphologic evolution and taxonomic turnover through time. Middle Miocene discoaster assemblages, for example, exhibit an extreme array of morphotypes, particularly within the 6-rayed forms possessing bifurcated ray tips. Other discoasters also show wide inter- and intra-specific morphologic variability; for example, both 4-rayed and 6-rayed variants of *Discoaster quinqueramus* were observed. The upper Miocene triquetrorhabdulid lineage also exhibits considerable variability in morphology, and transitional forms between *Triquetrorhabdulus rugosus* and *Amaurolithus primus* were observed. Subsequently, *T. rugosus* evolved into *Amaurolithus amplificus*, and, lastly, at the Miocene/Pliocene boundary, into *Ceratolithus acutus*. The latter transition appears to have been accompanied by the extinction of *T. rugosus*. These, and other, evolutionary transitions are well represented in the material recovered from Site 925. These detailed evolutionary transitions and the prevailing species-rich assemblages suggest that the material retrieved from Site 925 may be used to improve the resolution of upper Cenozoic nannofossil biostratigraphy.

Sedimentation rates at Site 925 varied from about 15 to 43 m/m.y., which is moderate to high for an open-ocean site (see "Sedimentation Rates" section, this chapter). Thus, considering (1) the apparent continuity in biogenic carbonate sedimentation over the past 40 m.y.; (2) the generally well-preserved character of the nannofossil assemblages; (3) the tropical location in moderately deep waters; and (4) the cyclic nature of the physical properties of the sediments, Site 925 fulfills the essential requirements for a biostratigraphic reference section that represents a tropical ocean characterized by moderately strong to weak upwelling conditions.

Pleistocene

The Pleistocene extends to approximately the level of the first appearance of medium-sized (≥4 µm) *Gephyrocapsa. Emiliania huxleyi* was observed in the first core-catcher sample in Holes 925B, 925D, and 925E in abundances indicating a position below oxygen isotopic Substage 5b. *Pseudoemiliania lacunosa* shows a sharp final decline in abundance that can be determined precisely. The now well-established succession of Pleistocene gephyrocapsid events, which relies largely on taxonomic subdivision in three size classes (Raffi et al., 1993), was observed in, for example, in Core 154-925C-13H and in Sample 154-925C-12H-CC (see Table 2 for details). The last occurrence (LO) of *Helicosphaera sellii* was observed within the range of large *Gephyrocapsa,* although apparently in the middle part of that range. This is approximately halfway between the "old" estimates, shortly below the appearance of large gephyrocapsids, derived from equatorial Pacific Ocean sites (ODP Site 677; Piston Core V28-239) and the Caribbean (DSDP Site 502), and the "young" estimates (near the top of the range of large gephyrocapsids) derived from the mid- to high-latitude North Atlantic and Mediterranean (see discussion in Raffi et al., 1993).

Pliocene

The upper Pliocene encompasses the interval between the successive extinctions of *Discoaster brouweri* and *Discoaster pentaradiatus.* The base of the middle Pliocene is defined by the extinction of *Reticulofenestra pseudoumbilicus.* The appearance of *Ceratolithus acutus* approximates the Miocene/Pliocene boundary. Both *Discoaster asymmetricus* and *Discoaster tamalis* occur in most samples assigned to the middle Pliocene; the former showed a first

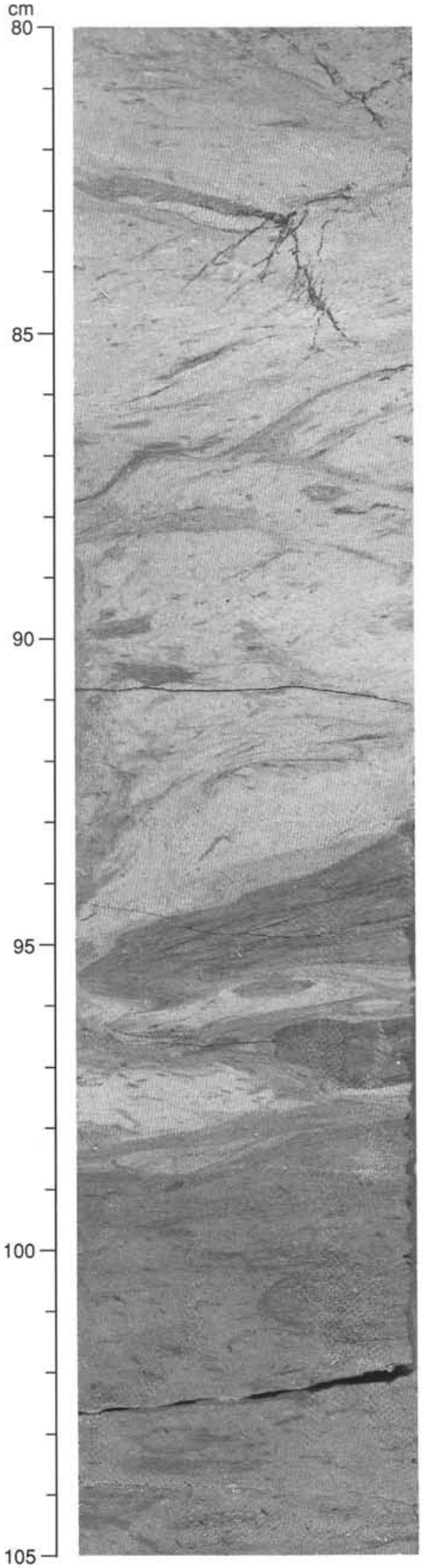

Figure 6. Photograph showing folded layers and contorted laminae in a slump deposit (interval 154-925A-56R-3, 80–105 cm).

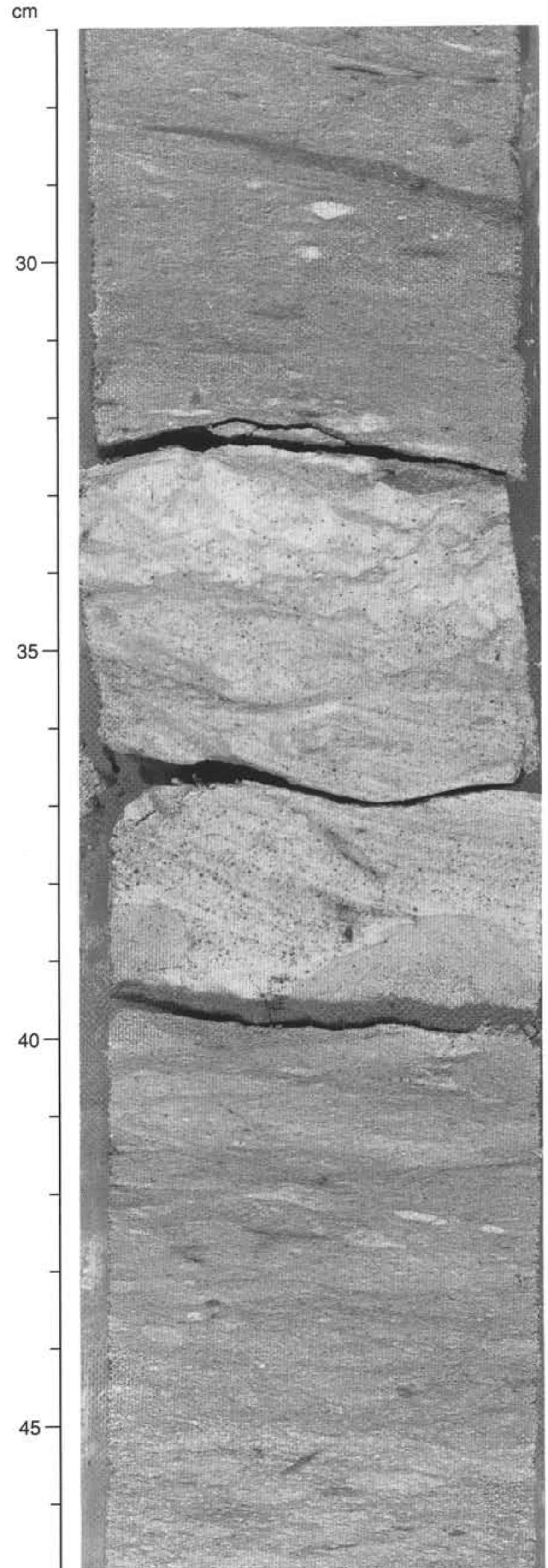

Figure 7. Photograph of a turbidite (interval 154-925A-63R-2, 27–47 cm).

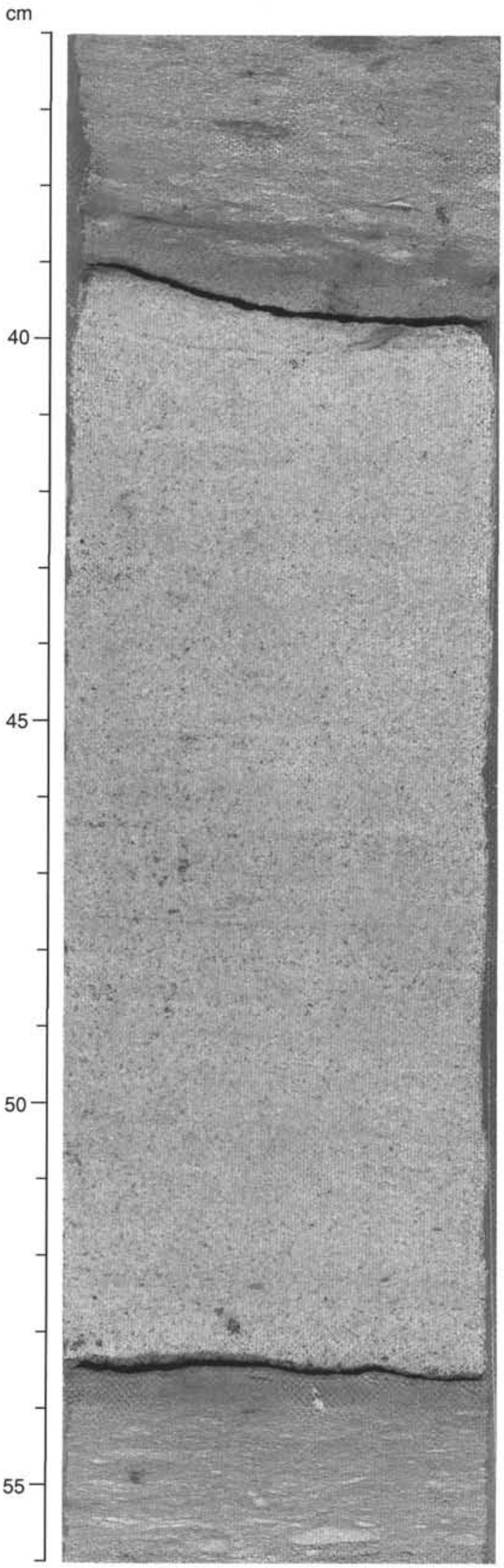

Figure 8. Well-sorted foraminifer sand bed from middle Eocene limestone sequence (Subunit IIIB) in interval 154-925A-69R-4, 36–56 cm.

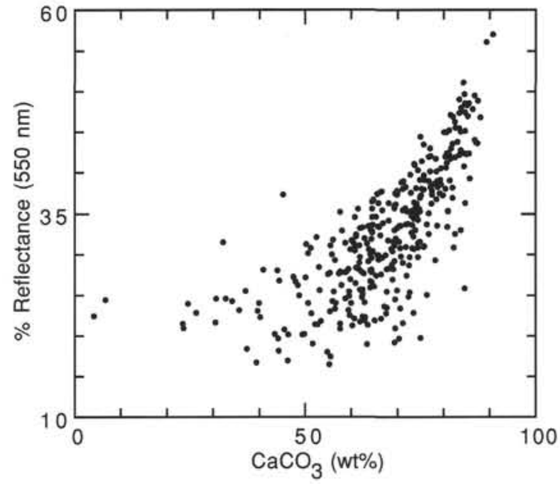

Figure 9. Percentage of carbonate content vs. percentage of reflectance at the 550-nm wavelength for Holes 925A, 925B, and 925C.

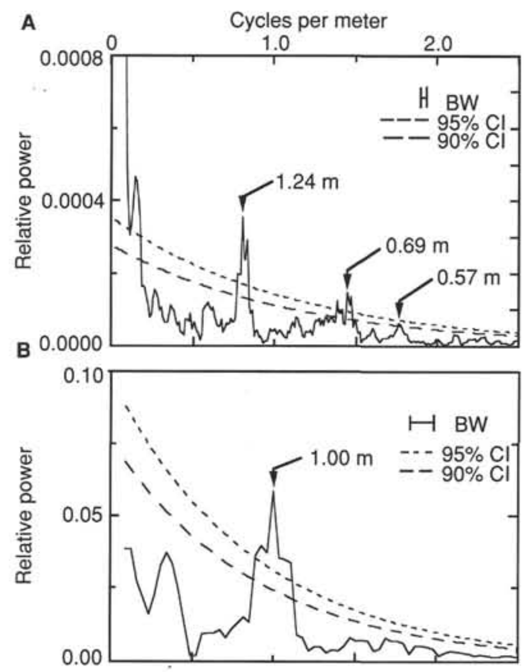

Figure 10. Fourier power spectra of the intervals from 0 to 100 mcd (**A**) and from 622 to 649 mcd (**B**), Site 925. Spectral analysis reflectance time series was based on the Fast Fourier transform and 8 degrees of freedom in the spectral estimates. The 95% and 90% CI lines indicate the approximate one-sided confidence intervals for the spectral background. The bar labeled "BW" indicates the bandwidth or frequency resolution of the spectrum.

occurrence (FO) slightly below that of the latter. Rare occurrences of *Amaurolithus* spp. (i.e., *Amaurolithus delicatus*) were observed to overlap with *D. tamalis* in Cores 154-925C-13H and -12H-CC. The extinction of *Amaurolithus primus,* which defines the Zone CN10/CN11 boundary, was observed between Samples 154-925C-14H-CC and -15H-1, 80 cm.

Ceratolithus armatus, a form that we consider as an intergrade between *Ceratolithus rugosus* and *Ceratolithus acutus,* was observed in Sample 154-925B-16H-3, 80 cm. The evolutionary sequence from *T. rugosus* to *C. acutus* involved a series of odd-looking, aberrant varieties of the ancestor species before the descendant *C. acutus* became firmly established. This sequence can be observed in Core

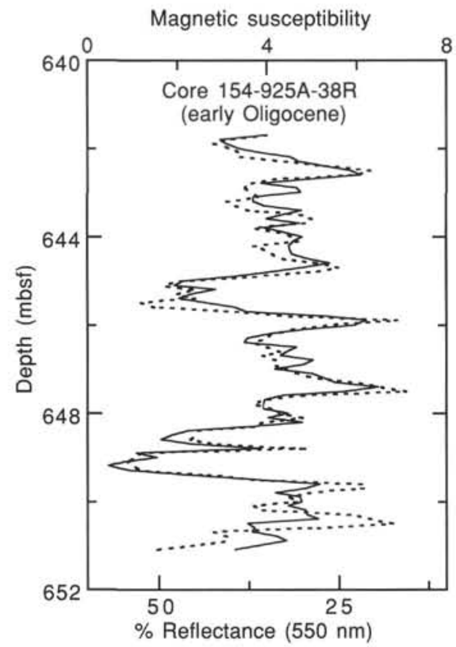

Figure 11. Comparison of percentage of reflectance at the 550-nm wavelength (solid line) and magnetic susceptibility (dashed line) values of Core 154-925A-38R.

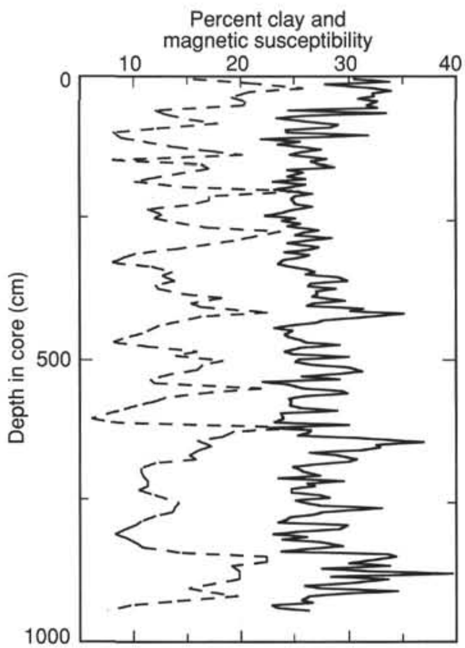

Figure 12. High-resolution record of magnetic susceptibility (8-cm sampling interval; dashed line) and clay-size (<4 μm) fraction (5-cm interval; solid line) vs. depth in Core 154-925C-8H.

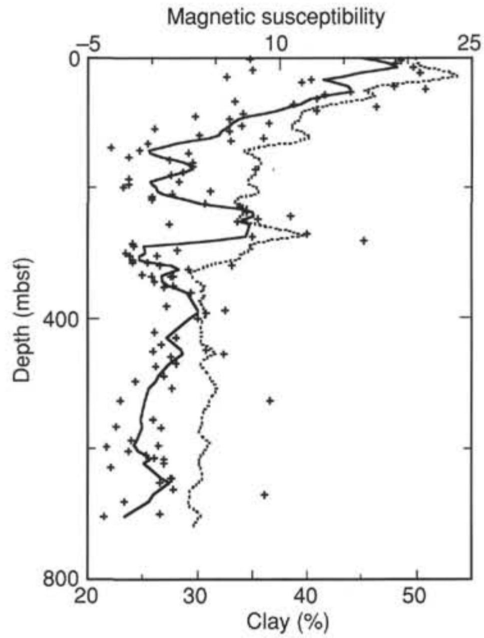

Figure 13. Clay-size fraction variation with depth at Site 925. The record from 0 to 300 m is from Hole 925B, and that from 300 m and below is from Hole 925A. Symbols represent discrete measurements of clay percentage. The solid line presents a moving average of the percentage of clay data, and the dashed line presents a moving average of magnetic susceptibility data from the same cores.

154-925D-16H, which also contains other rarely reported forms of *Ceratolithus,* including *Ceratolithus atlanticus,* which was described by Perch-Nielsen (1977) from the Ceara Rise (DSDP Site 354).

Miocene

Like several other Cenozoic stage or age boundaries, the position of the Serravallian/Tortonian boundary, or middle/upper Miocene boundary, is still debated. We approximate this boundary by the upper part of Zone CN7, which is defined by the total range of *Discoaster hamatus.* The extinction of *Helicosphaera ampliaperta* is used to approximate the lower/middle Miocene boundary, and the top of the interval with abundant *Sphenolithus delphix* is used to approximate the Oligocene/Miocene boundary.

All the classical upper Miocene nannofossil events were observed in the sequence at Site 925. The extinctions of *Discoaster quinqueramus* and *Amaurolithus amplificus* are clearly separated. The total range of *A. amplificus* was surprisingly long. The FO of *A. amplificus* appears only to be separated from that of *A. primus* by about 0.2 m.y. at Site 925, rather than the previous estimate of 0.8 m.y.). Assuming that these unusually deep occurrences are indigenous, this would indicate that the age estimated for this event in the equatorial Pacific and Indian oceans cannot be applied in the Ceara Rise region.

The base of the absence interval (paracme) of *R. pseudoumbilicus* was observed at the bottom of Section 154-925D-25H-1 and its upper limit is in Section 154-925D-21H-1. Enhanced carbonate dissolution characterizes some samples within the *R. pseudoumbilicus* paracme interval. Other samples within that interval were characterized by unusually high abundances of *Sphenolithus* spp. and *Reticulofenestra minuta.*

Zone CN8 was not subdivided because *Discoaster loeblichii,* the FO of which defines the base of Subzone CN8b, was observed only in a few samples within the range of *Discoaster berggrenii,* that is, within Subzone CN9a. Data from the equatorial Indian Ocean show a distribution of *D. loeblichii* (Rio et al., 1990) that is identical to the one observed at the Ceara Rise. However, Bukry's subdivision of Zone CN8 using *D. loeblichii* appears to be applicable in the eastern equatorial Pacific (Raffi and Flores, in press).

The LO of *Catinaster calyculus* was observed to fall consistently above the LO level of *Discoaster hamatus,* in accordance with Bukry (1973), but in contrast to results derived from the eastern equatorial Pacific and tropical Indian oceans (Raffi et al., in press). The LO of *Coccolithus miopelagicus* was observed half a core length below the FO of *Catinaster coalitus* (see data for Holes 925B and 925D in Table 2). This observation differs from observations made in the Pacific and Indian oceans (Bukry, 1973; Raffi et al., in press), where the LO of *C. miopelagicus* was observed to fall above the FO of *C. coalitus.*

The interval of relatively common *Discoaster kugleri* in the middle Miocene appears anomalously short in Site 925, which may be related to the possible occurrence of a short, slumped interval (see "Lithostratigraphy" section, this chapter). *Coronocyclus nitescens* was rare in its uppermost range, making it difficult to pinpoint a precise extinction level. Thin-walled elliptical morphotypes with serrated outlines were observed above the range of typical circular *C. nitescens*. In contrast, the LO of *Cyclicargolithus floridanus* is less difficult to determine, and was observed in Sample 154-925B-33H-3, 70 cm. Large and spiny specimens of *Sphenolithus* spp. were observed in Sample 154-925B-32H-7, 6 cm.

Discoaster deflandrei is a common to abundant member of the lower Miocene and Oligocene assemblages, and often shows considerable calcite overgrowth. Despite the overgrowth, it was possible to determine the rather distinct decline in abundance of *D. deflandrei*, which preceded its final disappearance, and which is considered a biostratigraphically meaningful marker event. The lower Miocene marker *Discoaster druggii* was not observed. The small but distinct species *Ericsonia obruta* last occurred in the lower Miocene Core 154-925A-18R and should be considered as a potential marker for subdividing the long stratigraphic interval between the FO of *Sphenolithus belemnos* and the LO of abundant *S. delphix*. The uppermost abundant occurrence of *Triquetrorhabdulus carinatus* was observed in Sample 154-925A-22R-CC. This sample also contains the LO of *Ericsonia fenestrata*. *Sphenolithus delphix* was observed only in Sample 154-925A-23R-3, 121 cm, about 10 m above the LO of *S. ciperoensis* in Section 154-925A-24R-1.

Oligocene

The lower/middle Oligocene boundary can be approximately recognized by the FO of *S. ciperoensis*. The LO of *Cyclicargolithus abisectus* (≥10 μm) was observed in upper Oligocene Core 154-925A-24R. The total ranges of *S. ciperoensis* and *Sphenolithus distentus* are important for the biostratigraphic subdivision of the Oligocene, as they provide four out of six nannofossil zonal boundary markers. *Sphenolithus distentus* evolved into *S. ciperoensis* in the lower upper Oligocene, where we observed an abundance of intergrading forms. Perhaps the crossover in abundance between the two species represents a less ambiguous marker event than the absolute FO of *S. ciperoensis* and the absolute LO of *S. distentus*, as suggested by Olafsson and Villa (1992).

A relatively large sphenolith species was observed in the lower Oligocene, which shows affinity to *S. distentus*, although it is generally larger and its entire range is below that of *S. distentus*; it appeared in Zone CP16 and disappeared within Zone CP17. This sphenolith has been reported previously from the identical stratigraphic interval in the equatorial Indian Ocean (Okada, 1990) and the western equatorial Pacific Ocean (Kroenke, Berger, Janecek, et al., 1991, p. 398).

The LO of *Reticulofenestra umbilicus* (≥14 μm), defining the top of Zone CP16, was preceded by low abundances in the highest part of its range. In terms of taxonomic ambiguity and relative abundance pattern, the best Oligocene nannofossil markers are considered to be the extinction of *S. ciperoensis* in the upper upper Oligocene, and the extinction of *Coccolithus formosus* in the lower lower Oligocene.

Eocene

The Eocene/Oligocene boundary is approximated by the LO of the last representative of the Paleogene lineage of rosette-shaped discoasters, *Discoaster saipanensis*. The upper/middle Eocene boundary is approximated by the LO of *Chiasmolithus grandis*. Cores 154-925A-54R and -55R contained discontinuous, rare occurrences of *Isthmolithus recurvus*, a species that is rarely reported from warm-water, low-latitude paleoenvironments.

Two distinct nannofossil events subdivide the upper Eocene, namely, the LOs of *Cribrocentrum reticulatum* and *Calcidiscus protoannula*. We noticed that the former species shows generally larger diameters (>10 μm) in the upper part of its range, and that the diameters decreased with depth. Common to abundant, large (about 20–25 μm) specimens of *Coccolithus eopelagicus* also characterize the Eocene assemblages. Sample 154-925A-65R-CC contains few *Sphenolithus intercalaris*. The uppermost occurrence of rare *Chiasmolithus grandis* was observed in Sample 154-925A-62R-CC. *Chiasmolithus grandis* is more abundant downward from Sample 154-925A-66R-CC. The lowermost cores in Hole 925A contain poorly preserved assemblages. The nannofossil assemblages in several of these samples show strong dominance in abundance of the holococcolith *Zygrhablithus bijugatus*.

The FO of the *Dictyococcites bisectus–Dictyococcites hesslandii* lineage was observed in Sample 154-925A-66R-CC. Core 154-925A-68R consists only of two small pieces of rock; these probably originated from different levels in the overlying middle Eocene strata according to their slight differences in nannofossil preservation and composition.

Sample 154-925A-69R-CC, the deepest sample recovered at Site 925, includes *Chiasmolithus grandis, Chiasmolithus solitus, Coccolithus formosus, Cyclicargolithus floridanus, Sphenolithus radians,* and *Zygrhablithus bijugatus*. This assemblage also contains reticulofenestrids that are up to 14 μm long, and thus belong to the *Reticulofenestra dictyoda–Reticulofenestra samodurovii–Reticulofenestra umbilicus* lineage. The fact that samples from overlying cores, notably Core 154-925A-67R, contain typical *R. umbilicus* (>14 μm), and the fact that the morphotypes in Sample 154-925A-69R-CC were up to, but did not exceed, 14 μm in length, suggest that the latter sample is close to the appearance of forms >14 μm, according to data presented by Backman and Hermelin (1986). Core 154-925A-68R contains >14-μm forms, but the stratigraphic placement of these samples is uncertain. The absence of *D. bisectus* and the presence of *C. floridanus* in Sample 154-925A-69R-CC support the interpretation that Hole 925A ended close to the Zone CP13/CP14 boundary in the middle part of the middle Eocene.

Planktonic Foraminifers

Planktonic foraminifers were studied most intensively in the middle Miocene to middle Eocene of Hole 925A and the Pleistocene to middle Miocene of Hole 925B. The middle Miocene interval was also studied in Hole 925C. In total, more than 300 samples from Site 925 were studied on board the ship. We aimed to constrain most datums to within 1.5 m (one section) by analyzing up to six samples per core, although fewer samples were studied in the lower, more lithified interval of Hole 925A. Lists of planktonic foraminifer datums from Holes 925A, 925B, and 925C are given in Table 3. Zonal assignments are summarized in Figure 14 for comparison with the nannofossil biozonation. Planktonic foraminifers indicate an almost continuous sequence at Site 925 from middle Eocene Zone P13 to the Holocene.

Preservation of planktonic foraminifers is very good through the late Miocene to the Holocene. Moderate dissolution has affected most samples in the middle Miocene, but biostratigraphic assignments are not affected. In the lower Miocene through most of the Oligocene, preservation is generally good. From the lower Oligocene through middle Eocene, the sediment is more lithified and foraminifer tests are recrystallized and often filled with sparry calcite. However, most of the zonal markers are relatively resistant to dissolution, so a series of datums can be reliably recorded.

Pleistocene

The Pleistocene is one of the most problematic intervals for planktonic foraminifer biostratigraphy at this site. The FO of *Globorotalia truncatulinoides*, which marks the base of Zone N22, is between Samples 154-925B-7H-4, 68–70 cm, and -7H-5, 65–67 cm. There is little stratigraphic overlap between the ranges of *G. truncatulinoides* and its ancestral form, *Globorotalia tosaensis*. The FO of *G. truncatulinoides* is accepted as the base of Zone N22. It is found consistently

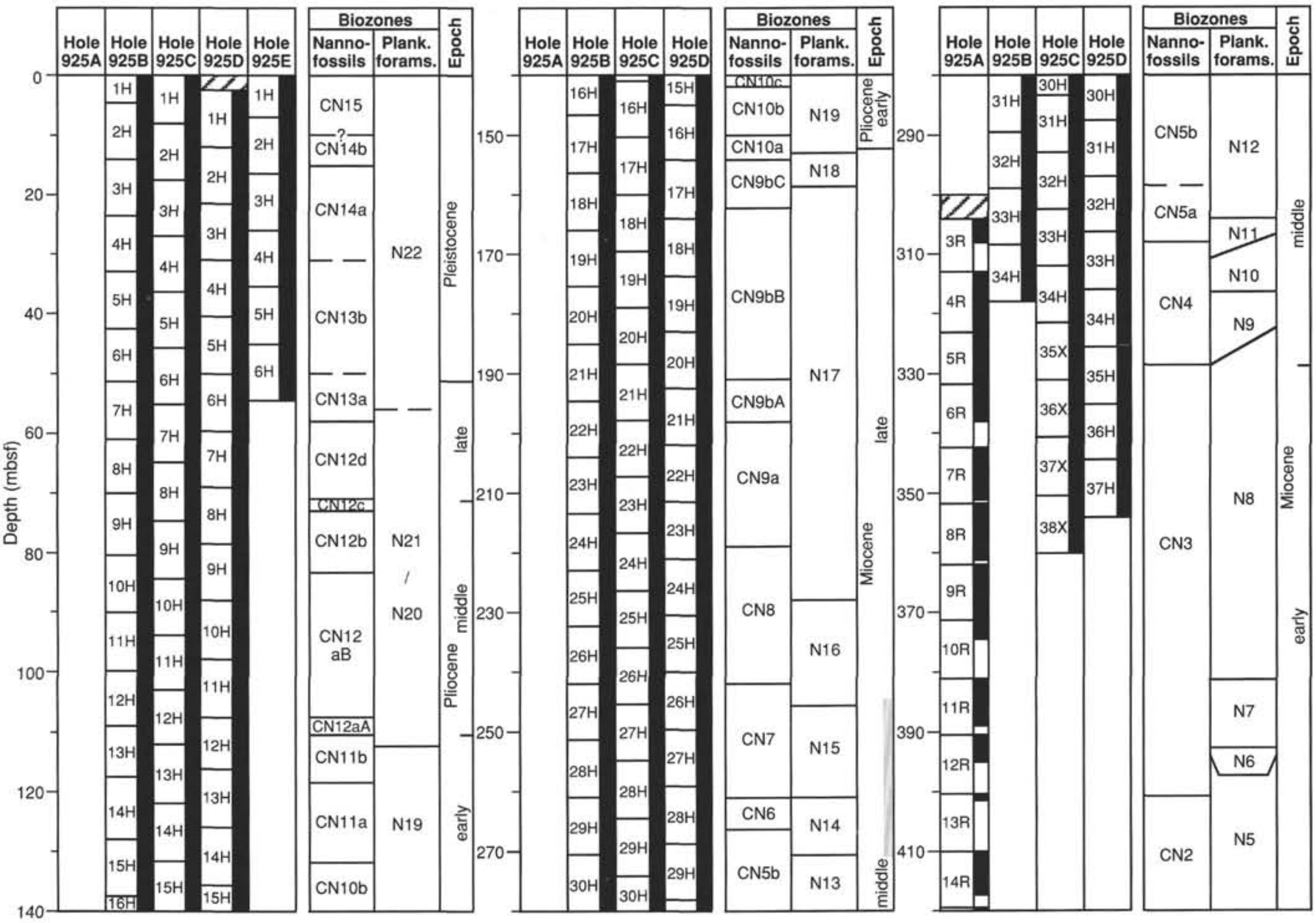

Figure 14. Calcareous nannofossil and planktonic foraminifer biozonations for Site 925. Note that depths are given in meters below seafloor (mbsf). Stippling indicates uncertainty in placement of epoch boundary.

above this, and its lowest occurrence coincides with levels found at other sites in the equatorial current system (e.g., Weaver and Raymo, 1989; Chaisson and Leckie, 1993).

The *Pulleniatina* lineage occurs sporadically above Sample 154-925B-4H-4, 65–67 cm. Below this sample, it occurs more continuously down to Sample 154-925B-8H-5, 65–67 cm. Three *Pulleniatina* morphotypes (*P. praecursor, P. obliquiloculata,* and *P. finalis*) occur together in the interval from Samples 154-925B-6H-2, 55–57 cm, to -7H-6, 68–70 cm, which crosses the Pleistocene/Pliocene boundary. In contrast, in the western equatorial Pacific (Leg 130, Chaisson and Leckie, 1993; Leg 144, Pearson, in press), the *Pulleniatina* morphotypes show good stratigraphic integrity, occurring in overlapping succession. However, in the eastern equatorial Pacific, forms ascribed to the "*praecursor*" morphotype occur up through the Pleistocene, and the "*obliquiloculata*" morphotype occurs sporadically below its generally accepted datum (Leg 138, Chaisson, in press). Bolli and Saunders (1985) also described this extended stratigraphic co-occurrence of morphotypes in the Atlantic. The FO of the *P. finalis* morphotype, between Samples 154-925B-7H-6, 68–70 cm, and -8H-1, 65–67 cm, was found at a greater depth than expected, and directly above an interval in which *Pulleniatina* is absent. This suggests that "*finalis*" is merely an ecophenotype of *P. obliquiloculata* and that its FO is probably controlled by local hydrographic conditions. The LO of *Globigerinoides fistulosus,* which approximates the Pleistocene/Pliocene boundary, is between Samples 154-925B-7H-3, 65–67 cm, and -7H-4, 68–70 cm, and it may be a more reliable datum.

The Pleistocene is characterized by marked faunal variations. *Globorotalia menardii, Globorotalia tumida, G. truncatulinoides, P. obliquiloculata,* and *Neogloboquadrina dutertrei* vary considerably in abundance and each is occasionally absent. These variations may indicate climatic cycles expressed through species sensitive to hydrographic change, but they were not studied at sufficient resolution on board the ship to investigate this possibility.

Pliocene

Zones N20 and N21 could not be differentiated because of the scarcity of the zonal marker, *Globorotalia tosaensis.* However, several other planktonic foraminifer datums were successfully recorded in the Pliocene. Of these, the most reliable are (1) the LO of *Globorotalia pertenuis* (which we regard as an extreme variant of *Globorotalia exilis,* characterized by seven or more chambers in the final whorl) between Samples 154-925B-9H-2, 65–67 cm, and -9H-3, 65–67 cm; (2) the LO of *Dentoglobigerina altispira* between Samples 154-925B-10H-7, 58–60 cm, and -11H-1, 65–67 cm; (3) the FO of *G. pertenuis* between Samples 154-925B-12H-3, 65–67 cm, and -12H-4, 54–56 cm; (4) the FO of *Globorotalia miocenica,* which marks the base of Zone N20, between Samples 154-925B-12H-7, 65–67 cm, and -13H-1, 66–68 cm; and (5) the LO of *Globoturborotalita nepenthes* between Samples 154-925B-14H-7, 10–12 cm, and -15H-1, 65–67 cm. The positions of these events are defined by species that have distinctive morphologies.

Note that three of the above datums were found to occur in or near core breaks. Several samples were taken from Hole 925C to further constrain the highest occurrence of *G. nepenthes* and also to aid in the construction of a composite section for the site. *G. nepenthes* was

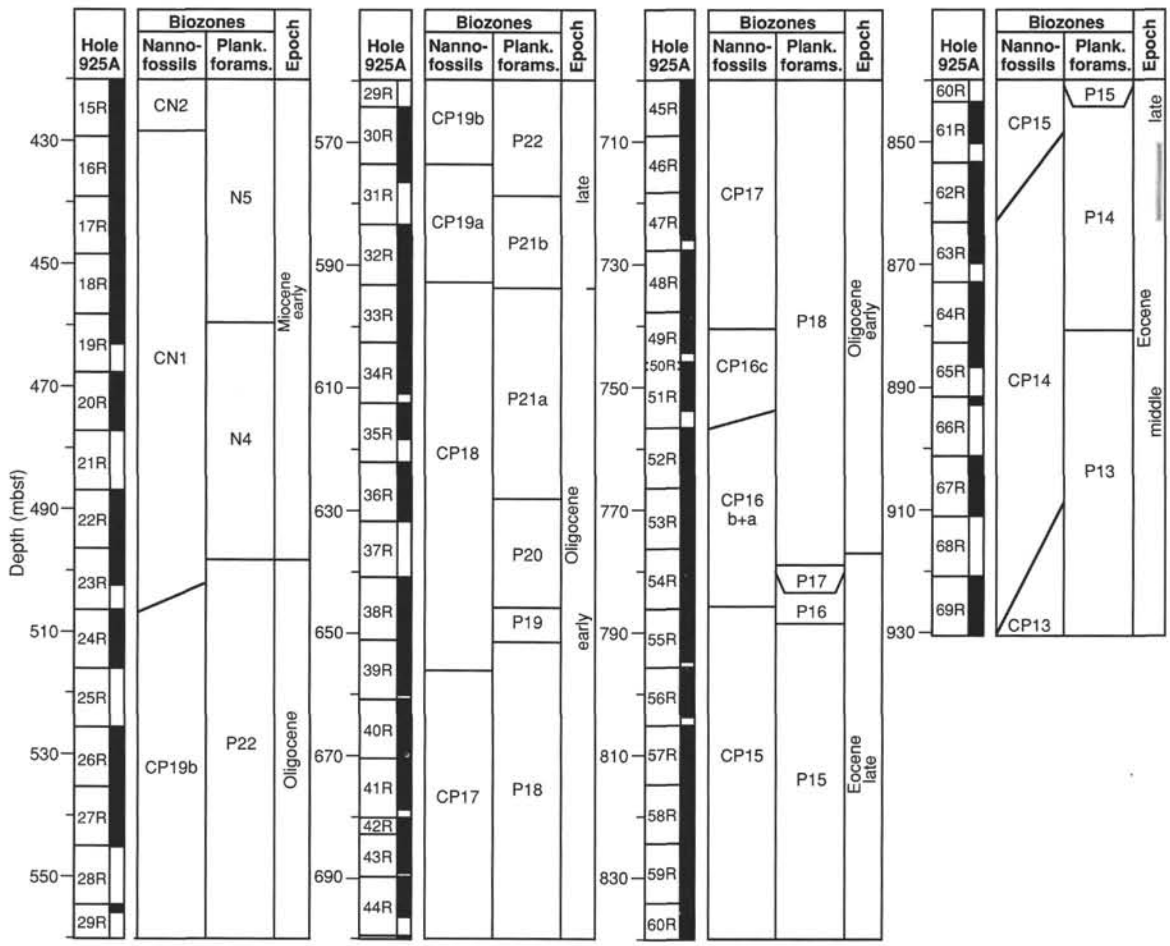

Figure 14 (continued).

found in all samples taken from Cores 154-925C-14H and -15H, the highest being Sample 154-925C-14H-5, 100–102 cm.

An interesting feature of the Pliocene in Hole 925B is the disappearance and subsequent reappearance of *Pulleniatina.* The stratigraphic position of these events is similar to that reported by Saito (1976) and Keigwin (1982) for other Atlantic and Caribbean sites. These records contrast with those from the Pacific Ocean, where *Pulleniatina* is present throughout the Pliocene (e.g., Keigwin, 1982; Chaisson and Leckie, 1993). The early Pliocene sinistral to dextral coiling shift in *Pulleniatina* (Berggren et al., 1985b) is also recorded at an appropriate level in Hole 925B.

Miocene

The FO of *Sphaeroidinella,* the earliest forms of which are distinguished from *Sphaeroidinellopsis* only by their minute dorsal sutural apertures, occurs between Samples 154-925B-17H-4, 65–67 cm, and -17H-5, 65–67 cm, and marks the base of Zone N19. The FO of *Globorotalia tumida,* which marks the base of Zone N18, is between Samples 154-925B-18H-1, 66–68 cm, and -18H-2, 66–68 cm. Contrary to the range given by Bolli and Saunders (1985), the *G. tumida* plexus does occur in the lower Pliocene. *G. tumida* and *G. plesiotumida* are infrequent but not always rare, and specimens that are morphologically intermediate are observed in Sample 154-925B-18H-1, 66–68 cm. However, as described by Bolli and Saunders (1985), *G. tumida* is absent from the middle Pliocene to the lower Pleistocene.

For most of the upper Miocene below Zone N18, the age constraint provided by planktonic foraminifers is less tight. This is partly because fewer datums are recognized and partly because the datums that were found are less reliable. For example, the FOs of *Globorotalia cibaoensis, Globigerinoides extremus,* and *Globorotalia plesiotumida* (the last marking the base of Zone N17) are defined by gradual transition from other forms and are to some extent subjective. The datums for the hirsutellids or scituline forms, such as *Globorotalia cibaoensis* and *G. margaritae,* were difficult to constrain. They are often rare in the >150-µm fraction and the morphological features that distinguish the "species" and "subspecies" within the plexus develop late in the life cycle of the organism. This makes identification of specimens from the fine fraction, presumably juveniles, unreliable for this group. Other forms, such as *Candeina nitida* and *Neogloboquadrina acostaensis* (the zonal marker for Zone N16), are rare and sporadic at the bottom of their ranges.

In Hole 925B, *Paragloborotalia mayeri* displays the full range of variation between the "*mayeri*" and "*siakensis*" forms, but is distinct from other co-occurring species. The LO of this species, which is used to recognize the base of Zone N15, is a well-constrained datum. It occurs between Samples 154-925B-28H-7, 65–67 cm, and -29H-1, 65–67 cm, probably in the core break. The FO of *Globoturborotalita nepenthes,* which marks the base of Zone N14, is probably also in a core break, between Cores 154-925B-29H and -30H. In some samples, specimens were found only in the <150-µm fraction, but the distinctive final chamber and apertural lip, coupled with high trochospire of this species, makes even small tests readily identifiable.

The *Fohsella* lineage provides a series of useful datums in the middle Miocene. The full complement of morphotypes, including *Fohsella lobata* and *Fohsella robusta,* are recognized in Hole 925B. The LO of *Fohsella,* which marks the base of Zone N13, is between

Table 3. Planktonic foraminifer datums recognized at Site 925.

Event	Age (Ma)	Sample range	Depth (mbsf)	Mean depth (mbsf)	Composite depth (m)	Mean composite depth (m)
Hole 925A:						
B *Fohsella "praefohsi"*	14.0	3R-2, 75–77 cm, to 3R-3, 80–83 cm	305.96–307.51	306.74	350.08–351.63	350.87
T *Fohsella peripheroronda*	14.6	3R-3, 80–83 cm, to 4R-1, 75–77 cm	307.51–314.46	310.99	351.63–354.23	352.93
B *Fohsella peripheroacuta*	14.7	4R-2, 75–77 cm, to 4R-3, 77–79 cm	315.96–317.48	316.72	355.73–357.25	356.50
T *Praeorbulina glomerosa* s.l.	14.8	4R-6, 75–77 cm, to 4R-7, 72–74 cm	321.96–323.43	322.70	361.73–363.20	362.48
T *Praeorbulina sicana*	14.8	4R-6, 75–77 cm, to 4R-7, 72–74 cm	321.96–323.43	322.70	361.73–363.20	362.48
B *Orbulina suturalis*	15.1	4R-7, 72–74 cm, to 5R-1, 75–77 cm	323.43–324.16	323.80	363.20–363.93	363.58
B *Praeorbulina circularis*	16.0	5R-4, 75–77 cm, to 5R-5, 75–77 cm	328.66–330.16	329.41	368.43–369.93	369.19
B *Praeorbulina glomerosa*	16.1	5R-4, 75–77 cm, to 5R-5, 75–77 cm	328.66–330.16	329.41	368.43–369.93	369.19
B *Praeorbulina sicana*	16.4	10R-CC to 11R-1, 75–77 cm	381.30–382.05	381.68	414.31–421.83	421.46
T *Catapsydrax dissimilis*	17.3	12R-1, 75–77 cm, to 12R-2, 75–77 cm	391.56–393.06	392.31	431.33–432.83	432.09
B *Globigerinatella* sp.	18.7	12R-2, 75–77 cm, to 12R-3, 75–77 cm	393.06–394.56	393.81	432.83–434.33	433.59
T *Globoquadrina binaiensis*	19.1	16R-3, 75–77 cm, to 16R-4, 75–77 cm	433.06–434.56	433.81	472.83–474.33	473.59
T *Paragloborotalia kugleri*	21.6	18R-7, 75–77 cm, to 19R-2, 75–77 cm	458.36–460.46	459.41	498.13–500.24	499.14
B *Globoquadrina binaiensis*	22.1	18R-7, 64–66 cm, to 19R-2, 75–77 cm	458.25–460.46	459.36	498.13–500.24	499.14
T *Globigerina angulisuturalis*	23.3	23R-3, 88–91 cm, to 23R-4, 77–79 cm	500.59–501.98	501.29	540.36–541.75	541.07
B *Paragloborotalia kugleri*	21.6	23R-2, 88–90 cm, to 23R-3, 77–79 cm	499.09–500.48	499.79	538.86–540.36	539.57
B *Globigerinoides primordius* (common)	24.5	24R-2, 20–22 cm, to 24R-3, 20–22 cm	508.01–509.51	508.76	547.78–549.28	548.45
B *Paragloborotalia pseudokugleri*	26.3	27R-5, 75–77 cm, to 27R-6, 75–77 cm	532.36–543.56	537.96	571.03–572.53	577.74
T *Paragloborotalia opima*	27.1	31R-1, 75–77 cm, to 32R-1, 75–77 cm	574.56–584.26	579.41	614.33–624.03	619.19
T *Chiloguembelina cubensis* (common)	28.5	32R-CC to 33R-1, 70–73 cm	593.10–593.82	593.46	632.88–633.60	633.24
B *Globigerina angulisuturalis*	29.7	36R-7, 60–62 cm, to 38R-6, 70–72 cm	631.71–649.61	640.70	671.49–689.39	680.48
T *Turborotalia ampliapertura*	30.3	38R-6, 70–72 cm, to 40R-1, 70–72 cm	649.61–661.51	655.56	689.39–701.29	695.34
T *Pseudohastigerina* spp.	32.5	49R-5, 70–72 cm, to 50R-2, 20–22 cm	744.31–747.81	746.06	784.09–787.59	785.84
T *Hantkenina alabamensis*	33.8	54R-1, 16–17 cm, to 54R-1, 72–74 cm	776.46–777.03	776.75	816.24–816.81	816.53
T *Turborotalia cerroazulensis*	33.9	54R-1, 72–74 cm, to 54R-1, 121–122 cm	777.03–777.42	777.23	816.81–817.20	817.01
T *Cribrohantkenina inflata*	34.0	54R-2, 114–115 cm, to 54R-3, 19–20 cm	777.91–779.49	778.70	817.69–819.27	818.48
T *Globigerinatheka index*	34.2	54R-3, 19–20 cm, to 54R-3, 82–83 cm	779.49–780.12	779.81	819.27–819.90	819.59
B *Turborotalia cunialensis*	35.1	54R-2, 114–115 cm, to 54R-3, 19–20 cm	777.91–779.49	778.70	817.69–819.27	818.48
T *Turborotalia pomeroli*	35.2	54R-4, 62–67 cm, to 54R-5, 72–73 cm	781.45–783.02	782.24	821.23–822.80	822.02
T *Globigerinatheka semiinvoluta*	35.2	54R-5, 72–73 cm, to 54R-6, 16–17 cm	783.02–783.96	783.49	822.02–823.74	823.27
B *Cribrohantkenina inflata*	35.4	55R-1, 32–33 cm, to 55R-2, 27–28 cm	786.32–787.77	787.05	826.10–827.55	826.83
B *Globigerinatheka semiinvoluta*	38.8	60R-3, 53–55 cm, to 60R-CC	837.74–843.80	840.77	877.52–883.58	880.55
T *Orbulinoides beckmanni*	40.2	64R-5, 63–65 cm, to 64R-CC	879.44–882.50	880.97	919.22–922.28	920.75
Hole 925B:						
B *Pulleniatina finalis*	1.4	7H-6, 68–70 cm, to 8H-1, 65–67 cm	60.19–62.16	61.18	63.51–65.25	64.38
B *Globigerinoides fistulosus*	1.7	7H-3, 65–67 cm, to 7H-4, 68–70 cm	55.66–57.19	56.43	58.98–60.51	59.74
T *Globigerina apertura*	1.9	6H-5, 55–57 cm, to 6H-6, 55–57 cm	49.06–50.56	49.81	51.70–53.20	52.45
T *Globigerinoides extremus*	1.9	7H-5, 68–70 cm, to 7H-6, 68–70 cm	58.69–60.19	59.44	62.01–63.51	62.76
B *Globorotalia truncatulinoides*	2.0	7H-4, 68–70 cm, to 7H-5, 65–67 cm	57.19–58.66	57.93	60.51–61.98	61.24
T *Globorotalia exilis*	2.2	8H-5, 65–67 cm, to 8H-6, 65–67 cm	68.16–69.66	68.91	71.25–72.75	72.00
T *Globorotalia miocenica*	2.3	8H-7, 53–55 cm, to 9H-1, 65–67 cm	71.04–71.66	71.35	74.13–75.97	75.05
Reappearance *Pulleniatina*	2.3	8H-6, 65–67 cm, to 8H-7, 53–55 cm	69.66–71.04	70.35	72.75–74.13	73.44
T *Globigerina woodi*	2.3	8H-6, 65–67 cm, to 8H-7, 53–55 cm	69.66–71.04	70.35	72.75–74.13	73.44
T *Globigerina decoraperta*	2.6	10H-1, 65–67 cm, to 10H-2, 65–67 cm	81.16–82.66	81.91	85.93–87.43	86.68
T *Globorotalia pertenuis*	2.6	9H-2, 65–67 cm, to 9H-3, 65–67 cm	73.16–74.66	73.91	77.47–78.97	78.22
T *Dentoglobigerina altispira*	3.0	10H-7, 58–60 cm, to 11H-1, 65–67 cm	90.09–90.66	90.38	94.86–98.91	96.88
T *Globorotalia multicamerata*	3.0	10H-6, 65–67 cm, to 10H-7, 58–60 cm	88.66–90.09	89.38	93.43–94.86	94.14
T *Sphaeroidinellopsis seminulina*	3.1	10H-7, 58–60 cm, to 11H-1, 65–67 cm	90.09–90.66	90.38	94.86–98.91	96.88
Disappearance *Pulleniatina*	3.5	12H-1, 54–56 cm, to 12H-2, 69–71 cm	100.05–101.7	100.88	109.18–110.83	110.00
B *Globorotalia pertenuis*	3.5	12H-3, 65–67 cm, to 12H-4, 54–56 cm	103.16–104.55	103.86	112.29–113.68	112.98
B *Globorotalia miocenica*	3.6	12H-7, 65–67 cm, to 13H-1, 66–68 cm	109.16–109.66	109.41	118.29–120.72	119.50
T *Globorotalia margaritae*	3.6	13H-2, 66–68 cm, to 13H-3, 60–62 cm	111.17–112.61	111.89	122.22–123.66	122.94
Pulleniatina, sinistral to dextral	4.0	13H-7, 51–53 cm, to 14H-1, 65–67 cm	118.52–119.16	118.84	129.57–130.48	130.02
T *Globoturborotalita nepenthes*	4.3	14H-7, 10–12 cm, to 15H-1, 10–12 cm	127.61–128.11	127.86	138.93–140.40	139.66
T *Globorotalia plesiotumida*	4.4	12H-7, 51–53 cm, to 13H-1, 66–68 cm	109.02–109.67	109.35	118.15–120.72	119.43
B *Globorotalia crassaformis* s.l.	4.7	13H-2, 66–68 cm, to 13H-3, 60–62 cm	111.17–112.61	111.89	122.22–123.66	122.94
T *Globorotalia cibaoensis*	5.0	16H-4, 65–67 cm, to 16H-5, 65–67 cm	142.66–144.16	143.41	156.46–157.96	157.21
T *Neogloboquadrina acostaensis*	5.1	15H-3, 65–67 cm, to 15H-4, 65–67 cm	131.66–133.16	132.41	143.95–145.45	144.70
T *Globoquadrina baroemoenensis*	5.4	16H-4, 65–67 cm, to 16H-5, 65–67 cm	142.66–144.16	143.41	156.46–157.96	157.21
B *Sphaeroidinella dehiscens*	5.6	17H-4, 65–67 cm, to 17H-5, 65–67 cm	152.16–153.66	152.91	166.56–168.06	167.31
B *Globorotalia tumida*	5.9	18H-1, 66–68 cm, to 18H-2, 66–68 cm	157.17–158.67	157.92	173.02–174.52	173.77
B *Globorotalia margaritae*	5.7	18H-5, 66–68 cm, to 18H-6, 66–68 cm	163.17–164.67	163.92	179.02–180.52	179.77
B *Globorotalia cibaoensis*	7.7	21H-4, 65–67 cm, to 21H-5, 65–67 cm	190.16–191.66	190.91	210.43–211.93	211.18
B *Candeina nitida*	8.0	24H-7, 65–67 cm, to 25H-2, 65–67 cm	223.16–225.16	224.16	249.76–254.10	251.93
B *Globigerinoides extremus*	8.0	25H-3, 65–67 cm, to 25H-4, 62–64 cm	226.66–228.13	227.40	255.60–257.07	256.34
B *Globorotalia plesiotumida*	8.2	25H-3, 65–67 cm, to 25H-4, 62–64 cm	226.66–228.13	227.40	255.60–257.07	256.34
B *Neogloboquadrina acostaensis*	10.0	27H-2, 65–67 cm, to 27H-3, 65–67 cm	244.16–245.66	244.91	274.30–275.80	275.05
T *Paragloborotalia mayeri*	10.3	28H-7, 65–67 cm, to 29H-1, 65–67 cm	261.16–261.66	261.41	290.94–294.46	292.70
B *Globigerina apertura*	10.8	29H-6, 65–67 cm, to 30H-2, 65–67 cm	269.16–272.66	270.91	301.96–306.93	304.44
B *Globoturborotalita nepenthes*	10.8	29H-7, 65–67 cm, to 30H-1, 65–67 cm	270.66–271.16	270.91	303.46–305.43	304.44
B *Globigerina decoraperta*	11.2	30H-3, 65–67 cm, to 30H-4, 65–67 cm	274.16–275.66	274.91	308.43–309.93	309.18
T *Fohsella fohsi* s.l.	11.8	30H-6, 65–67 cm, to 31H-1, 65–68 cm	278.66–280.66	279.66	312.93–316.51	314.72
B *Globorotalia lenguaensis*	12.3	32H-4, 65–67 cm, to 32H-5, 66–68 cm	294.66–296.17	295.42	332.95–334.46	337.70
B *Fohsella robusta*	12.7	32H-7, 65–67 cm, to 33H-1, 65–67 cm	299.16–299.66	299.41	337.45–339.04	338.24
B *Fohsella fohsi*	13.5	33H-4, 65–67 cm, to 33H-5, 65–67 cm	304.16–305.66	304.91	343.54–345.04	344.29
B *Fohsella "praefohsi"*	14.0	34H-1, 65–67 cm, to 34H-2, 65–67 cm	309.16–310.66	309.91	351.19–352.69	351.94
T *Fohsella peripheroronda*	14.6	34H-2, 65–67 cm, to 34H-4, 65–67 cm	310.66–313.66	312.16	352.69–355.69	354.19
Hole 925C:						
B *Orbulina* spp.	15.1	35X-2, 65–67 cm, to 35X-3, 65–67	323.65–325.15	324.40	364.16–365.66	364.91
B *Praeorbulina circularis*	16.0	36X-2, 65–67 cm, to 36X-3, 65–67	333.25–334.85	334.05	370.71–372.31	371.51
B *Praeorbulina glomerosa*	16.1	36X-2, 65–67 cm, to 36X-3, 65–67	333.25–334.85	334.05	370.71–372.31	371.51

Note: T = top, and B = base.

Samples 154-925B-30H-6, 65–67 cm, and -31H-1, 65–68 cm. Other *Fohsella* datums, including the bases of Zones N11 and N10, occur in close succession and indicate a relatively slow accumulation rate for the interval of Cores 154-925B-30H through -34H. The dissolved nature of samples in this interval also suggests a more condensed section.

The lower middle Miocene was also studied in the lower part of Hole 925C (Cores 154-925C-34H through -38X). The FO of *Orbulina suturalis,* which marks the base of Zone N9, occurs between Samples 154-925C-35X-2, 65–67 cm, and -35X-3, 65–67 cm. The FO of *Praeorbulina sicana,* which marks the base of Zone N8, occurs between Samples 154-925C-38X-7, 30–32 cm, and -39X-2, 65–67 cm.

Hole 925A was cored by RCB from a depth of 304 to 929.9 mbsf. Two isolated cores (Cores 154-925A-1R and -2R) were taken at higher levels in an interval that was later recovered completely by APC coring in Holes 925B, 925C, and 925D. Consequently, planktonic foraminifers from Hole 925A were studied in detail only in Core 154-925A-3R and below.

Sample 154-925A-3R-1, 76–78 cm, contains *Fohsella peripheroacuta* and *Fohsella "praefohsi"* but no *Fohsella fohsi* and, therefore, is assigned to Zone N11. The FO of *F. "praefohsi,"* which marks the base of Zone N11, occurs between Samples 154-925A-3R-2, 75–77 cm, and -3R-3, 80–83 cm. This level is a little higher than that recorded in Hole 925B. The inconsistency can be explained by the fact that the transition between *F. "praefohsi"* and *F. fohsi* is gradual, and preservation is not sufficient to observe reliably the imperforate band on the earlier chambers in the final whorl that is diagnostic of *F. fohsi.* The FO of *F. peripheroacuta,* which marks the base of Zone N10, is between Samples 154-925A-4R-2, 75–77 cm, and -4R-3, 77–79 cm.

The base of Zone N9, recognized by the FO of *Orbulina,* is between Samples 154-925A-4R-7, 72–74 cm, and -5R-1, 75–77 cm. The base of Zone N8, recognized by the FO of *Praeorbulina sicana,* is between Samples 154-925A-10R-CC and -11R-1, 75–77 cm. The FOs of praeorbuline forms intermediate between *P. sicana* and *Orbulina* are found in succession through Zone N8 (Samples 154-925A-5R-1, 75–77 cm, to -10R-CC and Samples 154-925C-35X-5, 65–67 cm, to -38X-7, 30–32 cm). This suggests fairly high sedimentation rates in the lower Miocene at this site.

The base of Zone N7 is recognized by the LO of *Catapsydrax dissimilis* between Samples 154-925A-12R-1, 75–77 cm, and -12R-2, 75–77 cm. *Catapsydrax dissimilis* and *Globigerinatella insueta* s. str. co-occur in only one sample (Sample 154-925A-12R-2, 75–77 cm), which alone is assigned to Zone N6. The short duration of Zone N6, in comparison with standard time scales, is almost certainly because of the criteria we use to recognize *G. insueta* s. str. (see Pearson, in press), not the result of a condensed section. In our definition, *G. insueta* s. str. requires areal apertures or bullae on the final "chamber." Forms lacking areal apertures or bullae, which were recorded as "Globigerinatella" sp., occur consistently down to Sample 154-925A-15R-4, 74–77 cm, at a level we assign to Zone N5.

The LO of *Paragloborotalia kugleri* marks the base of Zone N5 between Samples 154-925A-18R-5, 75–77 cm, and -18R-6, 75–77 cm. Immediately before its LO, *P. kugleri* was found only in the <150-μm fraction. The FO of *P. kugleri* marks the base of Zone N4 and approximates the position of the Oligocene/Miocene boundary. This datum occurs between Samples 154-925A-23R-2, 88–90 cm, and -23R-3, 88–91 cm.

Oligocene

The base of Zone P22 is marked by the LO of *Paragloborotalia opima,* which is differentiated from *Paragloborotalia nana* by size alone. We follow Bolli and Saunders (1985) and consider specimens >0.39 mm to be *P. opima.* The last such specimens occur between Samples 154-925A-31R-1, 75–77 cm, and -32R-1, 75–77 cm.

The LO of *Chiloguembelina cubensis,* by which we recognize the base of Subzone P21b, is between Samples 154-925A-32R-CC and -33R-1, 70–73 cm. *C. cubensis* co-occurs with *"Globigerina" angulisuturalis* to a level between Samples 154-925A-36R-7, 60–62 cm, and -38R-6, 70–72 cm, which represents the base of Zone P21a. The base of Zone P20 is marked by the LO of *Turborotalia ampliapertura* between Samples 154-925A-38R-6, 70–72 cm, and -40R-1, 70–72 cm. The base of Zone P19 is recognized by the LO of *Pseudohastigerina* between Samples 154-925A-49R-5, 70–72 cm, and -50R-1, 70–72 cm. The last members of *Pseudohastigerina* present are small evolute individuals assigned to *Pseudohastigerina naguewichiensis.*

Eocene

A series of planktonic foraminifer datums occurs near the Eocene/Oligocene boundary. Core 154-925A-54R was sampled at relatively high resolution (three samples per section) to investigate these faunal changes. The Eocene/Oligocene boundary is placed at the LO of *Hantkenina alabamensis,* which is between Samples 154-925A-54R-1, 16–17 cm, and -54R-1, 72–74 cm. Note, however, that *H. alabamensis* is scarce at its LO, only two poorly preserved individuals having been found. In Section 154-925A-54R-2 and below, *H. alabamensis* is very frequent.

The LO of *Hantkenina* occurs slightly above the LO of the *Turborotalia cerroazulensis* group, which is between Samples 154-925A-54R-1, 121–122 cm, and -54R-2, 72–73 cm. We use the LO of *T. cerroazulensis* to recognize the base of Zone P18, following Berggren and Miller (1988). The base of Zone P17 is marked by the LO of *Cribrohantkenina inflata,* which is between Samples 154-925A-54R-2, 114–115 cm, and -54R-3, 19–20 cm. Other datums that we recognized in Core 154-925A-54R are the LOs of *Globigerinatheka index* and *Globigerinatheka semiinvoluta,* and the FO of *Turborotalia cunialensis.* These forms are rare, however, in this material.

The base of Zone P16 is marked by the FO of *Cribrohantkenina* between Samples 154-925A-55R-1, 32–33 cm, and -55R-2, 27–28 cm. The base of Zone P15 is marked by the FO of *Globigerinatheka semiinvoluta,* which occurs sporadically down to a level between Samples 154-925A-59R-CC and -60R-3, 53–55 cm.

The short-ranging and distinctive species *Orbulinoides beckmanni* is a useful index fossil in the lower part of Hole 925A, where the sediments are more lithified and samples are generally poorly preserved. The LO of *O. beckmanni,* which marks the base of Zone P14, is between Samples 154-925A-64R-5, 63–65 cm, and -64R-CC. *O. beckmanni* was found down to the lowest sample examined (Sample 154-925A-68R-CC) and therefore was assigned to Zone P13. It is possible that this sample, a small rock fragment, was derived from a slightly higher level in the sequence. With the present information, the FO level of *O. beckmanni* cannot be constrained at the site. The thick sequence assigned to Zone P13, which is a short zone that lasted only 0.4 m.y., may be partly explained by the presence of slumps and turbidites in the lowest cores of Hole 925A (see "Lithostratigraphy" section, this chapter).

Benthic Foraminifers

Studies of benthic foraminifers were conducted mainly on core-catcher samples. In addition, certain samples from within cores were examined as a preliminary investigation of the relationship between assemblage changes and climatic cycles. Benthic foraminifers are well preserved but rare or few in abundance in the Pleistocene through middle Miocene. In the lower Miocene, preservation is poor and benthic foraminifers are very rare. A major faunal break is recognized within the early Oligocene. Many agglutinated foraminifer species occur in the lower part of the early Oligocene through the middle Eocene. Eocene and early Oligocene calcareous benthic foraminifers, which are few to common and moderately preserved, include several species that are restricted to the Paleogene. Details of these faunal characteristics follow.

In Cores 154-925B-1H through -11H, the benthic foraminifer fauna is characterized by marked abundance fluctuations of *Uviger-*

ina peregrina, Epistominella exigua, and *Nuttallides umbonifera.* For example, in Sample 154-925B-2H-3, 65–67 cm, more than 30% of benthic foraminifers belong to *N. umbonifera,* whereas in Samples 154-925B-3H-3, 65–67 cm, -4H-2, 65–67 cm, and -4H-CC more than 40% of benthic foraminifers are *U. peregrina. E. exigua* is frequent in the core-catcher samples of Cores 154-925B-2H, -3H, and -5H. A high abundance of *N. umbonifera* is considered to be indicative of Antarctic Bottom Water. *U. peregrina* and *E. exigua* are representative of glacial deep and glacial bottom waters, respectively. *E. exigua* is also abundantly distributed in the deeper part of NADW and the lower Circumpolar Deep Water. Another faunal association observed is similar to the Holocene NADW assemblage, and includes such forms as *Pyrgo murrhina, Globocassidulina subglobosa, Cibicidoides bradyi, Gyroidinoides soldanii, Oridorsalis umbonatus, Pullenia bulloides, Pullenia quinqueloba, Pullenia osloensis, Ioanella tumidulus, Ioanella pusillus,* and *Siphotextularia catenata.* The abundance fluctuations of these various species and assemblages observed at Site 925 suggest significant changes in deep-water circulation, which probably correspond to glacial-interglacial cycles.

In Samples 154-925B-12H-CC through -33H-CC, the main benthic foraminifer faunal components are similar to those observed at higher levels, except that *U. peregrina* and *E. exigua* are very rare or absent. Other spinose uvigerinids do occur, such as *Uvigerina hispida, U. hispidocostata,* and *U. proboscidea.* No major abundance fluctuations occur below Core 154-925B-12H-CC, which apparently points to a more stable environment. Minor abundance changes of *Globocassidulina subglobosa, Oridorsalis umbonatus,* and some cibicidoids were observed, however.

In Sample 154-925B-34H-CC and Samples 154-925A-2R-CC through -16R-CC, rare and poorly preserved benthic foraminifers occur. The fauna contains small numbers of several species, primarily *Globocassidulina subglobosa, Cibicidoids mundulus,* and *Oridorsalis umbonatus.*

In Samples 154-925A-17R-CC through -44R-CC, the most common species are *Globocassidulina subglobosa, Oridorsalis umbonatus,* and several species of cibicidoids and gyroidinoids. Another association includes *Stilostomella* spp., *Planulina renzi, Anomalinoides globolosus, Laticarinina pauperata,* and *Pullenia* spp. Various forms increase in abundance in the upper middle Oligocene (Sample 154-925A-35R-CC), including *Melonis barleeanus, Pullenia bulloides, Globocassidulina subglobosa, Oridorsalis umbonatus,* and several gyroidinoids. These replace an agglutinated dominated fauna that occurs down through the Eocene.

Samples 154-925A-47R-CC through -68R-CC include many agglutinated species, such as *Spiroplectammina spectabilis, Repmanina charoides, Thalmannammina conglobata,* and several species of *Bathysiphon, Ammodiscus, Gaudryina, Cyclammina, Karreriella,* and *Ammovertellina.* This agglutinated assemblage has been termed a "flysch-type" assemblage and indicates relatively low oxygen conditions (Gradstein and Berggren, 1981). The "flysch-type" fauna has previously been reported mainly from areas close to mobile belts, such as the Alps and the circum-Pacific, or from rapidly deposited sequences, such as the Late Cretaceous to early Oligocene of the North Sea. The calcareous benthic foraminifers in the assemblage are few to common and moderately preserved. Common species include *Nuttallides truempyi, Cibicidoides grimsdalei, Cibicidoides truncanus, Cibicidoides eocaenus,* and *Hanzawaia ammophila.* Note that in Sample 154-925A-65R-CC, calcareous foraminifers are very rare and poorly preserved.

Nuttallides truempyi and *Cibicidoides grimsdalei* are restricted to the Eocene (Samples 154-925A-56R-CC through -68R-CC). *Cibicidoides truncanus,* which has a previously reported stratigraphic range only from planktonic foraminifer Zones P13 to P16 (van Morkhoven et al., 1986), continues to occur until the earliest Oligocene at this site (Sample 154-925A-52R-CC). *Cibicidoides eocaenus, Hanzawaia ammophila,* and many agglutinated species persist throughout the Eocene to the early Oligocene (Samples 154-925A-47R-CC through -68R-CC).

Nuttallides truempyi is considered to be indicative of old and corrosive water masses (Tjalsma and Lohmann, 1983). The presence of *N. truempyi* in the middle and late Eocene, in association with many agglutinated foraminifers, indicates the influence of a corrosive and low-oxygenated water mass at Site 925.

PALEOMAGNETISM

Following procedures described in the "Explanatory Notes" chapter (this volume), we conducted paleomagnetic measurements on the archive halves of the APC cores with the cryogenic magnetometer. The natural remanent magnetization (NRM) at Site 925 is characterized by very high intensities and a steeply downward vertical component, which we take to reflect an overprint. Although a significant part of this large overprint was removed after alternating-field (AF) demagnetization at 20 and 30 mT, no characteristic component could be isolated by this treatment. Indeed, as we measured cores from Hole 925B, we quickly noticed that the declinations (which would be the primary parameter used to determine the succession of reversals at low latitudes) pointed systematically toward 0° (core coordinates), with no correction applied to account for the orientation of the cores in the horizontal plane (Fig. 15). Even more intriguing was the observation that the NRM of the working halves showed the same raw results: magnetization was primarily directed downcore and out of the split face, no matter whether an archive half, a working half, or a section intentionally split at an angle was measured. We ceased routine measurement of archive sections to perform detailed equipment checks (for reproducibility of the measurements, low fields within the magnetometer and the AF coils, baseline corrections, etc.). Successive tests confirmed that the equipment was indeed working properly.

In an effort to determine whether any ancient magnetization was detectable, we conducted measurements and stepwise AF demagnetization (up to 50 mT) on single samples from Cores 154-925B-4H, -7H, and -22H. After removal of the steep downward component by AF peak fields on the order of 10 mT, most of the demagnetization trajectories are characterized by a single component directed downward at a moderately shallow angle. No evidence was present for clustered northward declinations in the discrete sample results (Fig. 15); however, no coherent polarity pattern could be obtained for the intervals sampled across the base of the Jaramillo and Olduvai subchronozones in Cores 154-925B-4H and -7H (which we predicted on the basis of the nannofossil biostratigraphy). Although the clustered north declinations of the split sections remain unexplained, it is obvious that the sediment underwent a remagnetization during and/or after coring and thus carries an isothermal remanent magnetization (IRM). It seems also that the original magnetization was either very weak or was mostly remagnetized by the IRM.

To understand further the source of the problems, we attempted to characterize the main magnetic carriers of the remanence. The anhysteretic remanent magnetizations of five samples (imparted in the Schonstedt demagnetizer in a 0.01-mT direct current field and a 100-mT alternating field) showed a regular decrease upon thermal demagnetization up to the Curie temperature of magnetite (580°C) (Fig. 16A). We also performed stepwise acquisitions of IRMs of up to 1.2 tesla (T) using the ASC scientific pulse magnetizer; we followed this with stepwise AF demagnetization of the samples. Figures 16B and 16C show that most of the magnetization is acquired in relatively low fields (<100 mT). A rapid decay of the IRM intensity occurs with alternating-field treatments lower than 30 mT, followed by a more stable decay of a second component that represents between 20% and 40% of the initial intensity (Fig. 16D). Thus, we can tentatively assume that the lowest coercivity component seen in these experiments is carried by the same magnetic grains that carry the two downward components isolated during demagnetization of the NRM. If a primary component was carried by the higher coercivity fraction, it may be too small for detection in the NRM of the samples.

Because the NRM appears dominated by the IRM acquired during coring, it is likely that this parameter is primarily controlled by the concentration of permanently magnetizable material, presumably magnetite. If so, we can expect that both "NRM" (IRM) intensity and low-field susceptibility should display broadly similar downcore patterns. Indeed, short-wavelength variations of both indicators correlate well (Fig. 17). This being the case, "NRM" (IRM) could have some value as a complementary parameter for detailed correlation between holes. The longer wavelength variations are more difficult to interpret, perhaps because the field responsible for the remagnetization does not have fixed characteristics.

COMPOSITE SECTION

A continuous 350-m-thick sedimentary sequence extending from the middle Miocene through the late Pleistocene was recovered in the five holes drilled at Site 925. The continuity of the sedimentary sequence was verified by construction of a composite depth section that demonstrates overlap of cores from adjacent holes throughout most of the upper 300 m. On the composite depth scale (expressed in meters composite depth [mcd]), sedimentary features present in adjacent holes are aligned so that they occur at approximately the same depth. Working sequentially from the top, for each core in each hole a constant was added to the mbsf (meters below seafloor) depth to arrive at an mcd for that core. The depth offsets that comprise the composite depth section are given in Table 4.

Magnetic susceptibility data collected on the multisensor track (MST) and the color reflectance data from Holes 925A through 925E were the two remotely sensed lithologic parameters used to determine depth offsets of the composite depth section. Because of low-amplitude variations in bulk density, GRAPE wet bulk density was not a useful lithologic parameter for composite depth section construction at Site 925. Because measurements were not taken in every hole at Site 925, natural gamma was not useful for hole-to-hole correlation; however, correlations between magnetic susceptibility and natural gamma helped confirm the reliability of the weak magnetic susceptibility record seen in much of the sequence. Although magnetic susceptibility has a low-amplitude signal, oscillations in magnetic susceptibility were correlatable between offset holes throughout most of the section. Magnetic susceptibility measurements were taken at high sensitivity (but at lower sampling resolution; i.e., at 8 or 10 cm), where the amplitude of variations was particularly low (< ten units). Where the magnetic susceptibility signal was higher in amplitude, measurements taken at a lower sensitivity level but at a higher sampling resolution (generally 3 cm).

Color reflectance collected on the split cores (generally 5-cm sampling resolution) was very useful for hole-to-hole correlation, as the reflectance data often provided a higher relative signal-to-noise ratio than the susceptibility. In general, color reflectance was inversely correlated to susceptibility. Although large-scale lithologic features were recorded similarly by both susceptibility and reflectance, small scale (<1 m) features were often different. Correlations between holes based on both susceptibility and reflectance were integrated to arrive at a composite depth section for Site 925. Both of these records on the Site 925 composite depth scale are shown in Figure 18.

In general, the composite depth section demonstrates excellent agreement between the multiple holes at Site 925. Relative stretching and compression of sedimentary features in aligned cores indicate distortion of the cored sequence. The level of disturbance may be related to changes in sea state during coring. Because stretching and squeezing occur on scales of <9 m, it was not possible to align every feature accurately in the susceptibility and reflectance records by simply adding a constant to the mbsf core depth. Within-core depth-scale changes will also be required to align smaller scale sedimentary features. Several intervals at Site 925 were identified as containing slumps: 208–216 mbsf (236–244 mcd), 229 mbsf (259 mcd), and 272 mbsf (307 mcd). Even in these intervals, hole-to-hole correlation was possible through the slumped intervals. From 360 to 389 mcd (approximately 320–350 mbsf), the equivalent depth interval was recovered by rotary coring with an experimental drill bit (see "Operations" section, this chapter) in Hole 925A, by APC and XCB coring in Hole 925C, and by APC coring in Hole 925D. Over this interval, it was also possible to correlate between holes. Comparison of the three coring methods over this interval suggests that, where recovery is good, coring gaps and distortion are smaller in the rotary-cored intervals than in the intervals cored with the APC and XCB.

The depth offsets (Table 4, and CD-ROM, back pocket) required to transform mbsf depth to the mcd depth scale are plotted vs. mbsf depth in Figure 19. From 0 to 50 mbsf, the mcd scale growth relative to the mbsf scale is on the order of 5%. From 50 to about 200 mbsf, mcd scale growth is on the order of 10%. Data gaps between successive cores average 1.0 to 1.1 m. From 200 through 350 mbsf, the growth of the mcd scale is greater than 10%, indicating larger apparent gaps (average 1.3–1.6 m) between successive cores.

Additional verification of the hole-to-hole correlations of the composite depth scale was provided by the biostratigraphic data. When a nannofossil or foraminifer event was identified in more than one hole, the composite depths of the event were compared. At Site

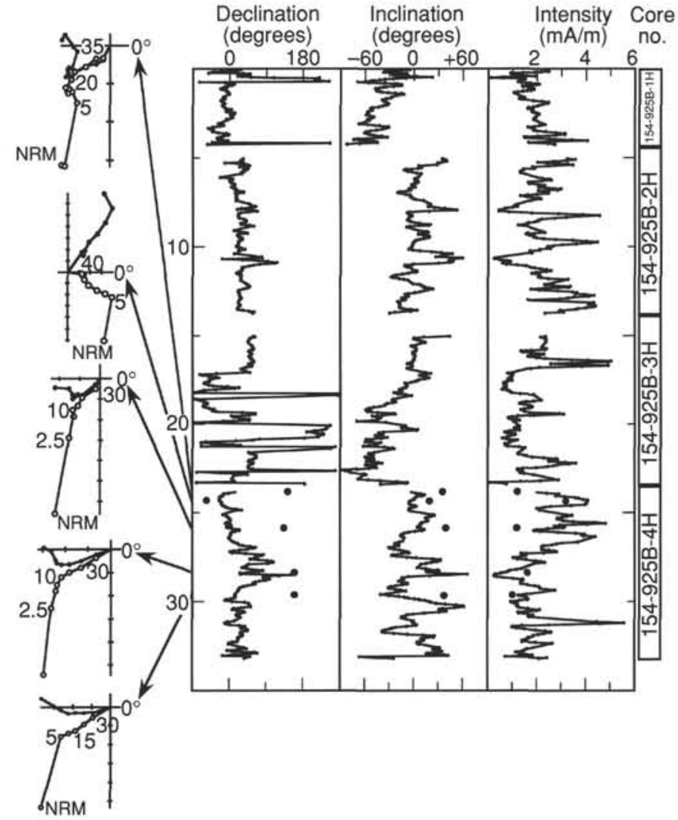

Figure 15. Downcore evolution of paleomagnetic remanence directions (after 20-mT alternating-field treatment) in Cores 154-925B-1H to -4H, along with selected orthogonal demagnetization diagrams for discrete samples taken from Core 154-925B-4H. Open points on the demagnetization diagrams show projection in the vertical plane, whereas closed points show projection in the horizontal plane. Azimuthal orientation (0° to right, 90° down, 180° left, 270° toward top of page) is given with respect to double line on core liner. Demagnetization treatment level (in mT) is shown next to corresponding open point. Tick marks denote intervals of 1 mA/m. Direction of 20-mT step for these discrete samples is marked with closed circles on the declination, inclination, and intensity panels.

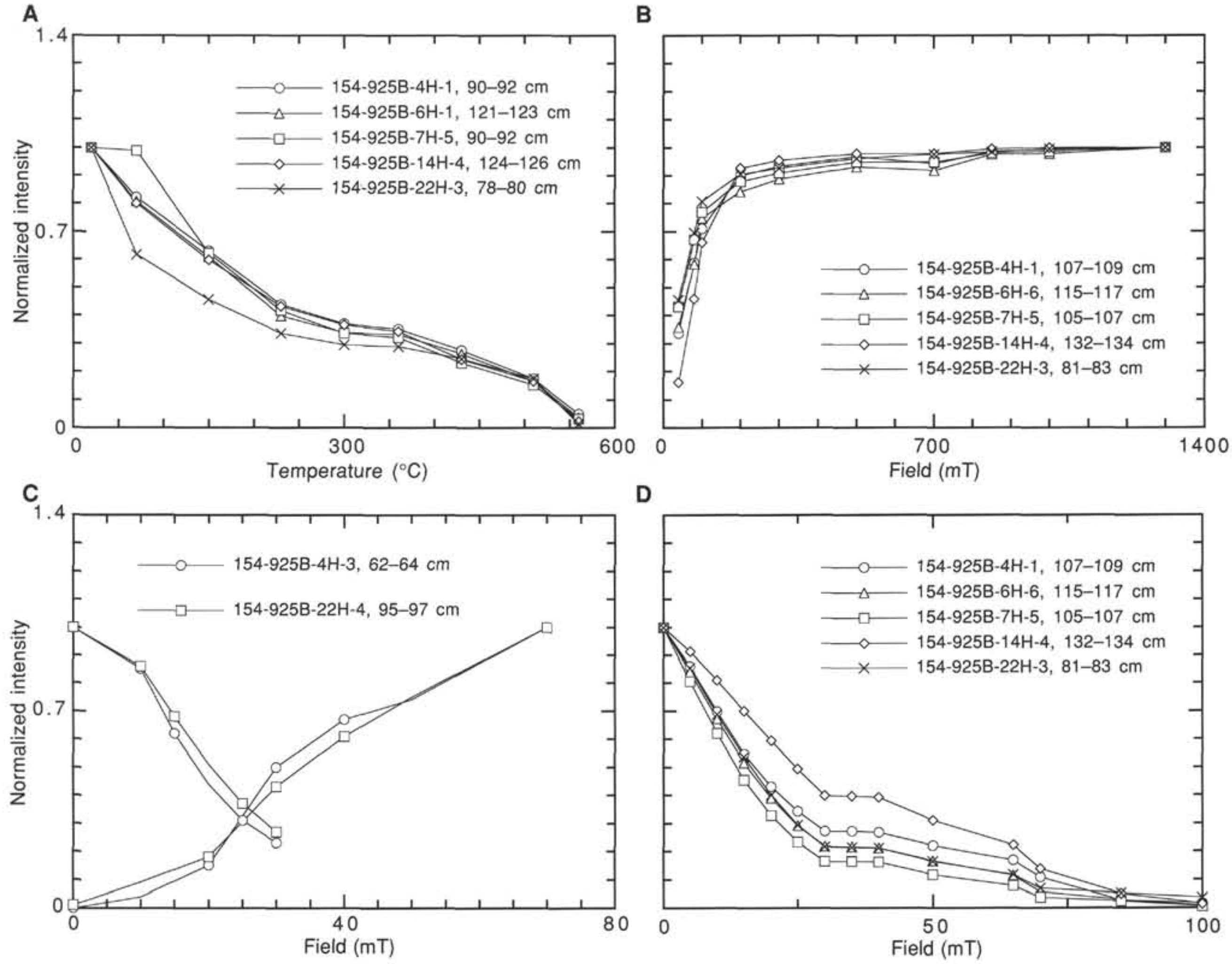

Figure 16. Results of discrete sample measurements from Hole 925B. **A.** Thermal demagnetization of applied ARM. **B.** IRM acquisition curves. **C.** IRM acquisition and AF demagnetization of IRM. **D.** Alternating-field demagnetization of applied IRM.

925, more than 25 nannofossil events and 5 foraminifer events were identified in more than one hole. At least 10 nannofossil events were identified in three holes at Site 925. Figure 20 shows 5 such events. The excellent agreement indicates that, within the limits imposed by core distortion and by the sampling interval of the datums, the validity of the composite section is confirmed by biostratigraphy.

Following construction of the composite depth section for Site 925, a single spliced record was assembled from the aligned cores. The Site 925 splice can be used as a sampling guide to recover a single continuous sedimentary sequence from the top 350 m of Site 925. The Site 925 splice also indicates that a continuous sequence (interrupted by three small slumps) can be sampled over approximately the past 15 m.y. The composite depths were aligned so that tie points between adjacent holes occurred at exactly the same depth in meters composite depth (within the sampling resolution of the magnetic susceptibility). In constructing the splice, we avoided intervals that were reported by the physical properties specialist or sedimentologists to have significant disturbance or distortion. The tie points for the Site 925 splice are given in Table 5, and spliced records of magnetic susceptibility and reflectance are illustrated in Figure 21.

SEDIMENTATION RATES

A sedimentary section just over 930 m thick covering the interval from the Holocene to the middle part of the middle Eocene was recovered at Site 925. Magnetostratigraphy was not obtained at Site 925 because of severe overprint problems, and the sedimentation rate record for Site 925 therefore was based only on the biostratigraphy of calcareous nannofossils and planktonic foraminifers.

Hole 925A was washed and spot-cored to 346.39 mcd, where continuous coring with the RCB began to total depth (TD) at 968.28 mcd. Hole 925B was cored with the APC from the mud line to 360.56 mcd, thus obtaining a short, continuously cored overlap with Hole 925A. Efforts were devoted to providing the highest resolution biostratigraphy in these holes, which represent the entire cored section at Site 925 (Figs. 22 and 23). Depths are given both in mbsf and mcd. The sedimentation rate history presented relies on linear interpolation between selected markers (Tables 6 and 7). The biostratigraphy was valuable for clarifying some ambiguities in the MST- and color reflectance-based correlations among holes (see discussion in "Composite Section" section, this chapter); it follows that the mcd scale is coherent with the biostratigraphic results.

The age control in the Pleistocene–latest Miocene time interval (0–6 Ma) is very accurate, with a large number of bioevents per unit time (>40 over the past 6 m.y.). Most nannofossil events in that interval have been tied directly to astronomically tuned oxygen isotope records, or to either the magnetostratigraphic record or the astronomically tuned Leg 138 MST records that recently were derived from the eastern equatorial Pacific (Raffi et al., 1993; Schneider, in press; Shackleton et al., in press).

Table 4. Composite depth section, Site 925.

Core and section	Section length (cm)	Depth (mbsf)	Offset (m)	Composite depth (mcd)
154-925A-				
1R-1	150	101.8	8.31	110.11
1R-2	150	103.3	8.31	111.61
1R-3	100	104.8	8.31	113.11
1R-4	65	105.8	8.31	114.11
1R-CC	17	106.45	8.31	114.76
2R-1	150	197.9	11.34	209.24
2R-2	150	199.4	11.34	210.74
2R-3	150	200.9	11.34	212.24
2R-4	130	202.4	11.34	213.74
2R-CC	13	203.7	11.34	215.04
3R-1	150	303.7	42.69	346.39
3R-2	150	305.2	42.69	347.89
3R-3	113	306.7	42.69	349.39
3R-CC	16	307.83	42.69	350.52
4R-1	150	313.7	38.34	352.04
4R-2	150	315.2	38.34	353.54
4R-3	150	316.7	38.34	355.04
4R-4	150	318.2	38.34	356.54
4R-5	150	319.7	38.34	358.04
4R-6	150	321.2	38.34	359.54
4R-7	74	322.7	38.34	361.04
4R-CC	16	323.44	38.34	361.78
5R-1	150	323.4	38.34	361.74
5R-2	150	324.9	38.34	363.24
5R-3	150	326.4	38.34	364.74
5R-4	150	327.9	38.34	366.24
5R-5	150	329.4	38.34	367.74
5R-6	150	330.9	38.34	369.24
5R-7	66	332.4	38.34	370.74
5R-CC	22	333.06	38.34	371.4
6R-1	150	333.1	38.34	371.44
6R-2	150	334.6	38.34	372.94
6R-3	130	336.1	38.34	374.44
6R-CC	35	337.4	38.34	375.74
7R-1	150	342.7	38.34	381.04
7R-2	150	344.2	38.34	382.54
7R-3	150	345.7	38.34	384.04
7R-4	150	347.2	38.34	385.54
7R-5	150	348.7	38.34	387.04
7R-6	123	350.2	38.34	388.54
7R-CC	15	351.43	38.34	389.77
8R-1	150	352.4	38.34	390.74
8R-2	150	353.9	38.34	392.24
8R-3	150	355.4	38.34	393.74
8R-4	150	356.9	38.34	395.24
8R-5	150	358.4	38.34	396.74
8R-6	127	359.9	38.34	398.24
8R-CC	15	361.17	38.34	399.51
9R-1	150	362	38.34	400.34
9R-2	150	363.5	38.34	401.84
9R-3	150	365	38.34	403.34
9R-4	150	366.5	38.34	404.84
9R-5	150	368	38.34	406.34
9R-6	150	369.5	38.34	407.84
9R-7	70	371	38.34	409.34
9R-CC	20	371.7	38.34	410.04
10R-1	150	371.7	38.34	410.04
10R-2	133	373.2	38.34	411.54
10R-CC	15	374.53	38.34	412.87
11R-1	150	381.3	38.34	419.64
11R-2	150	382.8	38.34	421.14
11R-3	150	384.3	38.34	422.64
11R-4	150	385.8	38.34	424.14
11R-5	150	387.3	38.34	425.64
11R-6	41	388.8	38.34	427.14
11R-CC	12	389.21	38.34	427.55
12R-1	150	390.8	38.34	429.14
12R-2	150	392.3	38.34	430.64
12R-3	148	393.8	38.34	432.14
12R-CC	3	395.28	38.34	433.62
13R-1	100	400.4	38.34	438.74
13R-2	78	401.4	38.34	439.74
13R-CC	3	402.18	38.34	440.52
14R-1	26	410	38.34	448.34
14R-2	150	410.26	38.34	448.6
14R-3	150	411.76	38.34	450.1
14R-4	150	413.26	38.34	451.6
14R-5	150	414.76	38.34	453.1
14R-6	121	416.26	38.34	454.6
14R-CC	5	417.47	38.34	455.81
15R-1	150	419.7	38.34	458.04
15R-2	150	421.2	38.34	459.54
15R-3	150	422.7	38.34	461.04
15R-4	150	424.2	38.34	462.54
15R-5	150	425.7	38.34	464.04
15R-6	150	427.2	38.34	465.54
15R-7	68	428.7	38.34	467.04
15R-CC	20	429.38	38.34	467.72
16R-1	150	429.3	38.34	467.64
16R-2	150	430.8	38.34	469.14
16R-3	150	432.3	38.34	470.64
16R-4	150	433.8	38.34	472.14
16R-5	150	435.3	38.34	473.64
16R-6	150	436.8	38.34	475.14
16R-7	50	438.3	38.34	476.64
16R-CC	8	438.8	38.34	477.14
17R-1	150	438.9	38.34	477.24
17R-2	150	440.4	38.34	478.74
17R-3	150	441.9	38.34	480.24
17R-4	150	443.4	38.34	481.74
17R-5	150	444.9	38.34	483.24
17R-6	100	446.4	38.34	484.74
17R-7	72	447.4	38.34	485.74
17R-CC	12	448.12	38.34	486.46
18R-1	150	448.6	38.34	486.94
18R-2	150	450.1	38.34	488.44
18R-3	150	451.6	38.34	489.94
18R-4	150	453.1	38.34	491.44
18R-5	150	454.6	38.34	492.94
18R-6	150	456.1	38.34	494.44
18R-7	70	457.6	38.34	495.94
18R-CC	15	458.3	38.34	496.64
19R-1	7	458.2	38.34	496.54
19R-2	150	458.27	38.34	496.61
19R-3	150	459.77	38.34	498.11
19R-4	150	461.27	38.34	499.61
19R-5	24	462.77	38.34	501.11
20R-1	150	467.8	38.34	506.14
20R-2	150	469.3	38.34	507.64
20R-3	150	470.8	38.34	509.14
20R-4	150	472.3	38.34	510.64
20R-5	150	473.8	38.34	512.14
20R-6	150	475.3	38.34	513.64
20R-7	68	476.8	38.34	515.14
20R-CC	19	477.48	38.34	515.82
22R-1	150	487.1	38.34	525.44
22R-2	150	488.6	38.34	526.94
22R-3	150	490.1	38.34	528.44
22R-4	150	491.6	38.34	529.94
22R-5	150	493.1	38.34	531.44
22R-6	150	494.6	38.34	532.94
22R-7	68	496.1	38.34	534.44
22R-CC	18	496.78	38.34	535.12
23R-1	150	496.7	38.34	535.04
23R-2	150	498.2	38.34	536.54
23R-3	150	499.7	38.34	538.04
23R-4	148	501.2	38.34	539.54
23R-CC	17	502.68	38.34	541.02
24R-1	150	506.3	38.34	544.64
24R-2	150	507.8	38.34	546.14
24R-3	150	509.3	38.34	547.64
24R-4	150	510.8	38.34	549.14
24R-5	150	512.3	38.34	550.64
24R-6	150	513.8	38.34	552.14
24R-7	50	515.3	38.34	553.64
26R-1	40	525.6	38.34	563.94
26R-2	150	526	38.34	564.34
26R-3	150	527.5	38.34	565.84
26R-4	150	529	38.34	567.34
26R-5	150	530.5	38.34	568.84
26R-6	150	532	38.34	570.34
26R-7	150	533.5	38.34	571.84
26R-8	24	535	38.34	573.34
26R-CC	38	535.24	38.34	573.58
27R-1	150	535.3	38.34	573.64
27R-2	150	536.8	38.34	575.14
27R-3	150	538.3	38.34	576.64
27R-4	150	539.8	38.34	578.14
27R-5	150	541.3	38.34	579.64
27R-6	150	542.8	38.34	581.14
27R-7	23	544.3	38.34	582.64
27R-CC	11	544.53	38.34	582.87
28R-1	24	544.9	38.34	583.24
29R-1	150	554.6	38.34	592.94
29R-2	38	556.1	38.34	594.44
29R-CC	11	556.48	38.34	594.82
30R-1	150	564.2	38.34	602.54
30R-2	150	565.7	38.34	604.04
30R-3	150	567.2	38.34	605.54
30R-4	150	568.7	38.34	607.04
30R-5	150	570.2	38.34	608.54
30R-6	150	571.7	38.34	610.04
30R-7	75	573.2	38.34	611.54
30R-CC	22	573.95	38.34	612.29
31R-1	150	573.8	38.34	612.14
31R-2	126	575.3	38.34	613.64
31R-CC	16	576.56	38.34	614.9
32R-1	150	583.5	38.34	621.84
32R-2	150	585	38.34	623.34
32R-3	150	586.5	38.34	624.84
32R-4	150	588	38.34	626.34
32R-5	150	589.5	38.34	627.84
32R-6	150	591	38.34	629.34
32R-7	63	592.5	38.34	630.84
32R-CC	20	593.13	38.34	631.47
33R-1	150	593.1	38.34	631.44
33R-2	150	594.6	38.34	632.94
33R-3	150	596.1	38.34	634.44
33R-4	150	597.6	38.34	635.94
33R-5	150	599.1	38.34	637.44
33R-6	150	600.6	38.34	638.94
33R-7	71	602.1	38.34	640.44
33R-CC	22	602.81	38.34	641.15
34R-1	150	602.8	38.34	641.14
34R-2	150	604.3	38.34	642.64
34R-3	150	605.8	38.34	644.14
34R-4	150	607.3	38.34	645.64
34R-5	150	608.8	38.34	647.14
34R-6	73	610.3	38.34	648.64
34R-CC	3	611.03	38.34	649.37
35R-1	150	612.4	38.34	650.74
35R-2	150	613.9	38.34	652.24
35R-3	150	615.4	38.34	653.74
35R-4	100	616.9	38.34	655.24
35R-5	53	617.9	38.34	656.24
35R-CC	10	618.43	38.34	656.77
36R-1	150	622.1	38.34	660.44
36R-2	150	623.6	38.34	661.94
36R-3	150	625.1	38.34	663.44
36R-4	150	626.6	38.34	664.94
36R-5	150	628.1	38.34	666.44
36R-6	150	629.6	38.34	667.94
36R-7	62	631.1	38.34	669.44
36R-CC	27	631.72	38.34	670.06
38R-1	150	641.4	38.34	679.74
38R-2	150	642.9	38.34	681.24
38R-3	150	644.4	38.34	682.74
38R-4	150	645.9	38.34	684.24
38R-5	150	647.4	38.34	685.74
38R-6	150	648.9	38.34	687.24
38R-7	55	650.4	38.34	688.74
38R-CC	33	650.95	38.34	689.29
39R-1	150	651.1	38.34	689.44
39R-2	150	652.6	38.34	690.94
39R-3	150	654.1	38.34	692.44
39R-4	150	655.6	38.34	693.94
39R-5	150	657.1	38.34	695.44
39R-6	100	658.6	38.34	696.94
39R-7	65	659.6	38.34	697.94
39R-CC	5	660.25	38.34	698.59
40R-1	150	660.8	38.34	699.14
40R-2	150	662.3	38.34	700.64
40R-3	150	663.8	38.34	702.14
40R-4	150	665.3	38.34	703.64
40R-5	150	666.8	38.34	705.14
40R-6	150	668.3	38.34	706.64
40R-7	39	669.8	38.34	708.14
40R-CC	20	670.19	38.34	708.53
41R-1	150	670.4	38.34	708.74
41R-2	100	671.9	38.34	710.24
41R-3	73	672.9	38.34	711.24
41R-CC	15	673.63	38.34	711.97
42R-1	150	680.1	38.34	718.44
42R-2	114	681.6	38.34	719.94
42R-CC	2	682.74	38.34	721.08
43R-1	150	683.1	38.34	721.44
43R-2	150	684.6	38.34	722.94
43R-3	150	686.1	38.34	724.44
43R-4	143	687.6	38.34	725.94
43R-CC	12	689.03	38.34	727.37
44R-1	150	689.7	38.34	728.04
44R-2	150	691.2	38.34	729.54
44R-3	150	692.7	38.34	731.04
44R-4	150	694.2	38.34	732.54
44R-5	53	695.7	38.34	734.04
44R-CC	9	696.23	38.34	734.57
45R-1	150	699.3	38.34	737.64
45R-2	150	700.8	38.34	739.14
45R-3	150	702.3	38.34	740.64
45R-4	150	703.8	38.34	742.14
45R-5	150	705.3	38.34	743.64
45R-6	150	706.8	38.34	745.14

Table 4 (continued).

Core and section	Section length (cm)	Depth (mbsf)	Offset (m)	Composite depth (mcd)
45R-7	62	708.3	38.34	746.64
45R-CC	27	708.92	38.34	747.26
46R-1	150	709	38.34	747.34
46R-2	150	710.5	38.34	748.84
46R-3	150	712	38.34	750.34
46R-4	150	713.5	38.34	751.84
46R-5	150	715	38.34	753.34
46R-6	150	716.5	38.34	754.84
46R-7	70	718	38.34	756.34
46R-CC	23	718.7	38.34	757.04
47R-1	150	718.3	38.34	756.64
47R-2	150	719.8	38.34	758.14
47R-3	150	721.3	38.34	759.64
47R-4	150	722.8	38.34	761.14
47R-5	150	724.3	38.34	762.64
47R-6	39	725.8	38.34	764.14
48R-1	150	727.9	38.34	766.24
48R-2	150	729.4	38.34	767.74
48R-3	150	730.9	38.34	769.24
48R-4	150	732.4	38.34	770.74
48R-5	150	733.9	38.34	772.24
48R-6	150	735.4	38.34	773.74
48R-7	66	736.9	38.34	775.24
48R-CC	18	737.56	38.34	775.9
49R-1	150	737.6	38.34	775.94
49R-2	150	739.1	38.34	777.44
49R-3	150	740.6	38.34	778.94
49R-4	150	742.1	38.34	780.44
49R-5	96	743.6	38.34	781.94
49R-CC	14	744.56	38.34	782.9
50R-1	150	746.1	38.34	784.44
50R-2	51	747.6	38.34	785.94
50R-CC	12	748.11	38.34	786.45
51R-1	150	747.1	38.34	785.44
51R-2	150	748.6	38.34	786.94
51R-3	150	750.1	38.34	788.44
51R-4	150	751.6	38.34	789.94
51R-5	55	753.1	38.34	791.44
51R-CC	1	753.65	38.34	791.99
52R-1	150	757	38.34	795.34
52R-2	150	758.5	38.34	796.84
52R-3	150	760	38.34	798.34
52R-4	150	761.5	38.34	799.84
52R-5	150	763	38.34	801.34
52R-6	150	764.5	38.34	802.84
52R-7	65	766	38.34	804.34
52R-CC	21	766.65	38.34	804.99
53R-1	124	766.6	38.34	804.94
53R-2	150	767.84	38.34	806.18
53R-3	150	769.34	38.34	807.68
53R-4	150	770.84	38.34	809.18
53R-5	150	772.34	38.34	810.68
53R-6	150	773.84	38.34	812.18
53R-7	35	775.34	38.34	813.68
54R-1	150	776.3	38.34	814.64
54R-2	150	777.8	38.34	816.14
54R-3	150	779.3	38.34	817.64
54R-4	150	780.8	38.34	819.14
54R-5	150	782.3	38.34	820.64
54R-6	150	783.8	38.34	822.14
54R-7	64	785.3	38.34	823.64
54R-CC	33	785.94	38.34	824.28
55R-1	150	786	38.34	824.34
55R-2	150	787.5	38.34	825.84
55R-3	150	789	38.34	827.34
55R-4	150	790.5	38.34	828.84
55R-5	150	792	38.34	830.34
55R-6	116	793.5	38.34	831.84
55R-CC	8	794.66	38.34	833
56R-1	150	795.6	38.34	833.94
56R-2	150	797.1	38.34	835.44
56R-3	150	798.6	38.34	836.94
56R-4	150	800.1	38.34	838.44
56R-5	150	801.6	38.34	839.94
56R-6	107	803.1	38.34	841.44
56R-CC	12	804.17	38.34	842.51
57R-1	150	805.2	38.34	843.54
57R-2	150	806.7	38.34	845.04
57R-3	150	808.2	38.34	846.54
57R-4	150	809.7	38.34	848.04
57R-5	150	811.2	38.34	849.54
57R-6	150	812.7	38.34	851.04
57R-7	68	814.2	38.34	852.54
57R-CC	24	814.88	38.34	853.22
58R-1	150	814.8	38.34	853.14
58R-2	150	816.3	38.34	854.64
58R-3	150	817.8	38.34	856.14
58R-4	150	819.3	38.34	857.64
58R-5	150	820.8	38.34	859.14
58R-6	150	822.3	38.34	860.64
58R-7	66	823.8	38.34	862.14
58R-CC	24	824.46	38.34	862.8
59R-1	150	824.5	38.34	862.84
59R-2	150	826	38.34	864.34
59R-3	150	827.5	38.34	865.84
59R-4	150	829	38.34	867.34
59R-5	150	830.5	38.34	868.84
59R-6	150	832	38.34	870.34
59R-7	76	833.5	38.34	871.84
59R-CC	3	834.26	38.34	872.6
60R-1	150	834.2	38.34	872.54
60R-2	150	835.7	38.34	874.04
60R-3	150	837.2	38.34	875.54
60R-4	150	838.7	38.34	877.04
60R-5	75	840.2	38.34	878.54
60R-CC	8	840.95	38.34	879.29
61R-1	150	843.8	38.34	882.14
61R-2	150	845.3	38.34	883.64
61R-3	150	846.8	38.34	885.14
61R-4	150	848.3	38.34	886.64
61R-5	100	849.8	38.34	888.14
61R-CC	9	850.8	38.34	889.14
62R-1	150	853.5	38.34	891.84
62R-2	150	855	38.34	893.34
62R-3	150	856.5	38.34	894.84
62R-4	150	858	38.34	896.34
62R-5	150	859.5	38.34	897.84
62R-6	150	861	38.34	899.34
62R-7	72	862.5	38.34	900.84
62R-CC	21	863.22	38.34	901.56
63R-1	150	863.1	38.34	901.44
63R-2	150	864.6	38.34	902.94
63R-3	150	866.1	38.34	904.44
63R-4	150	867.6	38.34	905.94
63R-5	53	869.1	38.34	907.44
63R-CC	13	869.63	38.34	907.97
64R-1	150	872.8	38.34	911.14
64R-2	150	874.3	38.34	912.64
64R-3	150	875.8	38.34	914.14
64R-4	150	877.3	38.34	915.64
64R-5	150	878.8	38.34	917.14
64R-6	150	880.3	38.34	918.64
64R-7	40	881.8	38.34	920.14
64R-CC	3	882.2	38.34	920.54
65R-1	150	882.5	38.34	920.84
65R-2	150	884	38.34	922.34
65R-3	74	885.5	38.34	923.84
65R-CC	3	886.24	38.34	924.58
66R-1	146	891.8	38.34	930.14
67R-1	150	901.4	38.34	939.74
67R-2	150	902.9	38.34	941.24
67R-3	150	904.4	38.34	942.74
67R-4	150	905.9	38.34	944.24
67R-5	150	907.4	38.34	945.74
67R-6	150	908.9	38.34	947.24
67R-7	68	910.4	38.34	948.74
67R-CC	26	911.08	38.34	949.42
68R-CC	2	911.1	38.34	949.44
69R-1	150	920.7	38.34	959.04
69R-2	150	922.2	38.34	960.54
69R-3	150	923.7	38.34	962.04
69R-4	150	925.2	38.34	963.54
69R-5	150	926.7	38.34	965.04
69R-6	149	928.2	38.34	966.54
69R-CC	25	929.69	38.34	968.03
154-925B-				
1H-1	150	0	0	0
1H-2	150	1.5	0	1.5
1H-3	129	3	0	3
1H-CC	20	4.29	0	4.29
2H-1	150	4.5	0.7	5.2
2H-2	150	6	0.7	6.7
2H-3	150	7.5	0.7	8.2
2H-4	150	9	0.7	9.7
2H-5	150	10.5	0.7	11.2
2H-6	100	12	0.7	12.7
2H-7	77	13	0.7	13.7
2H-CC	33	13.77	0.7	14.47
3H-1	150	14	2.91	16.91
3H-2	150	15.5	2.91	18.41
3H-3	150	17	2.91	19.91
3H-4	150	18.5	2.91	21.41
3H-5	150	20	2.91	22.91
3H-6	150	21.5	2.91	24.41
3H-7	42	23	2.91	25.91
3H-CC	9	23.42	2.91	26.33
4H-1	150	23.5	3.5	27
4H-2	150	25	3.5	28.5
4H-3	150	26.5	3.5	30
4H-4	150	28	3.5	31.5
4H-5	150	29.5	3.5	33
4H-6	150	31	3.5	34.5
4H-7	70	32.5	3.5	36
4H-CC	16	33.2	3.5	36.7
5H-1	150	33	3.94	36.94
5H-2	150	34.5	3.94	38.44
5H-3	150	36	3.94	39.94
5H-4	150	37.5	3.94	41.44
5H-5	150	39	3.94	42.94
5H-6	100	40.5	3.94	44.44
5H-7	63	41.5	3.94	45.44
5H-CC	21	42.13	3.94	46.07
6H-1	150	42.5	3.66	46.16
6H-2	150	44	3.66	47.66
6H-3	150	45.5	3.66	49.16
6H-4	150	47	3.66	50.66
6H-5	150	48.5	3.66	52.16
6H-6	150	50	3.66	53.66
6H-7	55	51.5	3.66	55.16
6H-CC	14	52.05	3.66	55.71
7H-1	150	52	4.34	56.34
7H-2	150	53.5	4.34	57.84
7H-3	150	55	4.34	59.34
7H-4	150	56.5	4.34	60.84
7H-5	150	58	4.34	62.34
7H-6	150	59.5	4.34	63.84
7H-7	51	61	4.34	65.34
7H-CC	17	61.51	4.34	65.85
8H-1	150	61.5	4.11	65.61
8H-2	150	63	4.11	67.11
8H-3	150	64.5	4.11	68.61
8H-4	150	66	4.11	70.11
8H-5	150	67.5	4.11	71.61
8H-6	150	69	4.11	73.11
8H-7	58	70.5	4.11	74.61
8H-CC	22	71.08	4.11	75.19
9H-1	150	71	5.33	76.33
9H-2	150	72.5	5.33	77.83
9H-3	150	74	5.33	79.33
9H-4	150	75.5	5.33	80.83
9H-5	150	77	5.33	82.33
9H-6	150	78.5	5.33	83.83
9H-7	49	80	5.33	85.33
9H-CC	20	80.49	5.33	85.82
10H-1	150	80.5	5.79	86.29
10H-2	150	82	5.79	87.79
10H-3	150	83.5	5.79	89.29
10H-4	150	85	5.79	90.79
10H-5	150	86.5	5.79	92.29
10H-6	150	88	5.79	93.79
10H-7	63	89.5	5.79	95.29
10H-CC	19	90.13	5.79	95.92
11H-1	150	90	9.27	99.27
11H-2	150	91.5	9.27	100.77
11H-3	150	93	9.27	102.27
11H-4	150	94.5	9.27	103.77
11H-5	150	96	9.27	105.27
11H-6	150	97.5	9.27	106.77
11H-7	54	99	9.27	108.27
11H-CC	18	99.54	9.27	108.81
12H-1	150	99.5	10.15	109.65
12H-2	150	101	10.15	111.15
12H-3	150	102.5	10.15	112.65
12H-4	150	104	10.15	114.15
12H-5	150	105.5	10.15	115.65
12H-6	150	107	10.15	117.15
12H-7	61	108.5	10.15	118.65
12H-CC	24	109.11	10.15	119.26
13H-1	150	109	12.07	121.07
13H-2	150	110.5	12.07	122.57
13H-3	150	112	12.07	124.07
13H-4	150	113.5	12.07	125.57
13H-5	150	115	12.07	127.07
13H-6	150	116.5	12.07	128.57
13H-7	57	118	12.07	130.07
13H-CC	21	118.57	12.07	130.64
14H-1	150	118.5	12.34	130.84
14H-2	150	120	12.34	132.34
14H-3	150	121.5	12.34	133.84
14H-4	150	123	12.34	135.34
14H-5	150	124.5	12.34	136.84
14H-6	150	126	12.34	138.34
14H-7	43	127.5	12.34	139.84
14H-CC	22	127.93	12.34	140.27
15H-1	150	128	13.31	141.31
15H-2	150	129.5	13.31	142.81
15H-3	150	131	13.31	144.31
15H-4	150	132.5	13.31	145.81
15H-5	150	134	13.31	147.31

Table 4 (continued).

Core and section	Section length (cm)	Depth (mbsf)	Offset (m)	Composite depth (mcd)
15H-6	150	135.5	13.31	148.81
15H-7	26	137	13.31	150.31
15H-CC	16	137.26	13.31	150.57
16H-1	150	137.5	14.82	152.32
16H-2	150	139	14.82	153.82
16H-3	150	140.5	14.82	155.32
16H-4	150	142	14.82	156.82
16H-5	150	143.5	14.82	158.32
16H-6	150	145	14.82	159.82
16H-7	41	146.5	14.82	161.32
16H-CC	20	146.91	14.82	161.73
17H-1	150	147	15.42	162.42
17H-2	150	148.5	15.42	163.92
17H-3	150	150	15.42	165.42
17H-4	150	151.5	15.42	166.92
17H-5	150	153	15.42	168.42
17H-6	150	154.5	15.42	169.92
17H-7	60	156	15.42	171.42
17H-CC	22	156.6	15.42	172.02
18H-1	150	156.5	16.87	173.37
18H-2	150	158	16.87	174.87
18H-3	150	159.5	16.87	176.37
18H-4	150	161	16.87	177.87
18H-5	150	162.5	16.87	179.37
18H-6	150	164	16.87	180.87
18H-7	49	165.5	16.87	182.37
18H-CC	26	165.99	16.87	182.86
19H-1	150	166	17.27	183.27
19H-2	150	167.5	17.27	184.77
19H-3	150	169	17.27	186.27
19H-4	150	170.5	17.27	187.77
19H-5	150	172	17.27	189.27
19H-6	150	173.5	17.27	190.77
19H-7	58	175	17.27	192.27
19H-CC	19	175.58	17.27	192.85
20H-1	150	175.5	18.08	193.58
20H-2	150	177	18.08	195.08
20H-3	150	178.5	18.08	196.58
20H-4	150	180	18.08	198.08
20H-5	150	181.5	18.08	199.58
20H-6	150	183	18.08	201.08
20H-7	56	184.5	18.08	202.58
20H-CC	17	185.06	18.08	203.14
21H-1	150	185	21.29	206.29
21H-2	150	186.5	21.29	207.79
21H-3	150	188	21.29	209.29
21H-4	150	189.5	21.29	210.79
21H-5	150	191	21.29	212.29
21H-6	150	192.5	21.29	213.79
21H-7	76	194	21.29	215.29
21H-CC	17	194.76	21.29	216.05
22H-1	150	194.5	21.71	216.21
22H-2	150	196	21.71	217.71
22H-3	150	197.5	21.71	219.21
22H-4	150	199	21.71	220.71
22H-5	150	200.5	21.71	222.21
22H-6	150	202	21.71	223.71
22H-7	69	203.5	21.71	225.21
22H-CC	42	204.19	21.71	225.9
23H-1	150	204	24.51	228.51
23H-2	150	205.5	24.51	230.01
23H-3	150	207	24.51	231.51
23H-4	150	208.5	24.51	233.01
23H-5	150	210	24.51	234.51
23H-6	150	211.5	24.51	236.01
23H-7	79	213	24.51	237.51
23H-CC	23	213.79	24.51	238.3
24H-1	150	213.5	25.17	238.67
24H-2	150	215	25.17	240.17
24H-3	150	216.5	25.17	241.67
24H-4	150	218	25.17	243.17
24H-5	150	219.5	25.17	244.67
24H-6	150	221	25.17	246.17
24H-7	60	222.5	25.17	247.67
24H-CC	24	223.1	25.17	248.27
25H-1	150	223	27.51	250.51
25H-2	150	224.5	27.51	252.01
25H-3	150	226	27.51	253.51
25H-4	150	227.5	27.51	255.01
25H-5	150	229	27.51	256.51
25H-6	150	230.5	27.51	258.01
25H-7	78	232	27.51	259.51
25H-CC	29	232.78	27.51	260.29
26H-1	150	232.5	27.78	260.28
26H-2	150	234	27.78	261.78
26H-3	150	235.5	27.78	263.28
26H-4	150	237	27.78	264.78
26H-5	150	238.5	27.78	266.28
26H-6	150	240	27.78	267.78
26H-7	80	241.5	27.78	269.28
26H-CC	31	242.3	27.78	270.08
27H-1	150	242	28.71	270.71
27H-2	150	243.5	28.71	272.21
27H-3	150	245	28.71	273.71
27H-4	150	246.5	28.71	275.21
27H-5	150	248	28.71	276.71
27H-6	150	249.5	28.71	278.21
27H-7	72	251	28.71	279.71
27H-CC	30	251.72	28.71	280.43
28H-1	150	251.5	28.35	279.85
28H-2	150	253	28.35	281.35
28H-3	150	254.5	28.35	282.85
28H-4	150	256	28.35	284.35
28H-5	150	257.5	28.35	285.85
28H-6	150	259	28.35	287.35
28H-7	78	260.5	28.35	288.85
28H-CC	31	261.28	28.35	289.63
29H-1	150	261	31.37	292.37
29H-2	150	262.5	31.37	293.87
29H-3	150	264	31.37	295.37
29H-4	150	265.5	31.37	296.87
29H-5	150	267	31.37	298.37
29H-6	150	268.5	31.37	299.87
29H-7	86	270	31.37	301.37
29H-CC	39	270.86	31.37	302.23
30H-1	150	270.5	32.84	303.34
30H-2	150	272	32.84	304.84
30H-3	150	273.5	32.84	306.34
30H-4	150	275	32.84	307.84
30H-5	150	276.5	32.84	309.34
30H-6	150	278	32.84	310.84
30H-7	71	279.5	32.84	312.34
30H-CC	29	280.21	32.84	313.05
31H-1	150	280	34.42	314.42
31H-2	150	281.5	34.42	315.92
31H-3	150	283	34.42	317.42
31H-4	150	284.5	34.42	318.92
31H-5	150	286	34.42	320.42
31H-6	150	287.5	34.42	321.92
31H-7	75	289	34.42	323.42
31H-CC	26	289.75	34.42	324.17
32H-1	150	289.5	36.86	326.36
32H-2	150	291	36.86	327.86
32H-3	150	292.5	36.86	329.36
32H-4	150	294	36.86	330.86
32H-5	150	295.5	36.86	332.36
32H-6	150	297	36.86	333.86
32H-7	69	298.5	36.86	335.36
32H-CC	41	299.19	36.86	336.05
33H-1	150	299	37.95	336.95
33H-2	150	300.5	37.95	338.45
33H-3	150	302	37.95	339.95
33H-4	150	303.5	37.95	341.45
33H-5	150	305	37.95	342.95
33H-6	150	306.5	37.95	344.45
33H-7	67	308	37.95	345.95
33H-CC	23	308.67	37.95	346.62
34H-1	150	308.5	42.04	350.54
34H-2	150	310	42.04	352.04
34H-3	150	311.5	42.04	353.54
34H-4	150	313	42.04	355.04
34H-5	150	314.5	42.04	356.54
34H-6	150	316	42.04	358.04
34H-7	73	317.5	42.04	359.54
34H-CC	29	318.23	42.04	360.27
154-925C-				
1H-1	150	0	0	0
1H-2	150	1.5	0	1.5
1H-3	150	3	0	3
1H-4	150	4.5	0	4.5
1H-5	150	6	0	6
1H-6	41	7.5	0	7.5
1H-CC	22	7.91	0	7.91
2H-1	150	8	0.72	8.72
2H-2	150	9.5	0.72	10.22
2H-3	150	11	0.72	11.72
2H-4	150	12.5	0.72	13.22
2H-5	150	14	0.72	14.72
2H-6	150	15.5	0.72	16.22
2H-7	45	17	0.72	17.72
2H-CC	17	17.45	0.72	18.17
3H-1	150	17.5	0.33	17.83
3H-2	150	19	0.33	19.33
3H-3	150	20.5	0.33	20.83
3H-4	150	22	0.33	22.33
3H-5	150	23.5	0.33	23.83
3H-6	150	25	0.33	25.33
3H-7	55	26.5	0.33	26.83
3H-CC	18	27.05	0.33	27.38
4H-1	150	27	1.49	28.49
4H-2	150	28.5	1.49	29.99
4H-3	150	30	1.49	31.49
4H-4	150	31.5	1.49	32.99
4H-5	150	33	1.49	34.49
4H-6	150	34.5	1.49	35.99
4H-7	59	36	1.49	37.49
4H-CC	17	36.59	1.49	38.08
5H-1	150	36.5	2.09	38.59
5H-2	150	38	2.09	40.09
5H-3	150	39.5	2.09	41.59
5H-4	150	41	2.09	43.09
5H-5	150	42.5	2.09	44.59
5H-6	150	44	2.09	46.09
5H-7	35	45.5	2.09	47.59
5H-CC	15	45.85	2.09	47.94
6H-1	150	46	2.16	48.16
6H-2	150	47.5	2.16	49.66
6H-3	150	49	2.16	51.16
6H-4	150	50.5	2.16	52.66
6H-5	150	52	2.16	54.16
6H-6	150	53.5	2.16	55.66
6H-7	45	55	2.16	57.16
6H-CC	20	55.45	2.16	57.61
7H-1	150	55.5	2.53	58.03
7H-2	150	57	2.53	59.53
7H-3	150	58.5	2.53	61.03
7H-4	150	60	2.53	62.53
7H-5	150	61.5	2.53	64.03
7H-6	150	63	2.53	65.53
7H-7	62	64.5	2.53	67.03
7H-CC	22	65.12	2.53	67.65
8H-1	150	65	4.82	69.82
8H-2	150	66.5	4.82	71.32
8H-3	150	68	4.82	72.82
8H-4	150	69.5	4.82	74.32
8H-5	150	71	4.82	75.82
8H-6	150	72.5	4.82	77.32
8H-7	50	74	4.82	78.82
8H-CC	19	74.5	4.82	79.32
9H-1	150	74.5	5.07	79.57
9H-2	150	76	5.07	81.07
9H-3	150	77.5	5.07	82.57
9H-4	150	79	5.07	84.07
9H-5	150	80.5	5.07	85.57
9H-6	150	82	5.07	87.07
9H-7	44	83.5	5.07	88.57
9H-CC	19	83.94	5.07	89.01
10H-1	150	84	6.16	90.16
10H-2	150	85.5	6.16	91.66
10H-3	150	87	6.16	93.16
10H-4	150	88.5	6.16	94.66
10H-5	150	90	6.16	96.16
10H-6	150	91.5	6.16	97.66
10H-7	44	93	6.16	99.16
10H-CC	11	93.44	6.16	99.6
11H-1	150	93.5	10.84	104.34
11H-2	150	95	10.84	105.84
11H-3	150	96.5	10.84	107.34
11H-4	150	98	10.84	108.84
11H-5	150	99.5	10.84	110.34
11H-6	100	101	10.84	111.84
11H-7	58	102	10.84	112.84
11H-CC	17	102.58	10.84	113.42
12H-1	150	103	11.25	114.25
12H-2	150	104.5	11.25	115.75
12H-3	150	106	11.25	117.25
12H-4	150	107.5	11.25	118.75
12H-5	150	109	11.25	120.25
12H-6	150	110.5	11.25	121.75
12H-7	26	112	11.25	123.25
12H-CC	30	112.26	11.25	123.51
13H-1	150	112.5	13.56	126.06
13H-2	150	114	13.56	127.56
13H-3	150	115.5	13.56	129.06
13H-4	150	117	13.56	130.56
13H-5	150	118.5	13.56	132.06
13H-6	130	120	13.56	133.56
13H-CC	16	121.3	13.56	134.86
14H-1	150	122	14.19	136.19
14H-2	150	123.5	14.19	137.69
14H-3	150	125	14.19	139.19
14H-4	150	126.5	14.19	140.69
14H-5	150	128	14.19	142.19
14H-6	150	129.5	14.19	143.69
14H-7	65	131	14.19	145.19
14H-CC	21	131.65	14.19	145.84
15H-1	150	131.5	15.05	146.55
15H-2	150	133	15.05	148.05
15H-3	150	134.5	15.05	149.55

Table 4 (continued).

Core and section	Section length (cm)	Depth (mbsf)	Offset (m)	Composite depth (mcd)
15H-4	150	136	15.05	151.05
15H-5	150	137.5	15.05	152.55
15H-6	150	139	15.05	154.05
15H-7	26	140.5	15.05	155.55
15H-CC	19	140.76	15.05	155.81
16H-1	150	141	15.39	156.39
16H-2	150	142.5	15.39	157.89
16H-3	150	144	15.39	159.39
16H-4	150	145.5	15.39	160.89
16H-5	150	147	15.39	162.39
16H-6	150	148.5	15.39	163.89
16H-7	72	150	15.39	165.39
16H-CC	29	150.72	15.39	166.11
17H-1	150	150.5	16.47	166.97
17H-2	150	152	16.47	168.47
17H-3	150	153.5	16.47	169.97
17H-4	150	155	16.47	171.47
17H-5	150	156.5	16.47	172.97
17H-6	150	158	16.47	174.47
17H-7	29	159.5	16.47	175.97
17H-CC	30	159.79	16.47	176.26
18H-1	150	160	17.22	177.22
18H-2	150	161.5	17.22	178.72
18H-3	150	163	17.22	180.22
18H-4	150	164.5	17.22	181.72
18H-5	150	166	17.22	183.22
18H-6	150	167.5	17.22	184.72
18H-7	67	169	17.22	186.22
18H-CC	27	169.67	17.22	186.89
19H-1	150	169.5	19.02	188.52
19H-2	150	171	19.02	190.02
19H-3	150	172.5	19.02	191.52
19H-4	150	174	19.02	193.02
19H-5	150	175.5	19.02	194.52
19H-6	150	177	19.02	196.02
19H-7	56	178.5	19.02	197.52
19H-CC	26	179.06	19.02	198.08
20H-1	150	179	19.54	198.54
20H-2	150	180.5	19.54	200.04
20H-3	150	182	19.54	201.54
20H-4	150	183.5	19.54	203.04
20H-5	150	185	19.54	204.54
20H-6	150	186.5	19.54	206.04
20H-7	62	188	19.54	207.54
20H-CC	27	188.62	19.54	208.16
21H-1	150	188.5	20.75	209.25
21H-2	150	190	20.75	210.75
21H-3	150	191.5	20.75	212.25
21H-4	150	193	20.75	213.75
21H-5	150	194.5	20.75	215.25
21H-6	150	196	20.75	216.75
21H-7	79	197.5	20.75	218.25
21H-CC	31	198.29	20.75	219.04
22H-1	150	198	21.67	219.67
22H-2	150	199.5	21.67	221.17
22H-3	150	201	21.67	222.67
22H-4	150	202.5	21.67	224.17
22H-5	150	204	21.67	225.67
22H-6	150	205.5	21.67	227.17
22H-7	79	207	21.67	228.67
22H-CC	41	207.79	21.67	229.46
23H-1	150	207.5	26.61	234.11
23H-2	150	209	26.61	235.61
23H-3	150	210.5	26.61	237.11
23H-4	150	212	26.61	238.61
23H-5	150	213.5	26.61	240.11
23H-6	150	215	26.61	241.61
23H-7	70	216.5	26.61	243.11
23H-CC	42	217.2	26.61	243.81
24H-1	150	217	22.56	239.56
24H-2	150	218.5	22.56	241.06
24H-3	150	220	22.56	242.56
24H-4	150	221.5	22.56	244.06
24H-5	150	223	22.56	245.56
24H-6	150	224.5	22.56	247.06
24H-7	79	226	22.56	248.56
24H-CC	22	226.79	22.56	249.35
25H-1	150	226.5	23.46	249.96
25H-2	150	228	23.46	251.46
25H-3	150	229.5	23.46	252.96
25H-4	150	231	23.46	254.46
25H-5	150	232.5	23.46	255.96
25H-6	150	234	23.46	257.46
25H-7	74	235.5	23.46	258.96
25H-CC	45	236.24	23.46	259.7
26H-1	150	236	26.83	262.83
26H-2	150	237.5	26.83	264.33
26H-3	150	239	26.83	265.83
26H-4	150	240.5	26.83	267.33
26H-5	150	242	26.83	268.83
26H-6	150	243.5	26.83	270.33
26H-7	87	245	26.83	271.83
26H-CC	21	245.87	26.83	272.7
27H-1	150	245.5	29.25	274.75
27H-2	150	247	29.25	276.25
27H-3	150	248.5	29.25	277.75
27H-4	150	250	29.25	279.25
27H-5	150	251.5	29.25	280.75
27H-6	150	253	29.25	282.25
27H-7	76	254.5	29.25	283.75
27H-CC	36	255.26	29.25	284.51
28H-1	150	255	29.83	284.83
28H-2	150	256.5	29.83	286.33
28H-3	150	258	29.83	287.83
28H-4	150	259.5	29.83	289.33
28H-5	150	261	29.83	290.83
28H-6	150	262.5	29.83	292.33
28H-7	72	264	29.83	293.83
28H-CC	20	264.72	29.83	294.55
29H-1	150	264.5	33.29	297.79
29H-2	150	266	33.29	299.29
29H-3	150	267.5	33.29	300.79
29H-4	150	269	33.29	302.29
29H-5	150	270.5	33.29	303.79
29H-6	150	272	33.29	305.29
29H-7	62	273.5	33.29	306.79
29H-CC	48	274.12	33.29	307.41
30H-1	150	274	34.99	308.99
30H-2	150	275.5	34.99	310.49
30H-3	150	277	34.99	311.99
30H-4	150	278.5	34.99	313.49
30H-5	150	280	34.99	314.99
30H-6	150	281.5	34.99	316.49
30H-7	82	283	34.99	317.99
30H-CC	29	283.82	34.99	318.81
31H-1	150	283.5	39.14	322.64
31H-2	150	285	39.14	324.14
31H-3	150	286.5	39.14	325.64
31H-4	150	288	39.14	327.14
31H-5	150	289.5	39.14	328.64
31H-6	150	291	39.14	330.14
31H-7	64	292.5	39.14	331.64
31H-CC	42	293.14	39.14	332.28
32H-1	150	293	41.02	334.02
32H-2	150	294.5	41.02	335.52
32H-3	150	296	41.02	337.02
32H-4	150	297.5	41.02	338.52
32H-5	150	299	41.02	340.02
32H-6	150	300.5	41.02	341.52
32H-7	66	302	41.02	343.02
32H-CC	35	302.66	41.02	343.68
33H-1	150	302.5	42.1	344.6
33H-2	150	304	42.1	346.1
33H-3	150	305.5	42.1	347.6
33H-4	150	307	42.1	349.1
33H-5	150	308.5	42.1	350.6
33H-6	150	310	42.1	352.1
33H-7	69	311.5	42.1	353.6
33H-CC	29	312.19	42.1	354.29
34H-1	150	312	38.14	350.14
34H-2	150	313.5	38.14	351.64
34H-3	150	315	38.14	353.14
34H-4	150	316.5	38.14	354.64
34H-5	150	318	38.14	356.14
34H-6	150	319.5	38.14	357.64
34H-7	60	321	38.14	359.14
34H-CC	37	321.6	38.14	359.74
35X-1	150	321.5	37.19	358.69
35X-2	150	323	37.19	360.19
35X-3	150	324.5	37.19	361.69
35X-4	150	326	37.19	363.19
35X-5	150	327.5	37.19	364.69
35X-6	17	329	37.19	366.19
35X-CC	40	329.17	37.19	366.36
36X-1	150	331.2	36.59	367.79
36X-2	150	332.7	36.59	369.29
36X-3	150	334.2	36.59	370.79
36X-4	150	335.7	36.59	372.29
36X-5	150	337.2	36.59	373.79
36X-6	105	338.7	36.59	375.29
36X-CC	49	339.75	36.59	376.34
37X-1	150	340.8	38.44	379.24
37X-2	150	342.3	38.44	380.74
37X-3	150	343.8	38.44	382.24
37X-4	150	345.3	38.44	383.74
37X-5	150	346.8	38.44	385.24
37X-6	150	348.3	38.44	386.74
37X-7	39	349.8	38.44	388.24
37X-CC	2	350.19	38.44	388.63
38X-1	150	350.4	47.04	397.44
38X-2	150	351.9	47.04	398.94
38X-3	150	353.4	47.04	400.44
38X-4	150	354.9	47.04	401.94
38X-5	150	356.4	47.04	403.44
38X-6	150	357.9	47.04	404.94
38X-7	50	359.4	47.04	406.44
38X-CC	36	359.9	47.04	406.94
154-925D-				
1H-1	150	2.5	-0.5	2
1H-2	150	4	-0.5	3.5
1H-3	150	5.5	-0.5	5
1H-4	150	7	-0.5	6.5
1H-5	150	8.5	-0.5	8
1H-6	150	10	-0.5	9.5
1H-7	74	11.5	-0.5	11
1H-CC	24	12.24	-0.5	11.74
2H-1	142	12	2.59	14.59
2H-2	150	13.42	2.59	16.01
2H-3	150	14.92	2.59	17.51
2H-4	150	16.42	2.59	19.01
2H-5	150	17.92	2.59	20.51
2H-6	150	19.42	2.59	22.01
2H-7	73	20.92	2.59	23.51
2H-CC	31	21.65	2.59	24.24
3H-1	150	21.5	3.26	24.76
3H-2	150	23	3.26	26.26
3H-3	150	24.5	3.26	27.76
3H-4	150	26	3.26	29.26
3H-5	150	27.5	3.26	30.76
3H-6	150	29	3.26	32.26
3H-7	59	30.5	3.26	33.76
3H-CC	22	31.09	3.26	34.35
4H-1	150	31	3.77	34.77
4H-2	150	32.5	3.77	36.27
4H-3	150	34	3.77	37.77
4H-4	150	35.5	3.77	39.27
4H-5	150	37	3.77	40.77
4H-6	150	38.5	3.77	42.27
4H-7	50	40	3.77	43.77
4H-CC	21	40.5	3.77	44.27
5H-1	150	40.5	4.54	45.04
5H-2	150	42	4.54	46.54
5H-3	150	43.5	4.54	48.04
5H-4	150	45	4.54	49.54
5H-5	150	46.5	4.54	51.04
5H-6	150	48	4.54	52.54
5H-7	50	49.5	4.54	54.04
5H-CC	24	50	4.54	54.54
6H-1	150	50	4.58	54.58
6H-2	150	51.5	4.58	56.08
6H-3	150	53	4.58	57.58
6H-4	150	54.5	4.58	59.08
6H-5	150	56	4.58	60.58
6H-6	150	57.5	4.58	62.08
6H-7	78	59	4.58	63.58
6H-CC	22	59.78	4.58	64.36
7H-1	150	59.5	5.68	65.18
7H-2	150	61	5.68	66.68
7H-3	150	62.5	5.68	68.18
7H-4	150	64	5.68	69.68
7H-5	150	65.5	5.68	71.18
7H-6	150	67	5.68	72.68
7H-7	47	68.5	5.68	74.18
7H-CC	32	68.97	5.68	74.65
8H-1	150	69	6.47	75.47
8H-2	150	70.5	6.47	76.97
8H-3	150	72	6.47	78.47
8H-4	150	73.5	6.47	79.97
8H-5	150	75	6.47	81.47
8H-6	128	76.5	6.47	82.97
8H-CC	34	77.78	6.47	84.25
9H-1	150	78.5	7.24	85.74
9H-2	150	80	7.24	87.24
9H-3	150	81.5	7.24	88.74
9H-4	150	83	7.24	90.24
9H-5	150	84.5	7.24	91.74
9H-6	150	86	7.24	93.24
9H-7	82	87.5	7.24	94.74
9H-CC	26	88.32	7.24	95.56
10H-1	150	88	9.35	97.35
10H-2	150	89.5	9.35	98.85
10H-3	150	91	9.35	100.35
10H-4	150	92.5	9.35	101.85
10H-5	150	94	9.35	103.35
10H-6	150	95.5	9.35	104.85
10H-7	76	97	9.35	106.35
10H-CC	37	97.76	9.35	107.11
11H-1	150	97.5	10.25	107.75
11H-2	150	99	10.25	109.25

Table 4 (continued).

Core and section	Section length (cm)	Depth (mbsf)	Offset (m)	Composite depth (mcd)
11H-3	150	100.5	10.25	110.75
11H-4	150	102	10.25	112.25
11H-5	150	103.5	10.25	113.75
11H-6	150	105	10.25	115.25
11H-7	47	106.5	10.25	116.75
11H-CC	30	106.97	10.25	117.22
12H-1	150	107	10.91	117.91
12H-2	150	108.5	10.91	119.41
12H-3	150	110	10.91	120.91
12H-4	150	111.5	10.91	122.41
12H-5	150	113	10.91	123.91
12H-6	150	114.5	10.91	125.41
12H-7	61	116	10.91	126.91
12H-CC	21	116.61	10.91	127.52
13H-1	150	116.5	12.41	128.91
13H-2	150	118	12.41	130.41
13H-3	150	119.5	12.41	131.91
13H-4	150	121	12.41	133.41
13H-5	150	122.5	12.41	134.91
13H-6	150	124	12.41	136.41
13H-7	62	125.5	12.41	137.91
13H-CC	50	126.12	12.41	138.53
14H-1	150	126	12.43	138.43
14H-2	150	127.5	12.43	139.93
14H-3	150	129	12.43	141.43
14H-4	150	130.5	12.43	142.93
14H-5	150	132	12.43	144.43
14H-6	150	133.5	12.43	145.93
14H-7	64	135	12.43	147.43
14H-CC	20	135.64	12.43	148.07
15H-1	150	135.5	14.73	150.23
15H-2	150	137	14.73	151.73
15H-3	150	138.5	14.73	153.23
15H-4	150	140	14.73	154.73
15H-5	150	141.5	14.73	156.23
15H-6	150	143	14.73	157.73
15H-7	72	144.5	14.73	159.23
15H-CC	19	145.22	14.73	159.95
16H-1	150	145	14.53	159.53
16H-2	150	146.5	14.53	161.03
16H-3	150	148	14.53	162.53
16H-4	150	149.5	14.53	164.03
16H-5	150	151	14.53	165.53
16H-6	150	152.5	14.53	167.03
16H-7	52	154	14.53	168.53
16H-CC	45	154.52	14.53	169.05
17H-1	150	154.5	16.87	171.37
17H-2	150	156	16.87	172.87
17H-3	150	157.5	16.87	174.37
17H-4	150	159	16.87	175.87
17H-5	150	160.5	16.87	177.37
17H-6	150	162	16.87	178.87
17H-7	72	163.5	16.87	180.37
17H-CC	43	164.22	16.87	181.09
18H-1	150	164	17.16	181.16
18H-2	150	165.5	17.16	182.66
18H-3	150	167	17.16	184.16
18H-4	150	168.5	17.16	185.66
18H-5	150	170	17.16	187.16
18H-6	150	171.5	17.16	188.66
18H-7	66	173	17.16	190.16
18H-CC	23	173.66	17.16	190.82
19H-1	150	173.5	17.77	191.27
19H-2	150	175	17.77	192.77
19H-3	150	176.5	17.77	194.27
19H-4	150	178	17.77	195.77
19H-5	150	179.5	17.77	197.27
19H-6	150	181	17.77	198.77
19H-7	83	182.5	17.77	200.27
19H-CC	38	183.33	17.77	201.1
20H-1	150	183	20.24	203.24
20H-2	150	184.5	20.24	204.74
20H-3	150	186	20.24	206.24
20H-4	150	187.5	20.24	207.74
20H-5	150	189	20.24	209.24
20H-6	90	190.5	20.24	210.74
20H-7	92	191.4	20.24	211.64
20H-CC	3	192.32	20.24	212.56
21H-1	150	192.5	22.41	214.91
21H-2	150	194	22.41	216.41
21H-3	150	195.5	22.41	217.91
21H-4	150	197	22.41	219.41
21H-5	150	198.5	22.41	220.91
21H-6	150	200	22.41	222.41
21H-7	78	201.5	22.41	223.91
21H-CC	33	202.28	22.41	224.69
22H-1	132	202	23.19	225.19
22H-2	150	203.32	23.19	226.51
22H-3	150	204.82	23.19	228.01
22H-4	150	206.32	23.19	229.51
22H-5	150	207.82	23.19	231.01
22H-6	125	209.32	23.19	232.51
22H-7	71	210.57	23.19	233.76
22H-CC	17	211.28	23.19	234.47
23H-1	150	211.5	23.78	235.28
23H-2	150	213	23.78	236.78
23H-3	150	214.5	23.78	238.28
23H-4	150	216	23.78	239.78
23H-5	150	217.5	23.78	241.28
23H-6	150	219	23.78	242.78
23H-7	66	220.5	23.78	244.28
23H-CC	18	221.16	23.78	244.94
24H-1	150	221	23.98	244.98
24H-2	150	222.5	23.98	246.48
24H-3	150	224	23.98	247.98
24H-4	150	225.5	23.98	249.48
24H-5	150	227	23.98	250.98
24H-6	150	228.5	23.98	252.48
24H-7	76	230	23.98	253.98
24H-CC	40	230.76	23.98	254.74
25H-1	150	230.5	24.98	255.48
25H-2	150	232	24.98	256.98
25H-3	150	233.5	24.98	258.48
25H-4	150	235	24.98	259.98
25H-5	150	236.5	24.98	261.48
25H-6	150	238	24.98	262.98
25H-7	72	239.5	24.98	264.48
25H-CC	42	240.22	24.98	265.2
26H-1	150	240	25.97	265.97
26H-2	150	241.5	25.97	267.47
26H-3	150	243	25.97	268.97
26H-4	150	244.5	25.97	270.47
26H-5	150	246	25.97	271.97
26H-6	150	247.5	25.97	273.47
26H-7	69	249	25.97	274.97
26H-CC	46	249.69	25.97	275.66
27H-1	150	249.5	26.9	276.4
27H-2	150	251	26.9	277.9
27H-3	150	252.5	26.9	279.4
27H-4	150	254	26.9	280.9
27H-5	150	255.5	26.9	282.4
27H-6	120	257	26.9	283.9
27H-7	35	258.2	26.9	285.1
27H-CC	18	258.55	26.9	285.45
28H-1	150	259	29.46	288.46
28H-2	150	260.5	29.46	289.96
28H-3	150	262	29.46	291.46
28H-4	150	263.5	29.46	292.96
28H-5	150	265	29.46	294.46
28H-6	150	266.5	29.46	295.96
28H-7	79	268	29.46	297.46
28H-CC	21	268.79	29.46	298.25
29H-1	150	268.5	28.89	297.39
29H-2	150	270	28.89	298.89
29H-3	150	271.5	28.89	300.39
29H-4	150	273	28.89	301.89
29H-5	150	274.5	28.89	303.39
29H-6	135	276	28.89	304.89
29H-CC	26	277.35	28.89	306.24
30H-1	150	278	30.9	308.9
30H-2	150	279.5	30.9	310.4
30H-3	150	281	30.9	311.9
30H-4	150	282.5	30.9	313.4
30H-5	150	284	30.9	314.9
30H-6	150	285.5	30.9	316.4
30H-7	64	287	30.9	317.9
30H-CC	33	287.64	30.9	318.54
31H-1	150	287.5	31.82	319.32
31H-2	150	289	31.82	320.82
31H-3	150	290.5	31.82	322.32
31H-4	150	292	31.82	323.82
31H-5	150	293.5	31.82	325.32
31H-6	150	295	31.82	326.82
31H-7	69	296.5	31.82	328.32
31H-CC	48	297.19	31.82	329.01
32H-1	150	297	33.85	330.85
32H-2	150	298.5	33.85	332.35
32H-3	150	300	33.85	333.85
32H-4	150	301.5	33.85	335.35
32H-5	150	303	33.85	336.85
32H-6	150	304.5	33.85	338.35
32H-7	70	306	33.85	339.85
32H-CC	32	306.7	33.85	340.55
33H-1	150	306.5	34.94	341.44
33H-2	150	308	34.94	342.94
33H-3	150	309.5	34.94	344.44
33H-4	150	311	34.94	345.94
33H-5	150	312.5	34.94	347.44
33H-6	150	314	34.94	348.94
33H-7	75	315.5	34.94	350.44
33H-CC	35	316.25	34.94	351.19
34H-1	150	316	37.49	353.49
34H-2	150	317.5	37.49	354.99
34H-3	150	319	37.49	356.49
34H-4	150	320.5	37.49	357.99
34H-5	150	322	37.49	359.49
34H-6	96	323.5	37.49	360.99
34H-CC	38	324.46	37.49	361.95
35H-1	150	325.5	38.19	363.69
35H-2	150	327	38.19	365.19
35H-3	150	328.5	38.19	366.69
35H-4	150	330	38.19	368.19
35H-5	150	331.5	38.19	369.69
35H-6	100	333	38.19	371.19
35H-7	65	334	38.19	372.19
35H-CC	30	334.65	38.19	372.84
36H-1	150	335	40.99	375.99
36H-2	150	336.5	40.99	377.49
36H-3	150	338	40.99	378.99
36H-4	150	339.5	40.99	380.49
36H-5	150	341	40.99	381.99
36H-6	150	342.5	40.99	383.49
36H-7	54	344	40.99	384.99
36H-CC	33	344.54	40.99	385.53
37H-1	150	344.5	48.39	392.89
37H-2	150	346	48.39	394.39
37H-3	150	347.5	48.39	395.89
37H-4	150	349	48.39	397.39
37H-5	150	350.5	48.39	398.89
37H-6	150	352	48.39	400.39
37H-7	62	353.5	48.39	401.89
37H-CC	45	354.12	48.39	402.51
154-925E-				
1H-1	150	0	-0.02	-0.02
1H-2	150	1.5	-0.02	1.48
1H-3	150	3	-0.02	2.98
1H-4	150	4.5	-0.02	4.48
1H-5	34	6	-0.02	5.98
1H-CC	29	6.34	-0.02	6.32
2H-1	150	7	0.83	7.83
2H-2	150	8.5	0.83	9.33
2H-3	150	10	0.83	10.83
2H-4	150	11.5	0.83	12.33
2H-5	150	13	0.83	13.83
2H-6	150	14.5	0.83	15.33
2H-7	73	16	0.83	16.83
2H-CC	16	16.73	0.83	17.56
3H-1	150	16.5	2.52	19.02
3H-2	150	18	2.52	20.52
3H-3	150	19.5	2.52	22.02
3H-4	150	21	2.52	23.52
3H-5	150	22.5	2.52	25.02
3H-6	150	24	2.52	26.52
3H-7	57	25.5	2.52	28.02
3H-CC	22	26.07	2.52	28.59
4H-1	150	26	3.17	29.17
4H-2	150	27.5	3.17	30.67
4H-3	150	29	3.17	32.17
4H-4	150	30.5	3.17	33.67
4H-5	150	32	3.17	35.17
4H-6	150	33.5	3.17	36.67
4H-7	59	35	3.17	38.17
4H-CC	17	35.59	3.17	38.76
5H-1	150	35.5	4.59	40.09
5H-2	150	37	4.59	41.59
5H-3	150	38.5	4.59	43.09
5H-4	150	40	4.59	44.59
5H-5	150	41.5	4.59	46.09
5H-6	150	43	4.59	47.59
5H-7	33	44.5	4.59	49.09
5H-CC	32	44.83	4.59	49.42
6H-1	150	45	6.79	51.79
6H-2	150	46.5	6.79	53.29
6H-3	150	48	6.79	54.79
6H-4	150	49.5	6.79	56.29
6H-5	150	51	6.79	57.79
6H-6	150	52.5	6.79	59.29
6H-7	54	54	6.79	60.79
6H-CC	39	54.54	6.79	61.33

Table 5. Splice tie-points, Site 925.

Hole, core, section (cm)	Top (cm)	Bottom (cm)	Depth (mbsf)	Composite depth (mcd)		Hole, core, section (cm)	Top (cm)	Bottom (cm)	Depth (mbsf)	Composite depth (mcd)	Offset (m)
925C-1H-5	53	53	6.33	6.53	tie to	925D-1H-4	3.5	3.5	7.03	6.53	-0.31
925D-1H-6	33.6	33.6	10.34	9.85	tie to	925C-2H-1	113	113	9.13	9.85	-0.29
925C-2H-7	13	13	17.13	17.86	tie to	925B-3H-1	94.4	94.4	14.94	17.86	1.9
925B-3H-3	124.6	124.6	18.25	21.16	tie to	925C-3H-3	33	33	20.83	21.16	-0.68
925C-3H-6	63	63	25.63	25.96	tie to	925D-3H-1	126.6	126.6	22.77	25.97	2.19
925D-3H-6	12.5	12.5	29.13	32.33	tie to	925C-4H-3	93.2	93.2	30.93	32.33	0.39
925C-4H-6	63	63	35.13	36.53	tie to	925D-4H-2	27.5	27.5	32.78	36.53	2.74
925D-4H-4	84.5	84.5	36.35	40.1	tie to	925C-5H-2	3	3	38.03	40.1	1.06
925C-5H-3	147.2	147.2	40.97	43.04	tie to	925D-4H-6	78.5	78.5	39.28	43.04	2.75
925D-4H-6	138.5	138.5	39.88	43.64	tie to	925C-5H-4	59	59	41.59	43.64	1.04
925C-5H-6	67	67	44.67	46.72	tie to	925D-5H-2	21.5	21.5	42.22	46.72	3.49
925D-5H-6	63.5	63.5	48.63	53.13	tie to	925C-6H-4	51	51	51.01	53.13	1.11
925C-6H-6	91.2	91.2	54.41	56.53	tie to	925D-6H-2	45.5	45.5	51.96	56.53	3.56
925D-6H-6	96.5	96.5	58.47	63.04	tie to	925C-7H-4	52	52	60.52	63.04	1.51
925C-7H-7	20	20	64.7	67.22	tie to	925D-7H-2	54.6	54.6	61.55	67.22	4.66
925D-7H-6	105.5	105.5	68.06	73.73	tie to	925C-8H-3	92	92	68.92	73.73	3.8
925C-8H-5	76	76	71.76	76.57	tie to	925D-8H-1	111.5	111.5	70.11	76.57	5.45
925D-8H-6	24.6	24.6	76.75	83.21	tie to	925C-9H-3	68	68	78.18	83.25	4.06
925C-9H-5	132	132	81.82	86.89	tie to	925B-10H-1	59.7	59.7	81.1	86.89	4.78
925B-10H-5	34.6	34.6	86.85	92.64	tie to	925C-10H-2	100.4	100.4	86.5	92.66	5.15
925C-10H-6	140.4	140.4	92.9	99.06	tie to	925D-10H-2	21.5	21.5	89.71	99.16	8.44
925D-10H-7	45.7	45.7	97.46	106.91	tie to	925C-11H-2	108.4	108.4	96.08	106.9	9.82
925C-11H-3	116.4	116.4	97.66	108.49	tie to	925D-11H-1	75.5	75.5	98.25	108.5	9.23
925D-11H-6	147.6	147.6	106.5	116.72	tie to	925C-12H-2	97.4	97.4	105.5	116.7	10.24
925C-12H-4	109.4	109.4	108.6	119.84	tie to	925D-12H-2	42.7	42.7	108.9	119.8	9.9
925D-12H-6	144.5	144.5	115.9	126.85	tie to	925C-13H-1	79.4	79.4	113.3	126.9	12.55
925C-13H-3	67.4	67.4	116.2	129.73	tie to	925D-13H-1	81.5	81.5	117.3	129.8	11.42
925D-13H-7	9.5	9.5	125.6	138.03	tie to	925C-14H-2	34.5	34.5	123.9	138	13.17
925C-14H-5	14.5	14.5	128.2	142.33	tie to	925D-14H-3	91.5	91.5	129.9	142.3	11.41
925D-14H-7	27.5	27.5	135.3	147.69	tie to	925C-15H-1	114.5	114.5	132.7	147.7	14.03
925C-15H-4	94.5	94.5	137	151.99	tie to	925D-15H-2	27.5	27.5	137.3	152	13.71
925D-15H-6	130.6	130.6	144.3	159.03	tie to	925C-16H-2	114.6	114.6	143.7	159	14.38
925C-16H-3	134.6	134.6	145.4	160.74	tie to	925D-16H-1	122.7	122.7	146.2	160.7	13.5
925D-16H-6	76.5	76.5	153.3	167.77	tie to	925C-17H-1	84.6	84.6	151.4	167.8	15.41
925C-17H-6	34.6	34.6	158.4	174.77	tie to	925D-17H-3	44.5	44.5	158	174.8	15.86
925D-17H-5	140.5	140.5	161.9	178.77	tie to	925C-18H-2	4.6	4.6	161.6	178.8	16.21
925C-18H-5	4.6	4.6	166.1	183.27	tie to	925D-18H-2	60.6	60.6	166.1	183.3	16.15
925D-18H-5	100.5	100.5	171	188.17	tie to	925B-19H-4	39.7	39.7	170.9	188.2	16.26
925B-19H-6	119.5	119.5	174.7	191.97	tie to	925C-19H-3	44.6	44.6	173	192	18.02
925C-19H-5	134.5	134.5	176.9	195.88	tie to	925D-19H-4	12.7	12.7	178.1	195.9	16.76
925D-19H-6	100.6	100.6	182	199.78	tie to	925C-20H-1	124.5	124.5	180.2	199.8	18.53
925C-20H-6	74.5	74.5	187.2	206.78	tie to	925D-20H-2	60.6	60.6	185.1	206.8	21.68
925D-20H-6	36.5	36.5	190.9	212.55	tie to	925C-21H-3	35.5	35.5	191.9	212.6	22.19
925C-21H-5	115.5	115.5	195.7	216.4	tie to	925D-21H-1	148.5	148.5	194	216.4	23.91
925D-21H-5	116.7	116.7	199.7	222.08	tie to	925C-22H-2	99.5	99.5	200.5	222.2	23.09
925C-22H-6	35.5	35.5	205.9	227.52	tie to	925D-22H-2	100.6	100.6	204.3	227.5	24.61
925D-22H-5	44.5	44.5	208.3	231.46	tie to	925B-23H-2	144.5	144.5	207	231.5	25.95
925B-23H-5	144.5	144.5	211.5	235.96	tie to	925C-23H-2	35.5	35.5	209.4	236	28.05
925C-23H-6	3.6	3.6	215	241.65	tie to	925D-23H-5	36.5	36.5	217.9	241.7	25.22
925D-23H-7	4.6	4.6	220.6	244.33	tie to	925C-24H-4	27.5	27.5	221.8	244.3	24
925C-24H-5	51.5	51.5	223.5	246.07	tie to	925D-24H-1	108.5	108.5	222.1	246.1	25.42
925D-24H-7	52.5	52.5	230.5	254.5	tie to	925C-25H-4	3.5	3.5	231	254.5	24.9
925C-25H-5	3.5	3.5	232.5	256	tie to	925D-25H-1	52.5	52.5	231	256	26.52
925D-25H-7	20.7	20.7	239.7	264.69	tie to	925C-26H-2	51.5	51.5	238	264.8	28.22
925C-26H-3	43.5	43.5	239.4	266.26	tie to	925D-26H-1	28.6	28.6	240.3	266.3	27.36
925D-26H-7	12.5	12.5	249.1	275.1	tie to	925C-27H-1	35.5	35.5	245.9	275.1	30.64
925C-27H-2	83.5	83.5	247.8	277.09	tie to	925D-27H-1	68.4	68.4	250.2	277.1	28.3
925D-27H-5	100.5	100.5	256.5	283.41	tie to	925B-28H-3	57	57	255.1	283.4	29.74
925B-28H-4	147	147	257.5	285.82	tie to	925C-28H-1	99.5	99.5	256	285.8	31.22
925C-28H-6	67.7	67.7	263.2	293.01	tie to	925B-29H-1	64.5	64.5	261.6	293	32.76
925B-29H-5	57.1	57.1	267.6	298.94	tie to	925D-29H-2	4.6	4.6	270.1	298.9	30.28
925D-29H-5	84.4	84.4	275.3	306.63	tie to	925B-30H-1	87	87	271.4	306.6	34.25
925B-30H-6	4.6	4.6	278.1	310.91	tie to	925D-30H-2	52.4	52.4	280	310.9	32.28
925D-30H-6	28.4	28.4	285.8	316.67	tie to	925B-31H-2	72	72	282.2	316.7	35.85
925B-31H-6	107.5	107.5	288.6	323.04	tie to	925C-31H-1	35.5	35.5	283.9	323	40.57
925C-31H-4	83.5	83.5	288.8	328.01	tie to	925B-32H-2	11	11	291.1	328	38.29
925B-32H-4	115.1	115.1	295.2	332.05	tie to	925D-32H-1	124.4	124.4	298.2	332.1	35.2
925D-32H-6	20.6	20.6	304.7	338.52	tie to	925B-33H-2	3.3	3.3	300.5	338.5	39.38
925B-33H-4	107	107	304.6	342.56	tie to	925D-33H-1	108.4	108.4	307.6	342.6	36.37
925D-33H-7	28.5	28.5	315.8	350.78	tie to	925B-34H-1	19	19	308.7	350.8	42.05
925B-34H-5	123	123	315.7	357.82	tie to	925A-4R-4	124.6	124.6	319.5	357.8	38.18
925A-4R-7	69.6	69.6	323.4	361.79	tie to	925A-5R-1	4.5	4.5	323.5	361.7	39.41
925A-5R-5	119.7	119.7	330.6	368.99	tie to	925C-36X-1	115.5	115.5	332.4	369.9	39.79
925C-36X-6	67.5	67.5	339.4	376.02	tie to	925D-36H-1	4.5	4.5	335.1	376	42.96
925D-36H-5	76.6	76.6	341.8	382.81	tie to	925A-7R-2	24.6	24.6	344.5	382.8	40.4
925A-7R-6	119.5	119.5	351.4	389.79	tie to	925A-8R-1	4.6	4.6	352.5	390.8	45.65
925A-8R-5	119.6	119.6	359.6	397.99	tie to	925C-38X-1	51.5	51.5	350.9	398	
925C-38X-3	139.6	139.6	354.8	401.89	tie to	925A-9R-2	9.5	9.5	363.6	402	
925A-69R-6	139.5	139.5	929.6	966.02							

The middle Miocene (about 9–16 Ma) contains another dense cluster of events in which both foraminifer and nannofossil indications show negligible scatter around the chosen rate line. The remaining time intervals (the late Miocene and the early Miocene to middle Eocene) contain considerably fewer events per unit time, and also show relatively larger departures of individual events from the chosen rate line. The foraminifer events that show the largest departures from the rate line appear affected by taxonomic ambiguities that cause difficulties when making consistent biostratigraphic assignments, whereas the nannofossil events that show relatively larger departures appear related to calibration problems. For example, the base of *Amaurolithus amplificus* seems to occur at a biostratigraphically lower position on the Ceara Rise than elsewhere.

Two planktonic foraminifer events occur in Holes 925B and 925A at virtually identical mcd depths (base of *Fohsella "praefohsi"* and base of *Fohsella peripheroronda;* Table 6). Two nannofossil events (tops of *Sphenolithus heteromorphus* and *Helicosphaera ampliaperta*) bracketing these two foraminifer events were chosen to establish a sedimentation rate that links the upper part of the section (Hole 925B) to the lower part (Hole 925A). Both the mbsf and mcd sedimentation rates are identical downhole from the point where the holes are made to connect, that is, from the top of *Sphenolithus heteromorphus* in Hole 925B (Figs. 22B and 22C).

A series of neatly aligned events occurs between about 13 and 16 Ma, revealing a sedimentation rate of 11 m/m.y. The top of *H. ampliaperta* clearly belongs to this series and is used as a tie-point (15.8 Ma). A different sedimentation rate is implied below this event, because the base of *S. heteromorphus,* which has been confidently calibrated to the magnetostratigraphy (Olafsson, 1991), occurs considerably deeper than would be expected by extrapolation of the trend above. The sedimentation rate between the top of *H. ampliaperta* and the base of *S. heteromorphus* is estimated at 30 m/m.y. Pronounced shifts in sediment bulk density, carbonate percentage, and pore-water chemistry (see "Physical Properties" and "Geochemistry" sections, this chapter) occur precisely at the sharp change in sedimentation rate, and it appears likely that these changes are related.

The number of events in the Oligocene section is low, but foraminifer and nannofossil data are in good agreement, suggesting a threefold decrease in rate from the high early Oligocene value (43 m/m.y.) to the latest Oligocene and early Miocene value of 15 m/m.y. The cluster of events in the latest Eocene is not well aligned, although the consistency among the three critical events provided by *Hantkenina alabamensis, Turborotalia cerroazulensis,* and *Discoaster saipanensis* suggests that the four foraminifer events plotted at 35.1–35.2 Ma are poorly calibrated (Fig. 22C). The late Eocene rates between 35.4 and 40.2 Ma are surprisingly poorly constrained, with only two markers available. The nannofossil marker *Chiasmolithus grandis* is known to be diachronous between the Mediterranean and the mid-latitude South Atlantic (Wei and Wise, 1989). Moreover, *C. grandis* is rare toward the end of its range at Site 925. All globigerinathekids are rare at Site 925, including the marker *Globigerinatheka semiinvoluta.* The sedimentation rates between about 35 and 42 Ma are constrained by only two reliable biostratigraphic events, the foraminifer *Orbulinoides beckmanni* and the nannofossil *Reticulofenestra umbilicus.* Consequently, the late Eocene sedimentation rate may be more variable than shown.

The sedimentation rates at Site 925, were not corrected for compaction, are summarized in Figure 23: the progressive decrease through the Oligocene from the peak values of the early Oligocene; the relatively low early Miocene rates, with the short pulse of drastically increased rates in the late early Miocene; and the following gradual increase from the early middle Miocene to the Holocene. Combined regional and global effects have created the sedimentation patterns we observe at Site 925. The average sedimentation rate throughout the cored interval is 24 m/m.y. on the mbsf scale (Fig. 23). Note that for the purpose of calculating fluxes, the mbsf scale should be used.

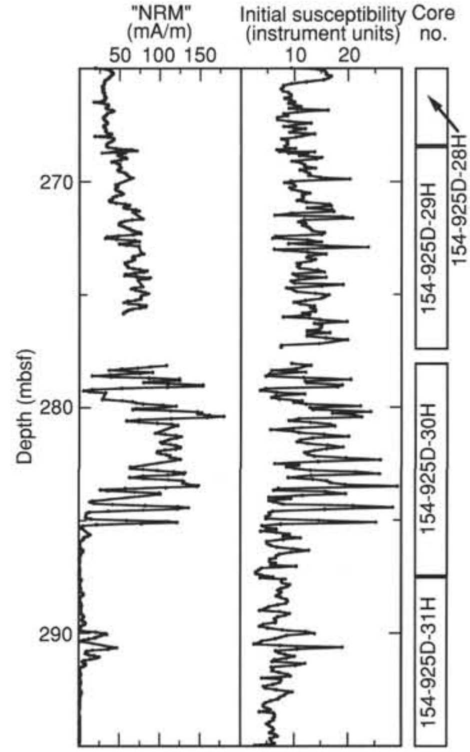

Figure 17. Comparison of the intensity of magnetization for archive half sections that have not been demagnetized ("NRM") and low-field magnetic susceptibility in four cores from Hole 925D.

GEOCHEMISTRY

Hydrocarbon Geochemistry

We routinely measured the volatile hydrocarbon content in sediment cores from Hole 925A, for a total of 60 analyses. Concentrations of methane remained at or near background levels at all depths. No heavier hydrocarbons were identified. These results suggest that biogenic methanogenesis was minimal at Site 925, probably because of the low organic carbon input. This interpretation is consistent with sediment total carbon measurements and interstitial-water sulfate determinations, which indicate low organic carbon inputs to the site and incomplete sulfate reduction throughout the section (see "Interstitial-water Geochemistry" and "Solid-phase Geochemistry" sections).

Interstitial-water Geochemistry

We collected interstitial waters from 59 samples at Site 925: 34 from Hole 925E at depths ranging from 1.45 to 53.95 mbsf, 9 from Hole 925B at depths ranging from 65.95 to 293.90 mbsf, and 16 from Hole 925A at depths ranging from 306.60 to 772.14 mbsf (Table 8). We did not recover any pore water from samples taken from Cores 154-925A-57R and -63R because of the low water content and impermeability of the sediments; therefore, we did not attempt deeper sampling. The samples from Holes 925A, 925B, and 925E are considered to constitute a single depth profile. The high frequency of sampling in the top 54 mbsf was undertaken primarily to obtain samples for shore-based oxygen isotope analyses; shipboard analyses were performed on a subset of these samples. Interstitial-water recovery from samples deeper than 660 mbsf in Hole 925A was low, so not all analyses could be performed on these samples. The calcium and magnesium concentrations of the samples from Cores 154-925A-42R-1, -45R-3, and -49R-3 were determined by Dionex ion chromatography because of the low sample volume. Chemical gradients in the interstitial waters at this site are influenced primarily by the

Table 6. Biostratigraphic events and sedimentation rate data from Holes 925A and 925B.

Marker species	Age (Ma)	Depth (mbsf)	(±)	Nannofossils (mbsf)	Foraminifers (mbsf)	Nannofossils (mcd)	Foraminifers (mcd)
Hole 925B:							
T *Pseudoemiliania lacunosa*	0.46	15.52–15.77	0.16	15.36		18.27	
Reentrance medium *Gephyrocapsa*	1.03	30.20–31.60	0.70	30.90		34.40	
Tl *Gephyrocapsa*	1.24	37.80–38.50	0.35	38.15		42.09	
B *Pulleniatina finalis*	1.4	60.19–62.16	0.98		61.18		65.40
Bl *Gephyrocapsa*	1.46	46.95–47.54	0.29	47.25		50.91	
T *Calcidiscus macintyrei*	1.6	48.45–49.04	0.29	48.75		52.41	
Bm *Gephyrocapsa*	1.67	49.95–50.54	0.29	50.25		53.91	
T *Globigerinoides fistulosus*	1.7	55.66–57.19	0.77		56.43		60.77
T *Globigerina apertura*	1.9	49.06–50.56	0.75		49.81		53.47
T *Globigerinoides extremus*	1.9	58.69–60.19	0.75		59.44		63.78
T *Discoaster brouweri*	1.95	57.75–58.45	0.35	58.10		62.44	
B *Globorotalia truncatulinoides*	2.0	57.19–58.66	0.73		57.93		62.27
Ba *Discoaster triradiatus*	2.15	64.15–64.90	0.38	64.53		68.64	
T *Globorotalia exilis*	2.2	68.16–69.66	0.75		68.91		73.02
T *Globorotalia miocenica*	2.3	71.04–71.66	0.31		71.35		76.07
Reappearance *Pulleniatina*	2.3	69.66–71.04	0.69		70.35		74.46
T *Globigerina woodi*	2.3	69.66–71.04	0.69		70.35		74.46
T *Discoaster pentaradiatus*	2.44	71.90–72.15	0.13	72.03		77.86	
T *Globigerina decoraperta*	2.6	81.16–82.66	0.75		81.91		87.70
T *Globorotalia pertenuis*	2.6	73.16–74.66	0.75		73.91		79.24
T *Discoaster surculus*	2.61	73.65–75.40	0.38	74.03		79.36	
T *Discoaster tamalis*	2.76	83.14–83.90	0.38	83.52		89.31	
T *Dentoglobigerina altispira*	3.0	90.09–90.66	0.28		90.38		97.91
T *Globorotalia multicamerata*	3.0	88.66–90.09	0.72		89.38		95.17
T *Sphaeroidinellopsis seminulina*	3.1	90.09–90.66	0.28		90.38		97.91
B *Globorotalia pertenuis*	3.5	103.16–105.55	1.20		104.36		114.51
Disappearance *Pulleniatina*	3.5	100.05–101.70	0.83		100.88		111.03
B *Globorotalia miocenica*	3.6	109.16–109.66	0.25		109.41		120.52
T *Sphenolithus*	3.62	106.65–107.40	0.38	107.03		117.18	
T *Reticulofenestra pseudoumbilicus*	3.77	110.70–110.92	0.11	110.81		122.88	
S to D *Pulleniatina*	4.0	118.52–119.16	0.32		118.84		131.04
T *Globigerina nepenthes*	4.3	127.61–128.11	0.25		127.86		140.68
T *Globorotalia plesiotumida*	4.4	109.02–109.67	0.33		109.35		120.45
B *Globorotalia crassaformis* s.l.	4.7	111.17–112.61	0.72		111.89		123.96
T *Globorotalia ciaboensis*	5.0	142.66–144.16	0.75		143.41		158.23
B *Ceratolithus rugosus*	5.04	142.40–143.15	0.38	142.77		157.60	
T *Neogloboquadrina acostaensis*	5.1	131.66–133.16	0.75		132.41		145.72
T *Ceratolithus acutus*	5.04	142.40–143.15	0.38	142.77		157.60	
B *Ceratolithus acutus*	5.34	147.25–148.60	0.67	147.93		163.35	
T *Triquetrorhabdulus rugosus*	5.34	147.11–147.25	0.07	147.18		162.30	
T *Globoquadrina baroemoenensis*	5.4	142.66–144.16	0.75		143.41		158.23
T *Discoaster quinqueramus*	5.56	153.80–154.60	0.40	154.20		169.62	
B *Sphaerodinella dehiscens*	5.6	152.16–153.66	0.75		152.91		168.33
T *Amaurolithus amplificus*	5.88	162.15–162.90	0.38	162.53		179.40	
B *Globorotalia tumida*	5.9	157.17–158.67	0.75		157.92		174.79
B *Globorotalia margaritae*	6.2	163.17–164.67	0.75		163.92		180.79
B *Amaurolithus amplificus*	6.5	190.65–191.40	0.38	191.03		212.32	
B *Amaurolithus primus*	7.3	198.30–198.65	0.17	198.48		220.19	
B *Globorotalia cibaoensis*	7.7	190.16–191.66	0.75		190.91		212.20
B *Candeina nitida*	8.0	223.16–225.16	1.00		224.16		250.50
B *Globigerinoides extremus*	8.0	226.66–228.13	0.73		227.40		254.91
B *Globorotalia plesiotumida*	8.2	226.66–228.13	0.73		227.40		254.91
B *Discoaster berggrenii*	8.4	218.80–219.15	0.17	218.98		244.15	
T *Catinaster calyculus*	9.3	242.61–242.80	0.09	242.71		270.95	
T *Discoaster hamatus*	9.4	243.00–243.08	0.04	243.04		271.75	
B *Discoaster neohamatus*	9.6	244.30–251.70	3.70	248.00		276.53	
B *Neogloboquadrina acostaensis*	10.0	244.16–245.66	0.75		244.91		273.62
T *Paragloborotalia mayeri*	10.3	261.16–261.66	0.25		261.41		291.27
B *Discoaster hamatus*	10.4	261.59–261.20	–0.19	261.40		291.26	
B *Catinaster coalitus*	10.7	266.30–267.20	0.45	266.75		298.12	
B *Coccolithus miopelagicus*	10.8	269.30–270.10	0.40	269.70		301.07	
B *Globigerina apertura*	10.8	269.16–272.66	1.75		270.91		303.01
B *Globigerina nepenthes*	10.8	270.66–271.16	0.25		270.91		303.01
B *Globigerina decoraperta*	11.2	274.16–275.66	0.75		274.91		307.75
Tc *Discoaster kugleri*	11.3	277.71–277.76	0.03	277.74		310.58	
Bc *Discoaster kugleri*	11.7	280.50–280.38	–0.06	280.44		314.07	
T *Fohsella fohsi* s.l.	11.8	278.66–280.66	1.00		279.66		313.29
B *Globorotalia lenguaensis*	12.3	294.66–296.17	0.75		295.42		332.28
B *Fohsella robusta*	12.7	299.16–299.66	0.25		299.41		336.82
T *Cyclicargolithus floridanus*	13.2	301.30–302.70	0.70	302.00		339.95	
B *Fohsella fohsi*	13.5	304.16–305.66	0.75		304.91		342.86
T *Sphenolithus heteromorphus*	13.6	308.25–308.50	0.13	308.38		346.33	
B *Fohsella "praefoshi"*	14.0	309.16–310.66	0.75		309.91		351.95
B *Fohsella peripheroronda*	14.6	310.66–313.66	1.50		312.16		354.20
Hole 925A:							
B *Fohsella peripheroacuta*	14.7	315.96–317.48	0.76		316.72		355.06
T *Praeorbulina glomerosa* s.l.	14.8	321.96–323.43	0.74		322.70		361.04
T *Praeorbulina sicana*	14.8	321.96–323.43	0.74		322.70		361.04
B *Orbulina suturalis*	15.1	323.43–324.16	0.37		323.80		362.14
T *Helicosphaera ampliaperta*	15.8	332.00–332.70	0.35	332.35		370.69	
B *Praeorbulina circularis*	16.0	328.66–330.16	0.75		329.41		367.75
B *Praeorbulina glomerosa*	16.1	328.66–330.16	0.75		329.41		367.75
B *Praeorbulina sicana*	16.4	381.30–382.05	0.38		381.68		420.02
T *Catapsydrax dissimilis*	17.3	391.55–393.06	0.75		392.31		430.65
B *Sphenolithus heteromorphus*	18.1	400.80–401.37	0.28	401.09		439.43	
T *Sphenolithus belemnos*	18.4	410.17–410.66	0.25	410.42		448.76	
B *Globigerinatella insueta* s.s.	18.7	393.06–394.56	0.75		393.81		432.15

Table 6 (continued).

Marker species	Age (Ma)	Depth (mbsf)	(±)	Nannofossils (mbsf)	Foraminifers (mbsf)	Nannofossils (mcd)	Foraminifers (mcd)
T *Globoquadrina binaiensis*	19.1	433.06–434.56	0.75		433.81		472.15
B *Sphenolithus belemnos*	19.7	428.60–428.90	0.15	428.75		467.09	
T *Paragloborotalia kugleri*	21.6	458.25–459.02	0.39		458.63		497.75
B *Globoquadrina binaiensis*	22.1	458.25–459.02	0.39		458.63		497.70
T *Globigerina angulisuturalis*	23.3	500.59–501.98	0.70		501.29		539.63
B *Paragloborotalia kugleri*	23.7	499.09–500.48	0.70		499.79		538.13
T *Sphenolithus delphix*	23.7	500.91–502.45	0.77	501.68		540.02	
Bc *Globigerinoides primordius*	24.5	508.01–509.51	0.75		508.76		547.10
T *Sphenolithus ciperoensis*	24.7	502.85–507.50	2.32	505.18		543.52	
B *Paragloborotalia pseudokugleri*	26.3	542.06–543.56	0.75		542.80		581.15
T *Sphenolithus distentus*	26.5	574.17–574.25	0.04	574.21		612.55	
T *Paragloborotalia opima*	27.1	574.56–584.26	4.85		579.41		617.75
B *Sphenolithus ciperoensis*	28.1	592.20–593.33	0.56	592.77		631.11	
Tc *Chiloguembelina cubensis*	28.5	593.10–593.82	0.36		593.46		631.80
B *Globigerina angulisuturalis*	29.7	631.71–651.04	9.66		641.38		679.72
B *Sphenolithus distentus*	30.4	654.60–657.00	1.20	655.80		694.14	
T *Turborotalia ampliapertura*	30.3	649.61–661.54	5.96		655.58		693.92
T > 14 µm *Reticulofenestra umbilicus*	32.1	739.81–741.21	0.70	740.51		778.85	
T *Coccolithus formosus*	32.7	753.66–757.01	1.68	755.34		793.68	
T *Pseudohastigerina*	32.5	744.31–747.81	1.75		746.06		784.40
T *Hantkenina alabamensis*	33.8	776.46–777.03	0.28		776.75		815.09
T *Turborotalia cerroazulensis*	33.9	777.03–777.42	0.19		777.23		815.57
T *Cribrohantkenina inflata*	34.0	777.91–779.49	0.79		778.70		817.04
T *Globigerinatheka index*	34.2	779.49–780.12	0.31		779.81		818.15
B *Turborotalia cunialensis*	35.1	777.91–779.49	0.79		778.70		817.04
T *Turborotalia pomeroli*	35.2	781.45–783.02	0.78		782.24		820.58
T *Globigerinatheka semiinvoluta*	35.2	783.02–783.96	0.47		783.49		821.83
T *Discoaster saipanensis*	34.2	785.91–786.27	0.18	786.09		824.43	
T *Cribrocentrum reticulatum*	35.0	792.25–792.62	0.19	792.44		830.78	
T *Calcidiscus protoannula*	35.4	794.72–804.29	4.78	799.51		837.85	
B *Cribrohantkenina inflata*	35.4	786.32–787.77	0.72		787.05		821.83
T *Chiasmolithus grandis*	37.1	850.89–863.43	6.27	857.16		895.50	
B > 14 µm *Reticulofenestra umbilicus*	42.2	911.34–929.94	9.30	920.64		958.98	
B *Globigerinatheka semiinvoluta*	38.8	837.74–843.80	3.03		840.77		825.39
T *Orbulinoides beckmanni*	40.2	879.44–882.50	1.53		880.97		879.11

Notes: T = top, Tl = top large (>5.5 µm), B = base, Bl = base large (>5.5 µm), Ba = base acme, S to D = sinistral to dextral coiling, Bc = base common, and Tc = top common. Medium size defined as 4.0–5.5 µm.

Table 7. Biostratigraphic control points for Site 925 sedimentation rates.

Biostratigraphic control point	Age (Ma)	Depth (mbsf)	Sedimentation rate (mbsf/m.y.)	Composite depth (m)	Sedimentation rate (mcd/m.y.)
Hole 925B:					
Top section	0.00	0.00		0.00	
T *P. lacunosa*	0.46	15.36	33	18.27	40
T *D. brouweri*	1.95	58.10	29	62.44	30
T *R. pseudoumbilicus*	3.77	110.81	29	122.88	33
T *A. amplificus*	5.88	162.78	25	179.40	27
T *D. hamatus*	9.4	243.04	23	271.75	26
Tc *D. kugleri*	11.3	277.74	18	310.58	20
T *S. heteromorphus*	13.6	308.38	13	346.33	16
Hole 925A:					
T *H. ampliaperta*	15.8	332.35	11	370.69	11
T *S. belemnos*	18.4	410.42	30	448.76	30
T *P. kugleri*	21.6	459.41	15	496.98	15
B *P. kugleri*	23.7	499.79	20	538.13	20
T *C. cubensis*	28.5	593.46	20	631.80	20
B *G. angulisuturalis*	29.7	641.38	40	679.72	40
T *C. formosus*	32.7	755.33	38	793.68	38
T *H. alabamensis*	33.75	776.75	20	815.09	20
T *O. beckmannii*	40.2	880.97	16	919.31	16
T Bottom of section, Site 925	43.2	929.94	16	968.28	16

Notes: T = top, Tc = top common, and B = bottom.

biogenic character of the sediments and by alteration reactions in the underlying basalt. Some pore-water profiles indicate that organic carbon and biogenic silica inputs to the site may have been greater than is reflected in the present sediment composition, particularly in the early to middle Miocene sediments near 400 mbsf.

Chlorinity measurements were hampered by analytical problems (see "Geochemistry" section, "Explanatory Notes" chapter, this volume, for discussion). Chlorinity, as measured by titration, generally increases with depth from standard seawater values of around 559 mM at the top of the section to values around 565 mM in our deepest samples (Fig. 24). Sodium concentrations, as calculated by charge balance, generally decrease downsection until 500 mbsf; below this level they increase again (Fig. 24). Considerable fluctuation is present within these trends. Sodium values range from a high of 490 mM near the top of the section to a low of 448 mM near 500 mbsf; the deepest samples for which calculations could be performed have higher sodium concentrations again (up to 473 mM). Salinity, as measured by a handheld refractometer, varies from 32.5 to 34.5 g/kg, with no recognizable trend with depth.

Alkalinity generally decreases in the top 150 m of the section to about 3.0 mM. Values then increase to a maximum of 10.6 mM at about 425 mbsf and gradually decrease to about 4.5 mM in our

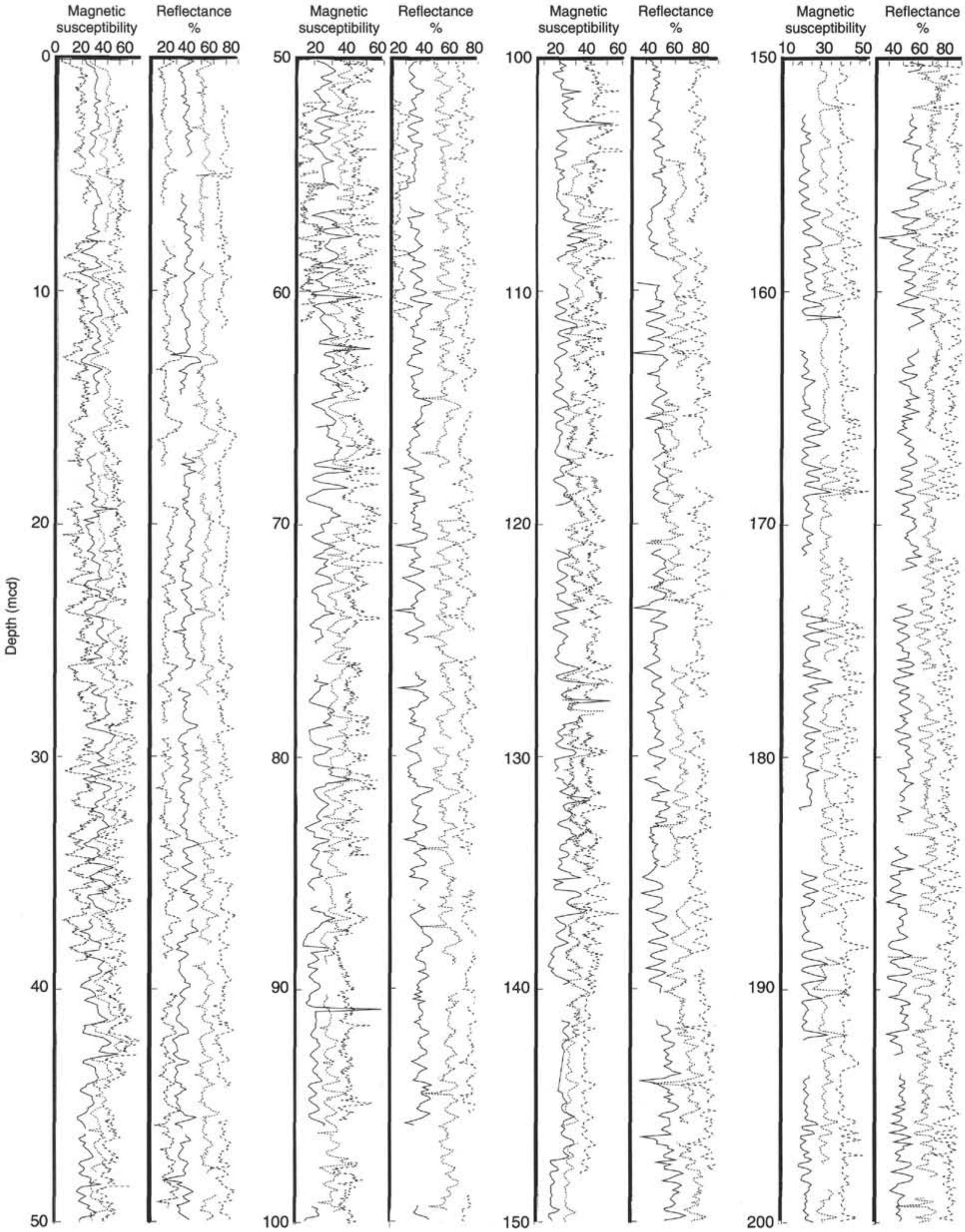

Figure 18. Magnetic susceptibility and reflectance from Site 925 on the composite depth (mcd) scale. Data are included on CD-ROM (back pocket). Plot lines are vertically offset from one another for clarity. Holes 925A and 925E = large dashed line (note that data for Hole 925A extend from 100 m on and for Hole 925E from 0 to 52 m only), Hole 925B = solid line, Hole 925C = dotted line, and Hole 925D = small dashed line. Magnetic susceptibility values are in uncorrected instrument units.

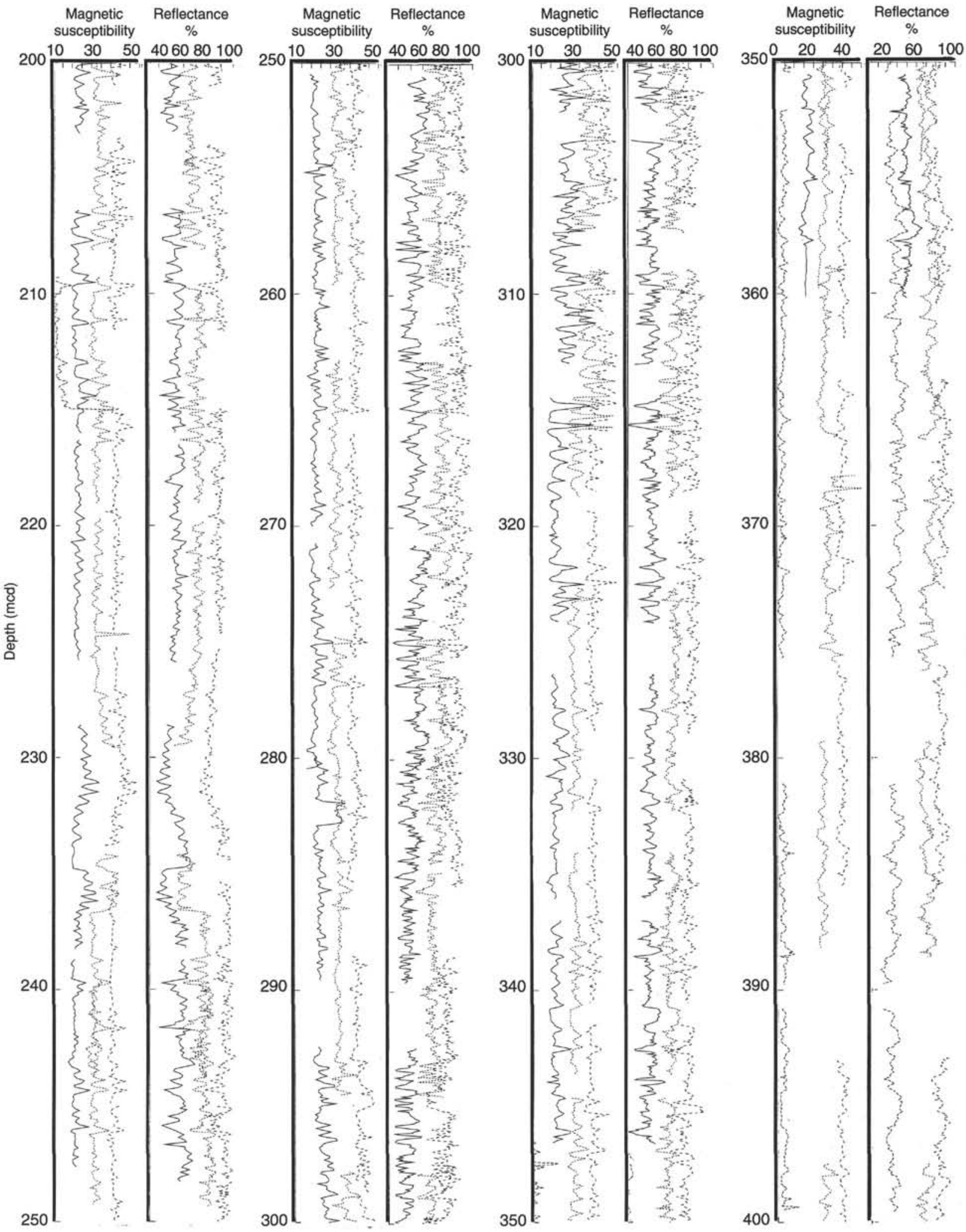

Figure 18 (continued).

deepest sample (Fig. 24). The alkalinity peak has much higher values than found at other low-latitude, pelagic carbonate sites (e.g., Leg 115, Swart and Burns, 1990; Site 758 of Leg 121, Shipboard Scientific Party, 1989; Leg 130, Kroenke, Berger, Janecek, et al., 1991; Leg 138, Mayer, Pisias, Janecek, et al., 1992). The pH varies erratically with depth, with most values ranging from 6.5 to 7.6 (Fig. 24). Around 400 and 600 mbsf, there are pronounced lows in pH, with values about 6.6. Dissolved silica concentrations are low (near 100 µM) in the top 200 mbsf of the section (Fig. 24). Values increase abruptly to near-saturation values of about 1000 µM between 200 and 400 mbsf, with a broad peak around 400 mbsf. Values gradually decrease to 383 µM in our deepest sample at 772 mbsf. This profile

Table 8. Summary of interstitial-water geochemistry results for samples from Holes 925A, 925B, and 925E.

Core, section, interval (cm)	Depth (mbsf)	Cl^- (mM)	Na^+ (mM)	Salinity (ppt)	Alkalinity (mM)	pH	SiO_2 (µM)	NH_4^+ (µM)	SO_4^{2-} (mM)	Mn^{2+} (µM)	Sr^{2+} (µM)	PO_4^{3-} (µM)	Li^+ (µM)	Ca^{2+} (mM)	Mg^{2+} (mM)	K^+ (mM)
154-925E-																
1H-1, 145–150	1.45	557					113	57	27.08	34.5	94	1.61	25			11.6
1H-2, 145–150	2.95	559					97	87	27.95	69.0		0.97	24	10.49	51.75	11.7
1H-3, 145–150	4.45	554		34.0	3.999	7.46	148	107	27.34	113.0	110	0.32	25			10.9
1H-4, 145–150	5.95	562					89	148	28.99	55.5			25			12.1
2H-1, 145–150	8.45	553					78	146	25.49	47.5	127	0.47	24			11.4
2H-2, 145–150	9.95						64	154	25.33	27.5		0.48	24			11.6
2H-3, 145–150	11.45	558	480	34.0	4.363	7.31	137	151	25.47	43.0		0.31	27	10.61	50.63	10.8
2H-4, 145–150	12.95	559					100	170	25.20	12.0	140	0.16	26			11.4
2H-5, 145–150	14.45						80	165	27.69	21.0			26			12.1
2H-6, 145–150	15.95	566	490	34.5	3.440	7.60	97	185	27.58				26	10.50	51.23	11.0
3H-1, 145–150	17.95	565							24.53	11.5	173		27			11.4
3H-2, 145–150	19.45								25.67				27			12.0
3H-3, 145–150	20.95	554	475	34.0	3.746	7.36	91	222	24.50			0.16	27	10.62	49.63	11.1
3H-4, 145–150	22.45	562							25.31	13.0	205		27			10.7
3H-5, 145–150	23.95								26.66				28			12.0
3H-6, 145–150	25.45	564	492	34.5	3.592	7.45	153	208	27.94			0.16	29	11.05	49.86	10.0
4H-1, 145–150	27.45	562							25.53	16.0	221		29			11.4
4H-2, 145–150	28.95								27.23				30			12.1
4H-3, 145–150	30.45	559	484	34.5	3.697	7.42	151	225	26.52			0.00	31	10.98	49.60	10.4
4H-4, 145–150	31.95	571							23.88	12.5	257		32			11.9
4H-5, 145–150	33.45								25.96			0.00	32			11.2
4H-6, 145–150	34.95	562	485	34.5	3.888	7.36	137	267	25.02				33	11.15	49.43	10.2
5H-1, 145–150	36.95	572							23.21	10.5	307		34			10.8
5H-2, 145–150	38.45								25.10				33			10.3
5H-3, 145–150	39.95	559	481	34.5	3.488	7.36	195	271	24.74			0.00	37	11.28	49.21	10.4
5H-4, 145–150	41.45	568							23.15	9.0	332		36			10.2
5H-5, 145–150	42.95								23.83				40			10.6
5H-6, 145–150	44.45	566	491	34.5	3.415	7.49	148	280	25.72			0.00	38	11.19	48.81	9.7
6H-1, 145–150	46.45	567							24.84	6.5	350		39			10.5
6H-2, 145–150	47.95								23.68				39			10.5
6H-3, 145–150	49.45			34.5	3.443	7.45	133	333	24.38			0.00	41	11.34	48.91	10.6
6H-4, 145–150	50.95	573							21.97	8.0	385		41			10.7
6H-5, 145–150	52.45								24.70				40			10.6
6H-6, 145–150	53.95	566	485	34.5	3.369	7.17	128	357	22.41			0.00	43	11.39	48.28	9.9
154-925B-																
8H-3, 145–150	65.95	563	482	34.5	3.430	7.38	139	536	23.28	5.0	487		69	11.27	48.48	9.8
11H-3, 145–150	94.45	559	469	34.0	3.052	7.14	128	574	18.88	2.5	625		67	11.92	47.75	9.3
14H-3, 145–150	122.95	565	482	34.0	2.988	7.49	124	616	21.26	2.0	812		89	12.82	46.41	8.2
17H-3, 145–150	151.45	563	470	34.0	3.079	7.32	121	621	17.45	1.5	848		113	13.85	45.77	8.9
20H-3, 145–150	179.95	565	474	33.5	3.464	7.26	139	601	18.78	2.0	942		152	15.04	45.51	8.5
23H-3, 145–150	208.45	567	480	33.5	4.347	7.32	163	670	20.42	2.0	1010		206	16.50	44.41	7.4
26H-3, 145–150	236.95	561	464	34.0	5.209	7.36	197	844	16.50	1.0	1108		284	18.27	43.57	7.8
29H-3, 145–150	265.45	565	469	34.0	6.537	7.32	241	893	16.43	3.0	1160		353	20.25	42.14	7.3
32H-3, 140–150	293.90	567	466	34.5	7.757	6.71	451	900	15.28	3.5	1250		440	22.43	41.38	7.2
154-925A-																
3R-2, 140–150	306.60	562	462	34.0	8.000	7.32	555	803	15.72	3.5	1252		491	23.80	40.95	5.9
6R-2, 140–150	336.00	569	468	34.5	9.412	7.56	901	953	17.00		1278		602	26.32	40.51	6.3
9R-3, 140–150	366.40	566	466	34.5	9.962	7.56	887	999	16.32	2.5	1258		668	27.91	37.81	6.6
12R-2, 140–150	393.70	563	458	34.0	9.684	6.63	972	907	13.66	3.5	1402		783	28.73	37.24	5.7
15R-3, 140–150	424.10	562	456	34.0	10.578	6.55	978	1045	12.90		1480		908	30.15	35.36	6.1
18R-3, 140–150	453.00	564	461	33.5	9.322	6.54	846	1192	13.30	2.5	1464		987	30.58	33.45	5.5
22R-3, 140–150	491.50	566	448	34.0			813	1259	9.29	1.5	1584		1053	30.26	32.21	5.6
26R-4, 140–150	530.40	563	450	33.5		7.60	777	1160	10.04	1.5	1686		1050	31.45	29.97	4.6
30R-3, 140–150	568.60	567	464	33.0	8.405	6.60	681	1293	9.47	0.5	1854		1074	30.85	28.49	4.9
33R-3, 140–150	597.50	567	462	33.0	7.540	6.62	609	1426	7.37	1.0	1926		1050	30.57	26.98	5.4
36R-3, 140–150	626.50	572	466		6.850	6.67	653	1279	5.22	0.5	2055		1100	32.03	23.71	4.0
39R-3, 140–150	655.50	574	473	32.5	4.582	7.44	530	1363	5.18	0.5			1118	34.34	21.14	4.1
42R-1, 140–150	681.50	564		33.0			518	1363	5.35		2152		1112	31.92	17.11	4.1
45R-3, 140–150	703.70	566					608	1200	6.67		2108		1090	29.57	17.52	3.4
49R-3, 130–150	741.90	564					471	1142	7.18		2000		946	32.17	19.09	4.1
53R-4, 130–150	772.14						383	933		2.5						

indicates the presence of solid-phase silica near 400 mbsf. Although rare, radiolarians and sponge spicules occur in Core 154-925A-15R (≈420 mbsf) and in Cores 154-925C-35X and -36X (≈320–340 mbsf). The pronounced low values above 400 mbsf reflect intense dissolution of any minor silica originally deposited within the upper sediment section. The rare siliceous microfossils observed at these levels presumably represent the last remnants of this deposit. The peak in alkalinity and a low in pH around 400 mbsf coincide with the peak in dissolved silica, suggesting that organic carbon inputs to the sediments may also have been greater at the time the siliceous sediments were deposited.

Sulfate decreases downhole, and ammonium increases to 600 mbsf and then decreases below that depth (Fig. 24), with the two profiles highly negatively correlated (r = –0.97; Fig. 25). Although sulfate decreases by 60% over the sampled sequence, it is never fully reduced. This is consistent with the observation that methane concentrations were near background levels throughout the cored sequence. Ammonium is a byproduct of organic matter degradation; thus, it would be expected to increase systematically with decreasing sulfate (Gieskes, 1981). The downcore gradients of these species vary throughout the section, with the rate of change of concentration with depth greatest in the top 100 mbsf of the section and deeper than about 400 mbsf. This suggests that organic carbon degradation is actively occurring in the deeper part of the section, as well as in the shallowest sediments at Site 925.

Dissolved manganese concentrations increase sharply from seawater values at the surface to 113 µM at 4.45 mbsf. Values then decrease to 21.0 µM by 14.45 mbsf and remain low throughout the remainder of the stratigraphic section (see Fig. 24 for the entire profile and Fig. 26 for an expanded view of the top 100 mbsf). This profile is consistent with a manganese redox boundary within the top meter of the sediment column. This boundary was observed by the sedimentologists as a distinct dark crust near the top of the section. The rapid increase in manganese in the pore waters reflects reduction and dissolution of solid-phase manganese below 1 mbsf and diffusion though the sedimentary column.

Strontium concentrations increase from a near-seawater value of 94 µM near the sediment-water interface to a maximum of 2152 µM at 681.50 mbsf; then they decrease slightly to 2000 µM in our deepest sample at 741.90 mbsf (Fig. 24). The strontium maximum here is unusually high, although even greater concentrations were measured on samples from DSDP Site 370 in the eastern Atlantic Ocean (Couture et al., 1977). The high strontium values indicate calcite recrystallization within the section. Consistent with this interpretation, highly recrystallized microfossils occur in the chalks and limestones of Unit III, and Section 154-925A-69R-4 of Subunit IIIB contains locally sparry calcite.

Phosphate exhibits a rapid decrease to values below the analytical detection limit by 11 mbsf (Fig. 27), and thus was not measured in samples recovered from deeper than 50 mbsf. The profile is consistent with the diffusion of phosphate into the sediments from bottom waters, with little contribution of phosphate released from the degradation of organic matter in the sediments.

Lithium pore-water values increase steadily from near seawater values of about 94 µM at the top of the section to about 1118 µM by 655.50 mbsf (Fig. 24). Lithium concentrations remain near 1000 µM to our deepest sample at 741.90 mbsf. Although the dissolution of biogenic silica has been suggested as a source of lithium to the pore waters (Gieskes, 1981), the lithium and silica profiles are actually quite different at Site 925 and at other pelagic sites as well (Leg 130, Kroenke, Berger, Janecek, et al., 1991; Leg 145, Rea, Basov, Janecek, Palmer-Julson, et al., 1993). High pore-water lithium concentrations in the range of those measured at Site 925 were determined in samples from the Guaymas Basin and from the Peru continental slope and are considered to have a nonsedimentary source, alteration of continental and oceanic crust (Gieskes et al., 1982; Martin et al., 1991).

Calcium concentrations increase (3.65 mM/100 m) whereas magnesium concentrations decrease (–4.69 mM/100 m) over the top 655.5 m (Fig. 24). These profiles reflect alteration of basement, with magnesium replacing calcium in altered basement rocks. Magnesium concentrations decrease faster than calcium concentrations increase near the top of the section; deeper in the section calcium values increase faster than magnesium values decrease. Calcium and magnesium are highly negatively correlated ($r = -0.92$), but the relationship breaks down at the bottom of the section.

Potassium concentrations decrease with depth from 11.6 mM at 1.45 mbsf to 4.1 mM at 741.90 mbsf (Fig. 24), presumably also because of the uptake of potassium during basement alteration.

In summary, the biogenic sediments are the primary influence on many of the chemical gradients in the interstitial waters at this site. Alteration reactions in the underlying basalt and subsequent diffusion through the sediment column control several profiles as well. The redox state of the sediments is intermediate, with manganese reduction occurring within the top meter of the section and sulfate never entirely depleted in the pore water. This reflects reduction of a moderate organic carbon input to the site. The high strontium values indicate that recrystallization has affected the biogenic carbonate component of the sediments. The high silica and alkalinity contents of the pore waters deeper in the section suggest that biogenic silica was a more important component of the original sedimentary deposits than is obvious by visual inspection of the cores. Calcium, magnesium, and lithium profiles appear to be generally controlled by the alteration of basalt and subsequent diffusion to the sediment-water interface.

Solid-phase Geochemistry

A total of 358 samples were measured for calcium carbonate content, comprising approximately a 3-m sampling interval from one complete stratigraphic section at Site 925 (Table 9). Three sets of closely spaced samples were analyzed from Cores 154-925A-38R, 154-925C-25H, and 154-925E-6H to compare with high-resolution physical properties, magnetic susceptibility, and color reflectance data. A subset of 140 samples was measured for total carbon, nitrogen, and sulfur content (Table 9).

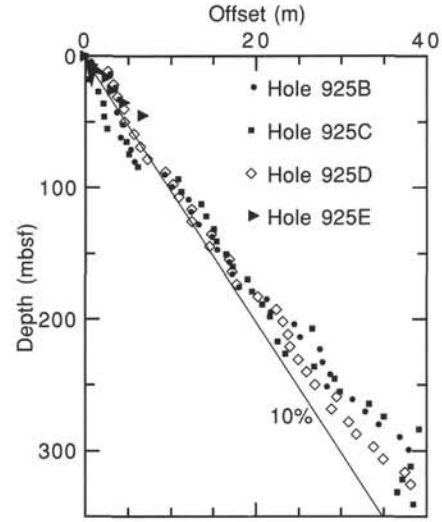

Figure 19. Depth offsets of successive cores on the mcd scale relative to mbsf depth, indicating the "growth" of the composite depth scale with increasing depth.

Calcium carbonate is the dominant sedimentary component, ranging from 50% to 80% throughout most of the sedimentary section cored at Site 925 (Fig. 28). Terrigenous material, most of which is derived from the Amazon River outflow, comprises the bulk of the noncarbonate portion of the sediments. Several broad-scale features are apparent in the carbonate concentration data. A significant decrease in the mean content is observed over the top 75 m of Site 925 (0–2.3 Ma), and near 300, 450, and 800 mbsf. These same features are evident in the 5-cm-spaced measurements of color reflectance (Fig. 28), so they do not represent a sampling bias in the carbonate data. The decrease in carbonate content over the Pleistocene is one of the more prominent features of the record, and the mean concentration (about 34%) over the top 20 m is lower than any other interval cored. Because the sedimentation rates are not drastically different in the late Pliocene to Pleistocene (see "Sedimentation Rates" section, this chapter), the decrease in content cannot be attributed to a simple dilution by terrigenous material (see "Accumulation Rates" section below). Two of the sections with a lower mean carbonate content (near 300 and 800 mbsf) correspond to intervals in which preservation of calcareous microfossils is poorer than in other parts of the cored section (see "Biostratigraphy" section, this chapter). Although worse preservation was not apparent near 450 mbsf, this interval contains rare siliceous microfossils, elevated silica concentrations, and alkalinity in the pore waters (Fig. 24), and large shifts in the physical properties data. This interval also contains the highest organic carbon and sulfur contents of samples measured at this site (Fig. 28). Our preliminary interpretation is that this sediment accumulated during a period of greater productivity when the biogenic flux included significant amounts of siliceous microfossils, most of which have since dissolved away.

Except for a few samples in the intervals of lower calcium carbonate content, the organic carbon, as measured for the difference of total carbon and carbonate carbon, is below 0.4%. In fact, many of the samples have concentrations below the detection limits of the technique and the difference between total carbon and carbonate carbon yielded negative values. Two of the samples with elevated organic carbon and sulfur levels were from discrete dark layers at 448.5 and 453.7 mbsf. Sulfur was only significant in samples from lithologic

Table 9. Concentrations of inorganic (carbonate) carbon, calcium carbonate, total carbon, organic carbon (total – inorganic), nitrogen, and sulfur in samples from Holes 925A, 925B, 925C, and 925E.

Core, section, interval (cm)	Depth (mbsf)	Inorganic carbon (%)	$CaCO_3$ (%)	Total carbon (%)	Organic carbon (%)	Nitrogen (%)	Sulfur (%)
154-925A-							
3R-1, 56–57	304.26	6.08	50.66				
3R-1, 78–79	304.48	7.89	65.75	7.88	0.00	0.00	0.00
3R-1, 105–106	304.75	6.77	56.41	6.82	0.05	0.06	0.00
3R-1, 112–114	304.82	8.78	73.16				
3R-2, 31–32	305.51	8.15	67.91				
3R-3, 88–90	307.58	7.73	64.41	7.62	0.00	0.00	0.00
4R-1, 48–50	314.18	9.02	75.14	8.77	0.00	0.00	0.00
4R-2, 28–30	315.48	8.56	71.30	8.49	0.00	0.00	0.00
4R-3, 75–77	317.45	7.77	64.72	7.74	0.00	0.00	0.00
4R-4, 62–64	318.82	9.79	81.55	9.74	0.00	0.00	0.00
4R-4, 100–102	319.20	8.35	69.56	8.26	0.00	0.00	0.00
4R-5, 26–28	319.96	8.85	73.72	8.62	0.00	0.00	0.00
4R-6, 99–101	322.19	8.95	74.55	8.92	0.00	0.00	0.00
4R-7, 21–23	322.91	9.28	77.30	9.14	0.00	0.00	0.00
5R-1, 47–49	323.87	8.76	72.97	8.65	0.00	0.00	0.00
5R-3, 86–88	327.26	8.89	74.05	8.74	0.00	0.00	0.00
5R-5, 68–70	330.08	9.81	81.72	9.69	0.00	0.00	0.00
6R-1, 55–57	333.65	3.86	32.15	3.87	0.01	0.00	0.00
6R-2, 103–105	335.63	8.86	73.80	8.75	0.00	0.00	0.00
6R-3, 12–13	336.22	6.03	50.23	5.94	0.00	0.00	0.00
6R-3, 75–77	336.85	9.47	78.89	9.13	0.00	0.00	0.00
7R-1, 43–45	343.13	8.32	69.31	8.38	0.06	0.00	0.00
7R-3, 40–42	346.10	9.11	75.89	8.96	0.00	0.00	0.00
7R-5, 97–99	349.67	8.87	73.89	8.79	0.00	0.00	0.00
8R-1, 121–123	353.61	8.90	74.14				
8R-3, 82–84	356.22	9.67	80.55	9.75	0.08	0.00	0.00
8R-5, 146–148	359.86	9.45	78.72				
9R-1, 28–30	362.28	5.28	43.98				
9R-3, 14–16	365.14	6.92	57.64	6.91	0.00	0.00	0.00
9R-5, 45–47	368.45	7.72	64.31				
10R-1, 10–12	371.80	7.39	61.56				
10R-1, 134–136	373.04	9.72	80.97	9.78	0.06	0.00	0.00
10R-2, 128–130	374.48	10.17	84.72				
11R-1, 22–24	381.52	10.16	84.63				
11R-3, 81–83	385.11	7.69	64.06	7.62	0.00	0.00	0.00
11R-5, 69–71	387.99	7.29	60.73				
12R-1, 36–38	391.16	7.15	59.56				
12R-2, 31–33	392.61	10.49	87.38	10.42	0.00	0.00	0.00
12R-3, 122–124	395.02	8.48	70.64				
13R-1, 39–41	400.79	10.18	84.80				
13R-2, 2–4	401.42	7.80	64.97	7.70	0.00	0.00	0.00
13R-2, 68–70	402.08	9.44	78.64				
14R-2, 30–32	410.56	8.63	71.89				
14R-3, 34–36	412.10	8.87	73.89	8.80	0.00	0.00	0.00
14R-5, 28–30	415.04	7.73	64.39				
15R-1, 101–103	420.71	5.42	45.15				
15R-3, 130–132	424.00	8.29	69.06	8.44	0.15	0.00	0.00
15R-5, 92–94	426.62	10.15	84.55				
15R-6, 35–37	427.55	9.53	79.38	9.45	0.00	0.00	0.00
16R-1, 33–35	429.63	5.33	44.40	5.25	0.00	0.00	0.07
16R-1, 108–110	430.38	10.42	86.80				
16R-2, 89–91	431.69	9.04	75.30	8.93	0.00	0.00	0.00
16R-3, 130–132	433.60	5.14	42.83	5.40	0.26	0.00	0.00
16R-5, 69–71	435.99	9.31	77.55				
17R-1, 98–100	439.88	9.42	78.47				
17R-3, 59–61	442.49	7.96	66.30	7.92	0.00	0.00	0.00
17R-3, 124–126	443.14	6.95	57.89	6.86	0.00	0.00	0.48
17R-5, 56–58	445.46	6.79	56.56				
17R-7, 59–60	447.99	0.50	4.17	1.54	1.04	0.10	1.22
18R-1, 65–67	449.25	9.18	76.47				
18R-3, 93–95	452.53	8.72	72.64	8.75	0.03	0.00	0.00
18R-4, 59–61	453.69	0.79	6.58	1.71	0.92	0.07	0.39
18R-5, 114–116	455.74	7.52	62.64				
19R-2, 61–63	458.88	8.79	73.22				
19R-3, 69–71	460.46	8.51	70.89	8.42	0.00	0.00	0.00
19R-4, 70–72	461.97	7.12	59.31				
20R-1, 62–64	468.42	9.23	76.89				
20R-3, 118–120	471.98	8.94	74.47	8.94	0.00	0.00	0.00
20R-5, 105–107	474.85	5.92	49.31	6.10	0.18	0.05	0.00
22R-1, 39–41	487.49	8.77	73.05				
22R-3, 35–37	490.45	7.76	64.64	7.78	0.02	0.00	0.00
22R-5, 44–46	493.54	7.42	61.81				
23R-1, 12–14	496.82	6.38	53.15				
23R-3, 75–77	500.45	8.99	74.89	9.02	0.03	0.00	0.00
23R-4, 75–77	501.95	8.97	74.72				
24R-1, 76–78	507.06	5.81	48.40				
24R-3, 86–88	510.16	7.32	60.98	7.39	0.07	0.00	0.57
24R-5, 144–146	513.74	7.50	62.48				
26R-2, 8–10	526.08	8.28	68.97				
26R-3, 132–134	528.82	8.18	68.14	8.27	0.09	0.00	0.00
26R-5, 130–132	531.80	8.87	73.89				
27R-1, 23–25	535.53	7.50	62.48				
27R-3, 81–83	539.11	9.11	75.89	9.05	0.00	0.00	0.00
27R-5, 118–120	542.48	9.22	76.80				
29R-1, 38–40	554.98	8.94	74.47				

Table 9 (continued).

Core, section, interval (cm)	Depth (mbsf)	Inorganic carbon (%)	$CaCO_3$ (%)	Total carbon (%)	Organic carbon (%)	Nitrogen (%)	Sulfur (%)
29R-1, 88–90	555.48	7.54	62.81	7.51	0.00	0.00	0.42
29R-2, 6–8	556.16	9.30	77.47				
30R-1, 28–30	564.48	8.99	74.89				
30R-3, 53–55	567.73	5.74	47.81	5.80	0.06	0.00	0.22
30R-5, 50–52	570.70	9.84	81.97				
31R-1, 47–49	574.27	10.22	85.13				
31R-1, 106–108	574.86	8.09	67.39	8.02	0.00	0.00	0.45
31R-2, 48–50	575.78	8.92	74.30				
32R-1, 130–132	584.80	9.28	77.30				
32R-3, 38–40	586.88	8.91	74.22	8.83	0.00	0.00	0.11
32R-5, 34–36	589.84	7.70	64.14				
33R-1, 95–97	594.05	8.00	66.64				
33R-3, 72–74	596.82	9.91	82.55	9.69	0.00	0.00	0.00
33R-5, 45–47	599.55	10.21	85.05				
34R-1, 74–76	603.54	7.98	66.47				
34R-3, 80–82	606.60	7.70	64.14	7.72	0.02	0.00	0.71
34R-5, 36–38	609.16	10.46	87.13				
35R-1, 107–109	613.47	8.92	74.30				
35R-3, 120–122	616.60	8.68	72.30	8.65	0.00	0.00	0.15
36R-1, 122–124	623.32	9.84	81.97				
36R-3, 14–16	625.24	9.43	78.55	9.57	0.14	0.00	0.06
36R-5, 50–52	628.60	8.39	69.89				
36R-5, 105–107	629.15	9.04	75.30				
38R-1, 23–25	641.63	9.23	76.89				
38R-1, 128–130	642.68	8.27	68.89				
38R-2, 51–53	643.41	8.85	73.72				
38R-2, 129–131	644.19	8.36	69.64				
38R-3, 28–30	644.68	7.40	61.64				
38R-3, 76–78	645.16	10.05	83.72	9.95	0.00	0.00	0.00
38R-3, 81–81	645.21	10.06	83.80				
38R-4, 3–3	645.93	6.26	52.15	6.32	0.06	0.00	0.12
38R-4, 47–49	646.37	9.09	75.72				
38R-4, 118–120	647.08	8.28	68.97				
38R-4,146–146	647.36	7.16	59.64				
38R-5, 24–26	647.64	8.46	70.47				
38R-5, 30–30	647.70	8.77	73.05				
38R-5, 115–117	648.55	10.03	83.55				
38R-5, 122–122	648.62	10.17	84.72				
38R-6, 24–26	649.14	10.72	89.30				
38R-6, 31–31	649.21	10.89	90.71				
38R-6, 72–72	649.62	8.17	68.06				
38R-6, 125–127	650.15	9.09	75.72				
38R-7, 5–7	650.45	9.88	82.30				
39R-1, 86–88	651.96	9.51	79.22				
39R-3, 117–119	655.27	6.65	55.39	6.70	0.05	0.00	0.00
39R-5, 49–51	657.59	8.39	69.89				
40R-1, 134–136	662.14	9.84	81.97				
40R-3, 58–60	664.38	6.74	56.14	6.72	0.00	0.06	0.20
40R-5, 59–61	667.39	10.57	88.05				
41R-1, 51–53	670.91	8.84	73.64				
41R-2, 71–73	672.61	7.46	62.14				
41R-3, 71–73	673.61	10.30	85.80	10.19	0.00	0.00	0.09
42R-1, 20–22	680.30	9.73	81.05				
42R-1, 91–93	681.01	9.70	80.80	9.69	0.00	0.00	0.00
42R-2, 45–47	682.05	9.44	78.64				
43R-1, 128–130	684.38	9.37	78.05				
43R-3, 65–67	686.75	9.29	77.39	9.29	0.00	0.00	0.16
43R-4, 84–86	688.44	10.50	87.47				
44R-1, 52–54	690.22	10.37	86.38				
44R-3, 43–45	693.13	7.55	62.89	7.58	0.03	0.00	0.13
44R-4, 80–82	695.00	7.62	63.47				
45R-1, 76–78	700.06	10.05	83.72				
45R-3, 130–132	703.60	8.32	69.31	8.33	0.01	0.00	0.61
45R-5, 134–136	706.64	8.35	69.56				
46R-1, 93–95	709.93	7.63	63.56				
46R-3, 71–73	712.71	9.38	78.14	9.15	0.00	0.00	0.00
46R-5, 108–110	716.08	8.12	67.64				
47R-1, 14–16	718.44	8.64	71.97				
47R-3, 30–32	721.60	8.47	70.56	8.36	0.00	0.00	0.00
47R-5, 84–86	725.14	9.18	76.47				
48R-1, 124–126	729.14	8.35	69.56				
48R-3, 144–146	732.34	7.81	65.06	7.76	0.00	0.00	0.00
48R-5, 92–94	734.82	7.04	58.64				
49R-1, 142–144	739.02	7.43	61.89				
49R-3, 63–65	741.23	7.47	62.23	7.54	0.07	0.00	0.06
49R-5, 4–6	743.64	7.49	62.39				
50R-1, 37–39	746.47	7.27	60.56	7.32	0.05	0.00	0.14
50R-2, 43–45	748.03	7.40	61.64				
51R-1, 72–73	747.82	8.32	69.31				
51R-3, 65–66	750.75	7.74	64.47	7.70	0.00	0.00	0.00
51R-5, 62–64	753.22	6.63	55.23				
52R-1, 74–75	757.74	5.97	49.73				
52R-3, 7–8	760.07	7.69	64.06	7.63	0.00	0.00	0.00
52R-5, 19–20	763.19	7.31	60.89				
53R-1, 114–116	767.74	7.18	59.81				
53R-3, 96–98	770.30	7.56	62.97	7.56	0.00	0.00	0.00
53R-5, 126–128	773.60	6.91	57.56				
54R-2, 110–111	778.90	6.01	50.06				
54R-4, 145–146	782.25	7.43	61.89	7.61	0.18	0.00	0.00
54R-6, 65–66	784.45	8.94	74.47				

Table 9 (continued).

Core, section, interval (cm)	Depth (mbsf)	Inorganic carbon (%)	$CaCO_3$ (%)	Total carbon (%)	Organic carbon (%)	Nitrogen (%)	Sulfur (%)
55R-1, 85–86	786.85	9.62	80.13				
55R-3, 54–55	789.54	8.33	69.39	8.41	0.08	0.00	0.00
55R-5, 112–113	793.12	7.50	62.48				
56R-1, 75–77	796.35	6.33	52.73				
56R-3, 75–77	799.35	6.69	55.73	6.97	0.28	0.00	0.10
56R-6, 73–75	803.83	6.58	54.81				
57R-1, 24–25	805.44	5.31	44.23				
57R-3, 117–118	809.37	6.71	55.89	6.63	0.00	0.00	0.00
57R-5, 25–26	811.45	6.19	51.56				
58R-1, 54–55	815.34	5.57	46.40				
58R-3, 66–68	818.46	6.29	52.40	6.24	0.00	0.00	0.19
58R-5, 73–74	821.53	8.11	67.56				
59R-1, 90–92	825.40	6.92	57.64	6.77	0.00	0.00	0.00
59R-3, 23–25	827.73	6.14	51.15				
59R-5, 108–110	831.58	8.12	67.64				
60R-1, 86–87	835.06	7.33	61.06				
60R-3, 25–26	837.45	7.23	60.23	7.16	0.00	0.00	0.00
60R-5, 63–64	840.83	6.92	57.64				
61R-1, 117–118	844.97	8.82	73.47				
61R-3, 58–59	847.38	4.82	40.15	4.89	0.07	0.00	0.20
61R-5, 28–29	850.08	8.44	70.31				
62R-1, 69–71	854.19	7.04	58.64				
62R-3, 88–89	857.38	6.77	56.39	6.82	0.05	0.00	0.08
62R-5, 91–92	860.41	8.05	67.06				
63R-1, 108–110	864.18	8.54	71.14				
63R-3, 124–125	867.34	9.01	75.05	8.84	0.00	0.00	0.00
63R-5, 15–16	869.25	7.43	61.89				
64R-1, 29–30	873.09	7.97	66.39				
64R-3, 54–55	876.34	7.87	65.56	7.65	0.00	0.00	0.00
64R-5, 139–141	880.19	8.69	72.39				
65R-1, 17–18	882.67	7.72	64.31				
65R-2, 37–39	884.37	7.37	61.39				
65R-3, 68–69	886.18	7.07	58.89	6.89	0.00	0.00	0.00
66R-1, 91–92	892.71	6.87	57.23	6.77	0.00	0.00	0.00
67R-1, 125–127	902.65	8.33	69.39				
67R-3, 125–127	905.65	7.54	62.81				
67R-5, 95–97	908.35	7.73	64.41				
69R-1, 145–146	922.15	9.91	82.58				
69R-3, 58–60	924.28	9.27	77.25	9.08	0.00	0.00	0.00
69R-5, 137–138	928.07	10.15	84.58				
154-925B-							
1H-1, 91–92	0.91	3.16	26.32	3.27	0.11	0.00	0.00
1H-3, 36–37	3.36	2.94	24.49	3.04	0.10	0.00	0.00
2H-1, 33–35	4.83	2.81	23.41				
2H-1, 103–104	5.53	2.83	23.57	3.13	0.30	0.00	0.00
2H-3, 56–57	8.06	4.80	39.98	5.14	0.34	0.00	0.00
2H-5, 52–53	11.02	3.69	30.74	3.70	0.01	0.00	0.00
2H-5, 76–77	11.26	3.93	32.74				
3H-1, 127–128	15.27	4.28	35.65	4.10	0.00	0.00	0.00
3H-3, 77–78	17.77	5.69	47.40	5.81	0.12	0.00	0.00
3H-5, 77–78	20.77	6.37	53.06	6.42	0.05	0.00	0.00
4H-1, 75–76	24.25	4.09	34.07	4.31	0.22	0.00	0.00
4H-3, 76–77	27.26	3.67	30.57	3.92	0.25	0.00	0.00
4H-5, 76–77	30.26	8.33	69.39	8.37	0.04	0.00	0.00
5H-1, 77–79	33.77	5.84	48.65	6.09	0.25	0.00	0.00
5H-3, 77–79	36.77	4.48	37.32	4.29	0.00	0.00	0.00
5H-6, 41–43	40.91	4.72	39.32	4.91	0.19	0.00	0.00
6H-2, 103–104	45.03	7.91	65.89	7.94	0.03	0.00	0.00
6H-4, 76–77	47.76	8.30	69.14	8.47	0.16	0.00	0.00
6H-6, 100–101	51.00	6.16	51.31	6.32	0.16	0.00	0.00
7H-1, 78–79	52.78	5.29	44.07	5.42	0.13	0.00	0.00
7H-3, 21–22	55.21	7.85	65.39	8.11	0.26	0.00	0.00
7H-5, 77–78	58.77	5.54	46.15	5.84	0.30	0.00	0.00
8H-1, 77–78	62.27	5.46	45.48	5.50	0.04	0.00	0.00
8H-3, 77–78	65.27	6.42	53.48	6.39	0.00	0.00	0.00
8H-5, 41–42	67.91	7.90	65.81	8.10	0.20	0.00	0.00
9H-1, 43–44	71.43	7.67	63.89	8.03	0.36	0.00	0.00
9H-3, 78–79	74.78	6.91	57.56	6.87	0.00	0.00	0.00
9H-5, 126–127	78.26	5.21	43.40	5.19	0.00	0.00	0.00
10H-1, 75–76	81.25	6.64	55.31	6.78	0.14	0.00	0.00
10H-3, 14–15	83.64	8.49	70.72	8.34	0.00	0.00	0.00
10H-5, 12–13	86.62	6.59	54.89	6.55	0.00	0.00	0.00
11H-1, 34–35	90.34	7.13	59.39	7.22	0.09	0.00	0.00
11H-3, 107–108	94.07	7.71	64.22	7.67	0.00	0.00	0.00
11H-5, 52–53	96.52	8.40	69.97	8.71	0.31	0.00	0.00
12H-1, 63–64	100.13	6.96	57.98				
12H-3, 17–18	102.67	7.99	66.56	8.07	0.08	0.00	0.00
12H-5, 41–42	105.91	7.21	60.06				
12H-7, 29–30	108.79	6.73	56.06				
13H-1, 88–89	109.88	7.88	65.64				
13H-3, 69–70	112.69	7.26	60.48	7.31	0.05	0.00	0.00
13H-5, 65–67	115.65	7.74	64.47				
14H-1, 33–34	118.83	7.74	64.47				
14H-3, 125–126	122.75	6.64	55.31	6.81	0.17	0.00	0.00
14H-5, 93–94	125.43	8.54	71.14				
15H-1, 78–79	128.78	8.39	69.89				
15H-3, 77–78	131.77	10.27	85.55	10.24	0.00	0.00	0.00
15H-5, 78–79	134.78	10.02	83.47				
16H-1, 75–76	138.25	10.27	85.55				

Table 9 (continued).

Core, section, interval (cm)	Depth (mbsf)	Inorganic carbon (%)	$CaCO_3$ (%)	Total carbon (%)	Organic carbon (%)	Nitrogen (%)	Sulfur (%)
16H-3, 115–116	141.65	8.36	69.64	8.53	0.17	0.00	0.00
16H-5, 75–76	144.25	7.93	66.06				
17H-1, 108–109	148.08	8.85	73.72				
17H-3, 69–70	150.69	8.02	66.81	7.90	0.00	0.00	0.00
17H-5, 53–54	153.53	9.26	77.14				
18H-1, 78–79	157.28	7.05	58.73				
18H-3, 106–107	160.56	8.95	74.55	9.09	0.14	0.00	0.00
18H-5, 121–122	163.71	7.65	63.72				
19H-1, 134–135	167.34	8.13	67.72				
19H-3, 132–133	170.32	9.00	74.97	9.08	0.08	0.00	0.00
19H-5, 132–133	173.32	9.22	76.80				
20H-1, 129–130	176.79	8.63	71.89				
20H-3, 90–91	179.40	10.03	83.55	10.01	0.00	0.00	0.00
20H-5, 47–48	181.97	7.71	64.22				
21H-1, 127–128	186.27	7.65	63.72				
21H-3, 135–136	189.35	8.74	72.80	8.77	0.03	0.00	0.00
21H-5, 137–138	192.37	7.76	64.64				
22H-1, 120–121	195.70	9.10	75.80				
22H-3, 50–51	198.00	8.18	68.14	8.28	0.10	0.00	0.00
22H-5, 125–126	201.75	9.09	75.72				
23H-1, 86–87	204.86	7.29	60.73				
23H-3, 33–34	207.33	7.17	59.73	7.20	0.03	0.00	0.00
23H-4, 57–58	209.07	9.85	82.05				
23H-5, 6–7	210.06	10.07	83.88				
23H-5, 46–47	210.46	7.72	64.31				
23H-6, 47–48	211.97	7.74	64.47				
23H-6, 132–133	212.82	9.01	75.05				
23H-7, 58–59	213.58	9.76	81.30				
24H-1, 45–46	213.95	9.98	83.13				
24H-3, 97–98	217.47	9.41	78.39	9.49	0.08	0.00	0.00
25H-1, 106–107	224.06	9.90	82.47				
25H-3, 100–101	227.00	8.01	66.72	7.88	0.00	0.00	0.00
25H-5, 91–92	229.91	9.72	80.97				
26H-1, 60–61	233.10	9.54	79.47				
26H-3, 116–117	236.66	9.72	80.97	8.86	0.00	0.00	0.00
26H-6, 135–136	241.35	8.25	68.72				
27H-1, 44–45	242.44	10.13	84.38				
27H-3, 130–131	246.30	6.08	50.65	6.27	0.19	0.00	0.00
27H-5, 70–71	248.70	9.66	80.47				
27H-6, 20–21	249.70	9.77	81.38				
27H-6, 133–134	250.83	9.92	82.63				
28H-1, 55–57	252.05	9.60	79.97				
28H-3, 56–58	255.06	9.69	80.72	9.74	0.05	0.00	0.00
28H-5, 52–54	258.02	8.83	73.55				
29H-1, 78–79	261.78	9.71	80.88				
29H-1, 95–96	261.95	8.72	72.64				
29H-3, 78–79	264.78	8.54	71.14	8.69	0.15	0.00	0.00
29H-3, 109–111	265.09	7.19	59.89				
29H-5, 78–79	267.78	8.78	73.14				
29H-5, 90–91	267.90	8.65	72.05				
30H-1, 64–65	271.14	7.29	60.73				
30H-3, 86–87	274.36	7.62	63.47	7.58	0.00	0.00	0.00
30H-5, 112–113	277.62	7.95	66.22				
31H-1, 132–133	281.32	4.91	40.90				
31H-3, 64–65	283.64	7.75	64.56	7.69	0.00	0.00	0.00
31H-5, 128–129	287.28	6.66	55.48				
32H-1, 139–140	290.89	7.75	64.56				
32H-3, 68–69	293.18	8.40	70.00	8.34	0.00	0.00	0.00
32H-5, 132–133	296.82	7.90	65.81				
33H-1, 108–109	300.08	7.22	60.14				
33H-3, 28–29	302.28	7.32	60.98	7.43	0.11	0.00	0.00
33H-5, 49–50	305.49	7.84	65.31				
34H-1, 107–108	309.57	8.54	71.14				
34H-3, 148–149	312.98	4.44	36.99	4.69	0.25	0.00	0.00
34H-5, 133–134	315.83	8.99	74.89				
154-925C-							
25H-3, 6–8	229.56	8.60	71.64				
25H-3, 19–21	229.69	10.02	83.47				
25H-3, 29–31	229.79	8.77	73.05				
25H-3, 45–47	229.95	7.15	59.56				
25H-3, 61–63	230.11	9.79	81.55				
25H-3, 79–81	230.29	8.45	70.39				
25H-3, 98–100	230.48	10.16	84.63				
25H-3, 116–118	230.66	9.54	79.47				
25H-3, 132–134	230.82	9.69	80.72				
25H-4, 2–4	231.02	10.43	86.88				
25H-4, 17–19	231.17	9.66	80.47				
25H-4, 40–42	231.40	10.17	84.72				
25H-4, 61–63	231.61	8.49	70.72				
25H-4, 76–78	231.76	10.24	85.30				
25H-4, 89–91	231.89	8.63	71.89				
25H-4, 104–106	232.04	9.25	77.05				
25H-4, 118–120	232.18	8.70	72.47				
25H-4, 138–140	232.38	9.76	81.30				
154-925E-							
6H-5, 9–11	51.09	4.34	36.15				
6H-5, 24–26	51.24	4.76	39.65				
6H-5, 39–41	51.39	4.91	40.90				
6H-5, 58–60	51.58	7.51	62.56				

Table 9 (continued).

Core, section, interval (cm)	Depth (mbsf)	Inorganic carbon (%)	$CaCO_3$ (%)	Total carbon (%)	Organic carbon (%)	Nitrogen (%)	Sulfur (%)
6H-5, 72–74	51.72	6.96	57.98				
6H-5, 90–92	51.90	4.58	31.15				
6H-5, 101–103	52.01	5.24	43.65				
6H-5, 115–117	52.15	4.65	38.73				
6H-5, 130–132	52.30	6.48	53.98				
6H-5, 142–144	52.42	7.01	58.39				

Unit III. This may reflect a sampling bias, as pyrite was observed throughout the cored sequence (see "Lithostratigraphy" section, this chapter) and significant sulfate reduction occurs within the top 100 mbsf (Fig. 24).

Comparisons with Reflectance and Magnetic Susceptibility

Magnetic susceptibility and color reflectance measurements were the primary data used to construct the composite stratigraphic sections for Site 925 (see "Composite Depths" section, this chapter). Variations in these measurements reflect the changing proportions of carbonate to lithogenic material. Figure 29 shows the comparison between the carbonate measurements and reflectance for the samples analyzed. Because the carbonate and reflectance data were used in defining the lithologic units, comparisons for each unit were made separately. Reflectance is linearly correlated to carbonate concentration, with $r = 0.82$, 0.80, and 0.70 for lithologic Units I, II, and III, respectively. However, the overall relationship is curvilinear with greater scatter for the lower reflectance values. This scatter is particularly significant in Unit III, where reflectance values of 20%–30% have associated calcium carbonate contents of 35%–80%.

Magnetic susceptibility also exhibits a high correlation with carbonate (Fig. 30), with higher values corresponding to low $CaCO_3$. The relationship appears to be more linear than that of carbonate and reflectance. The calcium carbonate is inversely correlated to magnetic susceptibility, with $r = -0.83$, -0.81, and -0.70 for lithologic Units I, II, and III, respectively.

Three sets of closely spaced samples document a high degree of correlation among $CaCO_3$ concentration, magnetic susceptibility, and reflectance in each of the lithologic units (Figs. 31A through 31C). To a first order, the density changes exhibit the same variations. The density relationships are discussed in greater detail in the "Physical Properties" section (this chapter). The correlation of carbonate to either magnetic susceptibility or reflectance is much greater when a smaller lithologic range is considered rather than the whole unit (Figs. 30 and 32; cf. Fig. 29). For example, the linear correlation of $CaCO_3$ to reflectance for Core 154-925E-6H in lithologic Unit I is 0.94, whereas it is 0.82 when samples spaced throughout the unit are considered. This comparison, and the changes in the slope of the linear correlations downsection, suggest that variations in the noncarbonate component need to be considered in the estimation of calcium carbonate from either the magnetic susceptibility or color reflectance data.

Accumulation Rates

The age model for Site 925, based on recognized biostratigraphic datums (see "Biostratigraphy" section, this chapter), was used to determine the mass accumulation rate (MAR) of the carbonate and noncarbonate sediment components (Fig. 33). Because the biostratigraphic age model provides the long-term (10^5 to 10^6 yr) changes in sedimentation rate, only the large-scale features in the accumulation rates are interpreted. MARs were determined on a subset of 273 of the 358 samples analyzed for calcium carbonate content, corresponding to those with dry-bulk-density measurements either from the same sample or from adjacent samples (see "Physical Properties" section, this chapter).

The mean accumulation rate of calcium carbonate ranges from a low near 10 $g/m^2/yr$ in the latest Pleistocene to a high near 60 $g/m^2/yr$ in the early Oligocene (Fig. 34). These rates are higher than typical pelagic carbonate sites in oligotrophic settings (i.e., western equatorial Pacific; see Kroenke, Berger, Janecek, et al., 1991) and are typical of the rates observed in the Neogene sections cored during ODP Leg 138 in the eastern equatorial Pacific (Mayer, Pisias, Janecek, et al., 1992). The lows in mean calcium carbonate concentration are also evident as accumulation lows. The decrease within the Pleistocene may be related to a decrease in biogenic carbonate production at this site because no significant change in preservation was observed. Consistent with this inference of higher productivity in the early Pleistocene is the observation that foraminifers that exist near the thermocline were more prevalent in the early Pleistocene compared with more recent deposits, suggesting that the thermocline was closer to the surface than at present (see "Biostratigraphy" section, this chapter). In general, the high rates of carbonate accumulation observed throughout the cored sequence is consistent with the observation that, except for a brief interval in the late Miocene, calcareous microfossils are relatively well preserved from the Oligocene to the Pleistocene.

Noncarbonate MAR reflects the input of terrigenous material largely derived from South America. The current source is Amazon River outflow. The increase in accumulation rate beginning near 5 Ma indicates that this source has been enhanced since that time, possibly associated with Andean uplift and erosion within the Pliocene.

PHYSICAL PROPERTIES

Physical properties reflect the initial sediment depositional environment, the type of sediment deposited, and any postdepositional changes related to either stress or diagenesis at Site 925. The variations in physical properties with depth below seafloor also control the seismic character at the site; thus, the physical properties are used to correlate core data with the seismic site survey data. At Site 925, changes in physical properties with depth below seafloor primarily reflect a stress history of gravitational consolidation, with a diagenetic overprint within several intervals.

Physical properties measured at Site 925 include index properties, acoustic compressional-wave velocity, shear strength, resistivity, and natural gamma. Measurement frequency varies from three per core over intervals of multiple holes to two per section within single-hole intervals.

Index Properties

Index properties reported here are bulk density, water content, porosity, dry density, and grain density. These properties represent the mass and volume phase relationships of the pore water and grains in the sediment. Measurement methods are described in the "Physical Properties" section of the "Explanatory Notes" chapter (this volume). All index data reported here are from discrete measurements and do not include bulk-density data from the GRAPE. With the exception of Hole 925D, GRAPE data at Site 925 are an unreliable measure of bulk density because of problems associated with an unstable power supply. In addition, GRAPE data collected within the XCB and RCB intervals of Site 925 are affected by variable sample diameter. The

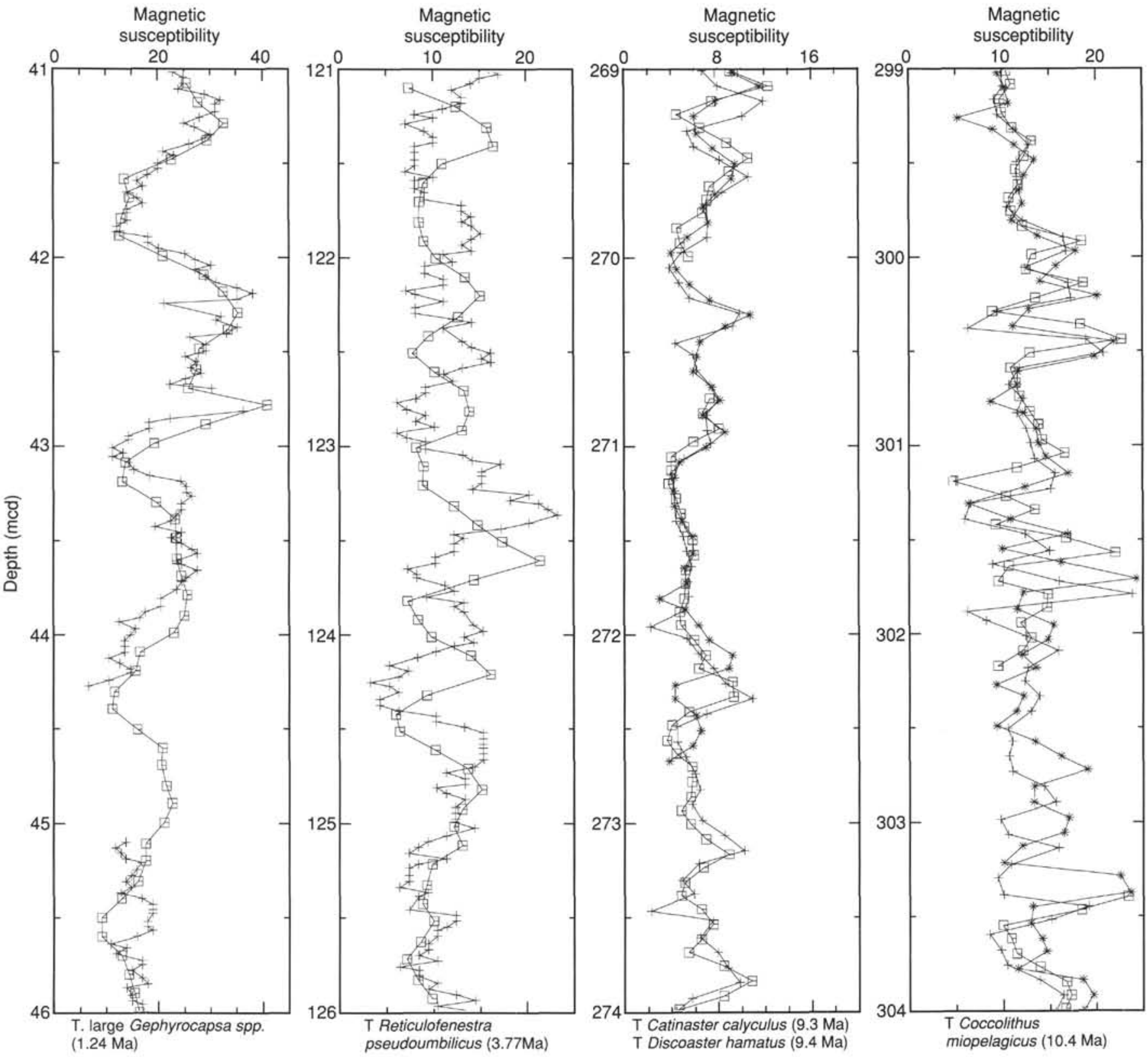

Figure 20. Nannofossil events identified in more than one hole at Site 925 and magnetic susceptibility data on the composite depth scale, providing verification of the composite depth offsets. Hole 925B = open squares, Hole 925C = asterisks, and Hole 925D = plus signs.

XCB and RCB data should never be used for interpretation of sediment bulk density except in rare cases when the liner is truly filled.

Bulk density, porosity, and water content are discussed together as a function of depth below seafloor; grain density and dry density are discussed in terms of lithologic units (see "Lithostratigraphy" section, this chapter). Bulk density generally increases with depth below seafloor, whereas porosity and water content decrease. These general trends vary in the sediment section in two ways: (1) by a change in the slope of the property-depth function, and (2) by offsets in the index property at specific depth intervals. Changes of the first type are normally associated with a change in sedimentation rates, whereas variations of the second kind are associated with diagenetic boundaries or unconformities.

At Site 925, bulk density shows a general increase with depth below seafloor from 1.5 Mg/m^3 at the seafloor to 2.35 Mg/m^3 at 928 mbsf, near the base of Hole 925A, whereas porosity and water content (expressed as percentage of dry mass) decrease from around 75% and 110% to around 15% and 8%, respectively (Fig. 35). Several changes in the index property gradients with depth occur throughout the section. These changes in gradients are usually bounded by offsets that roughly correlate with the boundaries between lithologic units (see "Lithostratigraphy" section, this chapter) and with changes in sedimentation rates (see "Biostratigraphy" section, this chapter). The changes appear most pronounced in the bulk-density profile, but they can also be seen in the porosity and water content data.

In the upper 20 m of the sediment column, within lithologic Subunit IA (nannofossil clay), bulk density increases with depth at a high gradient (0.01 Mg/m^4) (Figs. 35B through 35D and Table 10). Decreases in porosity and water content also occur over this interval. Below this depth, the downhole gradient of index properties decreases (0.001 Mg/m^4 for bulk density) from 20 mbsf to approximately 210 mbsf. At the base of this gradient, an inverse depth-

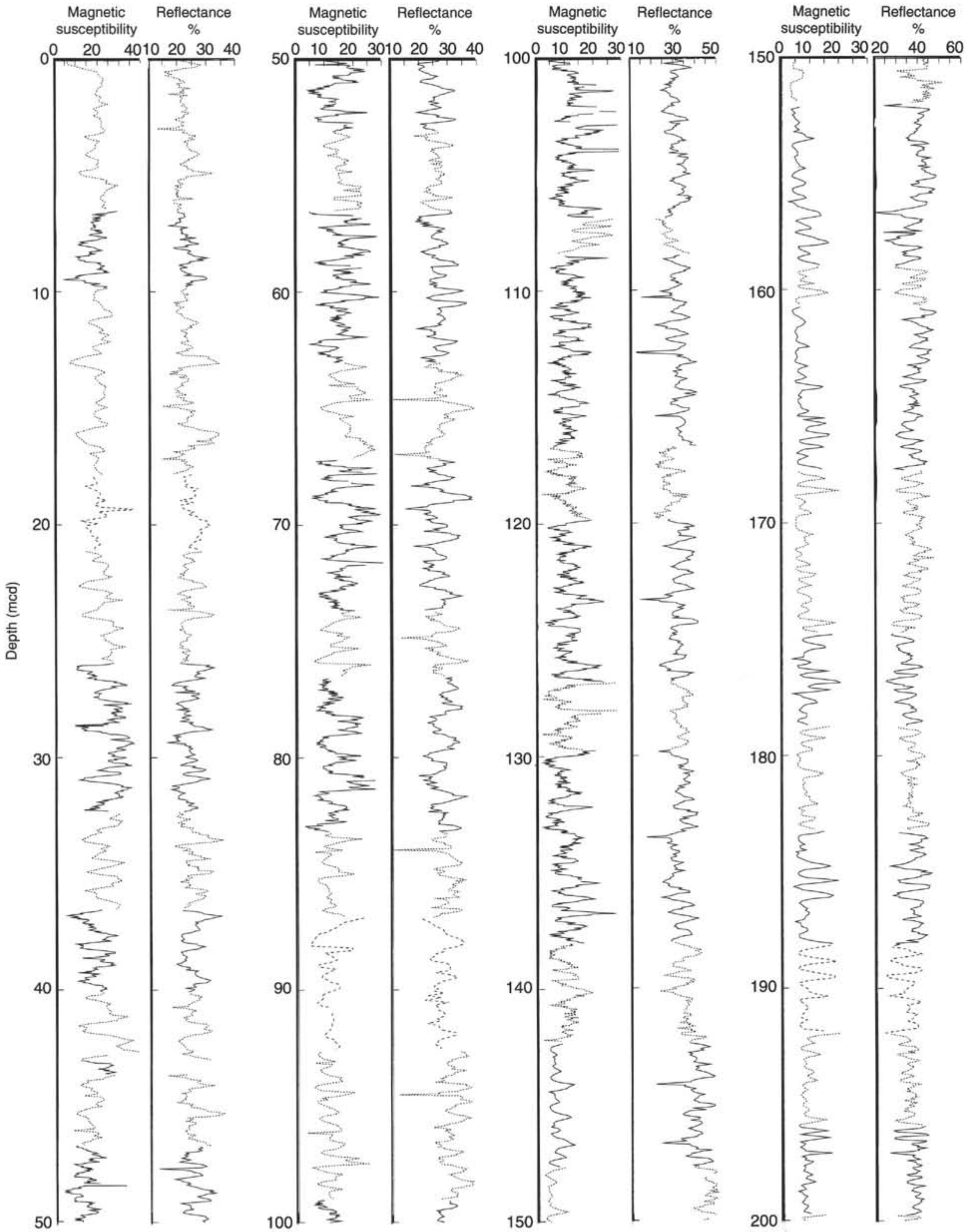

Figure 21. Spliced records of magnetic susceptibility and reflectance from the upper 400 mcd of Site 925. Tie points for forming the splice are given in Table 5. Hole 925A = large dashed line, Hole 925B = small dashed line, Hole 925C = dotted line, and Hole 925D = solid line.

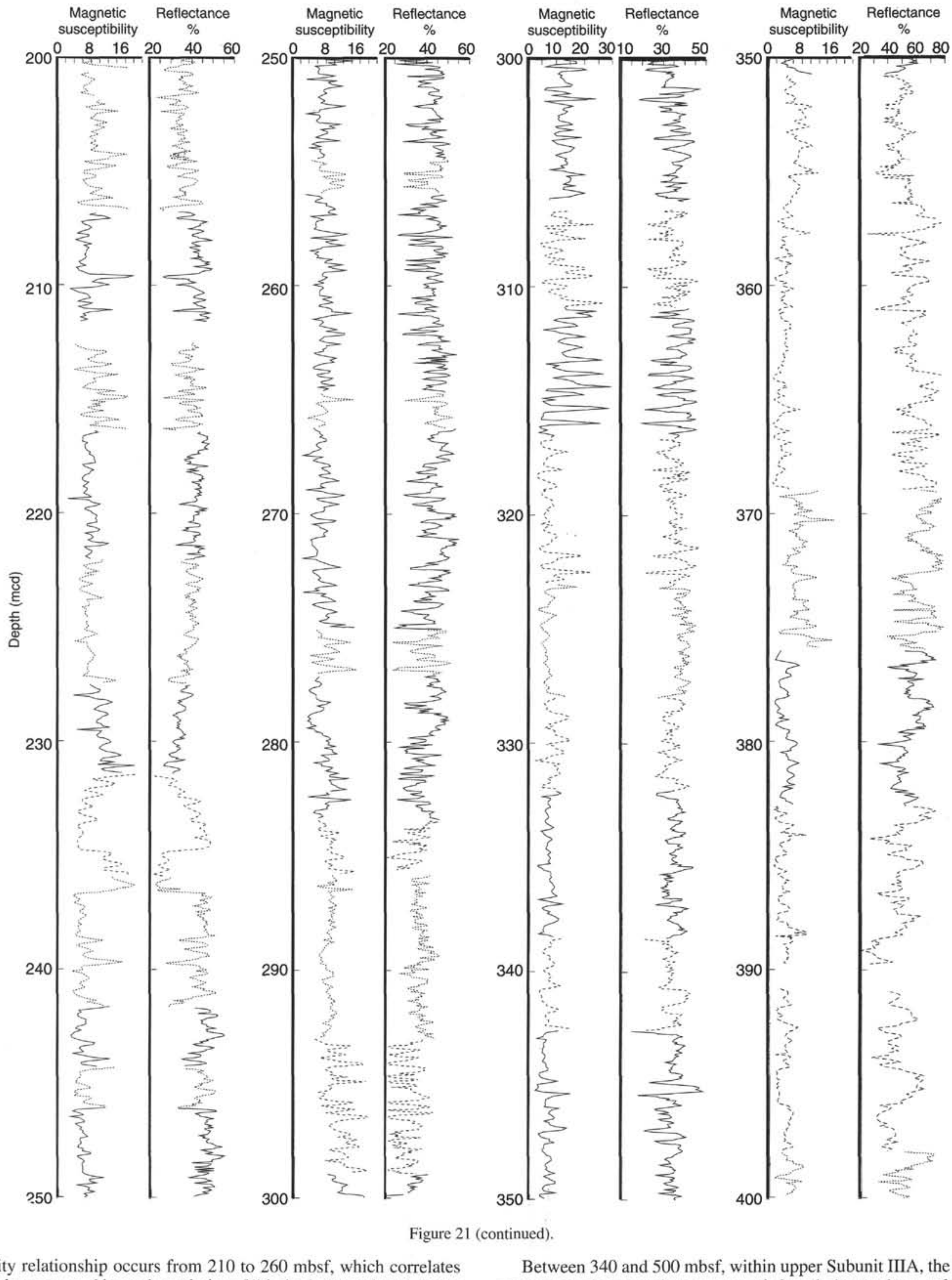

Figure 21 (continued).

density relationship occurs from 210 to 260 mbsf, which correlates with the upper and lower boundaries of lithologic Subunit IIB. Index properties over the interval from 280 to 340 mbsf show no dominant change with depth. A major offset in bulk density (–0.1 Mg/m^3), porosity (+9%), and water content (+12%) occurs at 340 mbsf, within lithologic Unit III, 50 m below the base of lithologic Unit II.

Between 340 and 500 mbsf, within upper Subunit IIIA, the index parameters show continuous normal downhole trends to values of 2.00 Mg/m^3 (gradient of 0.0012 Mg/m^4), 42% porosity, and 2% water content. At this depth (500 mbsf), another negative offset in bulk density (–0.1 Mg/m^3) is visible (Fig. 35A). Increasing porosity (+6%) and water content (+7%) display the same feature. Below this discon-

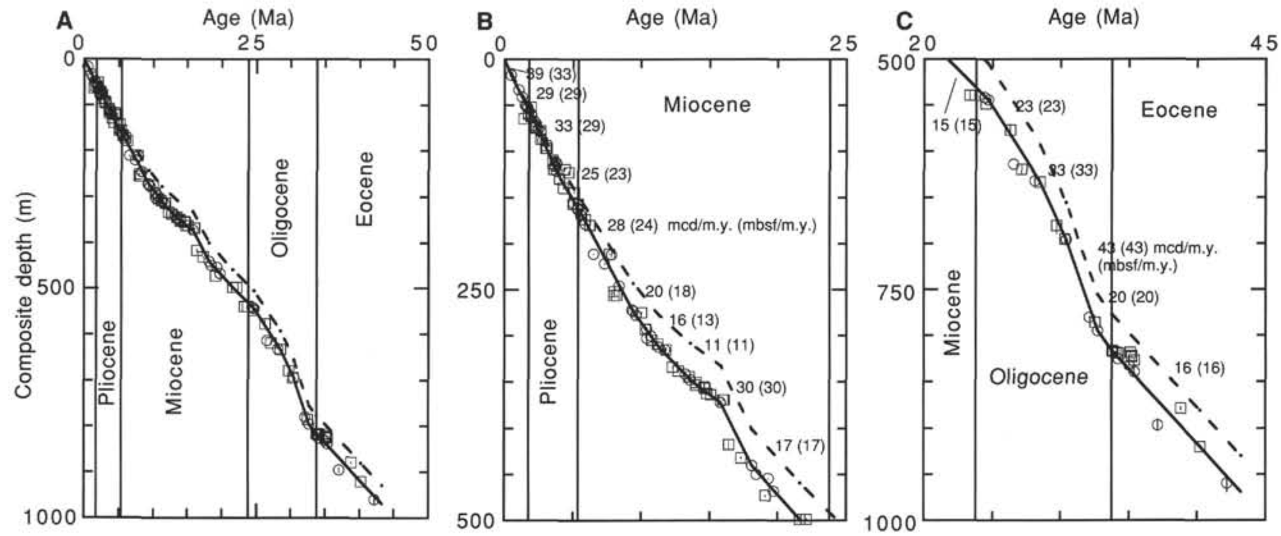

Figure 22. Age-depth plots of calcareous nannofossil (open circles) and planktonic foraminifer (open squares) events at Site 925, using data from Holes 925A and 925B. **A.** Middle Eocene to Holocene. **B.** Detail of early Miocene to Holocene. **C.** Detail of middle Eocene to early Miocene. The vertical bar within symbols represents depth uncertainty. The events are plotted on the mcd depth scale. The solid upper line represents the corresponding sedimentation rate line on the mbsf depth scale. Sedimentation rates are given on both scales: on the mcd scale and on the mbsf scale (in parentheses).

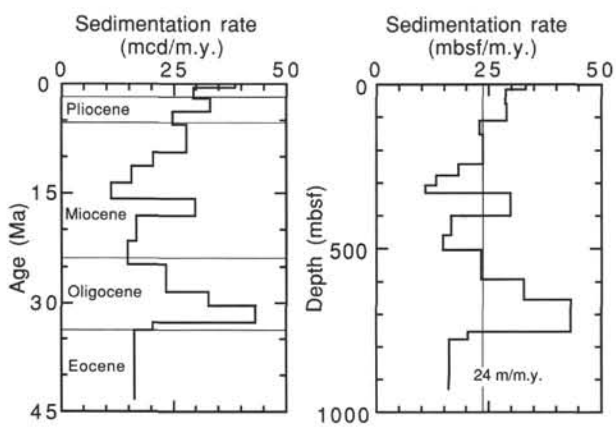

Figure 23. Plots of sedimentation rate at Site 925. The figure on the left shows sedimentation rate on the mcd scale vs. age. The figure on the right shows sedimentation rate on the mbsf scale vs. depth. The figure on the right also shows the average sedimentation rate at Site 925 using the mbsf scale.

tinuity to 700 mbsf, the index properties change again at a constant gradient with depth (0.0012 Mg/m^4).

The transition from Subunit IIIA to Subunit IIIB at 700 mbsf is marked by a pronounced positive offset in bulk density (+0.15 Mg/m^3), which reflects enhanced lithification of the sediments (chalk-limestone transition). Below this maximum, over the depth interval from 700 to 775 mbsf, a slight continuous decrease (increase) in density (porosity, water content) is followed by an increase (decrease) in the interval from 775 to 900 m. At the base of Hole 925A, bulk density increases at a high gradient (0.007 Mg/m^4), whereas porosity and water content decrease. Bulk density increases from 2.2 to 2.4 Mg/m^3, and porosity decreases from 25% to 15%.

The three large offsets in index properties at 340, 500, and 700 mbsf in Hole 925A are not associated with changes in sediment stress history. At 340 and 500 mbsf, bulk density decreases with depth across short depth intervals. If these offsets were associated with faulting in the section, displacements on the order of 100 m would be required to cause the observed offsets. This interpretation is not realistic given the biostratigraphic results and the generally flat-lying character of the seismostratigraphy on the rise. Consequently, these changes in index properties are likely associated with diagenetic processes or changes in source sediment. For example, a change from a kaolinite-dominated sediment to an illite-dominated sediment at the same depth below seafloor (effective stress) can reduce the bulk density by 10%. This reduction is caused by the clay fabric associated with each mineral (Mitchell, 1976). At 700 mbsf, Hole 925A, the offset in bulk density with depth is positive, suggesting that this boundary is an unconformity. However, if this boundary were an erosional unconformity, erosion of 150 to 200 m would be required to cause this change in density. Again, given the good biostratigraphic control over this interval, an unconformity is unlikely. A more plausible cause is a physicochemical change from 700 to 775 mbsf (Hole 925A), the interval where bulk density remains above the general downhole gradient. The two upper offsets, where bulk density decreases with depth across the boundary, are probably caused by a change in the type and amount of clay minerals.

Index property changes associated with meter and sub-meter lithologic cycles (see "Lithostratigraphy" section, this chapter) were evaluated by measuring three depth intervals at high resolution. Index properties and carbonate were measured in the three different lithologic units from Site 925: Section 154-925E-6H-5 (10 samples from 51.1 to 52.4 mbsf), Sections 154-925C-25H-3 and -4 (18 samples from 229.6 to 232.4 mbsf), and in Core 154-925A-38R (12 samples from 641.6 to 650.4 mbsf). In Section 154-925E-6H-5, index properties were determined using the constant volume method. In Section 154-925C-25H-3 and -4, index properties were determined based on dry and weight volume measurements with the Penta-Pycnometer. Bulk density calculated using wet volume measurements showed more scattering than those calculated using dry volumes. For Sections 154-925C-25H-3 and -4, dry volume and wet and dry mass were used to calculate index properties (see "Physical Properties" section, "Explanatory Notes" chapter, this volume). In Core 154-925A-38R, index properties were measured on cubes cut with the double-bladed saw.

These data are compared with carbonate content measured on the high-resolution samples along with results from the MST and color reflectance in Figures 31A through 31C ("Geochemistry" section, this chapter). The correlation of carbonate content to bulk-density data varies with the lithologic unit. In the shallow sections (154-925C-25H-3 and -25H-4; Fig. 31B), a weak correlation between bulk density, determined from GRAPE and carbonate, is observed. In the

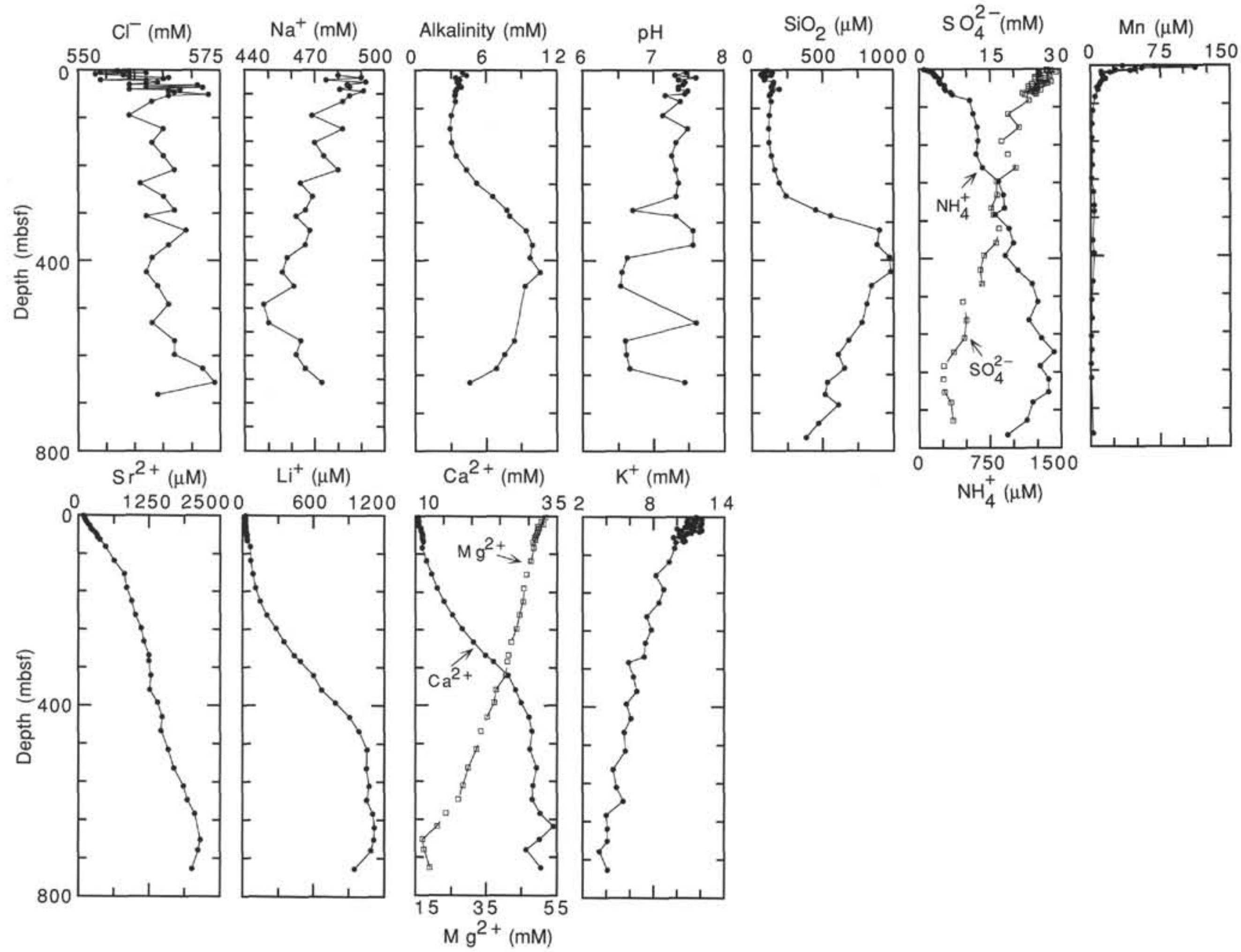

Figure 24. Interstitial-water geochemistry vs. depth, Site 925.

deeper interval (Core 154-925A-38R), sediments incompletely filled the core liner, which led to erroneously low GRAPE bulk-density values (Fig. 31C). Furthermore, meter to sub-meter amplitude variations observed in the GRAPE records from deep RCB sections are not indicative of true changes in sediment density, but are controlled by changes in the diameter of the sediment cores that do not completely fill the liner (Fig. 36).

Discrete index property measurements were used to determine a more precise relationship between bulk density and carbonate content for Site 925 (Fig. 37). It appears that higher density is associated with intervals of lower carbonate contents. Such a relationship is opposite to that observed in the equatorial Pacific, where the noncarbonate fraction consisted of diatoms and radiolarians (Mayer, 1979), and also opposite to that observed in other deep-sea pelagic carbonate sediments in which the noncarbonate fraction mainly consists of clay minerals (Herbert and Mayer, 1991). Detailed study of the interrelationships between index properties and composition requires additional mineralogical and fabric analyses, which will be conducted onshore.

As commonly observed in most carbonate-rich pelagic sediments (e.g., Bassinot et al., 1993), grain-density variations are a secondary control on bulk-density variations in sediments recovered at Site 925. At all scales of observation, bulk-density variations mainly reflect changes in porosity. The major offsets between bulk density measured in the three intervals (Fig. 37) probably result from the diagenetic or compositional changes (physicochemical) that occur in the sediment column. At finer scales of observation, over each interval studied, the

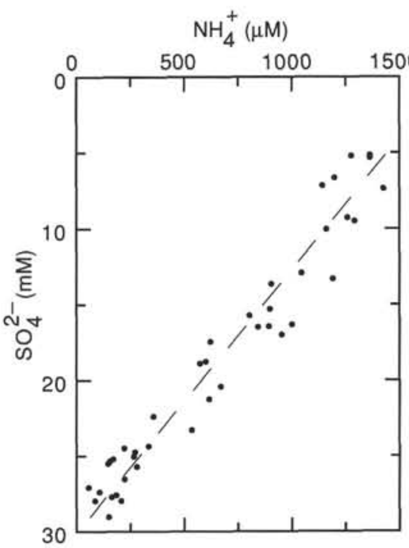

Figure 25. Interstitial-water ammonium vs. sulfate, showing the negative correlation of the two dissolved species.

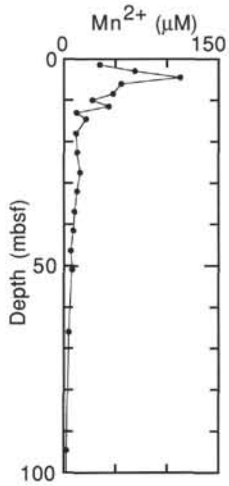

Figure 26. Expanded plot of interstitial-water manganese vs. depth in the upper 100 mbsf of the stratigraphic section.

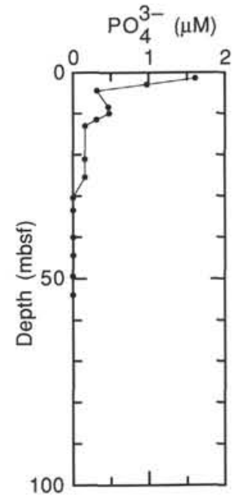

Figure 27. Interstitial-water phosphate vs. depth, as measured in samples from Hole 925E. Because phosphate levels dropped to zero within the top 40 mbsf of the section, no deeper samples were analyzed.

slope of the linear fit to the bulk-density vs. carbonate data increases with increased depth or gravitational consolidation. This is probably due to the compressibility changes for each sediment type that are caused by variations in composition or sediment fabric.

Acoustic Velocity

Acoustic velocity was measured using two discrete methods: the DSV and HF (see "Physical Properties" section, "Explanatory Notes" chapter, this volume). Wherever possible, discrete velocity was measured in both longitudinal and transverse directions. All data are corrected for the speed of sound of the pore fluid at the in situ temperature, using a gradient of 0.05°C/mbsf.

Within lithologic Unit I, acoustic velocity increases with depth below seafloor from values slightly lower than seawater velocity to average values of 1560 m/s (Figs. 38B through 38D and Table 11). Velocity becomes more variable at the base of lithologic Unit I with alternating high values, associated with darker (lower reflectance), clay-rich layers and low values, associated with lighter (higher reflectance), carbonate-rich layers.

In the upper 230 m of lithologic Unit II, velocity increases with depth from 1580 to 2280 m/s (Fig. 38A). Within this unit, intervals of low and high color reflectance alternate. Unlike Unit I, the higher velocity intervals are associated with high color reflectance intervals, and the lower velocity intervals are associated with the lower reflectance intervals. From 370 to 385 mbsf in Hole 925A, a velocity discontinuity occurs (Fig. 38A) with a large decrease from 2280 to 1680 m/s. over this same interval, velocity anisotropy increases slightly from an average of 0.5% to an average of 2%, suggesting the development of an anisotropic sediment fabric. this anisotropy shows large scatter, but it remains consistently high to the base of unit II; however, the absolute values of acoustic velocity gradually increase with depth.

Across the boundary between lithologic Units I and II (at 700 mbsf in Hole 925A), acoustic velocity increases 200 m/s for both longitudinal and transverse measurements. At this same interval, acoustic anisotropy begins to increase, suggesting the development of a fabric oriented in the horizontal plane with increasing depth.

In lithologic Unit III, acoustic velocity gradually increases with depth below seafloor, with the exception of one discontinuity that occurs at 748–749 mbsf in Hole 925A. Across this interval, velocity increases approximately 600 m/s in both longitudinal and transverse measurements. Acoustic anisotropy shows an offset across this interval, but it continues to increase with depth below this disconformity to 870 mbsf. At the bottom of Hole 925A, acoustic velocity sharply increases to the highest values measured at the site (3997 m/s). These high acoustic velocity measurements also show decreased anisotropy, suggesting a change in fabric at this depth (920–929 mbsf).

Undrained Shear Strength

Undrained shear strength is a measure of the development of sediment grain-to-grain and physicochemical bonds. This property is measured under no confining stress and is therefore described as a "friction angle (ϕ) = 0" test, or under no equivalent depth (stress) below seafloor. Thus, to characterize the strength of sediment with depth below seafloor, measurements must be made on the sediment over the full range of void ratios that exist within the stratigraphic section. No inference can be made about the strength of sediment at void ratios that are not measured. In comparison to this method, triaxial testing can be used to determine the strength characteristics of different lithologic units. By testing a series of three samples per lithologic unit under triaxial conditions, the friction angle and cohesion intercept can be determined. These values can then be applied to sediment of the same lithology at all void ratios. Because triaxial tests are relatively complex, it was not possible to complete any tests during this leg. Consequently, shear strength data are restricted to lithologic Unit I and the upper part of lithologic Unit II, where discrete measurements could be made using the miniature vane shear device and the pocket penetrometer (see "Physical Properties" section, "Explanatory Notes" chapter, this volume).

Undrained shear strength (S_u) increases with depth in the upper 70 mbsf from 7 kPa at the seabed to 30 kPa (Fig. 39 and Table 12). Below 70 mbsf, S_u shows an overall increase with depth, but with high variability. In sediment where carbonate controls the deformation behavior (>50% $CaCO_3$; Lee, 1982), shear strength increases with carbonate content. This suggests that the high strength intervals in Unit I are associated with higher carbonate content and vice versa. In the upper section of Unit II, S_u shows increased variability, probably associated with varying carbonate content. The overall shear strength increases with depth as does $CaCO_3$. A sharp increase in shear strength occurs at 272 mbsf in Hole 925B, at 278 mbsf in Hole 925C, and at 274 mbsf in Hole 925D (Fig. 39). This strength increase is only associated with the darker, clay-rich intervals and is best seen in Hole 925C where the alternating dark- and light-colored intervals were measured.

Normalized shear strength, which is represented by the ratio of S_u to the effective overburden stress (P_o'), can be used to assess the stress history of sediment. Normally consolidated sediment S_u/P_o' ratios vary from 0.2 to 0.22 (Ladd et al., 1977). At Site 925, S_u/P_o' are very

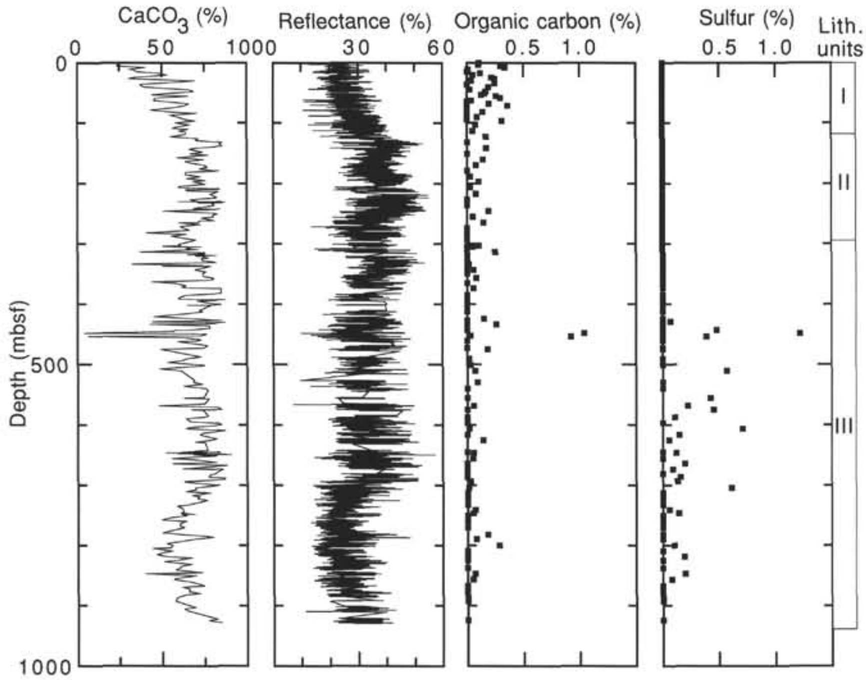

Figure 28. Calcium carbonate, color reflectance in the green (550 nm) band, organic carbon, and sulfur vs. depth, Site 925. Lithologic unit boundaries are shown on the right side of the diagram.

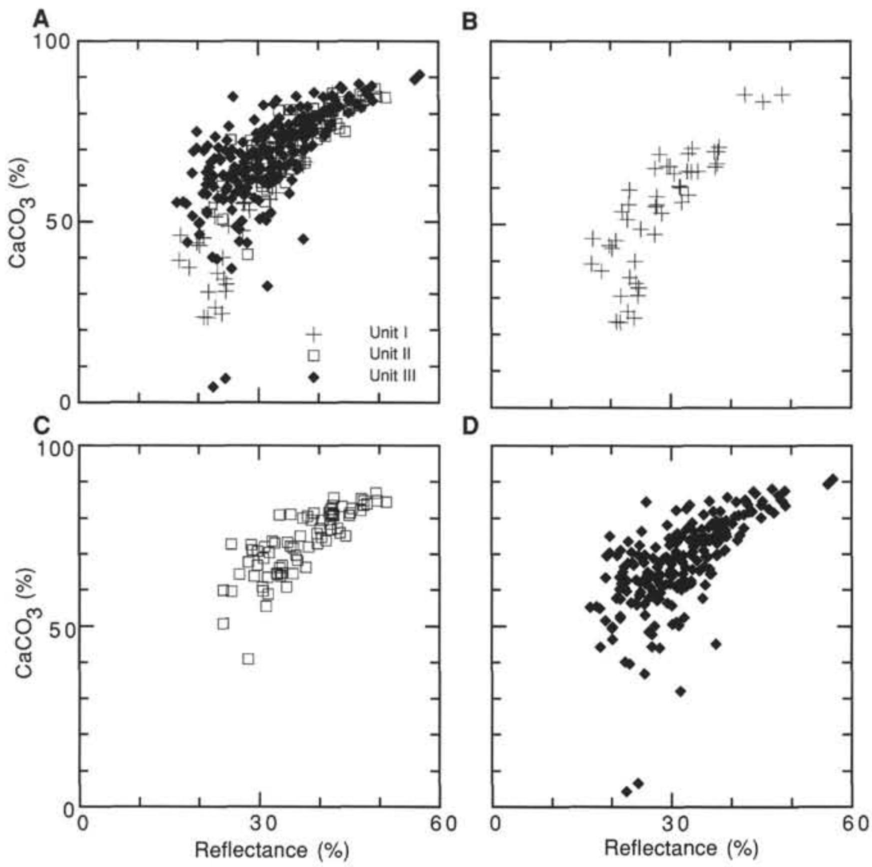

Figure 29. Calcium carbonate analyses from discrete samples vs. color reflectance values of the closest measurement, Site 925. **A.** Plot of all carbonate samples vs. color reflectance. **B, C,** and **D.** $CaCO_3$ vs. color reflectance for lithologic Units I, II, and III, respectively.

low and decrease with depth, suggesting that the sediments are underconsolidated (Fig. 40). Underconsolidated sediment has not developed the interparticle bonds required to support the overburden stresses caused by gravitational loading. In this case, the overburden stress is partially supported by the pore fluid, and excess pore fluid pressure could be present in the upper 270 m at Site 925. Below the increase in strength at 272–278 mbsf, only the carbonate-rich intervals remain underconsolidated. The clay-rich intervals have developed enough strength to support the overburden stress. The two sediment types (carbonate-rich and clay-rich) do not follow the same consolidation behavior and, therefore, the increase in strength in the clay-rich layers is not associated with stress changes. Rather, this

Table 10. Index properties measured on discrete samples for all holes at Site 925.

Core, section, interval (cm)	Depth (mbsf)	Water content (bulk wt %)	Water content (dry wt %)	Bulk density (Mg/m^3)	Grain density (Mg/m^3)	Dry density (Mg/m^3)	Porosity (%)
154-925A-							
1R-1, 19–21	102	36.34	57.08	1.711	2.771	1.089	60.69
1R-3, 20–22	105	36.52	57.52	1.688	2.689	1.071	60.16
2R-2, 20–22	200	33.99	51.50	1.721	2.649	1.136	57.11
2R-4, 15–17	203	30.58	44.05	1.841	2.836	1.278	54.94
3R-1, 38–40	304	36.19	56.71	1.716	2.780	1.095	60.61
3R-1, 53–55	304	33.86	51.19	1.779	2.856	1.177	58.79
3R-1, 112–114	305	33.13	49.55	1.807	2.908	1.208	58.45
3R-2, 31–33	306	30.41	43.70	1.848	2.850	1.286	54.86
3R-2, 90–92	306	30.15	43.16	1.869	2.902	1.306	55.00
3R-3, 23–25	307	29.34	41.52	1.891	2.914	1.336	54.15
3R-3, 88–90	308	32.21	47.51	1.850	2.997	1.254	58.16
4R-1, 21–23	314	30.75	44.40	1.849	2.877	1.281	55.49
4R-1, 48–50	314	30.09	43.05	2.009	3.426	1.404	59.01
4R-2, 28–30	315	28.71	40.27	1.959	3.097	1.397	54.90
4R-2, 81–83	316	27.87	38.64	1.891	2.810	1.364	51.46
4R-3, 75–77	317	30.86	44.63	1.860	2.924	1.286	56.02
4R-3, 131–133	318	31.83	46.69	1.819	2.852	1.240	56.52
4R-4, 8–10	318	29.93	42.72	1.860	2.854	1.303	54.34
4R-4, 100–102	319	28.67	40.19	1.919	2.957	1.369	53.70
4R-5, 26–28	320	29.28	41.40	1.875	2.857	1.326	53.58
4R-5, 107–109	321	29.46	41.76	1.923	3.034	1.356	55.29
4R-6, 4–6	321	28.33	39.53	1.971	3.105	1.413	54.51
4R-6, 99–101	322	30.93	44.78	1.888	3.031	1.304	56.98
4R-7, 21–23	323	27.92	38.73	1.907	2.862	1.375	51.97
5R-1, 47–49	324	23.37	30.50	1.933	2.649	1.481	44.09
5R-1, 129–131	325	23.43	30.60	1.899	2.571	1.454	43.43
5R-2, 13–15	325	24.13	31.80	1.919	2.656	1.456	45.19
5R-2, 85–87	326	26.22	35.53	1.989	2.989	1.468	50.90
5R-3, 86–88	327	24.33	32.16	1.909	2.644	1.445	45.35
5R-3, 146–148	328	25.04	33.40	1.890	2.633	1.417	46.19
5R-4, 14–16	328	25.39	34.02	1.952	2.822	1.457	48.38
5R-4, 109–111	329	21.56	27.48	1.970	2.640	1.546	41.46
5R-5, 68–70	330	24.45	32.37	1.901	2.628	1.436	45.36
5R-6, 61–63	332	29.92	42.70	1.871	2.891	1.311	54.65
5R-6, 130–132	332	29.57	41.99	1.888	2.923	1.330	54.51
5R-7, 51–53	333	30.48	43.84	1.866	2.915	1.297	55.50
6R-1, 21–23	333	27.24	37.43	1.824	2.577	1.327	48.50
6R-1, 55–57	334	26.78	36.57	1.885	2.720	1.380	49.26
6R-2, 29–31	335	26.63	36.30	1.820	2.535	1.336	47.32
6R-3, 48–50	337	30.93	44.79	1.832	2.831	1.265	55.31
6R-3, 75–77	337	31.48	45.95	1.815	2.812	1.244	55.78
7R-1, 43–45	343	30.27	43.41	1.836	2.797	1.280	54.24
7R-1, 98–100	344	30.02	42.91	1.839	2.790	1.287	53.89
7R-2, 41–43	345	33.98	51.46	1.775	2.848	1.172	58.86
7R-2, 98–100	345	30.58	44.05	1.841	2.837	1.278	54.95
7R-3, 40–42	346	30.87	44.65	1.836	2.839	1.269	55.30
7R-3, 116–118	347	31.10	45.14	1.816	2.789	1.251	55.13
7R-4, 40–42	348	29.92	42.69	1.845	2.802	1.293	53.87
7R-4, 118–120	348	31.79	46.61	1.811	2.822	1.236	56.22
7R-5, 42–44	349	30.49	43.87	1.843	2.837	1.281	54.85
7R-5, 97–99	350	28.33	39.54	1.840	2.685	1.319	50.89
7R-6, 57–59	351	31.19	45.34	1.807	2.765	1.243	55.03
7R-6, 118–120	351	28.73	40.31	1.849	2.738	1.318	51.86
8R-1, 12–14	353	29.60	42.05	1.838	2.760	1.294	53.11
8R-1, 121–123	354	29.42	41.69	1.866	2.837	1.317	53.58
8R-2, 2–4	354	29.17	41.19	1.861	2.802	1.318	52.98
8R-2, 72–74	355	30.06	42.97	1.836	2.784	1.284	53.87
8R-3, 2–4	355	29.94	42.73	1.811	2.696	1.269	52.93
8R-3, 82–84	356	30.93	44.78	1.839	2.856	1.270	55.52
8R-4, 9–11	357	27.58	38.09	1.898	2.810	1.374	51.10
8R-4, 90–92	358	30.12	43.09	1.834	2.780	1.281	53.90
8R-5, 5–7	358			1.843			
8R-5, 146–148	360	29.61	42.08	1.857	2.821	1.307	53.67
8R-6, 3–5	360	34.44	52.53	1.769	2.861	1.160	59.47
8R-6, 83–85	361	31.91	46.87	1.806	2.810	1.229	56.25
9R-1, 28–30	362	30.20	43.27	1.852	2.846	1.292	54.58
9R-1, 86–88	363	30.64	44.17	1.829	2.802	1.269	54.71
9R-2, 25–27	364	30.50	43.88	1.846	2.848	1.283	54.95
9R-2, 131–133	365	27.84	38.58	1.879	2.770	1.356	51.06
9R-3, 14–16	365	28.08	39.04	1.893	2.830	1.362	51.88
9R-3, 133–135	366	29.05	40.95	1.861	2.797	1.321	52.79
9R-4, 54–56	367	29.15	41.14	1.860	2.799	1.318	52.92
9R-4, 125–127	368			1.845			
9R-5, 45–47	368	28.93	40.71	1.849	2.750	1.314	52.22
9R-6, 36–38	370	29.89	42.62	1.840	2.786	1.290	53.68
9R-6, 122–124	371	27.57	38.06	1.882	2.762	1.363	50.65
9R-7, 53–55	372	29.09	41.02	1.877	2.851	1.331	53.30
10R-1, 10–12	372	28.39	39.64	1.854	2.729	1.327	51.36
10R-1, 134–136	373	29.57	41.99	1.847	2.786	1.301	53.31
10R-2, 48–50	374	30.54	43.97	1.831	2.802	1.272	54.60
10R-2, 128–130	374	32.66	48.50	1.797	2.835	1.210	57.30
11R-1, 22–24	382	32.60	48.37	1.809	2.874	1.219	57.57
11R-1, 145–147	383	30.24	43.34	1.834	2.788	1.279	54.12
11R-2, 45–47	383	30.30	43.48	1.815	2.731	1.265	53.68
11R-2, 125–127	384	30.47	43.82	1.826	2.778	1.269	54.30
11R-3, 15–17	384	27.95	38.80	1.867	2.741	1.345	50.93
11R-3, 81–83	385	27.18	37.33	1.840	2.619	1.340	48.83
11R-4, 26–28	386	28.30	39.47	1.870	2.774	1.341	51.66
11R-4, 144–146	387	27.97	38.83	1.877	2.773	1.352	51.25
11R-5, 69–71	388			1.856			
11R-5, 130–132	389	28.05	38.99	1.887	2.809	1.358	51.67
11R-6, 38–40	389	27.41	37.76	1.879	2.743	1.364	50.27
12R-1, 36–38	391	28.04	38.97	1.862	2.732	1.340	50.96
12R-1, 120–122	392	27.35	37.64	1.880	2.742	1.366	50.19
12R-2, 31–33	393	31.12	45.18	1.841	2.876	1.268	55.92
12R-2, 120–122	394	28.63	40.11	1.863	2.773	1.330	52.06
12R-3, 25–27	394	28.50	39.86	1.870	2.787	1.337	52.02
12R-3, 122–124	395	27.84	38.59	1.875	2.759	1.353	50.95
13R-1, 39–41	401	30.14	43.15	1.844	2.816	1.288	54.26
13R-2, 2–4	401	27.75	38.41	1.849	2.676	1.336	50.08
13R-2, 68–70	402	27.11	37.19	1.890	2.757	1.378	50.02
14R-2, 30–32	411	25.77	34.71	1.900	2.702	1.411	47.80
14R-2, 139–141	412	27.14	37.25	1.905	2.802	1.388	50.47
14R-3, 34–36	412	25.09	33.50	1.962	2.829	1.469	48.05
14R-4, 33–35	414	25.99	35.11	1.914	2.753	1.417	48.55
14R-4, 125–127	415	26.32	35.72	1.900	2.735	1.400	48.81
14R-5, 28–30	415	26.24	35.57	1.890	2.703	1.394	48.41
14R-5, 128–130	416	25.93	35.01	1.913	2.747	1.417	48.42
14R-6, 33–35	417	24.63	32.67	1.909	2.659	1.439	45.89
15R-1, 70–72	420	26.27	35.62	1.909	2.758	1.408	48.95
15R-1, 101–103	421	26.61	36.26	1.910	2.781	1.402	49.61
15R-2, 56–58	422	28.31	39.49	1.861	2.748	1.334	51.44
15R-2, 137–139	423	26.27	35.62	1.899	2.729	1.400	48.69
15R-3, 18–20	423	24.18	31.88		2.018	1.239	38.57
15R-3, 130–132	424	24.52	32.49	1.926	2.697	1.454	46.10
15R-4, 6–8	424	27.92	38.74	1.906	2.858	1.374	51.94
15R-4, 110–112	425	27.81	38.52	1.898	2.826	1.370	51.51
15R-5, 7–9	426	26.30	35.68	1.875	2.665	1.382	48.13
15R-5, 92–94	427	26.04	35.22	1.931	2.806	1.428	49.10
15R-6, 35–37	428	26.21	35.52	1.922	2.789	1.418	49.16
15R-6, 142–144	429	25.47	34.17	1.928	2.759	1.437	47.92
15R-7, 10–12	429	26.37	35.81	1.861	2.630	1.370	47.90
16R-1, 33–35	430	24.15	31.83	1.977	2.807	1.499	46.59
16R-1, 108–110	430	25.93	35.00	1.928	2.789	1.428	48.79
16R-2, 23–25	431	25.39	34.04	1.936	2.776	1.444	47.98
16R-2, 89–91	432	24.98	33.30	1.955	2.803	1.467	47.67
16R-3, 11–13	432	24.04	31.65	1.937	2.696	1.471	45.44
16R-3, 130–132	434	18.50	22.70	2.003	2.558	1.633	36.17
16R-4, 12–14	434	26.44	35.94	1.913	2.848	1.407	50.58
16R-4, 137–139	435	26.33	35.74	1.923	2.800	1.416	49.41
16R-5, 16–18	435	24.71	32.83	1.941	2.748	1.461	46.82
16R-5, 69–71	436	24.08	31.71	1.961	2.762	1.489	46.09
16R-6, 15–17	437	23.66	30.98	1.991	2.814	1.520	45.98
16R-6, 147–149	438	24.35	32.19	1.929	2.694	1.459	45.84
16R-7, 48–50	439	27.03	37.05	1.920	2.838	1.401	50.65
17R-1, 5–7	439	24.57	32.58	1.912	2.664	1.442	45.86
17R-1, 98–100	440	25.25	33.78	1.930	2.751	1.443	47.57
17R-2, 8–10	440	24.44	32.35	1.938	2.723	1.464	46.24
17R-2, 87–89	441	27.13	37.23	1.911	2.891	1.392	51.84
17R-3, 59–61	442	24.61	32.64	1.939	2.736	1.462	46.57
17R-3, 124–126	443	24.78	32.95	1.911	2.672	1.437	46.22
17R-4, 27–29	444	21.16	26.85	1.943	2.559	1.532	40.14
17R-4, 95–97	444	22.44	28.93	2.005	2.772	1.555	43.91
17R-5, 2–4	445	24.24	31.99	1.919	2.663	1.454	45.40
17R-5, 56–58	445	20.56	25.88	1.968	2.584	1.563	39.50
17R-6, 28–30	447	20.52	25.82	1.904	2.447	1.514	38.15
17R-6, 80–82	447	20.21	25.33	1.992	2.617	1.589	39.29
17R-7, 18–20	448	26.75	36.52	1.881	2.708	1.378	49.12
18R-1, 65–67	449	23.27	30.33	2.006	2.827	1.539	45.56
18R-1, 111–113	450	18.70	23.00	1.973	2.506	1.604	36.01
18R-2, 12–14	450			1.888			
18R-2, 145–147	452	18.91	23.31	2.025	2.622	1.642	37.37
18R-3, 40–42	452	22.78	29.50	1.988	2.752	1.535	44.20
18R-3, 93–95	453	23.19	30.19	1.968	2.726	1.512	44.55
18R-4, 34–36	453	25.59	34.39	1.934	2.783	1.439	48.30
18R-4, 59–61	454	27.72	38.34	1.921	2.892	1.389	51.97
18R-5, 52–54	455	23.64	30.95	1.983	2.791	1.514	45.75
18R-5, 114–116	456	22.94	29.76	1.945	2.654	1.499	43.53
18R-6, 21–23	456	23.62	30.93	1.969	2.812	1.504	46.52
18R-6, 126–128	457	25.49	34.20	1.947	2.813	1.451	48.43
18R-7, 68–70	458	25.27	33.82	1.944	2.793	1.453	47.97
19R-2, 17–19	458	24.58	32.60	1.955	2.777	1.474	46.91
19R-2, 61–63	459	24.89	33.13	1.936	2.744	1.454	47.02
19R-3, 69–71	460			1.923			
19R-3, 69–71	460	27.16	37.30	1.923	2.857	1.400	50.98
19R-3, 135–137	461			1.938			
19R-3, 135–137	461	24.02	31.61	1.938	2.699	1.473	45.44
19R-4, 70–72	462	20.06	25.10	1.898	2.414	1.517	37.17
20R-1, 123–125	469	22.65	29.29	1.984	2.787	1.534	44.94
20R-2, 34–36	470	23.84	31.31	1.941	2.695	1.478	45.16
20R-2, 123–125	471	23.32	30.40				
20R-3, 34–36	471	23.09	30.02	1.955	2.688	1.503	44.06
20R-3, 118–120	472	22.05	28.28	1.977	2.682	1.541	42.54
20R-4, 56–58	473	22.36	28.79	1.985	2.718	1.541	43.31
20R-4, 132–134	474	21.99	28.19	1.988	2.706	1.551	42.68

Table 10 (continued).

Core, section, interval (cm)	Depth (mbsf)	Water content (bulk wt %)	Water content (dry wt %)	Bulk density (Mg/m^3)	Grain density (Mg/m^3)	Dry density (Mg/m^3)	Porosity (%)
20R-5, 41–43	474	22.13	28.42	1.986	2.708	1.546	42.90
20R-5, 105–107	475	24.18	31.89	1.951	2.743	1.480	46.06
20R-6, 56–58	476	22.58	29.16	1.987	2.737	1.538	43.79
20R-6, 118–120	476	23.82	31.27	1.963	2.809	1.496	46.76
20R-7, 28–30	477	23.01	29.89	1.977	2.739	1.522	44.42
22R-1, 39–41	487	24.06	31.68				
22R-1, 116–118	488	25.94	35.02	2.068	3.216	1.532	52.36
22R-2, 47–49	489	22.45	28.94	1.978	2.707	1.534	43.33
22R-2, 104–106	490	22.85	29.63	1.969	2.709	1.519	43.93
22R-3, 35–37	490	22.65	29.28	1.963	2.683	1.519	43.40
22R-3, 118–120	491	23.00	29.87	1.977	2.792	1.522	45.47
22R-4, 31–33	492	22.37	28.81	1.988	2.727	1.543	43.40
22R-4, 92–94	493	23.04	29.94	1.965	2.711	1.513	44.20
22R-5, 44–46	494	22.94	29.77	1.978	2.735	1.524	44.28
22R-5, 106–108	494	23.83	31.29	1.964	2.754	1.496	45.68
22R-6, 108–110	496	23.14	30.11	1.986	2.768	1.526	44.86
22R-7, 44–46	497	23.01	29.89	2.010	2.820	1.547	45.14
23R-1, 12–14	497	24.61	32.65	1.923	2.752	1.450	47.33
23R-1, 119–121	498	21.13	26.79	1.991	2.664	1.570	41.06
23R-2, 96–98	499	23.95	31.50	1.955	2.797	1.487	46.83
23R-3, 75–77	500	26.77	36.56	1.900	2.763	1.391	49.65
23R-4, 75–77	502	22.12	28.40	2.002	2.746	1.559	43.22
24R-1, 4–6	506	20.84	26.33	1.980	2.624	1.567	40.28
24R-1, 76–78	507	25.14	33.58	1.923	2.726	1.440	47.19
24R-2, 60–62	508	25.62	34.44	1.934	2.785	1.438	48.35
24R-2, 140–142	509	25.72	34.63	1.830	2.516	1.360	45.95
24R-3, 86–88	510	24.77	32.92	1.910	2.670	1.437	46.18
24R-3, 144–146	511	25.71	34.60	1.886	2.661	1.402	47.33
24R-4, 61–63	511	20.93	26.47	1.792	2.235	1.417	36.61
24R-5, 6–8	512	25.87	34.91	1.889	2.677	1.400	47.71
24R-5, 144–146	514	25.43	34.11	1.889	2.651	1.408	46.88
24R-6, 68–70	514	25.96	35.06	1.899	2.710	1.406	48.12
24R-6, 143–145	515	24.46	32.38	1.923	2.684	1.452	45.90
26R-2, 137–139	527	24.28	32.07	1.893	2.600	1.434	44.87
26R-3, 16–18	528	24.64	32.70	1.895	2.624	1.428	45.58
26R-3, 132–134	529	23.57	30.84	1.938	2.673	1.481	44.58
26R-4, 4–6	529	23.41	30.57	1.932	2.649	1.479	44.14
26R-4, 136–138	530	23.57	30.85	1.943	2.687	1.485	44.72
26R-5, 69–71	531	22.04	28.27	1.967	2.659	1.534	42.33
26R-5, 130–132	532	24.14	31.81	1.954	2.746	1.482	46.02
26R-6, 64–66	533	23.34	30.44	1.966	2.729	1.507	44.78
26R-6, 145–147	533	23.17	30.16	1.979	2.751	1.520	44.75
26R-7, 114–116	535	22.05	28.28	2.007	2.754	1.564	43.19
27R-1, 23–25	536	21.91	28.05	1.979	2.679	1.546	42.32
27R-1, 130–132	537	23.00	29.87	1.956	2.686	1.507	43.92
27R-2, 21–23	537	24.16	31.87	1.926	2.677	1.461	45.43
27R-2, 108–110	538	23.73	31.11	1.951	2.715	1.488	45.19
27R-3, 15–17	538	23.28	30.34	1.961	2.713	1.504	44.55
27R-3, 81–83	539	22.82	29.58	1.938	2.633	1.496	43.19
27R-4, 21–23	540	23.21	30.22	1.916	2.601	1.472	43.41
27R-4, 94–96	541	21.34	27.12	2.019	2.741	1.588	42.05
27R-5, 25–27	542	23.03	29.92	1.949	2.669	1.500	43.80
27R-5, 118–120	542	22.01	28.22	1.975	2.675	1.540	42.43
27R-6, 31–33	543	21.97	28.15	1.968	2.656	1.535	42.19
27R-6, 128–130	544	23.22	30.24	1.950	2.682	1.497	44.19
29R-1, 38–40	555	19.91	24.86	2.004	2.628	1.605	38.94
29R-1, 88–90	555	20.17	25.27	2.000	2.634	1.597	39.38
29R-2, 6–8	556	20.82	26.30	1.946	2.548	1.541	39.55
30R-1, 28–30	564	21.08	26.72	1.993	2.666	1.572	41.01
30R-1, 107–109	565	20.31	25.49	2.007	2.657	1.600	39.80
30R-2, 30–32	566	19.61	24.39	1.984	2.571	1.595	37.97
30R-2, 140–142	567	22.06	28.30	1.936	2.589	1.509	41.69
30R-3, 53–55	568	20.36	25.56	1.977	2.594	1.575	39.29
30R-3, 109–111	568	25.58	34.37	1.863	2.592	1.386	46.51
30R-4, 78–80	569	24.20	31.93	1.919	2.660	1.454	45.32
30R-5, 50–52	571	22.80	29.54	1.934	2.622	1.493	43.05
30R-5, 134–136	572	22.10	28.36	1.936	2.590	1.508	41.76
30R-6, 41–43	572	21.08	26.71	1.965	2.603	1.551	40.42
30R-6, 121–123	573	22.42	28.90	1.930	2.592	1.497	42.23
31R-1, 47–49	574	24.92	33.20	1.883	2.609	1.414	45.81
31R-1, 106–108	575	21.53	27.43	1.983	2.667	1.556	41.66
31R-2, 48–50	576	21.01	26.59	1.957	2.583	1.546	40.13
32R-1, 130–132	585	19.86	24.78	1.968	2.550	1.577	38.14
32R-2, 35–37	585	20.31	25.49	1.964	2.564	1.565	38.95
32R-2, 119–121	586	20.16	25.25	2.005	2.644	1.601	39.45
32R-3, 38–40	587	19.48	24.19	2.010	2.619	1.618	38.21
32R-3, 126–128	588	20.14	25.21	1.978	2.584	1.580	38.87
32R-4, 33–35	588	21.14	26.81	1.931	2.531	1.522	39.84
32R-4, 119–121	589	20.95	26.51	1.980	2.631	1.565	40.51
32R-5, 34–36	590	19.58	24.35	2.010	2.625	1.617	38.42
32R-5, 127–129	591	19.59	24.37	2.006	2.616	1.613	38.36
32R-6, 26–28	591	19.71	24.55	1.979	2.566	1.589	38.07
32R-6, 85–87	592	21.73	27.75	1.936	2.570	1.515	41.04
33R-1, 23–25	593	21.31	27.09	1.989	2.670	1.565	41.38
33R-1, 95–97	594	20.82	26.30	2.014	2.701	1.595	40.94
33R-2, 17–19	595	22.42	28.89	1.957	2.656	1.518	42.82
33R-2, 67–69	595	20.79	26.24	2.009	2.687	1.592	40.77
33R-3, 12–14	596	22.33	28.76	1.981	2.709	1.539	43.19
33R-3, 72–74	597	23.93	31.46	1.905	2.611	1.449	44.49
33R-4, 51–53	598	21.39	27.21	1.984	2.663	1.560	41.43
33R-4, 120–122	599	21.48	27.35	1.986	2.671	1.559	41.62
33R-5, 45–47	600			2.044			
33R-6, 46–48	601	22.87	29.65	1.950	2.664	1.504	43.54
34R-1, 74–76	604	20.28	25.45	2.007	2.656	1.600	39.75
34R-1, 74–76	604			2.043			
34R-1, 130–132	604	23.14	30.11	2.013	2.837	1.547	45.47
34R-2, 23–25	605	20.83	26.32	2.003	2.676	1.586	40.74
34R-2, 94–96	605	21.57	27.51	1.990	2.687	1.561	41.91
34R-3, 33–35	606	21.05	26.66	2.016	2.717	1.592	41.41
34R-3, 80–82	607	20.24	25.38	2.024	2.691	1.615	40.00
34R-4, 71–73	608	19.86	24.78	2.020	2.660	1.618	39.14
34R-4, 132–134	609	18.59	22.84	2.063	2.684	1.679	37.43
34R-5, 36–38	609			1.971			
34R-5, 145–147	610	21.38	27.20	2.010	2.723	1.580	41.96
34R-5, 145–147	610			1.987			
34R-6, 40–42	611	19.39	24.05	2.040	2.678	1.644	38.60
35R-1, 16–18	613	18.48	22.67	2.046	2.644	1.668	36.91
35R-1, 107–109	613	20.17	25.26	2.008	2.651	1.603	39.53
35R-2, 26–28	614	20.97	26.53	2.010	2.699	1.589	41.14
35R-2, 114–116	615	20.56	25.88	2.012	2.681	1.598	40.37
35R-3, 43–45	616	20.72	26.13	2.040	2.752	1.617	41.25
35R-3, 43–45	616			2.071			
35R-3, 120–122	617	19.78	24.65	2.019	2.655	1.620	38.98
35R-4, 18–20	617	19.33	23.96	2.016	2.625	1.627	38.04
35R-4, 81–83	618	22.45	28.95	2.018	2.806	1.565	44.23
35R-4, 81–83	618			1.947			
35R-5, 27–29	618			1.992			
35R-5, 50–52	618	19.14	23.67	2.027	2.638	1.639	37.87
36R-1, 26–28	622	21.35	27.15	2.024	2.753	1.592	42.18
36R-1, 26–28	622			1.915			
36R-1, 122–124	623	20.43	25.67	1.988	2.621	1.582	39.64
36R-2, 49–51	624	20.40	25.62	2.015	2.679	1.604	40.12
36R-2, 106–108	625	20.87	26.38	1.990	2.649	1.575	40.55
36R-3, 14–16	625	20.40	25.62	1.970	2.580	1.568	39.22
36R-3, 81–83	626	22.01	28.22	1.993	2.718	1.554	42.81
36R-4, 22–24	627	20.23	25.35	1.999	2.635	1.595	39.47
36R-4, 105–107	628	19.14	23.67	2.042	2.670	1.651	38.16
36R-5, 105–107	629	19.04	23.52	2.042	2.664	1.653	37.94
36R-6, 15–17	630	19.79	24.67	2.047	2.717	1.642	39.55
36R-6, 119–121	631	21.02	26.61	2.019	2.721	1.594	41.41
36R-7, 39–41	631	21.81	27.89	1.981	2.679	1.549	42.18
38R-1, 23–25	642	18.84	23.22	2.026	2.620	1.644	37.25
38R-1, 128–130	643	19.20	23.76	2.036	2.660	1.645	38.16
38R-2, 51–53	643	20.89	26.41	1.978	2.623	1.565	40.34
38R-2, 129–131	644	19.01	23.47	2.065	2.711	1.672	38.31
38R-3, 28–30	645	19.13	23.66	2.067	2.723	1.672	38.60
38R-3, 76–78	645	22.18	28.51	1.977	2.690	1.538	42.81
38R-4, 47–49	646	18.75	23.07	2.043	2.651	1.660	37.39
38R-4, 118–120	647	19.06	23.55	2.044	2.670	1.655	38.03
38R-5, 24–26	648	19.34	23.97	2.040	2.676	1.646	38.51
38R-5, 115–117	649	21.33	27.11	1.985	2.661	1.562	41.32
38R-6, 24–26	649	24.38	32.24	1.912	2.652	1.446	45.49
38R-6, 125–127	650	19.21	23.78	2.067	2.726	1.670	38.75
38R-7, 5–7	650	21.38	27.20	1.980	2.652	1.556	41.32
39R-1, 4–6	651	21.32	27.09	1.985	2.661	1.562	41.31
39R-1, 86–88	652	20.23	25.36	2.030	2.703	1.620	40.09
39R-2, 45–47	653	20.06	25.09	2.033	2.699	1.625	39.80
39R-2, 82–84	653	18.69	22.98	2.077	2.719	1.689	37.89
39R-3, 13–15	654	19.08	23.58	2.068	2.723	1.674	38.52
39R-3, 117–119	655	17.66	21.45	2.104	2.719	1.733	36.28
39R-4, 3–5	656	20.51	25.80	2.013	2.680	1.600	40.30
39R-4, 64–66	656	20.04	25.06	2.003	2.633	1.601	39.17
39R-5, 49–51	658	19.26	23.85	2.013	2.616	1.626	37.85
39R-5, 142–144	659	18.68	22.97	2.029	2.619	1.650	36.99
39R-6, 54–56	659	19.90	24.85	1.935	2.483	1.550	37.59
39R-7, 31–33	660	17.83	21.69	2.066	2.651	1.698	35.95
40R-1, 134–136	662	19.70	24.53	2.002	2.614	1.608	38.50
40R-2, 98–100	663	18.69	22.99	2.026	2.614	1.647	36.96
40R-3, 58–60	664	17.13	20.67	2.174	2.830	1.802	36.34
40R-4, 62–64	666	17.18	20.74	2.074	2.633	1.718	34.78
40R-5, 59–61	667	21.39	27.21	2.054	2.828	1.615	42.90
40R-7, 2–4	670	17.40	21.07	2.160	2.819	1.784	36.70
41R-1, 51–53	671	17.21	20.79	2.077	2.640	1.719	34.89
41R-1, 107–109	671	17.13	20.66	2.054	2.592	1.702	34.33
41R-2, 71–73	673	15.25	17.99	2.120	2.625	1.797	31.56
41R-3, 71–73	674	20.06	25.09	2.008	2.645	1.605	39.31
42R-1, 20–22	680	16.56	19.84	1.956	2.386	1.632	31.60
42R-1, 91–93	681	13.37	15.43	2.041	2.411	1.768	26.64
42R-2, 45–47	682	11.80	13.38	2.129	2.488	1.878	24.52
43R-1, 3–5	683	19.11	23.63	1.997	2.575	1.616	37.26
43R-1, 128–130	684	15.78	18.74	2.121	2.653	1.786	32.67
43R-2, 59–61	685	19.59	24.37	2.008	2.622	1.615	38.41
43R-2, 144–146	686	15.88	18.87	2.138	2.689	1.798	33.13
43R-3, 21–23	686	19.26	23.85	2.047	2.687	1.653	38.48
43R-3, 65–67	687	16.79	20.18	2.072	2.610	1.724	33.96
43R-4, 84–86	688	19.34	23.98	2.032	2.659	1.639	38.36
43R-4, 139–141	689	15.81	18.78	2.142	2.694	1.803	33.06
44R-1, 52–54	690	20.42	25.66	2.009	2.668	1.599	40.06
44R-1, 109–111	691	20.30	25.47	1.987	2.611	1.583	39.36
44R-2, 31–33	692	16.19	19.31	2.144	2.718	1.797	33.87

Table 10 (continued).

Core, section, interval (cm)	Depth (mbsf)	Water content (bulk wt %)	Water content (dry wt %)	Bulk density (Mg/m^3)	Grain density (Mg/m^3)	Dry density (Mg/m^3)	Porosity (%)
44R-2, 140–142	693	16.14	19.24		2.096	1.504	28.25
44R-3, 43–45	693	13.96	16.22	2.195	2.695	1.889	29.91
44R-3, 74–76	693	14.50	16.95	2.204	2.739	1.885	31.19
44R-4, 80–82	695	13.04	14.99	2.185	2.632	1.900	27.81
45R-1, 76–78	700	11.57	13.08	2.212	2.608	1.956	24.98
45R-1, 140–142	701	13.33	15.37	2.216	2.698	1.920	28.82
45R-2, 19–21	701	12.00	13.64	2.241	2.673	1.972	26.24
45R-2, 119–121	702	13.11	15.09	2.228	2.708	1.936	28.52
45R-3, 130–132	704	11.62	13.15	2.268	2.698	2.004	25.73
45R-4, 75–77	705	16.52	19.79	2.223	2.893	1.856	35.85
45R-5, 39–41	706	12.54	14.34	2.228	2.680	1.949	27.28
45R-5, 134–136	707	12.84	14.73	2.221	2.682	1.936	27.83
45R-6, 47–49	707	12.53	14.33	2.224	2.672	1.945	27.20
45R-6, 114–116	708	11.80	13.38	2.211	2.617	1.951	25.47
46R-1, 40–42	709	12.26	13.98	2.235	2.677	1.961	26.75
46R-1, 93–95	710	13.65	15.81	2.185	2.688	1.886	29.82
46R-2, 4–6	711	12.15	13.83	2.190	2.621	1.924	26.60
46R-2, 111–113	712	13.68	15.85	2.122	2.581	1.832	29.03
46R-3, 9–11	712	12.66	14.50	2.210	2.655	1.930	27.31
46R-3, 71–73	713	12.24	13.94	2.194	2.633	1.926	26.85
46R-4, 6–8	714	12.74	14.59	2.178	2.631	1.901	27.74
46R-5, 61–63	716	11.79	13.36	2.215	2.623	1.954	25.49
46R-5, 108–110	716	13.26	15.29		3.466	2.284	34.09
46R-6, 2–4	717	12.60	14.42	2.187	2.639	1.912	27.57
46R-7, 13–15	718	12.76	14.63	2.215	2.668	1.932	27.59
47R-1, 14–16	718	12.06	13.72		2.920	2.099	28.11
47R-1, 140–142	720	13.30	15.34	2.193	2.658	1.901	28.47
47R-2, 32–34	720	12.78	14.65	2.203	2.649	1.921	27.48
47R-2, 80–82	721	12.65	14.49	2.213	2.660	1.933	27.33
47R-3, 30–32	722	13.19	15.19	2.162	2.600	1.877	27.82
47R-3, 147–149	723	13.58	15.72	2.159	2.614	1.866	28.63
47R-4, 68–70	723	13.79	16.00	2.206	2.705	1.902	29.70
47R-4, 117–119	724	13.09	15.07	2.164	2.600	1.881	27.66
47R-5, 84–86	725	13.99	16.27	2.110	2.550	1.815	28.82
48R-1, 54–56	728	15.00	17.64	2.155	2.706	1.832	32.32
48R-1, 124–126	729	13.71	15.89	2.157	2.643	1.861	29.57
48R-2, 51–53	730	15.35	18.14	2.141	2.699	1.812	32.86
48R-2, 89–91	730	16.42	19.65	2.063	2.608	1.724	33.88
48R-3, 144–146	732	15.06	17.73	2.158	2.684	1.833	31.71
48R-4, 35–37	733	14.78	17.35	2.150	2.686	1.832	31.79
48R-5, 92–94	735	14.84	17.42	2.094	2.587	1.783	31.07
48R-6, 146–148	737	14.44	16.88	2.159	2.685	1.848	31.19
48R-7, 57–59	737	13.66	15.82	2.181	2.682	1.883	29.79
49R-1, 142–144	739	14.18	16.53	2.196	2.736	1.884	31.14
49R-2, 50–52	740	13.62	15.77	2.196	2.707	1.897	29.92
49R-2, 147–149	741	14.43	16.86	2.149	2.666	1.839	31.01
49R-3, 63–65	741	14.34	16.74	2.135	2.635	1.829	30.60
49R-3, 129–131	742	15.35	18.13	2.135	2.688	1.807	32.76
49R-4, 46–48	743	14.58	17.06	2.124	2.628	1.814	30.96
49R-4, 144–146	744	14.18	16.53	2.140	2.638	1.837	30.36
49R-5, 4–6	744	14.45	16.88	2.146	2.660	1.836	30.99
50R-1, 37–39	746	14.24	16.61	2.153	2.664	1.847	30.67
50R-2, 43–45	748	13.70	15.87	2.152	2.607	1.857	28.78
51R-1, 38–40	747	14.91	17.52	2.159	2.679	1.837	31.42
51R-1, 70–72	748	13.02	14.97	2.170	2.607	1.888	27.59
51R-2, 14–16	749	13.82	16.04	2.172	2.648	1.872	29.30
51R-2, 60–62	749	14.24	16.60	2.157	2.642	1.850	29.98
51R-3, 67–69	751	14.77	17.33	2.111	2.587	1.800	30.44
51R-3, 124–126	751	15.12	17.81	2.115	2.610	1.795	31.21
51R-4, 11–13	752	13.68	15.85	2.133	2.575	1.841	28.49
51R-4, 73–75	752	15.38	18.18	2.114	2.621	1.789	31.75
51R-5, 60–62	753			2.021			
52R-1, 72–74	758	15.19	17.92	2.077	2.545	1.761	30.80
52R-1, 139–141	758	16.20	19.33	2.190	2.808	1.835	34.63
52R-2, 64–66	759	14.44	16.88	2.087	2.531	1.786	29.42
52R-2, 99–101	759	15.56	18.43	2.120	2.641	1.790	32.21
52R-3, 6–8	760	14.59	17.08	2.140	2.628	1.827	30.47
52R-3, 139–141	761	14.31	16.70	2.123	2.614	1.820	30.38
52R-4, 35–37	762	13.28	15.32	2.159	2.600	1.872	27.99
52R-4, 101–103	763	14.99	17.64	2.075	2.532	1.764	30.36
52R-5, 17–19	763	16.37	19.58	2.034	2.520	1.701	32.50
52R-5, 139–141	764	15.77	18.72	2.090	2.625	1.760	32.95
52R-6, 11–13	765	16.82	20.22	2.049	2.569	1.704	33.64
52R-6, 102–104	766	15.45	18.28	2.102	2.603	1.777	31.71
53R-1, 35–37	767	16.07	19.15	2.095	2.651	1.758	33.67
53R-1, 114–116	768	15.44	18.26		3.033	1.952	35.64
53R-2, 77–79	769	15.66	18.56	2.085	2.612	1.759	32.65
53R-2, 140–142	769	16.44	19.67	2.076	2.633	1.735	34.12
53R-3, 25–27	770	16.67	20.01	2.083	2.659	1.735	34.72
53R-3, 96–98	770	16.21	19.34	2.086	2.640	1.748	33.80
53R-4, 1–3	771	15.69	18.61	2.133	2.704	1.799	33.48
53R-4, 84–86	772	16.34	19.53	2.109	2.692	1.764	34.46
53R-5, 6–8	772	15.48	18.32	2.118	2.664	1.790	32.80
53R-5, 126–128	774	15.63	18.52	2.115	2.666	1.785	33.06
53R-6, 43–45	774	15.22	17.96	2.109	2.634	1.788	32.11
53R-6, 148–150	775	14.94	17.57	2.146	2.686	1.825	32.06
54R-1, 74–76	777	14.95	17.58	2.164	2.720	1.840	32.35
54R-1, 145–147	778	13.65	15.81	2.126	2.562	1.836	28.33
54R-2, 44–46	778	14.44	16.87	2.186	2.733	1.871	31.56
54R-2, 110–112	779	15.06	17.73	2.140	2.682	1.818	32.22
54R-3, 17–19	779	13.63	15.78	2.212	2.734	1.910	30.14
54R-3, 145–147	781	14.58	17.06		2.292	1.648	28.11
54R-4, 50–52	781	14.14	16.47	2.172	2.691	1.864	30.71
54R-4, 146–148	782	13.71	15.89	2.180	2.683	1.881	29.89
54R-5, 67–69	783	15.96	19.00	2.145	2.742	1.803	34.25
54R-5, 147–149	784	13.71	15.89	2.191	2.702	1.891	30.04
54R-6, 66–68	784	14.26	16.63	2.175	2.703	1.865	31.01
55R-1, 7–9	786	14.71	17.25	2.154	2.659	1.837	30.92
55R-1, 87–89	787	16.24	19.40	2.095	2.628	1.755	33.22
55R-2, 40–42	788	16.22	19.36	2.070	2.579	1.734	32.77
55R-2, 121–123	789	13.41	15.48	2.142	2.578	1.855	28.03
55R-3, 51–53	790	12.80	14.68	2.207	2.658	1.925	27.58
55R-3, 140–142	790	13.82	16.03	2.158	2.623	1.859	29.10
55R-4, 30–32	791	13.28	15.32	2.189	2.650	1.898	28.38
55R-4, 136–138	792	14.17	16.51	2.154	2.634	1.849	29.79
55R-5, 60–62	793	14.35	16.75	2.174	2.677	1.862	30.45
55R-5, 114–116	793	14.44	16.87	2.113	2.575	1.808	29.78
55R-6, 80–82	794	15.24	17.98	2.119	2.623	1.796	31.52
56R-1, 16–18	796	13.58	15.71	2.181	2.651	1.885	28.90
56R-1, 78–80	796	15.89	18.89	2.102	2.623	1.768	32.60
56R-2, 6–8	797	13.46	15.55	2.191	2.662	1.896	28.78
56R-2, 90–92	798	14.37	16.78	2.136	2.611	1.829	29.96
56R-3, 44–46	799	13.85	16.07	2.165	2.636	1.865	29.26
56R-3, 140–142	800	14.39	16.80	2.138	2.615	1.830	30.02
56R-4, 134–136	801	13.28	15.31	2.186	2.646	1.896	28.33
56R-5, 68–70	802	12.43	14.19	2.185	2.603	1.913	26.50
56R-5, 122–124	803	14.00	16.28	2.131	2.586	1.833	29.13
56R-6, 44–46	804	13.61	15.75	2.184	2.658	1.887	29.01
57R-1, 61–63	806	14.84	17.42	2.148	2.656	1.830	31.12
57R-1, 111–113	806	14.97	17.60	2.156	2.677	1.833	31.50
57R-2, 29–31	807	15.14	17.84	2.130	2.638	1.808	31.47
57R-2, 141–143	808	15.27	18.02	2.110	2.609	1.788	31.45
57R-3, 18–20	808	14.31	16.69	2.153	2.639	1.845	30.07
57R-3, 121–123	809	13.99	16.26	2.175	2.661	1.871	29.69
57R-4, 6–8	810	13.29	15.33	2.177	2.630	1.887	28.24
57R-4, 128–130	811	16.63	19.94	2.104	2.663	1.754	34.14
57R-5, 21–23	811	15.75	18.69	2.096	2.606	1.766	32.22
57R-5, 134–136	813	14.28	16.66	2.140	2.614	1.835	29.83
57R-6, 47–49	813	15.29	18.05	2.133	2.651	1.807	31.84
57R-6, 145–147	814	14.30	16.69	2.153	2.638	1.845	30.06
57R-7, 13–15	814	14.03	16.32	2.176	2.664	1.870	29.80
58R-1, 22–24	815	14.03	16.31	2.140	2.603	1.840	29.30
58R-1, 51–53	815	16.07	19.15	2.101	2.630	1.763	32.96
58R-2, 90–92	817	18.28	22.37	2.025	2.591	1.655	36.13
58R-2, 146–148	818	15.64	18.54	2.102	2.612	1.774	32.09
58R-3, 64–66	818	15.46	18.28	2.136	2.665	1.806	32.23
58R-3, 142–144	819	14.43	16.86	2.150	2.639	1.840	30.28
58R-4, 49–51	820	13.77	15.98	2.188	2.673	1.887	29.42
58R-4, 138–140	821	13.71	15.89	2.196	2.684	1.895	29.40
58R-5, 12–14	821	13.30	15.34	2.185	2.644	1.894	28.35
58R-5, 74–76	822	13.81	16.02	2.181	2.663	1.880	29.40
58R-6, 6–8	822	13.84	16.06	2.189	2.678	1.886	29.57
58R-6, 100–102	823	14.88	17.47	2.160	2.679	1.839	31.37
58R-7, 3–5	824	14.17	16.51	2.165	2.653	1.858	29.96
59R-1, 19–21	825	14.12	16.45	2.158	2.638	1.853	29.75
59R-1, 91–93	825	14.46	16.91	2.141	2.625	1.832	30.23
59R-2, 18–20	826	13.19	15.20	2.159	2.596	1.874	27.81
59R-2, 112–114	827	14.70	17.23	2.136	2.627	1.822	30.65
59R-3, 23–25	828	15.62	18.51	2.104	2.614	1.776	32.08
59R-3, 146–148	829	13.10	15.07	2.201	2.662	1.913	28.15
59R-4, 27–29	829			2.075			
59R-4, 60–62	830	13.60	15.74	2.181	2.652	1.884	28.94
59R-5, 107–109	832	13.63	15.77	2.175	2.644	1.879	28.93
59R-6, 10–12	832	14.20	16.55	2.154	2.634	1.848	29.85
59R-6, 143–145	833	15.12	17.82	2.141	2.657	1.817	31.60
59R-7, 56–58	834	13.60	15.74	2.181	2.652	1.885	28.95
60R-1, 32–34	835	13.18	15.19	2.190	2.647	1.901	28.18
60R-1, 82–84	835	14.08	16.39	2.173	2.663	1.867	29.88
60R-2, 70–72	836	13.70	15.87	2.168	2.635	1.871	28.98
60R-2, 132–134	837	15.19	17.91	2.164	2.702	1.835	32.08
60R-3, 21–23	837	13.45	15.54	2.178	2.639	1.885	28.59
60R-3, 45–47	838	14.32	16.71	2.186	2.697	1.873	30.55
60R-4, 2–4	839	15.61	18.49	2.149	2.697	1.814	32.74
60R-4, 137–139	840	13.25	15.27	2.158	2.596	1.872	27.90
60R-5, 60–62	841	13.67	15.83	2.187	2.665	1.888	29.17
61R-1, 114–116	845	13.25	15.28	2.202	2.672	1.910	28.49
61R-1, 131–133	845	14.73	17.27	2.174	2.697	1.854	31.25
61R-2, 3–5	845	13.78	15.99	2.217	2.724	1.912	29.83
61R-2, 82–84	846	13.44	15.53	2.206	2.688	1.910	28.95
61R-3, 56–58	847	14.52	16.99	2.167	2.674	1.853	30.73
61R-3, 88–90	848	13.60	15.75	2.169	2.632	1.874	28.80
61R-4, 84–86	849	13.05	15.01	2.211	2.677	1.923	28.17
61R-4, 126–128	850	12.82	14.70	2.228	2.693	1.943	27.87
61R-5, 28–30	850	12.33	14.07	2.227	2.668	1.953	26.81
62R-1, 15–17	854	12.68	14.53	2.224	2.680	1.942	27.54
62R-1, 70–72	854	13.72	15.90	2.169	2.637	1.871	29.04
62R-2, 55–57	856	14.08	16.38	2.186	2.685	1.878	30.04
62R-2, 113–115	856	15.77	18.72	2.193	2.788	1.847	33.75
62R-3, 73–75	857	13.13	15.11	2.212	2.682	1.922	28.34
62R-3, 85–87	857	15.11	17.80	2.160	2.691	1.834	31.86

Table 10 (continued).

Core, section, interval (cm)	Depth (mbsf)	Water content (bulk wt %)	Water content (dry wt %)	Bulk density (Mg/m^3)	Grain density (Mg/m^3)	Dry density (Mg/m^3)	Porosity (%)
62R-4, 91–93	859	14.49	16.94	2.190	2.712	1.873	30.96
62R-4, 146–148	859	12.43	14.19	2.226	2.671	1.950	27.00
62R-5, 42–44	860	12.48	14.26	2.217	2.659	1.941	27.02
62R-5, 91–93	860	12.22	13.92	2.240	2.683	1.966	26.73
62R-6, 7–9	861	11.51	13.01	2.237	2.645	1.980	25.14
62R-6, 118–120	862	14.77	17.33	2.159	2.671	1.840	31.12
62R-7, 63–65	863	11.50	12.99	2.236	2.642	1.979	25.10
63R-1, 21–23	863	11.75	13.31	2.230	2.644	1.968	25.57
63R-1, 109–111	864	11.58	13.09	2.210	2.605	1.954	24.98
63R-2, 24–26	865	12.37	14.11	2.219	2.656	1.945	26.79
63R-2, 101–103	866	12.04	13.69	2.209	2.625	1.943	25.98
63R-3, 4–6	866	12.51	14.30	2.240	2.697	1.960	27.35
63R-3, 121–123	867	10.82	12.14	2.241	2.618	1.998	23.68
63R-4, 5–7	868	13.38	15.44	2.186	2.649	1.893	28.54
63R-4, 141–143	869	10.85	12.17	2.222	2.591	1.981	23.54
63R-5, 16–18	869	13.46	15.56	2.209	2.694	1.912	29.03
64R-1, 126–128	874	10.75	12.04	2.279	2.673	2.034	23.91
64R-1, 134–136	874	12.99	14.92	2.224	2.694	1.935	28.18
64R-2, 37–39	875	11.02	12.38	2.256	2.651	2.008	24.27
64R-2, 73–75	875	11.67	13.21	2.243	2.661	1.981	25.55
64R-3, 12–14	876	12.32	14.06	2.191	2.608	1.921	26.35
64R-3, 85–87	877	11.94	13.56	2.215	2.630	1.951	25.82
64R-3, 124–126	877			2.141			
64R-4, 5–7	877	11.68	13.22	2.182	2.566	1.928	24.88
64R-4, 68–70	878	10.58	11.83	2.236	2.600	2.000	23.09
64R-5, 9–11	879	12.69	14.54	2.199	2.639	1.920	27.24
64R-5, 139–141	880	10.84	12.15	2.220	2.587	1.980	23.49
64R-6, 11–13	880	11.39	12.86	2.153	2.508	1.907	23.94
64R-6, 144–146	882	12.30	14.03	2.174	2.581	1.907	26.11
65R-1, 14–16	883	11.65	13.18	2.151	2.515	1.900	24.45
65R-1, 144–146	884	12.36	14.10	2.161	2.562	1.894	26.06
65R-2, 37–39	884	12.88	14.78	2.139	2.548	1.863	26.88
65R-2, 141–143	885	12.37	14.12	2.155	2.552	1.888	26.02
65R-3, 69–71	886	13.45	15.53		2.353	1.734	26.30
66R-1, 27–29	892	12.60	14.42	2.140	2.539	1.870	26.33
66R-1, 93–95	893	13.76	15.96	2.127	2.568	1.834	28.57
67R-1, 17–19	902	10.87	12.20	2.196	2.552	1.957	23.31
67R-1, 125–127	903	11.09	12.47	2.199	2.565	1.955	23.80
67R-2, 50–52	903	10.63	11.90	2.218	2.575	1.982	23.02
67R-2, 128–130	904	10.85	12.17	2.195	2.550	1.957	23.25
67R-3, 57–59	905	9.70	10.75	2.248	2.580	2.030	21.29
67R-3, 125–127	906	11.72	13.28	2.184	2.571	1.928	24.99
67R-4, 22–24	906	12.58	14.39	2.145	2.545	1.875	26.33
67R-4, 99–101	907	12.32	14.06	2.155	2.550	1.889	25.92
67R-5, 95–97	908	11.17	12.58	2.179	2.539	1.935	23.76
67R-6, 131–133	910	12.87	14.78	2.127	2.529	1.853	26.72
67R-7, 58–60	911	10.92	12.26	2.197	2.555	1.957	23.42
69R-1, 6–8	921	11.34	12.79	2.187	2.558	1.939	24.20
69R-1, 147–149	922	6.76	7.25	2.265	2.483	2.112	14.94
69R-2, 17–19	922	9.41	10.38	2.290	2.627	2.075	21.03
69R-2, 141–143	924	8.62	9.44	2.313	2.624	2.113	19.47
69R-3, 58–60	924	8.43	9.21	2.331	2.641	2.134	19.19
69R-3, 143–145	925	8.40	9.17	2.287	2.579	2.095	18.75
69R-4, 46–48	926	7.67	8.30	2.331	2.608	2.153	17.45
69R-5, 10–12	927	8.67	9.49	2.344	2.671	2.141	19.83
69R-5, 137–139	928	6.89	7.40	2.374	2.630	2.210	15.96
69R-6, 30–32	929	7.80	8.46	2.338	2.622	2.155	17.80
69R-CC, 7–9	930	9.44	10.43	2.249	2.568	2.036	20.72
154-925B-							
1H-1, 88–90	0.88	52.76	111.70	1.491	3.030	0.704	76.77
1H-3, 33–35	3.33	51.26	105.18	1.502	2.948	0.732	75.16
2H-1, 100–102	5.5	47.87	91.81	1.544	2.889	0.805	72.14
2H-3, 54–56	8.04	47.50	90.49	1.542	2.840	0.809	71.50
2H-5, 54–56	11	48.28	93.34	1.488	2.573	0.769	70.10
2H-7, 29–31	13.3	49.57	98.30	1.469	2.561	0.741	71.07
3H-1, 129–131	15.3	45.36	83.00	1.586	2.908	0.867	70.21
3H-3, 74–76	17.7	40.50	68.07	1.673	2.942	0.996	66.16
3H-5, 74–76	20.7	41.28	70.30	1.657	2.929	0.973	66.77
3H-7, 7–9	23.1	42.93	75.23	1.621	2.884	0.925	67.93
4H-1, 74–76	24.2	42.08	72.65	1.636	2.888	0.948	67.20
4H-3, 74–76	27.2	42.41	73.65	1.625	2.858	0.936	67.26
4H-5, 74–76	30.2	42.53	74.02	1.620	2.842	0.931	67.25
4H-7, 29–31	32.8	41.28	70.30	1.642	2.852	0.964	66.18
5H-1, 74–76	33.7	40.37	67.71	1.665	2.889	0.993	65.63
5H-3, 74–76	36.7	40.17	67.13	1.659	2.840	0.993	65.05
5H-4, 39–41	37.9	42.08	72.65	1.635	2.885	0.947	67.17
5H-6, 38–40	40.9	38.52	62.65	1.694	2.869	1.042	63.69
6H-2, 100–102	45	39.56	65.44	1.658	2.785	1.002	64.01
6H-4, 74–76	47.7	40.26	67.39	1.651	2.806	0.986	64.86
6H-6, 98–100	51	39.44	65.12	1.670	2.833	1.012	64.30
7H-1, 75–77	52.8	39.46	65.17	1.672	2.842	1.012	64.39
7H-3, 18–20	55.2	39.87	66.31	1.667	2.855	1.003	64.89
7H-5, 74–76	58.7	37.65	60.39	1.706	2.849	1.063	62.68
7H-7, 9–11	61.1	36.86	58.39	1.729	2.891	1.092	62.23
8H-1, 74–76	62.2	35.94	56.11	1.705	2.716	1.092	59.80
8H-3, 74–76	65.2	35.38	54.74	1.712	2.707	1.107	59.13
8H-5, 39–41	67.9	36.81	58.26	1.721	2.850	1.088	61.85
9H-1, 40–42	71.4	36.61	57.75	1.684	2.682	1.068	60.19
9H-3, 74–76	74.7	36.20	56.73	1.701	2.718	1.085	60.09

Core, section, interval (cm)	Depth (mbsf)	Water content (bulk wt %)	Water content (dry wt %)	Bulk density (Mg/m^3)	Grain density (Mg/m^3)	Dry density (Mg/m^3)	Porosity (%)
9H-5, 127–129	78.3	36.42	57.28	1.656	2.561	1.053	58.88
9H-7, 22–24	80.2	37.39	59.72	1.684	2.737	1.055	61.47
10H-1, 68–70	81.2	35.80	55.75	1.666	2.558	1.069	58.20
10H-3, 12–14	83.6	37.49	59.98	1.697	2.799	1.061	62.11
10H-5, 9–11	86.6	34.76	53.27	1.718	2.687	1.121	58.28
10H-7, 7–9	89.6	36.85	58.35	1.715	2.826	1.083	61.68
11H-1, 32–34	90.3	37.31	59.51	1.699	2.794	1.065	61.88
11H-3, 105–107	94.1	37.46	59.90	1.546	2.224	0.967	56.53
11H-5, 52–54	96.5	37.59	60.22	1.690	2.778	1.055	62.01
11H-7, 40–42	99.4	37.74	60.62	1.689	2.782	1.051	62.21
12H-1, 60–62	100	36.06	56.39	1.698	2.699	1.086	59.77
12H-3, 17–19	103	37.41	59.77	1.703	2.821	1.066	62.20
12H-5, 38–40	106	35.60	55.28	1.705	2.692	1.098	59.23
12H-7, 26–28	109	35.07	54.02	1.649	2.457	1.070	56.44
13H-1, 85–87	110	37.20	59.23	1.619	2.467	1.017	58.78
13H-3, 66–68	113	35.01	53.87	1.772	2.919	1.152	60.55
13H-5, 61–63	116	35.92	56.05	1.628	2.430	1.043	57.07
13H-7, 31–33	118	36.59	57.71	1.691	2.706	1.072	60.39
14H-1, 31–33	119	36.68	57.92	1.732	2.887	1.097	62.01
14H-3, 122–124	123	35.05	53.96	1.762	2.883	1.145	60.30
14H-5, 91–93	125	36.54	57.58	1.724	2.840	1.094	61.48
14H-7, 19–21	128	36.12	56.54	1.731	2.839	1.106	61.04
15H-1, 124–126	129	37.46	59.91	1.709	2.849	1.069	62.49
15H-3, 73–75	132	37.26	59.38	1.722	2.889	1.080	62.61
15H-5, 74–76	135	37.14	59.09	1.713	2.841	1.077	62.10
16H-1, 72–74	138	35.99	56.24	1.729	2.818	1.106	60.74
16H-3, 111–113	142	34.28	52.15	1.742	2.745	1.145	58.28
16H-5, 74–76	144	34.12	51.78	1.757	2.789	1.157	58.50
16H-7, 26–28	147	34.84	53.48	1.773	2.910	1.155	60.31
17H-1, 79–81	148	32.71	48.60	1.814	2.899	1.221	57.90
17H-3, 70–72	151	33.56	50.52	1.636	2.343	1.087	53.60
17H-5, 51–53	154	35.57	55.20	1.725	2.769	1.111	59.87
17H-7, 25–27	156	34.94	53.71	1.751	2.828	1.139	59.71
18H-1, 81–83	157	31.72	46.46	1.633	2.256	1.115	50.57
18H-3, 108–110	161	34.17	51.90	1.755	2.785	1.155	58.53
18H-5, 123–125	164	32.32	47.74	1.640	2.301	1.110	51.75
18H-6, 130–132	165	33.16	49.62	1.692	2.500	1.131	54.76
19H-1, 118–120	167	30.52	43.93	1.828	2.788	1.270	54.45
19H-3, 129–131	170	31.06	45.04	1.846	2.888	1.272	55.94
19H-5, 133–135	173	33.10	49.48	1.783	2.814	1.193	57.61
20H-1, 130–132	177	32.00	47.07	1.829	2.901	1.244	57.14
20H-3, 92–94	179	35.29	54.53	1.749	2.846	1.132	60.24
20H-5, 49–51	182	30.27	43.40	1.857	2.870	1.295	54.87
21H-1, 139–141	186	29.76	42.36	1.864	2.856	1.310	54.15
21H-3, 140–142	189	31.67	46.34	1.814	2.821	1.239	56.06
21H-5, 139–141	192	28.57	40.00	1.869	2.789	1.335	52.13
22H-2, 3–5	196	31.22	45.39	1.828	2.838	1.257	55.70
22H-3, 55–57	198	31.15	45.24	1.801	2.740	1.240	54.75
22H-5, 126–128	202	31.49	45.96	1.801	2.763	1.234	55.35
23H-3, 37–39	207	29.85	42.55	1.867	2.871	1.310	54.39
23H-5, 15–17	210	31.95	46.96	1.835	2.918	1.248	57.22
23H-7, 35–37	213	30.84	44.59	1.839	2.849	1.272	55.36
24H-3, 95–97	217	34.73	53.21	1.909	3.532	1.246	64.72
24H-5, 123–125	221	29.53	41.89	1.947	3.126	1.372	56.11
24H-7, 33–35	223	30.92	44.76	1.866	2.949	1.289	56.30
25H-1, 105–107	224	31.68	46.37	1.863	3.003	1.273	57.61
25H-3, 98–100	227	30.21	43.28	1.887	2.968	1.317	55.63
25H-5, 98–100	230	32.55	48.27	1.834	2.964	1.237	58.27
25H-7, 61–63	233	29.86	42.57	1.879	2.912	1.318	54.75
26H-1, 57–59	233	31.34	45.65	1.843	2.900	1.265	56.37
26H-3, 115–117	237	27.29	37.54	1.900	2.796	1.381	50.61
26H-6, 134–136	241	29.47	41.79	1.860	2.820	1.312	53.50
26H-7, 34–36	242	29.42	41.69	1.870	2.852	1.320	53.71
27H-1, 42–44	242	32.25	47.61	1.814	2.864	1.229	57.10
27H-3, 128–130	246	27.88	38.66	1.918	2.895	1.383	52.21
27H-5, 20–22	248	30.89	44.71	1.831	2.827	1.266	55.23
27H-7, 28–30	251	32.24	47.58	1.823	2.898	1.235	57.37
28H-1, 51–53	252	32.62	48.42	1.785	2.788	1.203	56.85
28H-3, 47–49	255	31.86	46.76	1.837	2.921	1.252	57.14
28H-3, 51–53	255	31.56	46.11	1.802	2.771	1.233	55.50
28H-4, 129–131	257	29.96	42.77	1.855	2.840	1.299	54.25
28H-4, 132–134	257	30.35	43.58	1.846	2.838	1.286	54.69
28H-5, 49–51	258	32.17	47.44	1.784	2.750	1.210	56.02
28H-7, 57–59	261	31.75	46.52	1.803	2.789	1.231	55.88
28H-7, 60–62	261	30.45	43.79	1.860	2.894	1.294	55.30
29H-1, 99–101	262	33.68	50.78	1.778	2.837	1.179	58.44
29H-5, 88–90	268	33.44	50.24	1.743	2.689	1.160	56.87
29H-7, 32–34	270	34.77	53.32	1.762	2.860	1.149	59.81
30H-1, 62–64	271	26.70	36.42	1.932	2.851	1.416	50.34
30H-3, 83–85	274			1.978			
30H-5, 109–111	278	27.19	37.35	1.678	2.202	1.221	44.53
31H-1, 129–131	281	26.67	36.38	1.926	2.833	1.412	50.15
31H-3, 58–60	284	27.00	36.98	1.921	2.841	1.403	50.63
31H-5, 134–136	287	26.37	35.82	1.945	2.869	1.432	50.08
32H-1, 145–147	291	29.22	41.27	1.868	2.830	1.322	53.27
32H-3, 62–64	293	29.85	42.54	1.868	2.876	1.311	54.43
32H-5, 126–128	297	27.76	38.43	1.840	2.650	1.329	49.85
33H-1, 109–111	300	27.50	37.94	1.896	2.799	1.374	50.89
33H-3, 30–32	302	28.79	40.43	1.869	2.803	1.331	52.52
33H-5, 43–45	305	29.37	41.59	1.822	2.694	1.287	52.23

Table 10 (continued).

Core, section, interval (cm)	Depth (mbsf)	Water content (bulk wt %)	Water content (dry wt %)	Bulk density (Mg/m³)	Grain density (Mg/m³)	Dry density (Mg/m³)	Porosity (%)
34H-1, 104–106	310	31.93	46.90	1.758	2.646	1.197	54.78
34H-2, 14–16	310	27.24	37.43	1.876	2.725	1.365	49.80
34H-3, 145–147	313	28.86	40.56	1.837	2.709	1.307	51.70
154-925C-							
1H-2, 71–73	2.21	49.52	98.10	1.516	2.863	0.765	73.27
1H-6, 26–28	7.76	49.01	96.11	1.523	2.860	0.777	72.85
2H-2, 72–74	10.2	45.53	83.58	1.595	2.985	0.869	70.89
2H-4, 14–16	12.6	49.95	99.82	1.531	3.023	0.766	74.65
2H-6, 52–54	16	45.85	84.66	1.574	2.884	0.852	70.44
3H-2, 108–110	20.1	41.23	70.16	1.639	2.830	0.963	65.97
3H-4, 17–19	22.2	42.05	72.57	1.639	2.902	0.950	67.27
3H-6, 114–116	26.1	43.17	75.95	1.625	2.931	0.924	68.48
4H-2, 110–112	29.6	44.11	78.93	1.608	2.923	0.899	69.25
4H-4, 59–61	32.1	43.41	76.72	1.621	2.927	0.917	68.67
4H-6, 105–107	35.6	40.84	69.04	1.653	2.868	0.978	65.90
5H-2, 49–51	38.5	40.71	68.65	1.667	2.929	0.989	66.25
5H-4, 100–102	42	40.99	69.48	1.637	2.801	0.966	65.51
5H-6, 101–103	45	39.33	64.82	1.660	2.777	1.007	63.73
6H-2, 106–108	48.6	40.11	66.96	1.660	2.840	0.994	64.99
6H-4, 14–16	50.6	38.77	63.32	1.671	2.784	1.023	63.25
6H-6, 32–34	53.8	39.90	66.40	1.676	2.903	1.007	65.30
7H-4, 47–49	60.5	38.43	62.41	1.674	2.771	1.031	62.80
7H-6, 54–56	63.5	38.98	63.88	1.677	2.829	1.023	63.82
8H-2, 120–122	67.7	37.43	59.83	1.721	2.902	1.077	62.89
8H-4, 19–21	69.7	37.91	61.06	1.687	2.786	1.047	62.41
8H-6, 119–121	73.7	35.63	55.35	1.741	2.839	1.121	60.53
9H-2, 60–62	76.6	37.61	60.29	1.674	2.708	1.044	61.44
9H-4, 85–87	79.9	35.83	55.83	1.711	2.735	1.098	59.84
9H-6, 69–71	82.7	42.75	74.67	1.615	2.837	0.925	67.40
10H-2, 108–110	86.6	39.59	65.53	1.684	2.915	1.018	65.09
10H-4, 112–114	89.6	38.11	61.57	1.689	2.812	1.045	62.83
10H-6, 69–71	92.2	40.70	68.62	1.645	2.814	0.975	65.33
11H-2, 125–127	96.3	35.72	55.57	1.667	2.560	1.072	58.13
11H-4, 92–94	98.9	36.67	57.91	1.722	2.844	1.091	61.65
11H-6, 44–46	101	37.40	59.75	1.695	2.785	1.061	61.90
12H-2, 74–76	105	38.15	61.67	1.702	2.872	1.053	63.36
12H-4, 74–76	108	35.20	54.33	1.638	2.427	1.061	56.28
12H-6, 73–75	111	36.45	57.35	1.710	2.774	1.087	60.83
13H-2, 74–76	115	35.34	54.64	1.746	2.840	1.129	60.24
13H-4, 84–86	118	36.07	56.43	1.731	2.834	1.107	60.95
13H-6, 74–76	121	35.30	54.55	1.731	2.775	1.120	59.64
14H-4, 81–83	127	35.82	55.80	1.726	2.795	1.108	60.36
14H-6, 79–81	130	36.19	56.72	1.678	2.630	1.071	59.28
15H-2, 68–70	134	37.33	59.56	1.624	2.492	1.018	59.16
15H-4, 80–82	137	35.81	55.78	1.676	2.596	1.076	58.57
15H-6, 62–64	140	35.53	55.10	1.658	2.515	1.069	57.49
16H-2, 110–112	144	34.57	52.83	1.693	2.585	1.108	57.14
16H-4, 69–71	146	34.40	52.44	1.748	2.775	1.146	58.69
17H-2, 15–17	152	33.36	50.05	1.788	2.851	1.191	58.21
17H-4, 111–113	156	33.55	50.50	1.774	2.812	1.178	58.09
17H-6, 68–70	159	31.76	46.54	1.816	2.836	1.239	56.30
18H-1, 89–91	161	33.48	50.32	1.796	2.892	1.195	58.69
18H-3, 72–74	164	31.80	46.62	1.810	2.817	1.235	56.18
18H-6, 85–87	168	31.49	45.97	1.804	2.775	1.236	55.47
19H-2, 66–68	172	31.45	45.89	1.807	2.781	1.238	55.47
19H-4, 88–90	175	29.98	42.82	1.822	2.733	1.276	53.32
19H-6, 81–83	178	33.41	50.17	1.763	2.762	1.174	57.49
20H-2, 106–108	182	30.91	44.73	1.827	2.811	1.262	55.11
20H-4, 82–84	184	30.40	43.68	1.801	2.692	1.253	53.44
20H-6, 69–71	187	29.46	41.76	1.858	2.816	1.311	53.44
21H-4, 109–111	194	29.84	42.54	1.855	2.831	1.301	54.03
21H-6, 91–93	197	33.02	49.29	1.762	2.730	1.180	56.78
22H-2, 92–94	200	29.70	42.25	1.851	2.810	1.302	53.68
22H-4, 121–123	204	30.28	43.43	1.844	2.827	1.286	54.51
22H-6, 129–131	207	29.24	41.32	1.789	2.586	1.266	51.05
23H-4, 108–110	213	30.23	43.33	1.843	2.820	1.286	54.39
23H-6, 116–118	216	31.87	46.79	1.787	2.740	1.217	55.58
24H-2, 18–20	219	27.79	38.48	1.733	2.362	1.252	47.00
24H-4, 27–29	222	26.42	35.90	1.743	2.329	1.282	44.94
24H-6, 105–107	226	28.34	39.54	1.705	2.312	1.222	47.15
25H-2, 50–52	229	30.44	43.75	1.796	2.679	1.249	53.36
25H-3, 6–8	230	30.81	44.52	1.773	2.628	1.227	53.32
25H-3, 19–21	230	32.88	48.98	1.794	2.838	1.204	57.57
25H-3, 29–31	230	31.26	45.49	1.815	2.795	1.247	55.38
25H-3, 61–63	230	31.86	46.75	1.798	2.778	1.225	55.90
25H-3, 79–81	230	30.16	43.18	1.841	2.807	1.286	54.20
25H-3, 98–100	230	33.37	50.08	1.783	2.835	1.188	58.09
25H-3, 116–118	231	33.08	49.42	1.770	2.765	1.185	57.15
25H-3, 132–134	231	31.76	46.54	1.809	2.812	1.235	56.09
25H-4, 2–4	231	33.54	50.46	1.768	2.790	1.175	57.88
25H-4, 17–19	231	31.90	46.84	1.803	2.800	1.228	56.15
25H-4, 40–42	231	31.81	46.64	1.752	2.620	1.195	54.40
25H-4, 61–63	232	30.55	44.00	1.673	2.319	1.162	49.89
25H-4, 76–78	232	32.42	47.98	1.806	2.849	1.220	57.16
25H-4, 89–91	232	30.52	43.92	1.841	2.834	1.279	54.85
25H-4, 104–106	232	31.07	45.07	1.835	2.851	1.265	55.64
25H-4, 118–120	232	30.04	42.94	1.879	2.927	1.314	55.09
25H-4, 138–140	232	31.91	46.86	1.820	2.860	1.239	56.68
25H-6, 37–39	234	30.96	44.85	1.815	2.775	1.253	54.86
26H-2, 67–69	238	28.70	40.26	1.706	2.331	1.217	47.80
26H-4, 18–20	241	34.06	51.66	1.771	2.841	1.168	58.89
26H-6, 95–97	244	24.30	32.11	1.970	2.798	1.491	46.72
27H-2, 59–61	248	29.26	41.36	1.745	2.462	1.235	49.85
27H-6, 21–23	253	29.55	41.94	1.799	2.634	1.267	51.89
27H-6, 115–117	254	29.58	42.00	1.788	2.604	1.259	51.63
28H-2, 29–31	257	29.36	41.57	1.856	2.801	1.311	53.20
28H-4, 96–98	260	29.76	42.36	1.889	2.940	1.327	54.87
28H-6, 132–134	264	29.75	42.34	1.869	2.872	1.313	54.27
29H-2, 72–74	267	28.73	40.31	1.823	2.657	1.299	51.11
29H-4, 130–132	270	28.84	40.52	1.868	2.802	1.329	52.57
29H-6, 101–103	273	24.73	32.86	1.928	2.716	1.451	46.56
30H-2, 121–123	277	29.10	41.05	1.738	2.433	1.232	49.36
30H-4, 85–87	279	24.11	31.78	1.926	2.673	1.461	45.33
30H-6, 122–124	283	24.30	32.11	1.926	2.684	1.458	45.68
31H-2, 75–77	286	27.83	38.56	1.893	2.811	1.366	51.41
31H-4, 82–84	289	25.18	33.66	1.985	2.899	1.485	48.79
31H-6, 50–52	292	27.83	38.57	1.888	2.797	1.363	51.29
32H-2, 76–78	295	28.85	40.55	1.848	2.743	1.315	52.05
32H-4, 79–81	298	26.80	36.61	1.878	2.703	1.375	49.13
32H-6, 69–71	301	28.55	39.95	1.849	2.725	1.321	51.52
33H-2, 67–69	305	26.95	36.89	1.932	2.869	1.411	50.81
33H-4, 97–99	308	27.60	38.13	1.890	2.789	1.369	50.93
33H-6, 131–133	311	28.36	39.58	1.870	2.778	1.340	51.77
34H-2, 135–137	315	29.90	42.64	1.823	2.731	1.278	53.20
34H-4, 98–100	317	26.39	35.85	1.899	2.735	1.398	48.91
35X-2, 92–94	324	28.39	39.64	1.836	2.676	1.315	50.87
35X-4, 132–134	327	28.65	40.16	1.824	2.657	1.301	51.02
35X-6, 9–11	329	29.14	41.11	1.816	2.662	1.287	51.65
36X-2, 96–98	334	29.61	42.06	1.798	2.634	1.266	51.96
36X-4, 129–131	337	30.27	43.42	1.809	2.711	1.262	53.47
36X-6, 35–37	339	29.98	42.82	1.789	2.630	1.253	52.36
37X-2, 31–33	343	31.51	46.02	1.782	2.701	1.220	54.82
37X-4, 53–55	346	29.91	42.67	1.817	2.714	1.274	53.06
37X-6, 93–95	349	30.54	43.97	1.775	2.619	1.233	52.92
38X-2, 96–98	353	29.25	41.34	1.815	2.666	1.285	51.83
38X-4, 107–109	356	27.63	38.17	1.847	2.664	1.337	49.81
38X-6, 59–61	358	29.19	41.21	1.827	2.699	1.294	52.06
154-925D-							
1H-4, 76–78	7.76	47.93	92.05	1.545	2.901	0.804	72.27
1H-6, 71–73	10.7	44.86	81.36	1.590	2.888	0.877	69.64
2H-4, 76–78	17.2	42.44	73.74	1.630	2.887	0.938	67.51
2H-6, 71–73	20.1	42.63	74.32	1.624	2.875	0.932	67.59
3H-2, 96–98	24	41.67	71.45	1.642	2.884	0.958	66.79
3H-6, 49–51	29.5	42.03	72.50	1.636	2.885	0.948	67.12
4H-2, 109–111	33.6	41.18	70.01	1.651	2.889	0.971	66.38
4H-6, 91–93	39.4	41.27	70.28	1.641	2.842	0.963	66.09
5H-4, 31–33	45.3	41.68	71.46	1.649	2.920	0.962	67.07
6H-2, 16–18	51.7	39.73	65.91	1.644	2.732	0.991	63.74
6H-6, 58–60	58.1	40.17	67.13	1.659	2.839	0.993	65.04
7H-4, 83–85	64.8	38.93	63.74	1.690	2.885	1.032	64.22
7H-6, 81–83	67.8	36.05	56.36	1.732	2.838	1.108	60.96
8H-2, 88–90	71.4	37.28	59.43	1.696	2.778	1.064	61.71
9H-4, 31–33	83.3	36.99	58.71	1.712	2.824	1.079	61.81
10H-4, 50–52	93	39.09	64.17	1.678	2.839	1.022	64.00
10H-6, 114–116	96.6	38.51	62.63	1.691	2.852	1.040	63.55
11H-2, 22–24	99.2	36.22	56.78	1.721	2.801	1.097	60.82
11H-4, 112–114	103	36.06	56.39	1.701	2.710	1.088	59.87
12H-2, 50–52	109	37.65	60.37	1.704	2.842	1.062	62.61
12H-6, 116–118	116	39.97	66.59	1.661	2.831	0.997	64.79
14H-4, 99–101	131	35.72	55.57	1.728	2.793	1.110	60.24
14H-6, 64–66	134	35.10	54.09	1.741	2.799	1.130	59.64
15H-2, 90–92	138	35.69	55.51	1.732	2.810	1.114	60.36
15H-6, 118–120	144	33.49	50.35	1.777	2.820	1.182	58.09
16H-4, 131–133	151	33.69	50.81	1.770	2.809	1.174	58.21
16H-6, 38–40	153	35.67	55.44	1.737	2.827	1.117	60.48
17H-4, 60–62	160	32.78	48.77	1.782	2.786	1.198	57.02
17H-6, 33–35	162	32.72	48.64	1.792	2.821	1.206	57.25
18H-2, 63–65	166	29.86	42.58	1.854	2.829	1.300	54.03
18H-4, 64–66	169	32.81	48.83	1.788	2.810	1.201	57.25
19H-6, 101–103	182	31.63	46.27	1.792	2.744	1.225	55.35
20H-4, 124–126	189	34.45	52.55	1.752	2.797	1.149	58.92
20H-6, 37–39	191	29.99	42.84	1.870	2.894	1.309	54.75
21H-2, 56–58	195	32.97	49.18	1.798	2.860	1.205	57.86
21H-6, 118–120	201	31.31	45.58	1.827	2.840	1.255	55.82
22H-3, 5–7	205	30.67	44.23	1.852	2.883	1.284	55.45
22H-3, 19–21	205	29.91	42.67	1.865	2.869	1.307	54.44
22H-3, 32–34	205	30.03	42.92	1.880	2.929	1.315	55.10
22H-3, 46–48	205	29.24	41.33	1.898	2.929	1.343	54.17
22H-3, 61–63	205	30.40	43.68	1.864	2.903	1.297	55.31
22H-3, 77–79	206	29.67	42.19	1.857	2.827	1.306	53.80
22H-3, 89–91	206	29.59	42.02	1.885	2.913	1.327	54.44
22H-3, 104–106	206	29.96	42.78	1.856	2.844	1.300	54.28
22H-3, 119–121	206	30.44	43.75	1.875	2.945	1.304	55.70
22H-3, 132–134	206	30.04	42.95	1.862	2.868	1.302	54.59
22H-3, 141–143	206	30.00	42.85	1.880	2.929	1.316	55.06
23H-4, 26–28	216	31.59	46.17	1.823	2.848	1.247	56.21
23H-6, 115–117	220	31.45	45.88	1.846	2.919	1.265	56.66
24H-2, 124–126	224	33.21	49.72	1.774	2.787	1.185	57.49

Table 10 (continued).

Core, section, interval (cm)	Depth (mbsf)	Water content (bulk wt %)	Water content (dry wt %)	Bulk density (Mg/m^3)	Grain density (Mg/m^3)	Dry density (Mg/m^3)	Porosity (%)
24H-6, 115–117	230	30.12	43.10	1.842	2.808	1.287	54.15
25H-2, 100–102	233	30.36	43.59	1.868	2.913	1.301	55.35
25H-6, 97–99	239	31.72	46.45	1.803	2.787	1.231	55.82
26H-2, 79–81	242	31.97	47.00	1.823	2.877	1.240	56.90
26H-4, 112–114	246	32.49	48.13	1.828	2.936	1.234	57.97
27H-4, 66–68	255	30.48	43.84	1.844	2.841	1.282	54.87
27H-6, 71–73	258	30.78	44.48	1.810	2.747	1.253	54.39
28H-2, 19–21	261	31.34	45.65	1.794	2.729	1.232	54.87
28H-5, 144–146	266	31.74	46.51	1.805	2.797	1.232	55.94
29H-2, 83–85	271	32.71	48.62	1.759	2.702	1.184	56.18
29H-4, 116–118	274	29.72	42.29	1.858	2.834	1.306	53.92
30H-4, 104–106	284	26.60	36.23	1.902	2.758	1.396	49.38
30H-5, 90–92	285	32.34	47.81	1.761	2.682	1.191	55.58
31H-2, 84–86	290	29.48	41.80	1.857	2.813	1.310	53.44
32H-4, 99–101	302	29.95	42.76	1.864	2.871	1.306	54.51
32H-6, 69–71	305	32.54	48.23	1.769	2.723	1.193	56.18
33H-2, 64–66	309	31.98	47.01	1.811	2.835	1.232	56.54
33H-4, 100–102	312	29.97	42.79	1.851	2.828	1.297	54.15
34H-2, 25–27	318	31.13	45.21	1.841	2.877	1.268	55.94
34H-2, 47–49	318	30.89	44.71	1.831	2.827	1.266	55.23
34H-2, 72–74	318	30.90	44.72	1.811	2.759	1.252	54.63
35H-2, 50–52	328	25.75	34.67	1.903	2.709	1.413	47.83
35H-4, 73–75	331	27.10	37.17	1.899	2.780	1.384	50.22
36H-6, 103–105	344	29.84	42.53	1.818	2.712	1.276	52.96
37H-2, 10–12	346	31.33	45.63	1.790	2.716	1.229	54.75
37H-6, 18–20	352	30.04	42.93	1.835	2.778	1.284	53.80
37H-7, 43–45	354	30.17	43.21	1.818	2.734	1.270	53.56

increase is probably associated with changes in the sediment physicochemical properties.

Resistivity

Resistivity at Site 925 was measured using two different probes (see "Physical Properties" section, "Explanatory Notes" chapter, this volume). Initially, variable sediment stiffness characteristics caused problems with consistent insertion of the probes, resulting in large data variability for Holes 925A and 925B. After completing Hole 925B, methods were evaluated and standardized so that Holes 925C and 925D provide the best quality data for the site (Table 13).

Electrical resistivity increases with depth below seafloor, as expected for sediment undergoing gravitational consolidation. Resistivity is dependent upon sediment porosity and tortuosity. The general trend of increasing resistivity with depth below seafloor is consistent with the index properties results of decreasing porosity with depth below seafloor (Fig. 41). Intervals in which electrical resistivity sharply increases with no similar increase in porosity suggests that tortuosity is high. High tortuosity is probably associated with sediment that has an altered microfabric (e.g., due to diagenesis). In Hole 925A, increases in resistivity with no large decreases in porosity occur over two intervals: from 600 to 640 mbsf and from ≈700 mbsf to the bottom of the hole.

In the upper 350 m of Site 925, measurements of resistivity were made in Holes 925B, 925C, and 925D (Fig. 42). The results from Hole 925B are not consistent with the other two holes below 150 mbsf, because of nonstandard probe insertion methods. However, correlation is good in Holes 925C and 925D. In Hole 925C, the large SIO probe was used, which measures across the entire diameter of the split core and therefore includes the disturbed outer sediment layer.

Natural Gamma

At Site 925, natural gamma activity of the sedimentary column was measured on whole-core sections using the MST, at a sampling interval that varied from 10 to 40 cm, and during downhole measurements of Holes 925A and 925C using the natural gamma spectrometry tool (NGT), at a sampling interval of 15 cm (see "Downhole Measurements" section, this chapter). Most gamma rays are emitted by the naturally occurring radioactive 40K and by a series of U and Th isotopes and their daughters. Because these elements tend to be most abundant in clay minerals, natural gamma variations at Site 925 depict lithologic variations resulting from changes in the relative abundance of carbonate and clay minerals (see "Lithostratigraphy" section, this chapter).

Using these natural gamma records, integration of the core data and log data is possible. For example, the natural gamma activities (API units) measured downhole and on whole cores are compared for Site 925A (Fig. 43). The logging depths were adjusted to mbsf using the natural gamma ray. Although more careful analyses will be performed onshore, it is relatively easy to identify the prominent features that are correlatable between the two records. This preliminary correlation suggests that no important offset is present between the cored records and those in situ (depth differences for the selected events vary from 0 to a maximum of about 1.5 m).

Elastic Rebound

Sediment is a material that deforms both elastically and plastically. Plastic deformation is typically observed as sediment consolidates over time during gravitational sediment loading. Although most of consolidation deformation (pore-fluid expulsion) is plastic and nonrecoverable, a portion of the deformation is elastic and will recover when the stress is removed. This recoverable elastic strain is referred to as elastic rebound when it is associated with stress relief of recovered sediment samples. Elastic rebound contributes to the growth of the site composite depth (see "Composite Section" section, this chapter) when compared to depth calculated in meters below seafloor, referenced to the drill string.

The elastic characteristics of a sediment are normally measured using one-dimensional consolidation testing (e.g., MacKillop et al., in press). These tests are normally performed on whole-round samples post cruise. One-dimensional consolidation testing will be conducted on Leg 154 sediment to characterize the elastic response of the sediment within each lithologic unit. For a preliminary assessment of the elastic rebound at this site, a coefficient of rebound (C_r) was assumed for the entire sediment section in each of the overlapping holes (925B, 925C, and 925D), based on consolidation tests performed on sediment of similar carbonate content (Valent et al., 1982).

The method used by MacKillop et al. (in press) to calculate elastic rebound for each index property interval was used with the calculated overburden stress from each hole. The method applies the known relationship of the rebound coefficient, measured in one-dimensional consolidation tests, for determining the amount of elastic rebound over specific effective stress ranges (equivalent to depth below seafloor) in terms of void ratio as follows:

$$\Delta e = C_r \log (P_o'), \qquad (1)$$

where Cr is the coefficient of rebound and P_o' is the effective overburden stress.

The change in void ratio is used to determine the length of growth over specific depth intervals, defined here as the discrete measurement intervals. At each depth interval, a change in length over the interval was calculated as follows:

$$\Delta L = \Delta e \,(L_o - nL_o), \qquad (2)$$

where ΔL is the expanded length of the depth interval caused by elastic rebound, and n is the measured porosity over the depth interval.

For the three primary holes used in the construction of the composite depth section, elastic rebound lengthening of the cored intervals is less than the composite depth offset lengthening (Fig. 44). However, the general shape of the composite depth offset "growth" is similar to the rebound curve, suggesting that the dominant mechanism lengthening the mcd scale at Site 925 is elastic stress relief. When comparing elastic rebound with mcd offset, two large increases in the mcd are observed at approximately 80 and 180 mbsf. These offsets could be the result of other coring problems, for example,

Table 11. Uncorrected and corrected acoustic velocity measured on discrete samples for all holes at Site 925.

Core, section, interval (cm)	Depth (mbsf)	Longitudinal acoustic velocity (m/s)	Transverse acoustic velocity (m/s)	Corrected longitudinal velocity (m/s)	Corrected transverse velocity (m/s)
154-925A-					
1R-1, 19	102	1528	1627	1477.24	1569.58
2R-2, 20	199.59		1911.8		1861.33
2R-4, 15	202.57		1998.9		1946.63
3R-1, 38	304.09		1869.1		1846.44
3R-1, 53	304.21		1949.4		1925.53
3R-1, 112	304.82		2133.7		2105.52
3R-2, 26	305.49		2148.8		2122.19
3R-2, 99	306.15		2059.5		2035.19
3R-3, 27	306.95		2278.1		2249.15
3R-3, 83	307.56		2161.7		2133.93
4R-1, 25	313.93		2093		2070.25
4R-1, 55	314.22		2200.2		2173.61
4R-2, 28	315.49		2125		2102.33
4R-3, 131	318.02		2131		2108.43
4R-4, 8	318.28		2230		2206.34
4R-4, 100	319.22		1923.36		1906.19
4R-5, 26	319.97		2039.58		2020.56
4R-5, 107	320.78		1813.14		1797.82
4R-6, 4	321.25		1876.23		1860.19
4R-6, 99	322.2		2066.27		2046.27
4R-7, 21	322.91		1972.92		1956.47
5R-2, 13	325.04		1786.4		1775.08
5R-2, 85	325.75		1885.56		1871.55
5R-3, 86	327.27		2098.39		2083.35
5R-3, 146	327.87		2014.64		2000.68
5R-4, 109	329		1982.09		1970.21
5R-5, 68	330.09		2086.48		2072.38
5R-6, 130	332.21		2135.9		2118.91
5R-7, 51	332.91		2236.3		2217.62
6R-1, 21	333.32		2093.95		2079.74
6R-1, 55	333.66		1780.69		1770.32
6R-2, 29	334.9		2167.7		2153.33
7R-1, 43	343.14	2048	2020	2035.94	2008.27
7R-1, 98	343.69	2088	2054	2075.73	2042.12
7R-2, 41	344.62	2109	2021	2095.68	2008.76
7R-2, 98	345.19	2135	2009	2122.45	1997.88
7R-3, 40	346.11	2179		2166.19	
7R-3, 116	346.87	2078	2016	2066.64	2005.3
7R-4, 40	347.6	2105	2155	2093.85	2143.32
7R-4, 118	348.39	2147	2197	2135.19	2184.64
7R-5, 42	349.13	2045	2088	2034.78	2077.35
7R-5, 97	349.68	2074	2149	2064.42	2138.72
7R-6, 57	350.78	2091	2086	2080.85	2075.9
7R-6, 118	351.39	2108	2086	2098.48	2076.67
8R-1, 12	352.53	2087	2100	2077.82	2090.7
8R-1, 121	353.62	2116	2149	2106.85	2139.56
8R-2, 2	353.93	2180	2186	2170.51	2176.46
8R-2, 72	354.62	2147	2160	2137.88	2150.77
8R-3, 2	355.43	2001	2034	1993.46	2026.21
8R-3, 82	356.23	2230	2217	2220.5	2207.61
8R-4, 9	357	2194	2205	2185.8	2196.72
8R-4, 90	357.81	2043	2099	2035.76	2091.36
8R-5, 5	358.46	2002	2055	2002	2055
8R-5, 146	359.87	2209	2193	2201.35	2185.46
8R-6, 3	359.94	2117	2127	2109.25	2119.17
8R-6, 83	360.74	2020	2065	2013.58	2058.3
9R-1, 28	362.29	1787	1849	1782.51	1844.2
9R-1, 86	362.87	1933	1944	1927.91	1938.85
9R-2, 25	363.76	2138	2106	2132.07	2100.25
9R-2, 131	364.82	1952	1973	1947.7	1968.61
9R-3, 14	365.15	1885	1942	1881.02	1937.77
9R-3, 133	366.33	2115	2126	2110.3	2121.25
9R-4, 54	367.05	2095	2133	2090.62	2128.46
9R-4, 125	367.76	2204	2149	2204	2149
9R-5, 45	368.46	1960	2035	1956.63	2031.36
9R-6, 36	369.87	2173	2138	2169.25	2134.37
9R-6, 122	370.73	2053	2096	2050.11	2092.99
9R-7, 53	371.54	2096	2142	2093.11	2138.98
10R-1, 10	371.81	1932	1988	1929.71	1985.57
10R-1, 134	373.05	2288	2276	2285.17	2273.2
10R-2, 48	373.69	2295	2221	2292.35	2218.52
10R-2, 128	374.49	2235	2175	2232.69	2172.82
11R-1, 22	381.53	1862	1814	1862.45	1814.42
11R-1, 145	382.76	1737	1754	1737.66	1754.67
11R-2, 45	383.26	1655	1688	1655.7	1688.73
11R-2, 125	384.06	1662	1692	1662.89	1692.93
11R-3, 15	384.46	1672	1705	1672.93	1705.97
11R-3, 81	385.12	1665	1690	1666.02	1691.05
11R-4, 26	386.07	1803	1803	1804.5	1804.5
11R-4, 144	387.25	1773	1819	1774.72	1820.81
11R-5, 69	388	1658	1695	1658	1695
11R-5, 130	388.61	1822	1807	1824.17	1809.14
11R-6, 38	389.19	1646	1698	1647.84	1699.96
12R-1, 36	391.17	1627	1685	1629.22	1687.38
12R-1, 120	392.01	1751	1787	1753.72	1789.84
12R-2, 31	392.62	1922	1900	1925.84	1903.76
12R-2, 120	393.51	1698	1754	1700.99	1757.19
12R-3, 25	394.06	1616	1655	1618.82	1657.96
12R-3, 122	395.03	1705	1723	1708.29	1726.36
13R-1, 39	400.8	1935	1895	1941.26	1901
13R-2, 2	401.43	1661	1754	1665.38	1758.89
13R-2, 68	402.09	1842	1871	1847.55	1876.73
14R-2, 30	410.57	1733	1803	1739.53	1810.07
14R-2, 139	411.66	1891	1921	1899.51	1929.78
14R-3, 34	412.11	1819	1850	1826.6	1857.86
14R-4, 33	413.6	1807	1838	1814.94	1846.21
14R-4, 125	414.52	1776	1827	1783.92	1835.38
14R-5, 28	415.05	1681	1762	1688.15	1769.85
14R-5, 128	416.05	1536	1612	1542.14	1618.76
14R-6, 33	416.6	1777	1822	1784.91	1830.32
15R-1, 70	420.41	1766	1811	1775.22	1820.7
15R-1, 101	420.72	1505	1585	1511.84	1592.58
15R-2, 56	421.77	1621	1682	1629.44	1691.09
15R-2, 137	422.58	1755	1792	1764.55	1801.96
15R-3, 18	422.89	1618	1675	1624.47	1681.94
15R-3, 130	424.01	1676	1726	1684.53	1735.05
15R-4, 6	424.27	1896	1918	1908.39	1930.68
15R-5, 7	425.78	1622	1684	1630.68	1693.36
15R-5, 92	426.63	1883	1897	1895.18	1909.36
15R-6, 35	427.56	1888	1905	1900.51	1917.73
15R-6, 142	428.63	1815	1819	1826.52	1830.57
15R-7, 10	428.81	1622	1661	1631.23	1670.68
16R-1, 33	429.64	1556	1621	1564.4	1630.12
16R-1, 108	430.39	1927	1892	1940.72	1905.23
16R-2, 23	431.04	1859	1881	1871.72	1894.02
16R-2, 89	431.7	1769	1784	1780.59	1795.79
16R-3, 11	432.42	1822	1859	1833.89	1871.38
16R-3, 130	433.61	1561	1611	1568.09	1618.55
16R-4, 12	433.93	1851	1883	1865.07	1897.56
16R-4, 137	435.18	1962	1931	1977.82	1946.32
16R-5, 16	435.47	1819	1835	1831.94	1848.17
16R-5, 69	436	1823	1859	1835.92	1872.43
16R-6, 15	436.96	1534	1605	1543.28	1615.16
16R-6, 147	438.28	1788	1811	1800.87	1824.21
16R-7, 48	438.79	1896	1853	1912.16	1868.43
17R-1, 5	438.96	1944	1918	1959.42	1933.01
17R-1, 98	439.89	1918	1900	1933.82	1915.53
17R-2, 8	440.49	1755	1811	1768	1824.85
17R-2, 87	441.28	1865	1867	1881.7	1883.74
17R-3, 59	442.5	1708	1733	1720.82	1746.2
17R-3, 124	443.15	1667	1708	1679.25	1720.86
17R-4, 27	443.68	1819	1843	1831.77	1856.11
17R-4, 95	444.36	1568	1642	1578.49	1653.51
17R-5, 2	444.93	1664	1708	1676.34	1721
17R-5, 56	445.47	1645	1715	1655.57	1726.49
17R-6, 28	446.69	1630	1688	1640.21	1698.95
17R-6, 80	447.21	1855	1863	1868.74	1876.86
17R-7, 18	447.59	1971	1957	1990.56	1976.28
18R-1, 65	449.26	1910	1931	1927.46	1948.84
18R-1, 111	449.72	1540	1599	1549	1608.71
18R-2, 145	451.56	1571	1632	1580.99	1642.78
18R-3, 40	452.01	1595	1610	1607.27	1622.51
18R-3, 93	452.54	1863	1891	1880.03	1908.55
18R-4, 34	453.45	2048	2013	2070.64	2034.87
18R-5, 52	455.13	1561	1610	1573.71	1623.53
18R-5, 114	455.75	1780	1843	1795.88	1860.03
18R-6, 126	457.37	1901	1864	1921.63	1883.83
19R-2, 17	458.45	1572	1549	1585.83	1562.43
19R-2, 61	458.89	1796	1811	1814.23	1829.53
19R-3, 69	460.47	1792	1819	1812.1	1839.71
19R-3, 135	461.13	1843	1854	1862.09	1873.32
19R-4, 70	469.04	1823	1820	1843.35	1840.28
20R-2, 34	469.65	1755	1792	1774.08	1811.9
20R-2, 123	470.54	1762	1785	1762	1785
20R-3, 34	471.15	1731	1760	1749.42	1779.05
20R-3, 118	471.99	1820	1835	1839.85	1855.18
20R-4, 56	472.87	1669	1717	1686.16	1735.16
20R-4, 132	473.63	1901	1909	1923.15	1931.34
20R-5, 41	474.22	1835	1851	1855.87	1872.24
20R-5, 105	474.86	1584	1614	1600.8	1631.45
20R-6, 56	475.87	1835	1839	1856.7	1860.8
20R-6, 118	476.49	1652	1760	1670.9	1781.47
20R-7, 28	477.09	1760	1827	1780.52	1849.12
22R-1, 39	487.5	1797	1820	1797	1820
22R-1, 116	488.27	1787	1827	1815.03	1856.3
22R-2, 47	489.08	1875	1884	1900.68	1909.93
22R-2, 104	489.65	1735	1782	1757.4	1805.64
22R-3, 35	490.46	1715	1782	1736.78	1805.53
22R-3, 118	491.29	1900	1896	1928.29	1924.17
22R-4, 31	491.92	1760	1813	1783.27	1837.7
22R-4, 92	492.53	1750	1797	1773.57	1821.86
22R-5, 44	493.55	1669	1748	1690.67	1771.78
22R-5, 106	494.17	1901	1888	1930.23	1916.83
22R-6, 108	495.69	1748	1782	1772.58	1807.55
22R-7, 44	496.55	1851	1868	1878.97	1896.49

Table 11 (continued).

Core, section, interval (cm)	Depth (mbsf)	Longitudinal acoustic velocity (m/s)	Transverse acoustic velocity (m/s)	Corrected longitudinal velocity (m/s)	Corrected transverse velocity (m/s)
23R-1, 12	496.83	1642	1683	1665.12	1707.29
23R-1, 119	497.9	1884	1879	1910.65	1905.51
23R-2, 96	499.17	1852	1828	1881.76	1856.99
23R-3, 75	500.46	1893	1876	1926.39	1908.79
23R-4, 75	501.96	1855	1835	1883.21	1862.6
24R-1, 4	506.34	1720	1774	1743.42	1798.92
24R-1, 76	507.06	1560	1585	1582.72	1608.46
24R-2, 140	509.21	1666	1704	1691.7	1730.9
24R-3, 86	510.17	1663	1689	1688.94	1715.77
24R-3, 144	510.75	1777	1812	1807.55	1843.77
24R-4, 61	511.42	1773	1792	1796.56	1816.07
24R-5, 6	512.37	1699	1737	1727.5	1766.8
24R-5, 144	513.75	1676	1744	1703.54	1773.84
24R-6, 68	514.49	1777	1826	1809.02	1859.82
24R-6, 143	515.24	1744	1737	1773.56	1766.32
26R-2, 137	527.38	1672	1734	1701.08	1765.3
26R-3, 16	527.67	1602	1650	1629.17	1678.83
26R-3, 132	528.83	1693	1734	1722.94	1765.42
26R-4, 4	529.05	1679	1720	1708.19	1750.65
26R-4, 136	530.37	1678	1730	1707.83	1761.73
26R-5, 69	531.2	1747	1784	1777.78	1816.11
26R-5, 130	531.81	1792	1807	1827.43	1843.04
26R-6, 64	532.65	1722	1769	1753.99	1802.77
26R-6, 145	533.46	1815	1834	1850.75	1870.51
26R-7, 114	534.65	1755	1773	1787.49	1806.16
27R-1, 23	535.54	1696	1755	1725.88	1787.02
27R-1, 130	536.61	1801	1839	1836.29	1875.81
27R-2, 21	537.02	1685	1759	1717.03	1793.93
27R-2, 108	537.89	1785	1799	1821	1835.57
27R-3, 15	538.46	1748	1784	1782.14	1819.58
27R-4, 21	540.02	1822	1854	1858.54	1891.85
27R-4, 94	540.75	1699	1773	1729.87	1806.64
27R-5, 25	541.56	1823	1846	1860.3	1884.26
27R-5, 118	542.49	1800	1826	1835.42	1862.46
27R-6, 31	543.12	1819	1857	1855.12	1894.66
27R-6, 128	544.09	1838	1834	1876.92	1872.75
29R-1, 38	554.99	1766	1831	1799.83	1867.39
29R-1, 88	555.49	1692	1751	1723.49	1784.74
29R-2, 6	556.17	1784	1807	1819.34	1843.27
30R-1, 28	564.49	1767	1784	1804.82	1822.56
30R-1, 107	565.28	1643	1710	1674.82	1744.49
30R-2, 30	566.01	1769	1807	1804.36	1843.91
30R-2, 140	567.11	1822	1838	1863.56	1880.3
30R-3, 53	567.74	1604	1692	1634.35	1725.8
30R-3, 109	568.3	1810	1784	1856.19	1828.85
30R-4, 78	569.49	1822	1822	1867.9	1867.9
30R-5, 50	570.71	1822	1803	1865.85	1845.93
30R-5, 134	571.55	1830	1846	1873.09	1889.86
30R-6, 41	572.12	1748	1822	1786.11	1863.45
30R-6, 121	572.92	1795	1838	1837.25	1882.32
31R-1, 47	574.28	1744	1748	1787.65	1791.86
31R-1, 106	574.87	1734	1838	1773.28	1882.19
31R-2, 48	575.79	1745	1803	1783.49	1844.12
32R-1, 130	584.81	1792	1788	1832.51	1828.33
32R-2, 35	585.36	1738	1792	1777.03	1833.52
32R-2, 119	586.2	1741	1762	1780.85	1802.83
32R-3, 38	586.89	1777	1807	1817.35	1848.74
32R-3, 126	587.77	1656	1738	1691.77	1777.45
32R-4, 33	588.34	1726	1774	1766.01	1816.29
32R-4, 119	589.2	1713	1762	1753.26	1804.63
32R-5, 34	589.85	1731	1766	1770.09	1806.7
32R-5, 127	590.78	1641	1727	1676.2	1766.03
32R-6, 26	591.27	1792	1803	1833.85	1845.37
32R-6, 85	591.86	1570	1632	1604.69	1669.51
33R-1, 23	593.34	1727	1799	1769.75	1845.44
33R-1, 95	594.06	1792	1838	1837.74	1886.15
33R-2, 17	594.78	1955	1955	2012.36	2012.36
33R-2, 67	595.28	1679	1755	1719.17	1798.93
33R-3, 12	596.23	1697	1748	1740.76	1794.46
33R-3, 72	596.83	1920	1850	1978.12	1903.9
33R-4, 51	598.12	1688	1762	1729.88	1807.68
33R-4, 120	598.81	1846	1880	1896.62	1932.53
33R-5, 45	599.56	1903	1886	1903	1886
33R-6, 46	601.07	1784	1854	1834.04	1908.1
34R-1, 74	603.55	1827	1838	1827	1838
34R-1, 130	604.11	1920	1903	1981.68	1963.57
34R-2, 94	605.25	1904	1939	1960.07	1997.18
34R-3, 33	606.14	1815	1878	1865.47	1932.09
34R-3, 80	606.61	1762	1846	1807.98	1896.53
34R-4, 71	608.02	1846	1854	1895.75	1904.19
34R-4, 132	608.63	1575	1677	1609.57	1716.25
34R-5, 36	609.17	1895	1929	1895	1929
34R-5, 145	610.26	1792	1822	1792	1822
34R-6, 40	610.71	1870	1903	1921.01	1955.85
35R-1, 16	612.57	1854	1920	1902.31	1971.86
35R-1, 107	613.48	1862	1903	1914.52	1957.89
35R-2, 26	614.17	1832	1887	1885.12	1943.41
35R-2, 114	615.05	1878	1929	1933.02	1987.09
35R-3, 43	615.84	1929	1940	1929	1940
35R-3, 120	616.61	1846	1903	1897.63	1957.92
35R-4, 18	617.09	1874	1933	1926.03	1988.41
35R-4, 81	617.72	1933	1956	1933	1956
35R-5, 27	618.18	1850	1913	1850	1913
36R-1, 26	622.37	1931	1937	1931	1937
36R-1, 122	623.33	1982	1987	2044.62	2049.94
36R-2, 49	624.1	1720	1796	1767.72	1848.09
36R-2, 106	624.67	1982	1967	2046.5	2030.52
36R-3, 14	625.25	1903	1912	1960.53	1970.09
36R-3, 81	625.92	1886	1903	1948.03	1966.17
36R-4, 22	626.83	1734	1842	1782.3	1896.6
36R-4, 105	627.66	1912	1938	1969.1	1996.68
36R-5, 105	629.16	1895	1920	1951.12	1977.63
36R-6, 15	629.76	1823	1874	1877.29	1931.42
36R-6, 119	630.8	1827	1886	1884.44	1947.28
36R-7, 39	631.5	1938	1969	2004.21	2037.39
38R-1, 23	641.64	1903	1946	1961.69	2007.41
38R-1, 128	642.69	1871	1920	1929.39	1981.54
38R-2, 51	643.42	1956	1982	2023.9	2051.75
38R-2, 129	644.2	1883	1938	1942.78	2001.38
38R-3, 28	644.69	1770	1846	1823.24	1903.99
38R-3, 76	645.17	1965	1946	2038.44	2018
38R-4, 47	646.38	1920	1992	1981.22	2057.98
38R-4, 118	647.09	1862	1925	1920.71	1987.82
38R-5, 24	647.65	1903	1933	1965.32	1997.33
38R-5, 115	648.56	1886	1878	1952.07	1943.5
38R-6, 24	649.15	1799	1797	1865.46	1863.31
38R-6, 125	650.16	1958	1992	2025.17	2061.56
38R-7, 5	650.46	2039	2069	2117.07	2149.43
39R-1, 4	651.15	1982	1992	2055.88	2066.64
39R-1, 86	651.97	1956	1964	2025.96	2034.54
39R-2, 45	653.06	1982	2020	2053.65	2094.48
39R-2, 82	653.43	1870	1946	1930.59	2011.71
39R-3, 13	654.24	1846	1946	1906.24	2013.06
39R-3, 117	655.28	1756	1850	1807.39	1907.12
39R-4, 3	655.64	1982	2039	2055.37	2116.74
39R-4, 64	656.25	1988	2008	2059.86	2081.34
39R-5, 49	657.6	1863	2002	1924.11	2072.75
39R-5, 142	658.53	1893	1965	1954.88	2031.76
39R-6, 54	659.15	1992	2002	2061.97	2072.69
39R-7, 31	659.92	1839	1950	1895.98	2014.19
40R-1, 134	662.15	1946	1930	2015.24	1998.08
40R-2, 98	663.29	1880	1870	1942.16	1931.49
40R-3, 58	664.39	1624	1731	1669.58	1782.88
40R-4, 62	665.93	1803	1868	1857.2	1926.24
40R-5, 59	667.4	1804	1862	1871.8	1934.32
40R-7, 2	669.83	1870	1934	1932.66	2001.1
41R-1, 51	670.92	1796	1807	1851.02	1862.71
41R-1, 107	671.48	1939	1988	2002.36	2054.66
41R-2, 71	672.62	1784	1873	1833.28	1927.4
41R-3, 71	673.62	2020	1982	2099.91	2058.88
42R-1, 20	680.31	1891	1946	1948.21	2006.63
42R-1, 91	681.02	1920	1955	1969.63	2006.49
42R-2, 45	682.06	1822	1947	1863.17	1994.08
43R-1, 3	683.14	1903	1878	1972.44	1945.6
43R-1, 128	684.39	1748	1822	1799.25	1877.75
43R-2, 59	685.2	1983	2006	2061.56	2086.43
43R-2, 144	686.05	1862	1982	1921.49	2049.54
43R-3, 21	686.32	1964	2001	2041.5	2081.51
43R-3, 65	686.76	1826	1903	1884.81	1966.96
43R-4, 84	688.45	1814	1871	1880.23	1941.54
43R-4, 139	689	1727	1818	1778.51	1875.17
44R-1, 52	690.23	1807	1791	1876.2	1858.95
44R-1, 109	690.8	1752	1778	1815.93	1843.88
44R-2, 31	691.52	1686	1792	1736.76	1849.46
44R-2, 140	692.61	1720	1819	1764.04	1868.33
44R-3, 43	693.14	1766	1903	1815.37	1960.45
44R-3, 74	693.45	1815	1887	1869.55	1946.03
44R-4, 80	695.01	1870	1994	1921.8	2053
45R-1, 76	700.07	2157	2228	2220.11	2295.4
45R-1, 140	700.71	1842	1965	1895.2	2025.65
45R-2, 19	701	1932	2079	1985.27	2140.81
45R-2, 119	702	1803	1926	1853.62	1983.88
45R-3, 130	703.61	1956	2014	2010.03	2071.33
45R-4, 75	704.56	1943	2054	2018.34	2138.38
45R-5, 39	705.7	1869	1989	1921.71	2048.8
45R-5, 134	706.65	1828	1937	1879.61	1995.04
45R-6, 47	707.28	1899	2059	1953.58	2123.32
45R-6, 114	707.95	2055	2094	2115.01	2156.35
46R-1, 40	709.41	2164	2286	2234.47	2364.79
46R-1, 93	709.94	1861	1976	1919.13	2041.66
46R-2, 4	710.55	2010	2104	2070.55	2170.44
46R-2, 111	711.62	2173	2150	2250.95	2226.28
46R-3, 9	712.1	2001	2135	2062.99	2205.71
46R-3, 71	712.72	2146	2139	2216.36	2208.9
46R-4, 6	713.57	2000	2134	2063.25	2206.16
46R-5, 61	715.62	2172	2159	2241.03	2227.19
46R-5, 108	716.09	1881	2073	1950.7	2157.98
46R-6, 2	716.53	2025	2104	2090.12	2174.39

Table 11 (continued).

Core, section, interval (cm)	Depth (mbsf)	Longitudinal acoustic velocity (m/s)	Transverse acoustic velocity (m/s)	Corrected longitudinal velocity (m/s)	Corrected transverse velocity (m/s)
46R-7, 13	718.14	1973	2098	2035.16	2168.42
47R-1, 14	718.45	2069	2146	2138.87	2221.26
47R-1, 140	719.71	1892	2006	1951.28	2072.77
47R-2, 32	720.13	1929	2039	1988.53	2105.64
47R-2, 80	720.61	2014	2092	2078.73	2161.92
47R-3, 30	721.61	1946	2067	2007.69	2136.74
47R-3, 147	722.78	1903	2025	1963.96	2094.17
47R-4, 68	723.49	1854	2001	1914.19	2071.3
47R-4, 117	723.98	1973	2069	2036.57	2139.02
47R-5, 84	725.15	2055	2140	2127.34	2218.57
48R-1, 54	728.45	1811	1891	1874.68	1960.54
48R-1, 124	729.15	1902	2067	1966.33	2143.2
48R-2, 51	729.92	1819	1925	1884.69	1998.73
48R-2, 89	730.3	1724	1823	1784.87	1891.2
48R-3, 144	732.35	1882	2059	1950.41	2141.16
48R-4, 35	732.76	1829	2059	1893.8	2141.49
48R-5, 92	734.83	1717	1938	1773.03	2009.69
48R-6, 146	736.87	1849	1972	1914.84	2047.07
48R-7, 57	737.48	1890	2022	1955.78	2097.48
49R-1, 142	739.03	1856	2020	1922.71	2099.27
49R-2, 50	739.61	1925	2020	1994.08	2096.2
49R-2, 147	740.58	1870	2006	1937.79	2084.21
49R-3, 63	741.24	1923	2063	1993.93	2144.85
49R-3, 129	741.9	1862	1973	1933.44	2053.4
49R-4, 46	742.57	1855	1979	1922.01	2055.45
49R-4, 144	743.56	1881	2048	1948.77	2128.59
49R-5, 4	743.65	1842	1946	1908.35	2020.21
50R-1, 37	746.48	1848	1973	1914.68	2049.19
50R-2, 43	748.04	1842	2034	1904.33	2110.27
51R-1, 38	747.49	2202	2392	2300.09	2508.19
51R-1, 70	747.81	2543	2625	2658.07	2747.79
51R-2, 14	748.75	2334	2498	2437.13	2616.5
51R-2, 60	749.21	2258	2455	2356.87	2572.32
51R-3, 67	750.78	2473	2568	2594.62	2699.39
51R-3, 124	751.35	2140	2262	2233.03	2366.2
51R-4, 73	752.34	2262	2442	2368.42	2566.5
51R-5, 60	753.21	2212	2391	2212	2391
52R-1, 72	757.73	2138	2295	2231.45	2403.02
52R-1, 139	758.4	2238	2384	2354.27	2516.38
52R-2, 64	759.15	2264	2509	2364.59	2633.14
52R-2, 99	759.5	2076	2204	2168.72	2308.79
52R-3, 6	760.07	2204	2442	2303.05	2564.19
52R-3, 139	761.4	2302	2488	2410.39	2615.1
52R-4, 35	761.86	2310	2480	2410.35	2596.03
52R-4, 101	762.51	2322	2439	2432.64	2561.36
52R-5, 17	763.18	2176	2276	2280.24	2390.29
52R-5, 139	764.4	2118	2277	2218.44	2393.5
52R-6, 11	764.62	2056	2231	2152.66	2345.27
52R-6, 102	765.53	2090	2274	2184.23	2385.99
53R-1, 35	766.96	2175	2328	2284.36	2453.73
53R-1, 114	767.75	2124	2361	2234.85	2498.77
53R-2, 77	768.62	2126	2259	2227.57	2374.02
53R-2, 140	769.25	2181	2350	2293.31	2480.92
53R-3, 25	769.6	2088	2204	2192.72	2321.01
53R-3, 96	770.31	2175	2337	2285.94	2465.57
53R-4, 1	770.86	2068	2238	2167.22	2354.66
53R-4, 84	771.69	2076	2165	2179.34	2277.63
53R-5, 126	773.61	2129	2240	2233.8	2356.31
53R-6, 43	774.28	2178	2323	2284.71	2444.79
53R-6, 148	775.33	2276	2374	2392.97	2501.54
54R-1, 74	777.05	2340	2414	2465.65	2547.96
54R-3, 17	779.48	2394	2528	2517.13	2665.7
54R-3, 145	780.76	2221	2391	2319.54	2505.59
54R-4, 50	781.31	2488	2543	2624.67	2685.95
54R-4, 146	782.27	2326	2405	2442.02	2529.25
54R-5, 147	783.78	2399	2535	2523.83	2674.79
54R-6, 66	784.47	2502	2631	2643.01	2787.38
55R-1, 7	786.08	2340	2480	2463.11	2618.72
55R-1, 87	786.88	2543	2620	2700.98	2788.01
55R-2, 40	787.91	2047	2187	2147.01	2301.54
55R-2, 121	788.72	2250	2428	2353.29	2548.72
55R-3, 51	789.52	2470	2573	2593.22	2706.99
55R-3, 140	790.41	2470	2610	2600.72	2756.39
55R-4, 30	790.81	2329	2504	2441.99	2635.09
55R-4, 136	791.87	2336	2494	2456	2631.26
55R-5, 60	792.61	2254	2447	2368.37	2582.38
55R-5, 114	793.15	2290	2424	2405.6	2553.91
55R-6, 80	794.31	2149	2354	2257.08	2484.31
56R-1, 16	795.77	2393	2544	2516.53	2684.07
56R-1, 78	796.39	2066	2191	2169.91	2308.22
56R-2, 6	797.17	2262	2442	2372.03	2570.74
56R-2, 90	798.01	2095	2310	2193.32	2430.11
56R-3, 140	800.01	2136	2310	2239.11	2431.07
56R-4, 134	801.45	2242	2484	2349.59	2616.76
56R-5, 68	802.29	2600	2702	2736.23	2849.44
56R-5, 122	802.83	2274	2366	2388.5	2490.21
56R-6, 44	803.55	2227	2401	2336.45	2528.72
57R-1, 61	805.82	2238	2401	2357.81	2539.44
57R-1, 111	806.32	2161	2366	2274.1	2502.25
57R-2, 29	807	2096	2298	2202.33	2426.44
57R-2, 141	808.12	2204	2405	2322.17	2546.4
57R-3, 18	808.38	2264	2442	2383.2	2581.25
57R-4, 6	809.77	2414	2548	2541.78	2690.78
57R-5, 21	811.42	2117	2322	2229.65	2458.22
57R-5, 134	812.55	2367	2528	2498.04	2678.04
57R-6, 47	813.18	2151	2374	2266.52	2515.5
57R-6, 145	814.16	2217	2414	2333.01	2552.18
57R-7, 13	814.33	2274	2424	2395.16	2562.16
58R-1, 22	815.03	2413	2543	2547.71	2693.07
58R-1, 51	815.32	2076	2298	2188.06	2436.1
58R-2, 90	817.21	1996	2250	2110.48	2396.55
58R-2, 146	817.77	2217	2406	2342.55	2554.58
58R-3, 64	818.44	2151	2374	2269.75	2519.48
58R-3, 142	819.23	2498	2620	2649.56	2787.22
58R-4, 49	819.8	2441	2558	2581.4	2712.61
58R-4, 138	820.69	2323	2475	2450.03	2619.71
58R-5, 12	820.93	2361	2528	2487.48	2673.55
58R-5, 74	821.55	2392	2528	2527.23	2679.53
58R-6, 6	822.37	2351	2513	2482.6	2663.94
58R-6, 100	823.31	2197	2360	2319.18	2501.56
58R-7, 3	823.84	2276	2460	2401.34	2607.08
59R-1, 19	824.7	2237	2414	2357.36	2554.75
59R-1, 91	825.42	2182	2414	2298.53	2557.44
59R-2, 18	826.19	2637	2777	2794.85	2952.61
59R-2, 112	827.13	2217	2393	2339.74	2536.64
59R-3, 23	827.74	2068	2182	2179.82	2306.86
59R-3, 146	828.97	2498	2609	2642.12	2766.62
59R-4, 27	829.69	2323	2505	2451.06	2654.56
59R-4, 60	829.61	2302	2432	2427.67	2572.69
59R-5, 107	831.58	2418	2604	2557.73	2766.78
59R-6, 143	833.44	2171	2420	2294.52	2574.49
59R-7, 56	834.07	2572	2674	2731.88	2847.24
60R-1, 32	834.53	2391	2528	2524.87	2678.13
60R-1, 82	835.03	2262	2445	2389.24	2594.33
60R-2, 70	836.41	2640	2737	2809.99	2920.14
60R-2, 132	837.03	2151	2357	2275.34	2507.13
60R-3, 45	837.66	2202	2418	2326.12	2568.5
60R-3, 21	837.54	2653	2737	2835.22	2931.36
60R-4, 2	838.73	2094	2335	2214.77	2486.17
60R-4, 137	846.1	2278	2522	2406.6	2680.59
61R-2, 82	846.13	2418	2533	2563.41	2693.03
61R-3, 56	847.36	2119	2391	2237.43	2542.87
61R-3, 88	847.69	2604	2690	2773.19	2870.94
61R-4, 84	849.15	2364	2573	2499.93	2734.85
61R-4, 126	849.57	2414	2641	2554.47	2810.05
61R-5, 28	850.09	2488	2685	2631.66	2853.08
62R-1, 15	853.66	2359	2488	2492.71	2637.2
62R-1, 70	854.21	2225	2387	2350.57	2532.12
62R-2, 55	855.56	2249	2442	2382.52	2600.23
62R-2, 113	856.13	2401	2543	2574.29	2738.22
62R-3, 85	857.36	2064	2323	2183.64	2475.67
62R-3, 73	857.3	2610	2737	2804.27	2951.41
62R-4, 91	858.92	2206	2418	2339.65	2579.51
62R-4, 146	859.47	2413	2578	2552.27	2737.59
62R-5, 42	859.93	2351	2528	2483.27	2681.58
62R-5, 91	860.42	2426	2625	2565.67	2789.3
62R-6, 7	861.08	2547	2702	2691.93	2865.67
62R-6, 118	862.19	2174	2348	2305.5	2502.14
62R-7, 63	863.14	2573	2760	2721.53	2931.62
63R-1, 21	863.32	2743	2864	2915.9	3053.02
63R-1, 109	864.19	2516	2778	2657.5	2951.52
63R-2, 24	864.85	2388	2620	2525.07	2785.93
63R-2, 101	865.62	2625	2754	2786.55	2932.36
63R-3, 4	866.15	2484	2674	2636.46	2851.51
63R-3, 121	867.32	2910	3068	3091.87	3270.84
63R-4, 5	867.66	2320	2558	2459.1	2728.15
63R-4, 141	869.02	2827	3025	2998	3221.63
63R-5, 16	869.27	2323	2578	2465.6	2754.82
64R-1, 126	874.07	2562	2760	2705.79	2927.6
64R-1, 134	874.15	2303	2502	2440.42	2665.04
64R-2, 73	875.04	2404	2620	2539.64	2781.93
64R-3, 12	875.93	2366	2558	2501.91	2717.61
64R-3, 85	876.66	2488	2669	2635.8	2839.82
64R-4, 68	877.99	2759	2798	2921.99	2965.77
64R-5, 9	878.9	2326	2543	2462.94	2707.58
64R-5, 139	880.2	2636	2777	2787.95	2946.16
64R-5, 124	880.12	3834	3677	4164.03	3979.48
64R-6, 11	880.42	2547	2727	2691.53	2893.35
64R-6, 144	881.75	2336	2489	2469.03	2640.6
65R-1, 15	882.65	2428	2589	2562.68	2742.7
65R-1, 145	883.95	2361	2453	2497.45	2600.62
65R-2, 38	884.38	2250	2499	2377.83	2657.68
65R-2, 142	885.42	2455	2679	2603.17	2856.41
65R-3, 70	886.2	2275	2513	2403.36	2670.55
66R-1, 28	892.08	2588	2703	2758.06	2889.06
66R-1, 94	892.74	2301	2490	2446.77	2661.59
67R-1, 18	901.58	2437	2646	2572.12	2806.05
67R-1, 126	902.66	2435	2747	2573.24	2924.23

Table 11 (continued).

Core, section, interval (cm)	Depth (mbsf)	Longitudinal acoustic velocity (m/s)	Transverse acoustic velocity (m/s)	Corrected longitudinal velocity (m/s)	Corrected transverse velocity (m/s)
67R-2, 51	903.41	2564	2704	2724.8	2869.88
67R-2, 129	904.19	2590	2702	2743.69	2869.7
67R-3, 58	904.98	2727	2846	2882.98	3016.31
67R-3, 126	905.66	2368	2503	2506.43	2658.18
67R-4, 23	906.13	2162	2519	2283.45	2685.41
67R-4, 100	906.9	2414	2611	2564.16	2787.57
67R-5, 96	908.36	2657	2732	2824.43	2909.33
67R-6, 132	910.22	2420	2446	2577.13	2606.64
67R-7, 59	910.99	2589	2833	2746.28	3022.41
69R-1, 6	920.77	2445	2558	2593.09	2720.55
69R-1, 147	922.18	3579	3779	3774.4	3997.52
69R-2, 17	922.38	2835	2911	3008.76	3094.5
69R-2, 141	923.62	2883	3055	3049.24	3242.31
69R-3, 58	924.29	2864	2942	3025.75	3112.95
69R-3, 143	925.14	2808	2962	2959.86	3131.48
69R-4, 46	925.67	3702	3660	3951.01	3903.21
69R-5, 10	926.81	2815	3078	2977.56	3273.41
69R-5, 107	928.08	3047	3212	3199.6	3382.04
69R-6, 30	928.51	3719	3660	3977.47	3910.06
69R-CC, 7	929.78	2883	3091	3049.4	3287.2
154-925B-					
1H-1, 88	0.89	1451	1462	1376.548	1386.445
1H-1, 33	3.34	1481		1405.464	
1H-3, 100	5.505	1500	1512	1426.505	1437.354
2H-1, 125	5.765		1518		1442.159
2H-1, 54	8.045	1511		1438.257	
2H-3, 54	11.045	1443	1495	1376.087	1423.297
2H-5, 29	13.295	1511	1521	1439.011	1448.078
2H-7, 129	15.295	1523	1512	1454.234	1444.201
3H-1, 74	17.745	1573	1580	1499.518	1505.878
3H-3, 74	20.745	1568	1575	1494.288	1500.644
3H-5, 7	23.075	1569	1575	1496.354	1501.81
3H-7, 74	24.245	1556	1539	1484.657	1469.172
4H-1, 74	27.245	1573	1576	1500.656	1503.386
4H-3, 74	30.245	1584	1584	1512.298	1512.298
4H-5, 29	32.795	1580	1584	1509.219	1512.869
4H-7, 74	33.745	1593	1601	1522.124	1529.427
5H-1, 74	36.745	1598	1571	1524.64	1500.043
5H-3, 39	37.895	1608	1601	1537.934	1531.529
5H-4, 38	40.88	1611	1584	1540.54	1515.832
5H-6, 100	45	1604	1627	1533.777	1554.794
6H-2, 74	47.745	1621	1623	1550.643	1552.473
6H-4, 98	50.99	1636	1627	1564.772	1556.536
6H-6, 75	52.75	1626	1645	1555.685	1573.069
7H-1, 18	55.19	1638	1623	1569.305	1555.532
7H-3, 74	58.745	1653	1636	1583.995	1568.378
7H-5, 9	61.095	1644	1632	1578.904	1567.832
7H-7, 74	62.245	1626	1605	1563.379	1543.956
8H-1, 74	65.245	1640	1641	1573.715	1574.636
8H-3, 39	67.895	1681	1673	1613.768	1606.394
8H-5, 40	71.4	1638		1574.667	
9H-1, 74	74.5	1646		1583.902	
9H-3, 74	74.745	1673		1606.758	
9H-5, 127	78.275	1683	1637	1619.459	1576.823
9H-7, 22	80.225	1656	1582	1591.128	1522.692
10H-1, 65	81.165	1634		1574.889	
10H-1, 74	81.21	1663	1640	1598.564	1577.3
10H-3, 9	83.625	1648	1591	1584.508	1531.745
10H-5, 7	86.595	1738	1735	1673.847	1671.064
10H-7, 10	89.585	1672	1673	1607.565	1608.49
11H-1, 32	90.32	1604		1544.958	
11H-3, 105	94.05	1635	1553	1576.143	1499.803
11H-5, 52	96.525	1666	1622	1603.253	1562.464
11H-7, 40	99.405	1656	1639	1597.294	1581.473
12H-1, 60	100.11	1668	1544	1611.669	1495.612
12H-3, 17	102.675	1662		1603.953	
12H-5, 38	105.885	1719	1645	1655.697	1586.937
12H-7, 26	108.765	1730	1673	1670.071	1616.891
13H-1, 85	109.945	1682		1622.666	
13H-1, 104	110.05	1688	1596	1626.937	1541.304
13H-3, 66	112.665	1707	1558	1646.223	1507.212
13H-5, 65	115.63	1677	1667	1617.739	1608.431
13H-7, 62	118.715	1638		1582.357	
14H-1, 31	118.815	1669	1647	1610.477	1589.983
14H-1 , 46	118.97		1554		1504.205
14H-3, 122	122.725	1673	1650	1614.648	1593.214
14H-5, 91	125.415	1661	1554	1605.433	1505.256
14H-7, 19	127.695	1616		1565.883	
15H-1, 124	129.235	1608	1617	1558.588	1567.042
15H-3, 73	131.74	1585	1569	1535.802	1520.775
15H-5, 74	134.745	1603	1563	1555.072	1517.4
16H-1, 72	138.235	1574	1578	1531.567	1535.354
16H-3, 111	141.655	1509	1620	1466.071	1570.626
16H-5, 74	144.195	1515	1626	1472.391	1577.02
16H-7, 26	146.73	1608	1594	1567.621	1554.312
17H-1, 100	147.895	1619	1620	1572.28	1573.223
17H-3, 60	150.65	1681	1682	1636.562	1637.51
17H-5, 51	153.48	1610	1598	1567.334	1555.959

Core, section, interval (cm)	Depth (mbsf)	Longitudinal acoustic velocity (m/s)	Transverse acoustic velocity (m/s)	Corrected longitudinal velocity (m/s)	Corrected transverse velocity (m/s)
17H-7, 25	156.305	1610	1591	1568.041	1550.013
18H-1, 81	157.28	1655	1696	1610.025	1648.801
18H-3, 108	160.54	1640	1601	1594.722	1557.821
18H-5, 123	163.7	1711	1692	1662.814	1644.864
18H-6, 130	165.35	1664	1633	1616.608	1587.333
19H-1, 118	167.29	0	1633		1591.586
19H-5, 130	173.315	1614	1643	1574.373	1601.955
20H-1, 130	176.75	0	1664		1621.584
20H-3, 92	179.46	1619	1598	1582.141	1562.08
20H-5, 49	181.97	1727	1678	1682.863	1636.302
21H-1, 139	186.395	1712	1696	1669.827	1654.602
21H-3, 140	189.4	1644	1627	1605.46	1589.244
21H-5, 139	192.395	1717	1718	1676.297	1677.25
22H-1, 110	195.815	1543	1533	1508.873	1500.182
22H-3, 45	198	1522	1614	1490.38	1578.868
22H-5, 120	201.73	1694	1620	1648.982	1584.622
23H-3, 31	207.34	1697	1763	1658.435	1722.658
23H-5, 7	210.11	1687	1654	1649.863	1617.717
23H-7, 16	213.255	1675	1682	1638.103	1646.222
24H-3, 97	217.46		1703		1661.013
24H-5, 118	220.705	1699	1710	1662.16	1674.04
24H-7, 27	222.8	1701	1664	1666.901	1630.448
25H-1, 107	224.06	1630	1627	1598.144	1594.576
25H-3, 97	226.975	1713	1714	1681.614	1679.522
25H-5, 109	230.035		1678		1644.007
25H-7, 37	232.49	1717	1682	1684.765	1650.467
26H-1, 60	233.085	1703	1718	1669.836	1684.676
26H-3, 97	236.57	1715	1727	1684.315	1696.824
26H-7, 37	241.855	1699	1696	1667.876	1665.82
27H-1, 42	242.42	1613	1613	1584.854	1584.986
27H-3, 128	246.28	1743	1751	1710.598	1720.926
27H-5, 68	248.44	1653	1670	1624.457	1641.828
27H-7, 37	251.325	1691		1662.421	
28H-1, 52	252.015	1671	1667	1644.206	1639.298
28H-3, 40	255.91	1671	1667	1643.551	1639.145
28H-5, 48	258.99	1728	1732	1699.363	1703.161
28H-7, 49	261	1747		1718.698	
29H-1, 99	261.99	1667		1640.411	
29H-3, 108	265.075	1800		1770.083	
29H-5, 89	267.885	1804		1773.203	
29H-5, 72	267.8	1744		1720.264	
29H-7, 34	270.33		1664		1638.351
30H-1, 54	271.05		1829		1803.451
30H-3, 85	274.34		1831		1831
30H-5, 110	277.595		1844		1821.792
31H-1, 130	281.31		1862		1837.285
31H-3, 60	283.59		1861		1836.935
31H-5, 145	287.345		1910		1885.488
32H-1, 147	290.98		1967		1940.406
32H-3, 63	293.125		2778		2742
32H-5, 127	296.765		2025		2000.186
33H-1, 111	300.1		1846.337		1826.109
33H-1, 139	300.4		1949.636		1927.962
33H-3, 30	302.3		1963.494		1940.856
33H-5, 43	305.43		1995.267		1972.599
34H-1, 104	309.545	1802	1814	1802	1795.102
34H-2, 14	310.145	1669	1684	1669	1748.686
34H-3, 146	312.96	1662	1677	1662	1748.584
34H-5, 137	315.87	1825	2183	1825	2158.438
154-925C-					
2H-2, 76	10.24	1512	1528	1438.25	1452.72
2H-4, 13	12.635	1496	1514	1420.54	1436.76
2H-6, 55	16.035	1515	1505	1442.38	1433.32
3H-4, 20	22.185	1518	1528	1449.23	1458.34
3H-6, 115	26.145	1552	1567	1479.64	1493.27
4H-2, 112	29.61	1533	1532	1462.19	1461.28
4H-4, 62	32.105	1569	1565	1495.94	1492.31
4H-6 , 108	35.565	1560	1584	1491.13	1513.04
5H-2, 52	38.505	1572	1559	1502.25	1490.37
5H-4, 101	42.005	1603	1568	1531.93	1499.93
5H-6, 104	45.025	1593	1577	1525.14	1510.47
6H-2, 107	48.565	1605	1603	1535.47	1533.64
6H-4, 18	50.66	1588	1559	1522.01	1495.35
6H-6, 33	53.825	1625	1599	1554.41	1530.61
7H-4, 50	60.485	1625	1593	1558.2	1528.75
7H-6, 56	63.55	1634	1622	1565.98	1554.96
8H-2, 123	67.715	1628	1618	1562.17	1552.96
8H-4, 20	69.695	1621	1618	1556.56	1553.79
8H-6, 111	73.65	1667	1628	1601.62	1565.59
9H-2, 63	76.615	1619	1609	1556.9	1547.65
9H-4, 85	79.85	1685	1622	1620.12	1561.8
9H-6, 71	82.7	1579	1583	1515.5	1519.18
10H-2, 109	86.585	1609	1596	1546	1534
10H-6, 72	92.205	1610	1576	1547.76	1516.31
11H-2, 125	96.25	1720	1659	1657.45	1600.73
11H-4, 94	98.93	1677	1628	1614.53	1569.07
11H-6, 72	101.445	1664	1622	1602.72	1563.73
12H-2, 75	105.245	1621	1612	1562.19	1553.82

Table 11 (continued).

Core, section, interval (cm)	Depth (mbsf)	Longitudinal acoustic velocity (m/s)	Transverse acoustic velocity (m/s)	Corrected longitudinal velocity (m/s)	Corrected transverse velocity (m/s)
12H-4, 75	108.245	1689	1632	1632.68	1579.35
12H-6, 75	111.24	1666	1622	1607.47	1566.47
13H-2, 75	114.745	1689	1618	1630.12	1563.89
13H-4, 75	117.795	1639	1535	1583.44	1486.16
13H-6, 75	120.745	1708	1676	1649.58	1619.71
14H-4, 75	127.28	1733	1635	1673.55	1581.98
14H-6, 75	130.27	1549	1595	1502.65	1545.9
15H-2, 75	133.715	1581	1503	1533.43	1459.94
15H-4, 75	136.775	1595	1568	1547.6	1522.16
16H-2, 120	143.65	1658	1655	1609.31	1606.49
16H-4, 75	146.22	1641	1618	1592.51	1570.84
17H-2, 10	152.125	1687	1605	1637.35	1560
17H-4, 105	156.08	1647	1641	1600.48	1594.81
17H-6, 75	158.715	1781	1734	1728.91	1684.58
18H-6, 95	168.4	1647	1574	1604.74	1535.36
19H-2, 65	171.655	1647	1622	1605.33	1581.57
19H-4, 90	174.89	1734	1673	1690.24	1632.23
19H-6, 82	177.815	1610	1633	1569.85	1591.71
20H-2, 100	181.53	1636	1676	1596.9	1634.99
20H-4, 75	184.285	1691	1659	1651.01	1620.49
20H-6, 65	187.165	1815	1713	1769.62	1672.52
22H-2, 100	200.46	1614	1632	1580.15	1597.4
22H-6, 125	206.77		1894		1851.21
24H-2, 19	218.685	1712	1687	1681.75	1657.62
24H-4, 25	221.76		1865		1831.31
24H-6, 106	225.555		1800		1767.82
25H-2, 50	228.5		1847		1809.44
25H-4, 41	231.405		1833		1795.97
25H-6, 38	234.375		1841		1804.04
26H-2, 69	238.18		1831		1799.84
26H-4, 20	240.69		1793		1756.92
26H-6, 96	244.455		1768		1740.76
27H-2, 60	247.595		1814		1784.11
27H-6, 114	254.145		1892		1859.93
28H-2, 30	256.795		1863		1831.6
28H-4, 97	260.465		1842		1811.24
28H-6, 134	263.83		1909		1877.21
29H-2, 73	266.725		1806		1779.79
29H-4, 131	270.305		1818		1791.51
29H-6, 96	272.96		1879		1854.49
30H-2, 121	276.71		1878		1852.92
30H-4, 88	279.365		1854		1832.08
30H-6, 123	282.725		1877		1855.09
31H-2, 73	285.74		1850		1826.78
31H-4, 84	288.83		1881		1858.92
31H-6, 52	291.51		1906		1882.86
32H-2, 76	295.26		1860		1838.54
32H-4, 83	298.31		1902		1881.55
32H-6, 70	301.195		1975		1952.68
33H-2, 68	304.675		1856		1837.37
33H-4, 97	307.97		1877		1858.71
33H-6, 130	311.305		1909		1890.64
34H-2, 130	314.825		1884		1866.54
34H-4, 100	317.49		1885		1869.55
35H-2, 93	323.925	1869	1869	1854.79	1854.79
35H-4, 133	327.325	1815	1828	1802.35	1815.17
35H-6, 10	329.095	1877	1954	1863.76	1939.66
36H-2, 97	333.665	1903	1936	1890.51	1923.08
36H-4, 130	336.995	1860	1899	1848.59	1887.1
36H-6, 36	339.055	1866	1910	1855.28	1898.77
37H-2, 32	342.615	1754	1794	1744.93	1784.51
37H-4, 54	345.835	1817	1849	1808.37	1840.07
37H-6, 94	349.235	2067	2057	2056.96	2047.06
38H-2, 97	352.865	1938	1991	1930.36	1982.94
38H-4, 107	355.975	2011	2064	2003.99	2056.62
154-925D-					
1H-4, 77	7.765	1527	1534	1460.935	1467.341
1H-6, 71	10.71	1547	1549	1483.19	1485.028
3H-2, 98	23.97	1585	1607	1526.139	1546.525
3H-6, 50	29.495	1587	1545	1530.154	1491.072
4H-2, 111	33.6	1582	1607	1522.092	1545.221
4H-6, 92	39.415	1611	1594	1551.939	1536.156
5H-4, 34	45.325	1603	1620	1544.238	1560.008
6H-2, 18	51.67	1618	1629	1566.958	1577.273
6H-6, 60	58.09	1641	1647	1590.971	1596.61
7H-4, 84	64.835	1603	1629	1545.2	1582.098
7H-6, 84	67.82	1678	1698	1632.427	1651.35
7H-6, 83	71.39	1637	1617	1595.53	1576.524
9H-4, 32	83.315	1626	1627	1596.911	1597.875
10H-4, 53	93.015	1632	1604	1605.881	1578.763
10H-6, 116	96.65	1615	1617	1591.896	1593.839
11H-2, 23	99.225	1572	1610	1551.672	1588.684
12H-2, 51	109.005	1559	1635	1544.342	1618.886
12H-6, 116	115.66	1662	1635	1651.735	1625.065
14H-4, 90	131.445	1614	1631	1613.824	1630.821
14H-6, 60	134.12	1679	1648	1680.812	1649.745
15H-2, 100	137.95	1588	1605	1592.262	1609.354
15H-6, 120	144.19	1713	1583	1727.683	1595.531
16H-4, 125	150.78	1614	1622	1631.755	1639.933
16H-6, 45	152.915	1664	1625	1685.331	1645.337
17H-4, 45	159.65	1664	1648	1689.243	1672.757
17H-6, 70	162.365	1711	1686	1740.053	1714.203
18H-2, 60	166.115	1691	1708	1715.974	1733.482
18H-4, 60	169.12		1739		1769.621
19H-6, 104	182.025		1728		1768.094
20H-4, 125	188.745		1741		1788.1
20H-6, 38	190.875		1767		1813.795
21H-2, 56	194.56		1710		1759.676
21H-6, 119	201.185		1716		1770.114
22H-3, 6	204.875		1807		1870.37
22H-3, 20	205.015		1823		1886.437
22H-3, 33	205.145		1835		1900.225
22H-3, 47	205.285		1858		1923.875
22H-3, 62	205.435		1840		1906.153
22H-3, 78	205.595		1853		1918.369
22H-3, 90	205.715		1863		1930.034
22H-3, 105	205.865		1836		1901.031
22H-3, 120	206.015		1852		1920.144
22H-3, 133	206.145		1827		1892.048
22H-3, 142	206.235		1820		1885.202
23H-4, 27	216.265		1818		1894.342
23H-6, 116	220.155		1844		1927.543
24H-2, 125	223.745		1763		1847.549
24H-6, 116	229.655		1853		1947.359
25H-2, 100	233		1821		1917.786
25H-6, 98	238.975		1801		1902.938
27H-4, 70	254.68		1813		1931.773
27H-6, 70	257.705		1793		1911.294
28H-2, 21	260.7		1795		1917.988
28H-6, 147	266.455		1834		1972.151
29H-2, 87	270.85		1794		1931.659
29H-4, 115	274.155		1819		1958.315
30H-4, 102	283.53		1824		1961.374
30H-5, 94	284.92		1867		2032.665
31H-2, 81	289.825		1905		2076.842
32H-4, 100	302.495		1874		2060.03
32H-6, 70	305.195		2017		2245.847
33H-2, 65	308.645		1867		2067.5
33H-4, 101	312.005		1853		2045.466
34H-2, 26	317.755		1863		2069.046
34H-2, 38	317.925		1905		2118.146
34H-2, 48	317.975		1896		2107.095
34H-2, 72	318.22		2037		2280.119
35H-2, 50	327.5		1911		2105.536
35H-6, 104	343.535		1919		2161.022
37H-2, 10	346.1		2058		2354.177
37H-6, 19	352.185		1892		2143.111

mechanical expansion of the cored intervals (flow-in), or a large change in C_r at this depth interval. The value of C_r is dependent upon sediment composition; therefore, it must be measured by onshore testing of whole-round core samples post cruise.

Summary

Sediment physical properties at Site 925 show variations with depth below seafloor that reflect compositional and diagenetic changes in the sediment column. Although the effects of gravitational consolidation dominate as seen by the general trends of increasing bulk density and acoustic velocity with depth (Fig. 45), large offsets in all physical properties data over short depth intervals suggest that large physicochemical changes are also important. These changes are probably associated with diagenetic processes and changes in sediment source. In the upper part of the section, shear strength data suggest that the normal consolidation process is inhibited. If true, then the sediment column is under conditions of high excess fluid pressure and, therefore, more susceptible to failure. Post-cruise consolidation test results will be used to interpret the stress history at Site 925.

Correlation of log data to core data suggests no accumulated core offset with depth below seafloor and no apparent stretch of the core

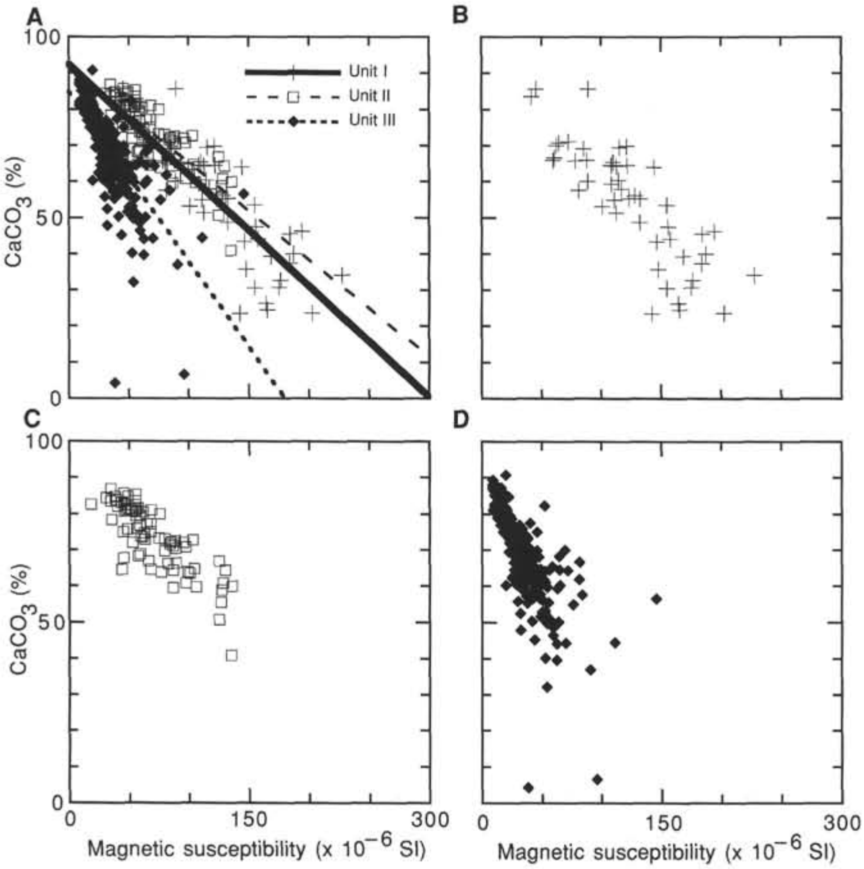

Figure 30. Calcium carbonate analyses from discrete samples vs. magnetic susceptibility values of the closest measurement, Site 925. **A.** Plot of all carbonate samples vs. magnetic susceptibility. Linear regression lines for each unit are shown. **B, C,** and **D.** $CaCO_3$ vs. magnetic susceptibility for lithologic Units I, II, and III, respectively.

section at low resolution. Estimated elastic rebound is likely the largest contributor to the "growth" of the composite depth offset. Post-cruise consolidation test results will better quantify this effect.

The acoustic impedance at Site 925 is dominated by changes in velocity rather than in bulk density. Large impedance contrasts cause high-amplitude seismic reflections. Based on discrete measurements, these large events occur at 0.10, 0.67, and 0.96 s two-way traveltime (TWT) (Fig. 46, solid lines). Smaller events occur at 0.18, 0.44, and 0.79 s TWT (Fig. 46, dashed lines). From the seabed to the bottom of the drilled interval, these contrasts can be correlated with reflection events interpreted from the seismostratigraphy (Fig. 46; see "Site Summary" section, this chapter).

DOWNHOLE MEASUREMENTS

Logging Operations and Log Quality

Downhole measurements at Site 925 were conducted in two phases. Hole 925C was logged with the Schlumberger Quad, FMS, and GHMT tool strings over the interval from 347 to 56 mbsf. Repeat logs of the Quad and FMS tool strings were recorded at this hole to test the repeatability of standard- and high-resolution-mode logs. The magnetometer component of the GHMT tool string failed on downhole transit, so total field log data were not recorded; the susceptibility channel was stable, however (Table 14). Hole 925A was logged 6 days later with the Quad and FMS tool strings between 907 and 205 mbsf (Table 15). The wireline heave compensator was employed during both logging efforts to compensate for moderate (about 0.5 m) ship heave. Logging depths were set initially using the measured base of pipe datum; logging depths were further adjusted by comparing the core and log natural gamma measurements and shifting the log depths appropriately. A summary of the logging tool strings used during Leg 154 and discussion of their measurement principles is provided in the "Downhole Measurements" section of the "Explanatory Notes" chapter (this volume).

All Quad data were recorded at 900 ft/hr cable speed to enable simultaneous high-resolution and standard-resolution logging. High-resolution density, neutron porosity, and induction resistivity logs are recorded and processed real-time at this logging speed. The density and porosity logs are recorded at 2.5-cm sample intervals as opposed to the standard 15-cm sample interval. The density data are processed to optimize the gamma count rates for the near-detector-source spacing (18 cm). The high-resolution resistivity data are recorded at 15 cm, and the data are processed to enhance thin bed resolution. The FMS and GHMT logs were both recorded at 1800 ft/hr.

Delays associated with borehole bridging problems prevented the full suite of logging measurements from being obtained at this site. Quad logging at Hole 925A encountered an impassable bridge near 427 mbsf; the tool string was retrieved and the hole was reamed to 450 mbsf. After a second deployment, another impassable bridge was encountered near 500 mbsf. Finally, the side-entry sub (SES) was used to break through the bridges and permit logging from total depth (907 mbsf) to 274 mbsf. A complete FMS log at Hole 925A (907–231 mbsf) was conducted using the remaining time allotted for downhole measurements.

The Quad logs for Holes 925A and 925C are shown at the end of this chapter. The log data at Hole 925C are of generally excellent quality throughout the entire logged sequence. The log data at Hole 925A deteriorate markedly below ~360 to ~730 mbsf; many log measurements were adversely affected by extreme borehole diameter fluctuations associated with regular borehole washouts. This depth coincides with a level where circulation (pumping) rate was increased slightly. Logging data from the two holes were combined by splicing at 311.26 mbsf; selected logs are shown adjacent to the lithostratigraphic units (see "Lithostratigraphy" section, this chapter) in Figure 47.

Closer inspection of an interval below 360 mbsf illustrates the effect of borehole washout on two common log parameters, density and velocity. Caliper data between 410 and 510 mbsf indicate regular

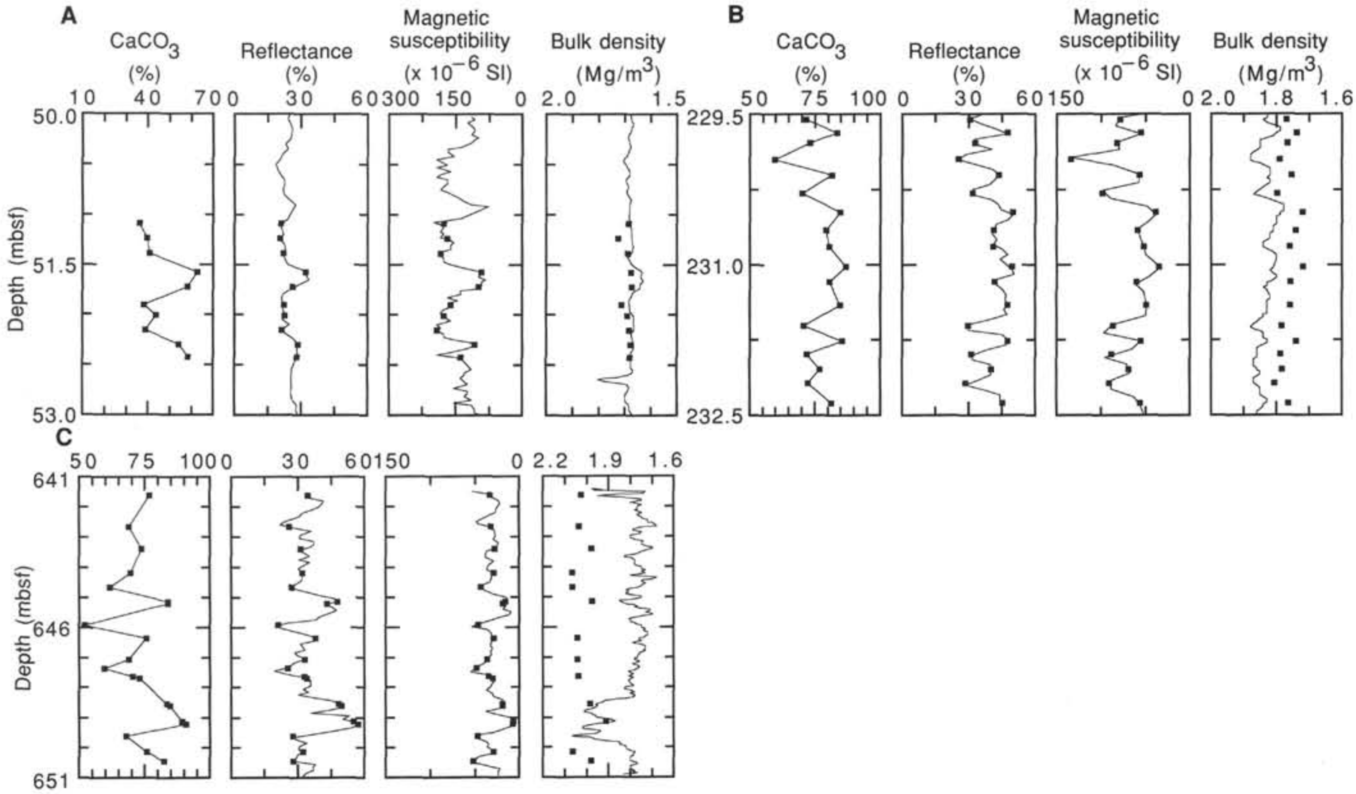

Figure 31. Calcium carbonate, reflectance, magnetic susceptibility, bulk density–GRAPE and discrete samples vs. depth for three sets of closely spaced samples at Site 925. The magnetic susceptibility and density scales are inverted. Solid squares on each plot represent the discrete values used in the scatter plots in Figures 32 and 37. For $CaCO_3$ and density, these values are the actual measurements on discrete samples. For reflectance and magnetic susceptibility, the values are linearly interpolated from the closest measurements. The GRAPE data has been smoothed with a 9-point Gaussian filter and duplicate measurements were averaged. Note changes in scale throughout. **A.** Core 154-925E-6H. **B.** Core 154-925C-25H. **C.** Core 154-925A-38R. Much of the variation in the GRAPE signal in this interval is related to sample diameter and gaps (see "Physical Properties" section, this chapter). The offset between GRAPE and the discrete measurements of density observed in Cores 154-925C-25H and 154-925A-38R is discussed in the "Physical Properties" section (this chapter).

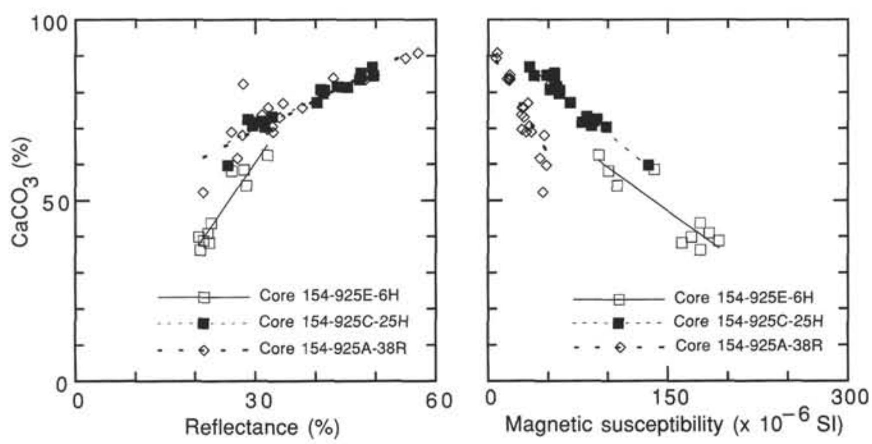

Figure 32. Calcium carbonate vs. reflectance and magnetic susceptibility for high-resolution study of Cores 154-925E-6H, 154-925C-25H, and 154-925A-38R, from lithologic Units I, II, and III, respectively. The linear regression lines for samples from each core are shown. Correlation coefficients (r) for reflectance are 0.94 (Core 154-925E-6H samples), 0.96 (Core 154-925C-25H samples), and 0.87 (Core 154-925A-38R samples). Correlation coefficients (r) for magnetic susceptibility are –0.90 (Core 154-925E-6H samples), –0.97 (Core 154-925C-25H samples), and –0.78 (Core 154-925A-38R samples).

intervals where the borehole diameter increases rapidly from values near the bit diameter (~10 in.) to at least 18 in. (the maximum caliper reading). The FMS images recorded over this interval demonstrate that the washouts reflect sidewall drilling erosion of the rhythmic carbonate-rich to clay-rich bedding cycles observed in the cores (see "Lithostratigraphy" section, this chapter). The sharpness of the washout features prevents the density tool from maintaining close contact with the borehole wall. As a result, the tool is forced to measure some combination of seawater and formation density, resulting in anomalously low densities. Comparison with the measured core wet bulk densities (Fig. 48) illustrates the importance of this effect on the log densities (this also applies to the photoelectric effect log, which uses the same measurement principle). Similarly, the variable borehole diameter induces "cycle skipping" in the sonic velocity log, in which the instrument picks incorrect first arrival times used in the velocity calculation. This log can be improved greatly after post-cruise processing of the full-waveform sonic data.

Log Repeatability

Main and repeat Quad logs recorded at Hole 925C were used to assess the precision of the various standard and high-resolution

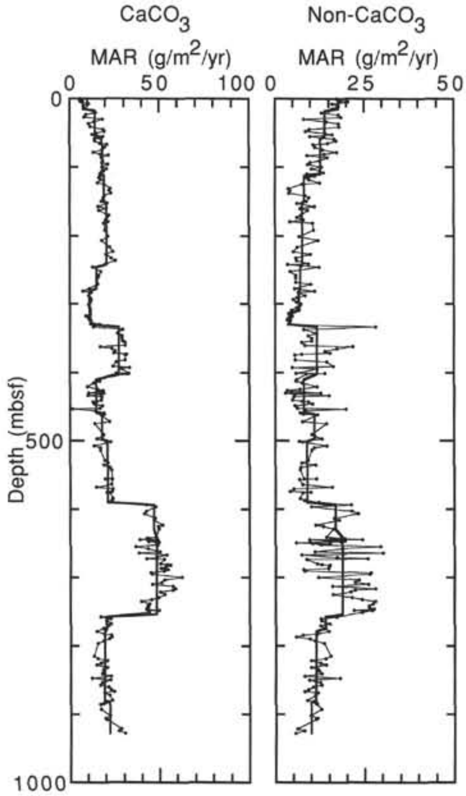

Figure 33. Mean calcium carbonate and noncarbonate accumulation rates vs. depth, Site 925. Solid circles represent values calculated from discrete carbonate and associated dry-bulk-density measurements. The age and sedimentation rates for each sample were based on linear interpolation between selected age datums (see "Sedimentation Rates" section, this chapter). The thick solid line in the plots is the mean value of the MARs between each of the selected age datums. Note that the scale for the carbonate is twice the range of the noncarbonate MAR in the separate plots.

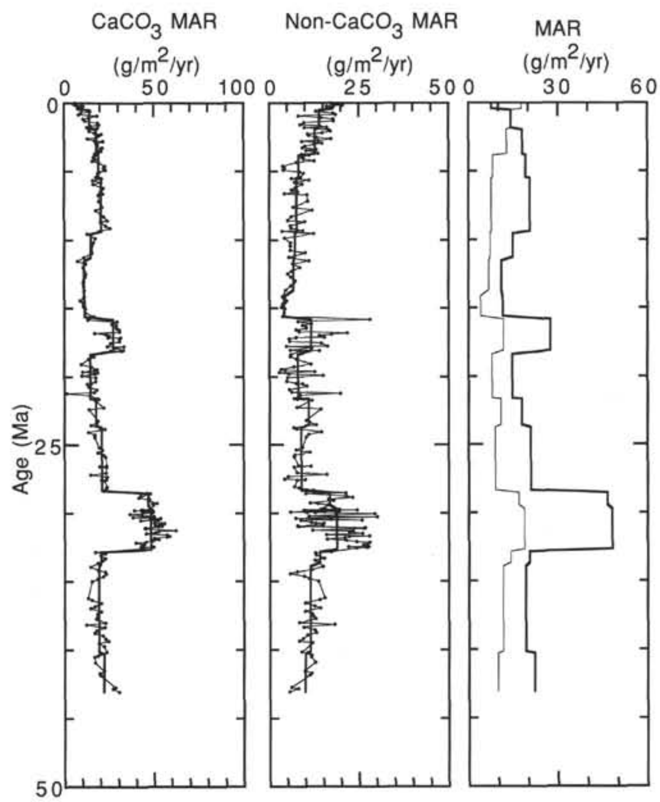

Figure 34. Calcium carbonate, noncarbonate, and mean accumulation rates vs. age, Site 925. Note that the scale for the carbonate is twice the range of the noncarbonate MAR in the separate plots. Mean rates are plotted on the same scale.

log measurements. Figure 49 shows the standard main and repeat gamma-ray, density, photoelectric effect, resistivity, velocity, and caliper logs for the interval from 220 to 240 mbsf in Hole 925C. Comparison of the main and repeat logs over this 20-m interval demonstrates a high degree of measurement precision. Much of the observed error can be attributed to slight depth offsets caused by uncompensated ship heave. The intrinsic vertical resolution (interval over which an accurate measurement is obtained) varies with log type, ranging from 38 cm for the HLDT density tool, to between 46 and 75 cm for the gamma-ray and SFL resistivity tools, to almost 2 m for the long-spaced sonic velocity tool (Allen et al., 1988). Analyses of Leg 138 core and log density data demonstrated that the HLDT resolution in eastern equatorial Pacific sediments was closer to 0.8–1.0 m (Harris et al., in press).

The high-resolution density and resistivity logs show repeatable improvements in log resolution (Fig. 49). The shipboard processing applied to the density logs employs a forward modeling scheme to optimize the density measurement using the near-detector-source spacing (18 cm). The main and repeat high-resolution density logs exhibit a high degree of covariance over the 240–220 mbsf interval despite very low-amplitude density variations. Core density measurements from Core 154-925C-25H are shown for comparison (see "Physical Properties" section, this chapter). The processed photoelectric effect logs also show increased resolution. Photoelectric absorption occurs when emitted gamma rays are reduced to lower energies by Compton scattering; these gamma rays are then absorbed by large atomic number (large photoelectric cross section) atoms. For carbonate-rich pelagic and hemipelagic sediments such as those recovered at this site, Ca predominates, so increased photoelectric log values can be expected to reflect increased $CaCO_3$ abundances.

Core-log Data Comparisons

Bulk density, magnetic susceptibility, natural gamma activity, and *P*-wave velocity are all measured on core sections and in logs. Comparison of the magnetic susceptibility and natural gamma records as measured on cores and in logs is shown for the uppermost 300 mbsf of Hole 925C in Figure 50. The figure demonstrates the very good correspondence between the core and log measurements.

The vertical resolution of the various log measurements is limited to between 0.5 and 1.0 m, as discussed above. Thus, the resolution of orbital-scale bedding cycles is primarily dependent upon sedimentation rate. For most Schlumberger logging tool measurements (those with vertical resolutions near 75 cm), nominal sedimentation rates must exceed 1.5, 3, and 6 cm/k.y. to achieve e-folding resolution of bedding cycles at the eccentricity (100 k.y.), tilt (41 k.y.), and precession (23–19 k.y.) orbital periodicities, respectively (deMenocal et al., 1992).

Comparison of the core and log susceptibility, density, and natural gamma measurements for the interval between 200 and 220 mbsf in Hole 925C illustrates the strong similarity between the core and log data sets, as well as the general signal attenuation inherent in the log-derived measurements (Fig. 51). The average sedimentation rate for this interval is 2.4 cm/k.y. (see "Sedimentation Rates" section, this chapter), so most tools are capable of resolving only the longest orbital bedding cycles (>100 k.y.). An exception to this is the high-resolution density log (shown as the solid line in the center panel of Fig. 51); this measurement approaches 18-cm resolution, which translates to ~15- to 20-k.y. temporal resolution.

The core and log natural gamma measurements between 600 and 700 mbsf at Site 925 are shown in Figure 52. In this interval, the bedding cycles are relatively expanded in depth because of the relatively

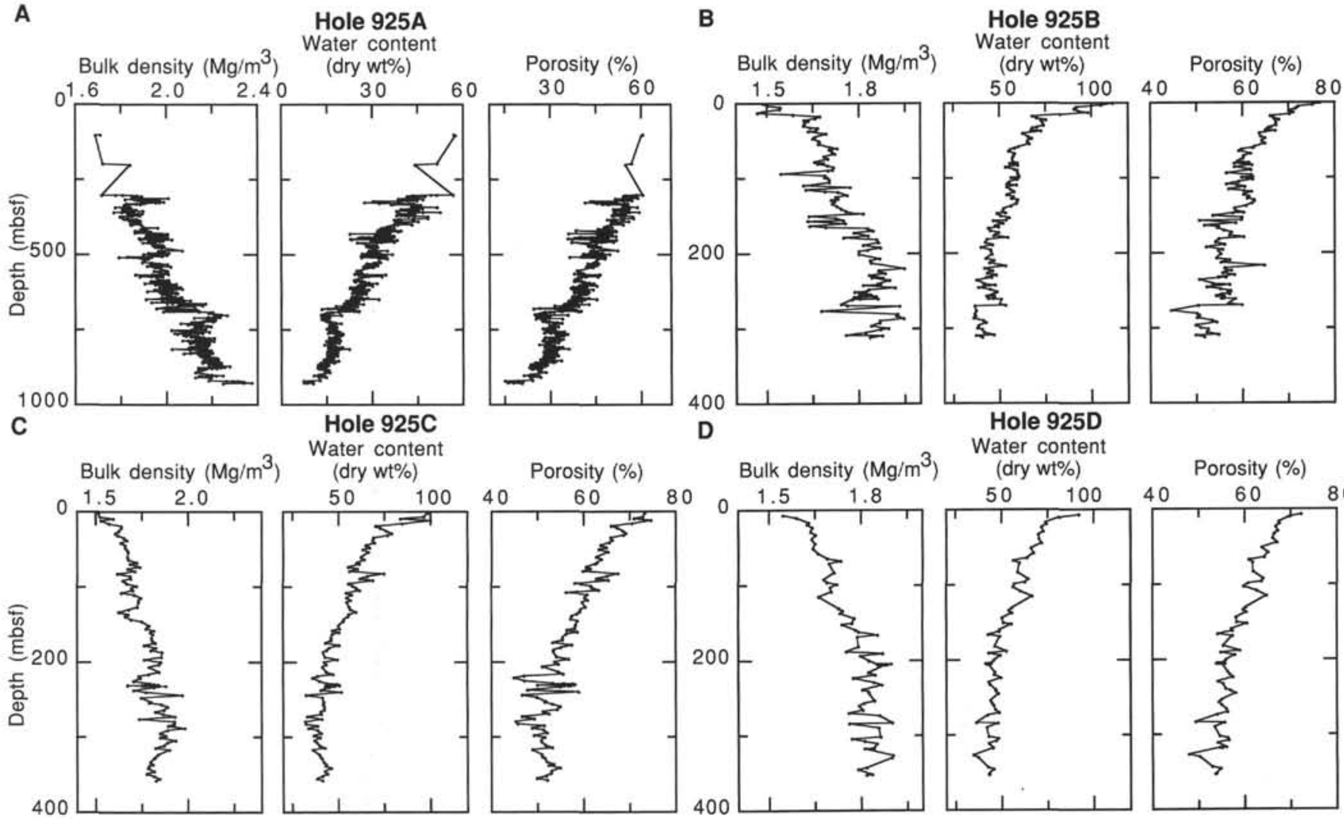

Figure 35. Bulk density, water content, and porosity vs. depth, Site 925. Note differences in scales.

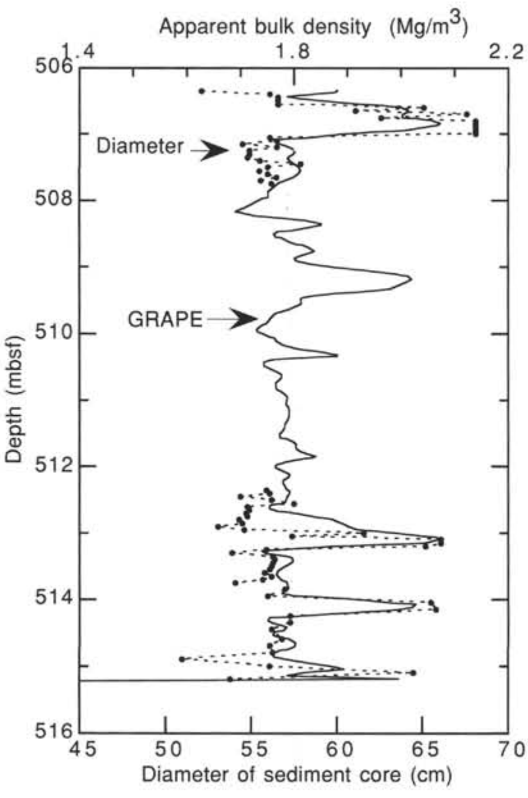

Figure 36. Comparison of GRAPE apparent bulk density calculations from an RCB interval of Hole 925A with measurement of core diameter.

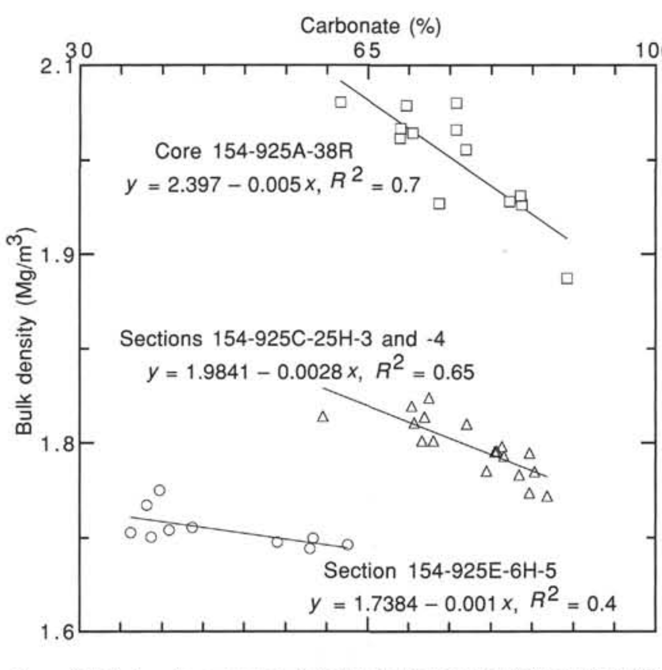

Figure 37. Carbonate content vs. bulk density for three depth intervals at Site 925 showing increased correlation of $CaCO_3$ to bulk density with depth in the sediment section.

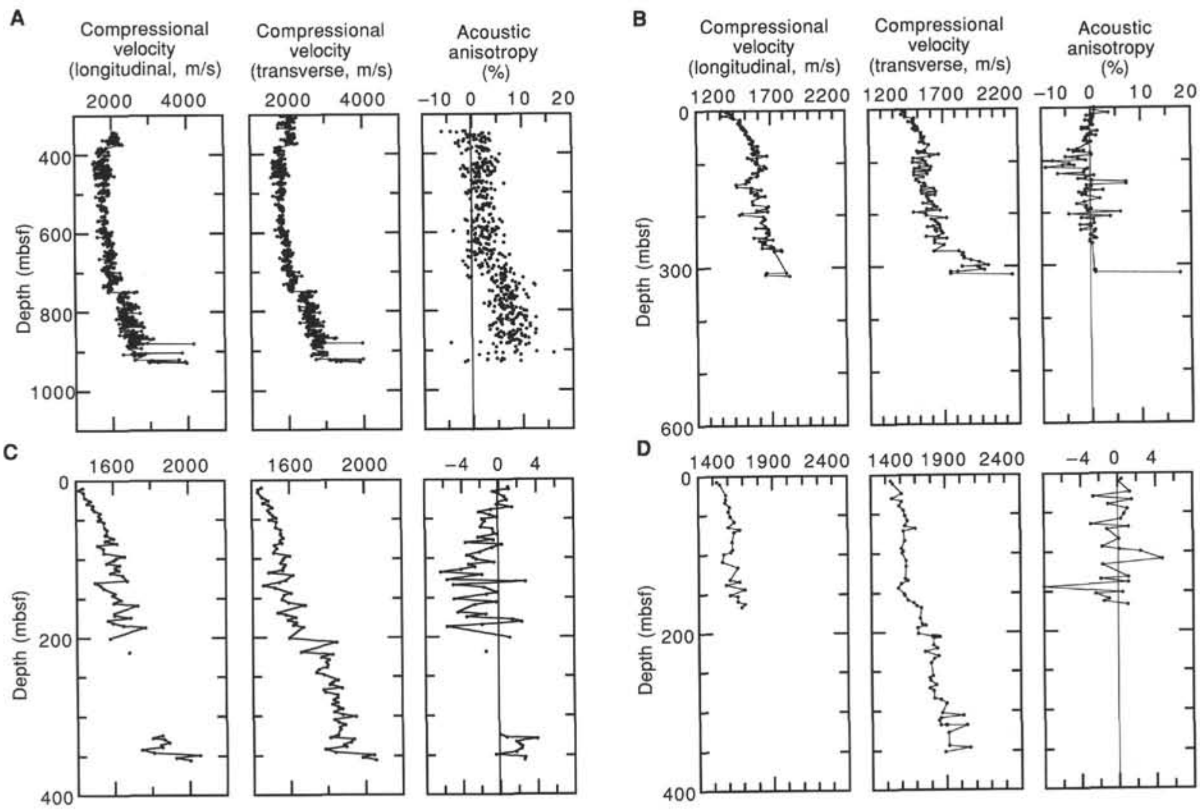

Figure 38. Acoustic velocity vs. depth measured along the core axis longitudinal and transverse to the axis of the core, and acoustic anisotropy vs. depth for Holes 925A (**A**), 925B (**B**), 925C (**C**), and 925D (**D**).

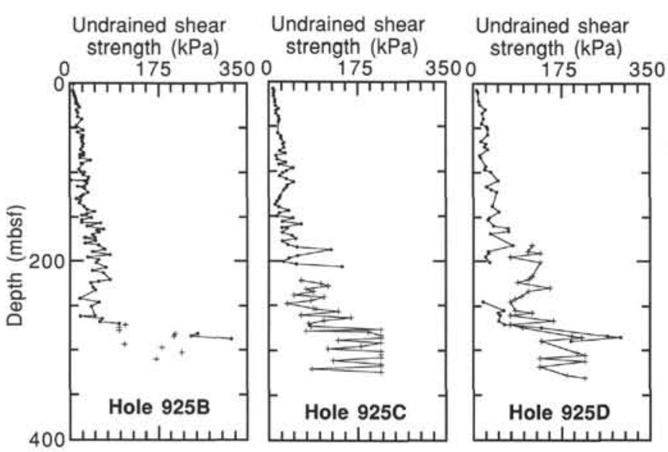

Figure 39. Undrained shear strength (kPa) measured using the miniature vane shear device (solid circles) and the pocket penetrometer (plus signs) on cores from Holes 925B, 925C, and 925D.

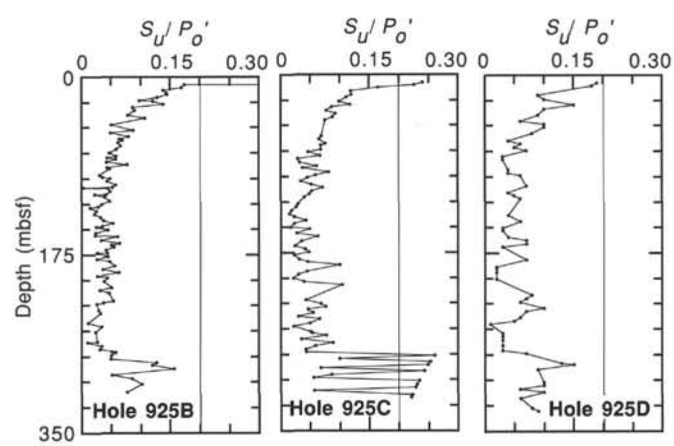

Figure 40. S_u/P_o' ratios calculated from undrained shear strength and bulk density for cores from Holes 925B, 925C, and 925D.

high sedimentation rates (3–4 cm/k.y.; see "Sedimentation Rates" section, this chapter). Note that the natural gamma log resolves the 1- to 1.3-m bedding cycles seen in the core-derived measurements.

Comparison of Core and Log Physical Properties Measurements

The core and log density data agree extremely well, whereas the core velocity data indicate significantly slower velocities than the log values between 150 and 750 mbsf (Fig. 53). Core density data have been corrected for elastic rebound, and the velocity data have been corrected to a temperature gradient of 50°C/km; both log density and velocity data have been filtered to remove borehole washout effects and related velocity (first-arrival cycle skipping) errors. The excellent agreement between the core and log densities demonstrates that the log data are still reliable despite very poor borehole conditions. The slower core velocities are curious in that the offsets are not a simple function of sub-bottom depth; the magnitude of the offset and its variability downhole argue for unrecovered changes in sediment moduli associated with recovery.

Log Interpretation and Lithology

The natural gamma, density, sonic velocity, and resistivity logs provide confirmation of major lithologic unit boundaries derived

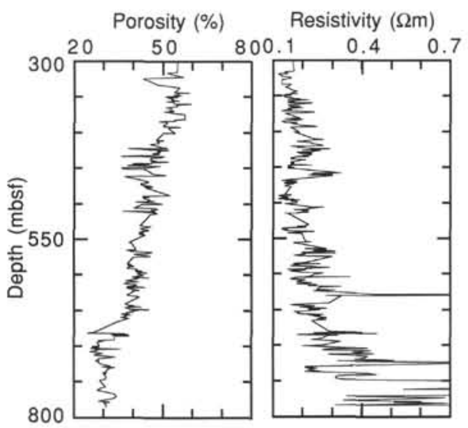

Figure 41. Porosity vs. depth compared with electrical resistivity vs. depth for Hole 925A.

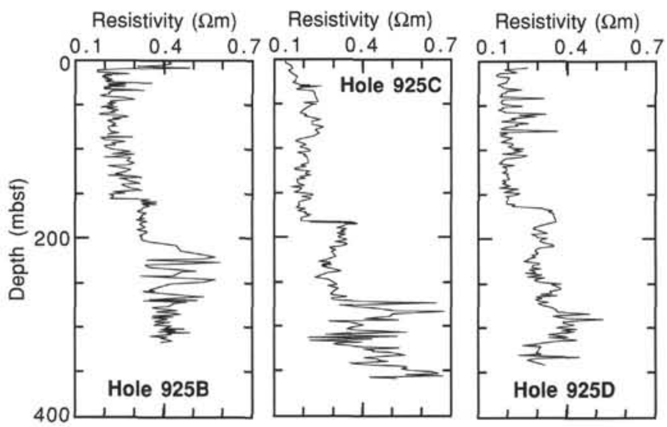

Figure 42. Electrical resistivity vs. depth for Holes 925B, 925C, and 925D.

from core descriptions (Fig. 47). The boundary separating Unit I, described as nannofossil clay alternating with clayey nannofossil ooze (see "Lithostratigraphy" section, this chapter), from Unit II, a nannofossil ooze with varying clay content, is clearly visible on the natural gamma log, which illustrates the decreasing clay content toward the base of Unit I and the lower average natural gamma-ray values for Subunit IIA (135 mbsf). The clay content decreases further in Subunit IIB before increasing again in Subunit IIC (210 mbsf), which contains bands of clay. Increased lithification produces a steady density increase throughout Unit II; higher carbonate content in this unit (average 72%) is reflected by increased photoelectric effect log values relative to Unit I (53% average carbonate content).

The natural gamma values decrease suddenly at the boundary between Units II and III, where the clay bands present at the base of Subunit IIC cease. A dramatic increase in sonic velocity is observed at and below the Unit II/III boundary (290 mbsf), reflecting increased rigidity associated with the transition to nannofossil chalk (Subunit IIIA). The log data suggest a marked increase in terrigenous content below 450 mbsf, in the middle of Subunit IIIA. The gradual increase in the photoelectric effect log within Subunit IIIA implies an increasing carbonate content with depth within this subunit (see "Lithostratigraphy" section, this chapter). The increased lithification associated with the Subunit IIIA–IIIB transition from nannofossil chalk to limestone (700 mbsf) is identified by significant increases in log density; below this boundary, the log velocity attains high and relatively stable values.

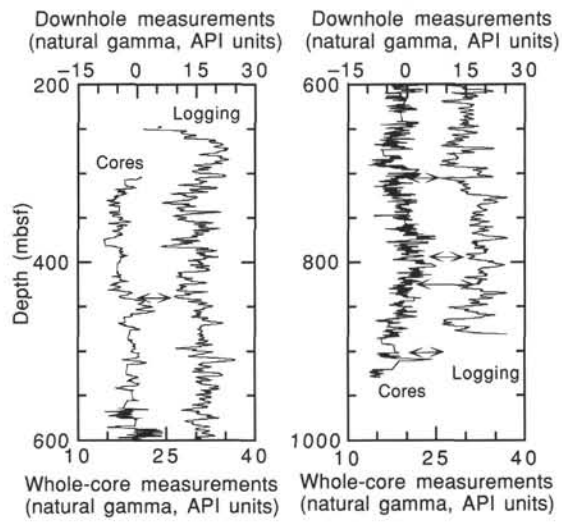

Figure 43. Whole-core natural gamma measurements compared with downhole natural gamma measurements, Site 925.

Velocity/Resistivity Relationship

Based on internal consistencies of the compressional-wave velocity and electrical resistivity profiles, we divided the data into three intervals to address velocity-resistivity changes during consolidation of the sedimentary series: top of the logged interval to 400 mbsf, from 400 to 700 mbsf, and from 700 mbsf to the bottom of the logged interval at about 930 mbsf. Compressional-wave velocity is plotted vs. electrical resistivity in Figure 54. Because electrical resistivity is controlled by porosity changes, this illustrates the changing relationship of velocity to porosity with depth in the sediment column. The different intervals occupy overlapping fields that tend toward lower porosities (higher resistivities) and increasing velocities with depth. In the top interval (from the top of the logged interval at 60–400 mbsf), velocity changes substantially (1450–2300 m/s), with very little change in electrical resistivity (1–1.3 Ωm). The middle interval (400–700 mbsf) shows more scattering. Velocities range from 2150 to about 2700 m/s over a wider range of electrical resistivity (1.4–2.2 Ωm). Finally, the bottom interval (700–930 mbsf) shows the strongest resistivity-velocity relationship, with velocity increasing from 2350 to 2900 m/s as resistivity increases from 1.7 to 2.8 Ωm.

The rapid rise in velocity with little change in electrical resistivity (top interval) can be confidently attributed to increasing cementation and grain-to-grain bonding in the upper part of the sedimentary column. The ooze-chalk transition occurs in this interval (at about 290 mbsf; see "Lithostratigraphy" section, this chapter). The bottom interval exhibits a typical porosity-velocity relationship for carbonate rocks (e.g., Wyllie et al., 1956).

Borehole Temperature

The temperature logging tool at the head of the Quad tool string indicated a borehole fluid temperature of 31.5°C at total depth (913 mbsf; Fig. 55). This temperature is significantly less than expected from the regional geothermal gradient because the hole was circulated with seawater during drilling and before logging. The data were collected approximately 17 hr after wiper trip circulation. The 5°C warmer uplog profile reflects borehole warming (thermal rebound) over approximately 2 hr.

Synthetic Seismogram

The density and velocity logs were filtered in a preliminary way to remove bad data caused by borehole washouts. Reflection coeffi-

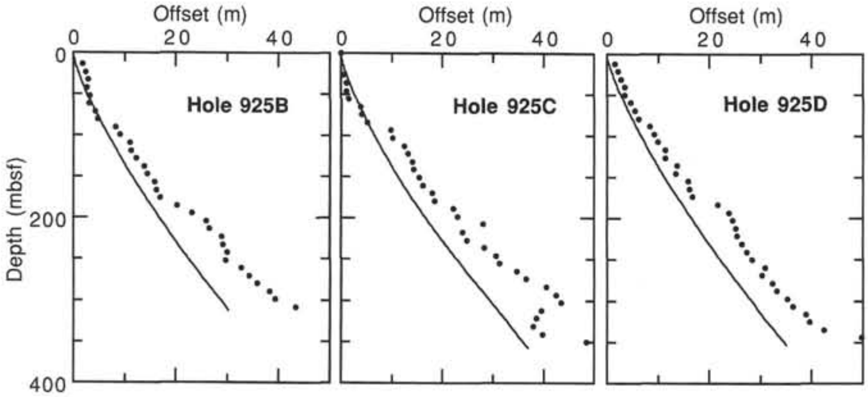

Figure 44. Estimated length of core expansion caused by elastic rebound of recovered core samples (solid line) compared with the composite depth offset for Holes 925B, 925C, and 925D.

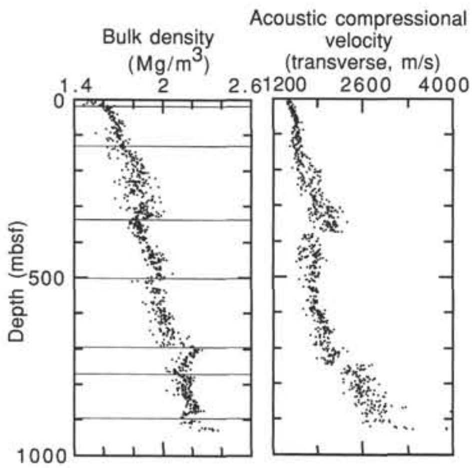

Figure 45. Bulk density and acoustic compressional velocity vs. depth for all holes at Site 925. The horizontal lines denote changes in gradient of bulk density with depth.

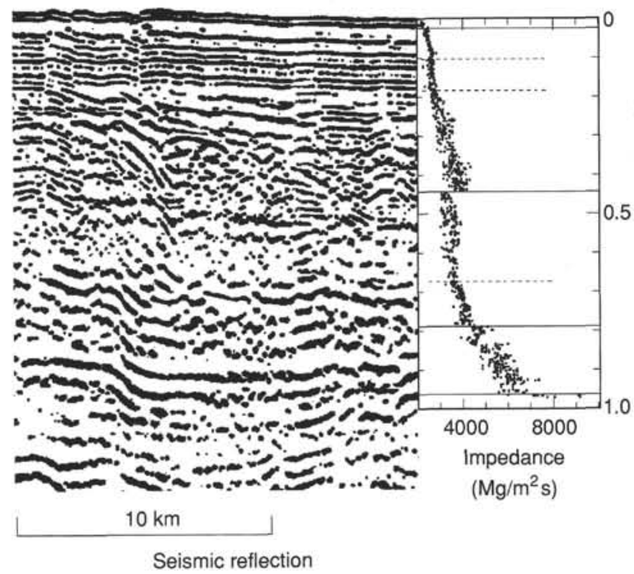

Figure 46. Acoustic impedance calculated from discrete measurement on core samples for Site 925 compared with the seismic reflection data.

cient data were then calculated and interpolated to 1-ms TWT increments. This time-series was then convolved with the (air-gun) source wavelet (Fig. 56) derived from stacking and averaging the mud-line response from ten CDP shotpoints. The resulting synthetic seismogram is shown compared to the Site 925 seismic line taken during the site survey (*Ewing* Cruise 9209, Line 2, Shotpoints 9590–9610; see Mountain and Curry, this volume) in Figure 57.

The synthetic seismogram from this site reproduces several features apparent in the seismic line; however, there are several notable differences as well. The main reflectors are associated with major changes in sediment lithification centered near 454, 536, and 587 mbsf. The sharp reflector near 454 mbsf may represent the clay-rich layer responsible for the bridge that interfered with logging operations (see Fig. 48). The synthetic seismogram seems to reproduce the general character of the Site 925 seismics, with moderate-amplitude reflectors between 4.10 and 4.25 s TWT; higher frequency, low-amplitude reflectors between 4.25 and 4.45 s TWT; and larger amplitude and longer wavelength reflectors below this level. However, in detail, the synthetic seismogram does not show all of the character apparent in the seismic line, which may be, in part, a result of the relatively noisy log density and velocity data that resulted from the poor borehole conditions.

Shore-based Log Processing

Additional processing of the Site 925 logs and display was conducted onshore by the Borehole Research Group. The results are presented at the end of this chapter and on the CD-ROM disc in the back pocket of this volume.

SUMMARY AND CONCLUSIONS

Situated on the shallowest part of the Ceara Rise, Site 925 will provide the reference section for the study of the paleoceanography of the western equatorial Atlantic Ocean. The upper 350 m of section, cored in three parallel holes to ensure completeness, comprises a truly continuous sequence of pelagic foraminifer and nannofossil ooze grading to chalk at the base, covering the last 16 m.y. without any break. Preservation of calcareous microfossils is generally very good to excellent, and numerous high-resolution studies will be possible in these sediments. Below this, a 400-m-thick sequence of lower Miocene and Oligocene, greenish, rhythmically bedded chalk was recovered with the RCB. Again, the preservation of calcareous microfossils is very good although the sediments become progressively more lithified with burial depth. In general, recovery was high in this sequence, and the downhole logs provide continuity over the inter-core gaps. In the upper and middle Eocene part of the section, the sediment grades toward a hard limestone with pervasive recrystallization; we ended drilling at the point where we judged that the sediments offered few opportunities for paleoceanographic investigations. Pore-water studies provide additional evidence that significant carbonate recrystallization is proceeding in the deepest part of section.

The warm western areas of the tropical oceans are generally considered to represent the regions of most rapid evolution in the marine plankton, and this idea is supported by the calcareous microfossils (foraminifers and calcareous nannofossils) recovered at Site 925.

Table 12. Undrained shear strength from miniature vane shear measurements and unconfined compression test results from the pocket penetrometer for all holes at Site 925.

Core, section, interval (cm)	Depth (mbsf)	Undrained shear strength (kPa)	Residual shear strength (kPa)	Pocket penetrometer (kg/cm²)	S_u from PP (kPa)
154-925B-					
1H-2, 10	1.6	3.5	2.5		
1H-1, 101	1.01	8.3	5.5		
2H-3, 55	8.05	6.9	3.8		
2H-5, 60	11.1	9.0	5.5		
2H-7, 30	13.3	8.7	6.0		
3H-1, 130	15.3	10.6	6.8		
3H-3, 75	17.75	12.9	8.7		
3H-5, 75	20.75	13.9	6.9		
3H-7, 8	23.08	12.0	5.0		
4H-1, 75	24.25	15.6	8.2		
4H-3, 75	27.25	20.3	11.7		
4H-5, 75	30.25	14.3	4.9		
4H-7, 30	32.8	16.1	6.3		
5H-4, 40	37.9	16.5	6.8		
5H-6, 38	40.88	24.9	12.0		
6H-2, 10	44.1	18.9	7.4		
6H-4, 75	47.75	14.0	6.6		
6H-6, 10	50.1	21.0	8.7		
7H-1, 75	52.75	26.6	14.2		
7H-3, 20	55.2	15.9	6.8		
7H-5, 75	58.75	27.4	10.7		
7H-7, 10	61.1	23.2	9.6		
8H-1, 75	62.25	25.5	13.7		
8H-3, 75	65.25	23.9	11.2		
8H-5, 40	67.9	26.8	12.1		
9H-1, 10	71.1	25.2			
9H-3, 75	74.75	21.7			
9H-5, 128	78.28	28.0			
9H-7, 23	80.23	21.1			
10H-1, 74	81.24	28.5			
10H-3, 13	83.63	21.4			
10H-5, 10	86.6	41.0	3.6		
10H-7, 10	89.6	23.8			
11H-1, 32	90.32	26.1	8.5		
11H-3, 15	93.15	24.7	9.9		
11H-5, 53	96.53	18.6	6.8		
11H-7, 41	99.41	21.7	6.1		
12H-7, 62	109.1	3.3	3.3		
12H-1, 62	100.1	29.6			
12H-3, 18	102.7	27.7			
12H-5, 39	105.9	37.5			
12H-7, 27	108.8	35.3			
13H-1, 86	109.9	30.9			
13H-3, 67	112.7	34.3			
13H-5, 72	115.7	16.2			
13H-5, 62	115.6	29.9			
13H-7, 33	118.3	29.0			
14H-3, 123	122.7	36.4			
14H-5, 84	125.3	26.9			
14H-7, 20	127.7	22.5			
15H-1, 123	129.2	11.8			
15H-3, 83	131.8	20.6			
15H-5, 85	134.9	18.6			
16H-1, 82	138.3	27.9			
16H-3, 112	141.6	33.6			
16H-5, 75	144.3	48.5			
16H-7, 28	146.8	33.2			
17H-1, 115	148.2	23.8			
17H-3, 75	150.8	42.4			
17H-5, 53	153.5	23.6			
17H-7, 25	156.3	22.8			
18H-1, 85	157.4	60.8			
18H-3, 118	160.7	33.9			
18H-5, 125	163.8	66.9			
18H-6, 130	165.3	53.2			
19H-1, 133	167.3	58.0			
19H-3, 128	170.3	45.5			
19H-5, 139	173.4	28.9			
19H-5, 145	173.5	31.7			
19H-5, 122	173.2	49.2			
20H-1, 128	176.8	51.5			
20H-3, 90	179.4	30.6			
20H-5, 54	182	56.6			
21H-1, 132	186.3	69.0			
21H-3, 133	189.3	45.0			
21H-5, 148	192.5	79.7			
22H-1, 119	195.7	35.0			
22H-3, 53	198	57.6			
22H-5, 130	201.8	51.9			
23H-1, 93	204.9	89.0			
23H-3, 22	207.2	71.0			
23H-5, 22	210.2	44.7			
23H-7, 6	213.1	66.4			
24H-5, 127	220.8	80.2			
24H-7, 19	222.7	56.6			
25H-1, 113	224.1	40.6			
25H-3, 15	226.2	37.0			
25H-5, 86	229.9	46.3			
25H-7, 59	232.6	51.4			
27H-1, 50	242.5	19.5			
27H-3, 118	246.2	58.1			
27H-5, 78	248.8	44.7			
27H-7, 46	251.5	43.2			
28H-7, 37	260.9	49.9			
29H-1, 89	261.9	20.6			
29H-3, 97	265	63.8			
29H-5, 79	267.8	59.2			
29H-7, 41	270.4	97.7			
30H-1, 70	271.2			2.25	110.32875
30H-3, 85	274.4			2.0	98.07
30H-5, 100	277.5			2.0	98.07
31H-1, 130	281.3	252.0		4.25	208.39875
31H-3, 60	283.6	239.0		4.2	205.947
31H-5, 135	287.4	318.0			
32H-1, 80	290.3			4.5	220.6575
32H-3, 102	293.5			2.2	107.877
32H-5, 127	296.8			3.7	181.4295
32H-6, 117	298.2			4.5	220.6575
32H-7, 42	298.9			3.4	166.719
33H-1, 52	299.5			4.5	220.6575
33H-3, 40	302.4			4.5	220.6575
33H-4, 87	304.4			4.5	220.6575
34H-1, 142	309.9			3.5	171.6225
34H-3, 75	312.3			4.5	220.6575
34H-5, 50	315			4.5	220.6575
154-925C-					
1H-6, 27	7.77	8.7	5.0		
2H-2, 86	10.36	11.3	7.2		
2H-4, 5	12.55	10.2	6.8		
2H-6, 44	15.94	9.5	6.0		
3H-2, 117	20.17	12.6	9.8		
3H-4, 33	22.33	13.1	6.8		
3H-6, 124	26.24	14.0	7.9		
4H-2, 121	29.71	18.9			
4H-4, 50	32	15.1			
4H-6, 115	35.65	15.3			
5H-2, 98	38.98	20.0			
5H-4, 111	42.11	20.6			
5H-6, 92	44.92	19.4			
7H-2, 13	57.13	18.4			
7H-4, 59	60.59	24.9			
7H-6, 47	63.47	24.6			
8H-2, 130	67.8	31.0			
8H-4, 9	69.59	28.5			
8H-6, 130	73.8	30.7			
9H-2, 71	76.71	21.9			
9H-4, 93	79.93	32.9	15.0		
9H-6, 60	82.6	14.5	4.9		
10H-2, 120	86.7	17.3	8.0		
10H-4, 139	89.89	33.4	11.0		
10H-6, 60	92.1	21.3	7.9		
11H-2, 125	96.25	48.5	21.9		
11H-4, 102	99.02	35.8	16.1		
11H-6, 36	101.4	28.5	13.7		
12H-2, 75	105.3	22.1	8.8		
12H-4, 89	108.4	34.7			
12H-6, 83	111.3	49.5			
13H-2, 85	114.9	37.6			
13H-4, 81	117.8	35.9			
13H-6, 83	120.8	30.6	11.0		
14H-4, 85	127.4	23.5	10.2		
14H-6, 85	130.4	21.5	7.6		
15H-2, 67	133.7	15.6			
15H-4, 59	136.6	12.4			
15H-6, 58	139.6	20.1			
16H-2, 107	143.6	39.0			
16H-4, 68	146.2	20.7	8.8		
16H-6, 123	149.7	16.1	7.1		
17H-2, 20	152.2	47.2			
17H-4, 98	156	27.2	7.9		
17H-6, 86	158.9	63.9			
18H-2, 85	162.4	25.5			
18H-3, 70	163.7	36.8			
18H-6, 104	168.5	26.6	11.9		
19H-2, 60	171.6	45.8			
19H-4, 100	175	53.5			

Table 12 (continued).

Core, section, interval (cm)	Depth (mbsf)	Undrained shear strength (kPa)	Residual shear strength (kPa)	Pocket penetrometer (kg/cm^2)	S_u from PP (kPa)
19H-6, 75	177.8	26.3	10.2		
20H-2, 110	181.6	37.3			
20H-4, 64	184.1	55.4			
20H-6, 71	187.2	122.5			
21H-4, 112	194.1	57.1			
21H-6, 87	196.9	40.2			
22H-2, 109	200.6	29.4	4.5		
22H-4, 118	203.7	54.0			
22H-6, 126	206.8	144.0			
24H-2, 218.5					
24H-4, 22	221.7			1.3	63.7455
24H-6, 102	225.5			2.1	102.9735
25H-2, 48	228.5			2.4	117.684
25H-4, 36	231.4			1.5	73.5525
25H-6, 47	234.5			1.8	88.263
26H-2, 67	238.2			1.0	49.035
26H-4, 23	240.7			2.2	107.877
26H-6, 90	244.4			1.7	83.3595
27H-2, 55	247.6			0.75	36.77625
27H-6, 26	253.3			1.8	88.263
27H-6, 118	254.2			1.9	93.1665
28H-2, 36	256.9			2.8	137.298
28H-4, 106	260.6			1.3	63.7455
28H-6, 130	263.8			3.3	161.8155
29H-2, 70	266.7			2.2	107.877
29H-4, 127	270.3			1.6	78.456
29H-6, 93	272.9			1.7	83.3595
30H-2, 118	276.7			4.5	220.6575
30H-3, 106	278.1			1.5	73.5525
30H-4, 87	279.4			4.0	196.14
30H-6, 127	282.8			4.5	220.6575
31H-2, 70	285.7			4.5	220.6575
31H-4, 79	288.8			2.8	137.298
31H-6, 49	291.5			4.5	220.6575
32H-2, 74	295.2			3.7	181.4295
32H-4, 81	298.3			2.4	117.684
32H-6, 76	301.3			4.5	220.6575
33H-2, 66	304.7			4.5	220.6575
33H-4, 95	308			4.5	220.6575
33H-6, 90	310.9			2.6	127.491
34H-2, 141	314.9			4.5	220.6575
34H-4, 101	317.5			4.5	220.6575
34H-6, 90	320.4			1.75	85.81125
35X-2, 100	324			4.5	220.6575
154-925D-					
1H-4, 77	7.77	7.4	6.6		
1H-6, 71	10.71	9.8	8.3		
1H-6, 0	10	0	0		
2H-4, 130	17.72	6.9	2.4		
2H-4, 16	16.58	8.0	4.1		
2H-6, 99	20.41	10.6	3.2		
3H-2, 98	23.98	13.7	4.9		
3H-6, 50	29.5	24.9	14.5		
4H-2, 118	33.68	18.4	8.8		
4H-6, 103	39.53	21.3	9.6		
5H-4, 47	45.47	16.7	8.5		
5H-6, 92	48.92	27.7	9.8		
6H-2, 30	51.8	29.8	16.7		
6H-6, 50	58	29.0	15.3		
7H-4, 93	64.93	15.9	6.6		
7H-6, 92	67.92	25.0	13.1		
8H-2, 103	71.53	23.6	12.1		
8H-4, 110	74.6	29.6	15.0		
9H-2, 90	80.9	14.2	7.1		
9H-4, 43	83.43	15.1	6.0		
10H-4, 66	93.16	25.4	11.3		

Core, section, interval (cm)	Depth (mbsf)	Undrained shear strength (kPa)	Residual shear strength (kPa)	Pocket penetrometer (kg/cm^2)	S_u from PP (kPa)
10H-6, 124	96.74	23.6	11.2		
11H-2, 37	99.37	36.1	15.0		
12H-2, 42	108.9	50.4			
12H-6, 108	115.6	26.3			
13H-2, 110	119.1	37.0			
13H-4, 110	122.1	47.7			
15H-2, 110	138.1	37.5			
15H-6, 128	144.3	51.5			
16H-4, 134	150.8	31.2			
16H-6, 35	152.9	29.6			
17H-4, 60	159.6	40.0			
17H-6, 48	162.5	68.4			
18H-2, 66	166.2	70.4			
18H-4, 60	169.1	33.6			
19H-6, 104	182	77.8		2.4	117.72
20H-4, 132	188.8	30.2		2.2	107.91
20H-6, 34	190.8	30.2		2.7	132.435
21H-2, 69	194.7	24.9		1.5	73.575
21H-6, 125	201.3	32.3		2.7	132.435
22H-2, 26	203.6			2.4	117.72
22H-6, 26	209.6			2.7	132.435
23H-4, 67	216.7			2.4	117.72
23H-6, 120	220.2			2.25	110.3625
24H-2, 130	223.8			1.8	88.29
24H-6, 120	229.7			3.1	152.055
25H-2, 110	233.1			2.25	110.3625
25H-6, 124	239.2			1.95	95.6475
26H-2, 104	242.5			1.7	83.385
26H-4, 84	245.3	20.0		1.5	73.575
27H-4, 70	254.7	61.1		1.7	83.385
27H-6, 70	257.7	49.8		2.4	117.72
28H-2, 21	260.7	53.4		1.5	73.575
28H-5, 147	266.5	50.9		3.25	159.4125
29H-2, 87	270.9	62.1		1.5	73.575
29H-4, 115	274.2	135.3		2.0	98.1
29H-5, 42	274.9			2.4	117.72
29H-5, 47	275			2.75	134.8875
29H-5, 52	275			4.0	196.2
29H-5, 60	275.1			2.6	127.53
29H-5, 65	275.2			3.25	159.4125
29H-5, 70	275.2			3.4	166.77
29H-5, 75	275.3			3.1	152.055
29H-5, 80	275.3			2.8	137.34
29H-5, 85	275.4			3.0	147.15
29H-5, 90	275.4			2.75	134.8875
29H-5, 95	275.5			2.75	134.8875
29H-5, 100	275.5			4.4	215.82
29H-5, 105	275.6			3.75	183.9375
29H-5, 110	275.6			3.25	159.4125
29H-5, 115	275.7			3.2	156.96
29H-5, 120	275.7			4.1	201.105
29H-5, 125	275.8			2.6	127.53
29H-5, 130	275.8			2.5	122.625
30H-4, 102	283.5	266.1		4.0	196.2
30H-5, 94	284.9	291.7		4.4	215.82
31H-2, 81	289.8	193.6		2.75	134.8875
31H-4, 80	292.8	262.6		4.5	220.725
32H-4, 100	302.5			4.2	206.01
32H-6, 70	305.2			4.5	220.725
33H-2, 69	308.7			2.7	132.435
33H-4, 105	312.1			4.5	220.725
34H-2, 77	318.3			2.7	132.435
35H-2, 54	327.5			3.8	186.39
35H-4, 75	330.8			4.5	220.725
36H-4, 140	340.9			4.5	220.725
36H-6, 110	343.6			4.5	220.725
37H-2, 11	346.1			4.5	220.725

Preservation is excellent, providing ideal material for detailed taxonomic and ecologic studies. An added attraction of the sequence is its proximity to many of the classic localities from which many of the species of Neogene tropical foraminifers were first described. Site 925 offers the continuity and temporal control that is invariably lacking in the classic land sections.

During the last 16 m.y. of global climatic deterioration, sedimentation rates have gradually increased from a low of about 10 m/m.y. in the middle Miocene to about 33 m/m.y. during the Pleistocene (see Fig. 23). This increase is chiefly accounted for by an increasing flux of terrigenous material that presumably originates in the Amazon River; indeed, during the Pleistocene the biogenic carbonate flux has actually decreased (see Fig. 34).

A composite section has been constructed on the basis of magnetic susceptibility and color reflectance data that will enable high-resolution sampling to be conducted with maximum efficiency and minimum waste of samples. The plots in Figure 21 show spliced magnetic susceptibility and reflectance records for the upper 400 m composite depth (the section down to 360 mbsf). At this time, we still do not fully understand the processes by which the sedimentary section becomes expanded during APC and XCB coring. The composite section also enables us to generate accurate spliced records of natural

Table 13. Electrical resistivity measured at discrete intervals for all holes at Site 925.

Core, section, interval (cm)	Depth (mbsf)	Resistivity (Ωm)	Core, section, interval (cm)	Depth (mbsf)	Resistivity (Ωm)	Core, section, interval (cm)	Depth (mbsf)	Resistivity (Ωm)	Core, section, interval (cm)	Depth (mbsf)	Resistivity (Ωm)
154-925A-			14R-5, 125	416	0.23	24R-2, 140	509.2	0.22	36R-1, 126	623.4	0.31
1R-1, 30	102.1	0.84	14R-6, 32	416.6	0.23	24R-3, 88	510.2	0.17	36R-2, 53	624.1	0.24
1R-3, 20	105	0.12	15R-1, 74	420.4	0.27	24R-3, 148	510.8	0.22	36R-5, 49	628.6	0.45
2R-2, 20	199.6	0.14	15R-1, 107	420.8	0.16	24R-4, 64	511.4	0.20	36R-5, 108	629.2	0.45
2R-1, 62	198.5	0.12	15R-2, 63	421.8	0.20	24R-5, 7	512.4	0.20	36R-6, 18	629.8	0.72
2R-1, 27	198.2	0.11	15R-2, 133	422.5	0.18	24R-5, 147	513.8	0.22	36R-6, 118	630.8	0.28
6R-3, 47	336.6	0.15	15R-3, 11	422.8	0.20	24R-6, 68	514.5	0.18	36R-7, 56	631.7	0.33
6R-3, 79	336.9	0.14	15R-3, 136	424.1	0.25	24R-6, 146	515.3	0.19	38R-1, 26	641.7	0.29
6R-1, 18	333.3	0.13	15R-4, 14	424.3	0.29	25R-2, 9	515.4	0.14	38R-1, 131	642.7	0.21
6R-1, 60	333.7	0.16	15R-4, 126	425.5	0.25	25R-2, 140	516.7	0.14	38R-2, 53	643.4	0.16
5R-1, 50	323.9	0.16	15R-5, 20	425.9	0.20	25R-3, 20	515.5	0.15	38R-2, 131	644.2	0.18
5R-1, 133	324.7	0.16	15R-5, 89	426.6	0.26	25R-3, 136	516.7	0.19	38R-3, 27	644.7	0.17
5R-3, 30	326.7	0.16	15R-6, 31	427.5	0.23	25R-4, 17	515.5	0.19	38R-3, 74	645.1	0.24
5R-3, 80	327.2	0.13	15R-6, 139	428.6	0.24	26R-5, 70	531.2	0.22	38R-4, 46	646.4	0.23
4R-6, 57	321.8	0.13	15R-7, 18	428.9	0.20	26R-6, 65	532.7	0.21	38R-4, 116	647.1	0.19
4R-6, 106	322.3	0.13	16R-1, 38	429.7	0.18	26R-5, 132	531.8	0.21	38R-5, 23	647.6	0.23
4R-4, 55	318.8	0.15	16R-1, 118	430.5	0.23	26R-6, 145	533.5	0.18	38R-5, 114	648.5	0.28
4R-4, 99	319.2	0.12	16R-2, 29	431.1	0.19	26R-7, 115	534.7	0.21	38R-6, 23	649.1	0.22
4R-2, 31	315.5	0.17	16R-2, 83	431.6	0.19	27R-1, 20	535.5	0.14	38R-6, 123	650.1	0.22
4R-2, 110	316.3	0.14	16R-3, 7	432.4	0.23	27R-1, 130	536.6	0.13	38R-7, 4	650.4	0.26
7R-1, 45	343.2	0.17	16R-3, 137	433.7	0.22	27R-2, 24	537	0.13	39R-1, 89	652	0.23
7R-1, 100	343.7	0.18	16R-4, 15	434	0.20	27R-2, 112	537.9	0.15	39R-2, 50	653.1	0.20
7R-2, 43	344.6	0.17	16R-4, 140	435.2	0.22	27R-3, 19	538.5	0.14	39R-2, 86	653.5	0.17
7R-2, 102	345.2	0.17	16R-5, 20	435.5	0.18	27R-3, 78	539.1	0.14	39R-3, 17	654.3	0.19
7R-3, 43	346.1	0.16	16R-5, 65	436	0.17	27R-4, 32	540.1	0.17	39R-3, 116	655.3	0.18
7R-3, 120	346.9	0.18	16R-6, 20	437	0.16	27R-4, 99	540.8	0.24	39R-4, 86	656.5	0.19
7R-4, 38	347.6	0.16	16R-6, 149	438.3	0.17	27R-5, 29	541.6	0.18	39R-5, 58	657.7	0.27
7R-4, 124	348.4	0.14	16R-7, 65	439	0.17	27R-5, 126	542.6	0.15	39R-5, 135	658.5	0.22
7R-5, 104	349.7	0.13	17R-1, 4	438.9	0.16	27R-6, 27	543.1	0.20	39R-6, 64	659.2	0.26
7R-5, 45	349.2	0.16	17R-1, 98	439.9	0.21	27R-6, 122	544	0.20	39R-7, 36	660	0.24
7R-6, 64	350.8	0.14	17R-2, 15	440.6	0.19	29R-1, 40	555	0.21	40R-1, 140	662.2	0.28
7R-6, 122	351.4	0.14	17R-2, 85	441.3	0.18	29R-1, 90	555.5	0.23	40R-2, 96	663.3	0.25
8R-1, 11	352.5	0.16	17R-3, 65	442.6	0.17	29R-2, 4	556.1	0.17	40R-3, 57	664.4	0.28
8R-1, 124	353.6	0.17	17R-3, 129	443.2	0.16	30R-1, 34	564.5	0.28	40R-4, 59	665.9	0.23
8R-2, 6	354	0.19	17R-4, 33	443.7	0.16	30R-1, 114	565.3	0.21	42R-1, 81	680.9	0.29
8R-2, 75	354.7	0.15	17R-4, 92	444.3	0.17	30R-2, 36	566.1	0.28	42R-2, 44	682	0.40
8R-3, 5	355.5	0.17	17R-5, 7	445	0.17	30R-2, 139	567.1	0.24	44R-2, 40	691.6	0.26
8R-3, 85	356.3	0.22	17R-5, 54	445.4	0.16	30R-3, 50	567.7	0.27	44R-2, 140	692.6	0.23
8R-4, 13	357	0.18	17R-6, 33	446.7	0.16	30R-3, 120	568.4	0.31	44R-3, 46	693.2	0.27
8R-4, 90	357.8	0.17	17R-6, 83	447.2	0.19	30R-4, 80	569.5	0.20	44R-4, 84	695	0.33
8R-5, 9	358.5	0.17	17R-7, 24	447.6	0.23	30R-5, 50	570.7	0.31	45R-1, 139	700.7	0.27
8R-5, 144	359.8	0.15	17R-7, 60	448	0.15	30R-6, 45	572.2	0.20	45R-2, 16	701	0.20
8R-6, 8	360	0.23	18R-1, 72	449.3	0.16	30R-6, 114	572.8	0.21	45R-2, 117	702	0.25
8R-6, 86	360.8	0.22	18R-1, 110	449.7	0.15	31R-1, 57	574.4	0.17	45R-3, 125	703.6	0.34
8R-4, 65	357.6	0.15	18R-2, 10	450.2	0.17	31R-1, 114	574.9	0.20	45R-4, 74	704.5	0.42
8R-4, 109	358	0.16	18R-2, 148	451.6	0.15	31R-2, 60	575.9	0.30	45R-5, 30	705.6	0.30
9R-1, 30	362.3	0.19	18R-3, 37	452	0.16	32R-1, 55	584.1	0.22	45R-5, 132	706.6	0.27
9R-1, 88	362.9	0.17	19R-2, 14	458.4	0.33	32R-1, 126	584.8	0.21	45R-6, 41	707.2	0.27
9R-2, 28	363.8	0.15	19R-2, 67	458.9	0.24	32R-2, 41	585.4	0.17	45R-6, 123	708	0.43
9R-2, 133	364.8	0.16	19R-3, 66	460.4	0.23	32R-2, 128	586.3	0.26	43R-1, 2	683.1	0.24
9R-3, 16	365.2	0.19	19R-3, 138	461.2	0.22	32R-3, 36	586.9	0.17	43R-1, 120	684.3	0.45
9R-3, 133	366.3	0.16	19R-3, 97	460.7	0.30	32R-3, 134	587.8	0.19	43R-2, 67	685.3	0.23
9R-4, 56	367.1	0.20	19R-4, 75	462	0.30	32R-4, 38	588.4	0.18	43R-2, 136	686	0.18
9R-4, 128	367.8	0.15	19R-4, 142	462.7	0.20	32R-4, 125	589.3	0.16	43R-3, 26	686.4	0.32
9R-5, 47	368.5	0.16	19R-5, 12	462.9	0.19	32R-5, 41	589.9	0.23	43R-3, 75	686.9	0.29
9R-5, 138	369.4	0.16	20R-1, 10	467.9	0.17	32R-5, 134	590.8	0.25	46R-1, 98	710	0.37
9R-6, 38	369.9	0.14	20R-1, 121	469	0.13	32R-6, 24	591.2	0.29	46R-3, 17	712.2	0.44
9R-6, 124	370.7	0.13	20R-2, 38	469.7	0.18	32R-6, 82	591.8	0.21	46R-5, 114	716.1	0.42
9R-7, 55	371.6	0.17	20R-2, 130	470.6	0.17	33R-1, 30	593.4	0.23	46R-3, 78	712.8	0.29
10R-1, 12	371.8	0.17	20R-3, 39	471.2	0.14	33R-1, 104	594.1	0.15	47R-1, 12	718.4	0.41
10R-1, 137	373.1	0.24	20R-3, 122	472	0.18	33R-2, 22	594.8	0.21	47R-1, 133	719.6	0.38
10R-2, 50	373.7	0.21	20R-4, 59	472.9	0.14	33R-2, 75	595.4	0.17	47R-2, 77	720.6	0.47
10R-2, 130	374.5	0.14	20R-4, 137	473.7	0.17	33R-3, 20	596.3	0.16	47R-3, 28	721.6	0.51
11R-1, 25	381.6	0.19	20R-5, 44	474.2	0.16	33R-3, 77	596.9	0.19	47R-3, 134	722.6	0.32
11R-1, 147	382.8	0.14	20R-5, 109	474.9	0.15	33R-4, 58	598.2	0.20	47R-5, 77	725.1	0.70
11R-2, 46	383.3	0.20	20R-6, 59	475.9	0.15	33R-4, 124	598.8	0.27	48R-1, 47	728.4	0.36
11R-2, 127	384.1	0.18	20R-6, 121	476.5	0.14	33R-5, 51	599.6	0.26	48R-1, 122	729.1	0.37
11R-3, 17	384.5	0.18	20R-7, 27	477.1	0.16	33R-6, 49	601.1	0.24	48R-2, 57	730	0.21
11R-3, 83	385.1	0.15	22R-1, 38	487.5	0.27	34R-1, 81	603.6	0.23	48R-2, 88	730.3	0.25
11R-4, 23	386	0.13	22R-1, 114	488.2	0.14	34R-1, 138	604.2	0.21	48R-3, 148	732.4	0.21
11R-4, 146	387.3	0.14	22R-2, 45	489.1	0.16	34R-2, 30	604.6	0.36	48R-4, 34	732.7	0.25
11R-5, 71	388	0.18	22R-2, 105	489.7	0.13	34R-2, 102	605.3	0.18	48R-5, 90	734.8	0.22
11R-5, 134	388.6	0.16	22R-3, 38	490.5	0.12	34R-3, 38	606.2	0.17	48R-6, 141	736.8	0.26
11R-6, 39	389.2	0.17	22R-3, 116	491.3	0.13	34R-3, 83	606.6	0.16	48R-7, 61	737.5	0.21
12R-1, 35	391.2	0.19	22R-4, 30	491.9	0.15	34R-4, 78	608.1	0.16	49R-1, 146	739.1	0.33
12R-1, 125	392.1	0.20	22R-4, 95	492.6	0.13	34R-4, 138	608.7	0.21	49R-2, 55	739.7	0.42
12R-2, 36	392.7	0.24	22R-5, 44	493.5	0.15	34R-5, 45	609.3	0.21	49R-3, 72	741.3	0.45
12R-2, 124	393.5	0.25	22R-5, 110	494.2	0.12	34R-5, 143	610.2	0.19	49R-4, 52	742.6	0.32
12R-3, 30	394.1	0.16	22R-6, 54	495.1	0.14	34R-6, 44	610.7	0.18	50R-1, 33	746.4	0.31
13R-1, 42	400.8	0.19	22R-6, 111	495.7	0.17	35R-1, 20	612.6	0.23	50R-2, 47	748.1	0.34
13R-2, 7	401.5	0.17	22R-7, 43	496.5	0.14	35R-1, 110	613.5	0.20	52R-1, 68	757.7	1.98
13R-2, 74	402.1	0.18	23R-1, 11	496.8	0.19	35R-2, 30	614.2	0.18	52R-2, 60	759.1	0.89
14R-2, 35	410.6	0.24	23R-1, 122	497.9	0.16	35R-2, 119	615.1	0.18	52R-4, 56	762.1	0.54
14R-2, 136	411.6	0.27	23R-2, 95	499.2	0.18	35R-3, 47	615.9	0.25	53R-5, 123	773.6	0.68
14R-3, 38	412.1	0.23	23R-3, 79	500.5	0.18	35R-3, 125	616.7	0.22	53R-4, 75	771.6	0.35
14R-3, 124	413	0.16	23R-4, 77	502	0.14	35R-4, 21	617.1	0.22	53R-1, 35	767	1.59
14R-4, 38	413.6	0.20	24R-1, 5	506.4	0.23	35R-4, 86	617.8	0.33	54R-1, 146	777.8	0.34
14R-4, 128	414.5	0.18	24R-1, 76	507.1	0.27	35R-5, 30	618.2	0.26	54R-2, 117	779	0.60
14R-5, 32	415.1	0.20	24R-2, 62	508.4	0.22	36R-1, 30	622.4	0.25	54R-3, 30	779.6	0.51

Table 13 (continued).

Core, section, interval (cm)	Depth (mbsf)	Resistivity (Ωm)
54R-4, 65	781.5	0.69
54R-6, 48	784.3	0.31
55R-1, 30	786.3	1.60
55R-2, 27	787.8	0.66
154-925B-		
1H-1, 90	0.9	0.41
1H-3, 24	3.24	0.43
2H-1, 110	5.6	0.39
2H-3, 66	8.16	0.49
2H-2, 90	6.9	0.31
2H-4, 40	9.4	0.26
2H-5, 55	11.05	0.18
2H-7, 30	13.3	0.18
3H-1, 124	15.24	0.28
3H-2, 40	15.9	0.21
3H-2, 90	16.4	0.20
3H-2, 130	16.8	0.20
3H-3, 10	17.1	0.22
3H-3, 40	17.4	0.20
3H-3, 90	17.9	0.20
3H-3, 125	18.25	0.20
3H-3, 80	17.8	0.19
3H-5, 10	20.1	0.20
3H-5, 70	20.7	0.20
3H-5, 90	20.9	0.22
3H-5, 130	21.3	0.21
3H-6, 35	21.85	0.22
3H-6, 55	22.05	0.21
3H-6, 100	22.5	0.23
3H-6, 145	22.95	0.23
3H-7, 7	23.07	0.20
3H-4, 10	18.6	0.19
3H-4, 55	19.05	0.20
3H-4, 90	19.4	0.21
3H-4, 130	19.8	0.21
4H-2, 20	25.2	0.36
4H-2, 60	25.6	0.28
4H-2, 130	26.3	0.26
4H-3, 33	26.83	0.21
4H-3, 60	27.1	0.25
4H-3, 96	27.46	0.27
4H-3, 140	27.9	0.21
4H-4, 60	28.6	0.22
4H-4, 100	29	0.24
4H-4, 130	29.3	0.27
4H-5, 30	29.8	0.23
4H-5, 67	30.17	0.20
4H-5, 101	30.51	0.20
4H-5, 147	30.97	0.22
4H-6, 22	31.22	0.20
4H-6, 68	31.68	0.20
4H-6, 110	32.1	0.21
4H-7, 5	32.55	0.20
4H-1, 20	23.7	0.22
4H-1, 80	24.3	0.21
4H-1, 130	24.8	0.24
5H-1, 80	33.8	0.33
5H-1, 130	34.3	0.23
5H-2, 110	35.6	0.22
5H-3, 82	36.82	0.22
5H-4, 33	37.83	0.22
5H-5, 60	39.6	0.19
5H-6, 34	40.84	0.20
5H-7, 15	41.65	0.27
6H-2, 955	53.55	0.23
6H-2, 20	44.2	0.30
6H-3, 80	46.3	0.22
6H-4, 32	47.32	0.22
6H-4, 84	47.84	0.24
6H-5, 30	48.8	0.21
6H-6, 107	51.07	0.23
6H-7, 30	51.8	0.20
7H-1, 70	52.7	0.19
7H-1, 110	53.1	0.24
7H-2, 70	54.2	0.22
7H-2, 110	54.6	0.21
7H-3, 25	55.25	0.23
7H-3, 130	56.3	0.25
7H-4, 95	57.45	0.23
7H-5, 81	58.81	0.22
7H-5, 120	59.2	0.24
7H-6, 30	59.8	0.19
7H-7, 16	61.16	0.18
8H-1, 83	62.33	0.26
8H-2, 94	63.94	0.28
8H-2, 136	64.36	0.25
8H-3, 40	64.9	0.26
8H-3, 82	65.32	0.23
8H-4, 40	66.4	0.25
8H-4, 145	67.45	0.22
8H-5, 45	67.95	0.21
9H-1, 47	71.47	0.24
9H-2, 64	73.14	0.23
9H-3, 82	74.82	0.21
9H-4, 40	75.9	0.21
9H-3, 24	74.24	0.24
9H-7, 29	80.29	0.22
10H-1, 80	81.3	0.25
10H-2, 80	82.8	0.21
10H-4, 50	85.5	0.21
10H-5, 70	87.2	0.19
10H-6, 107	89.07	0.20
10H-5, 10	86.6	0.29
10H-7, 10	89.6	0.21
11H-2, 50	92	0.27
11H-3, 50	93.5	0.23
11H-4, 50	95	0.24
11H-6, 50	98	0.21
11H-5, 50	96.5	0.20
11H-1, 5	90.05	0.23
11H-3, 111	94.11	0.24
12H-1, 67	100.2	0.23
12H-3, 26	102.8	0.29
12H-5, 28	105.8	0.23
12H-7, 39	108.9	0.20
12H-5, 32	105.8	0.30
12H-7, 32	108.8	0.23
13H-1, 80	109.8	0.29
13H-3, 72	112.7	0.28
13H-5, 57	115.6	0.30
13H-7, 38	118.4	0.28
14H-1, 38	118.9	0.21
14H-3, 128	122.8	0.29
14H-5, 95	125.5	0.27
14H-7, 26	127.8	0.24
15H-1, 128	129.3	0.21
15H-1, 118	129.2	0.26
15H-2, 70	130.2	0.29
15H-3, 90	131.9	0.33
15H-4, 80	133.3	0.25
15H-5, 67	134.7	0.27
15H-6, 69	136.2	0.28
16H-1, 85	138.4	0.32
16H-2, 70	139.7	0.26
16H-3, 126	141.8	0.27
16H-4, 98	143	0.28
16H-5, 71	144.2	0.29
16H-6, 74	145.7	0.33
17H-1, 107	148.1	0.23
17H-2, 100	149.5	0.27
17H-3, 66	150.7	0.22
17H-4, 68	152.2	0.23
17H-5, 62	153.6	0.23
17H-6, 104	155.5	0.22
17H-7, 42	156.4	0.18
18H-1, 85	157.4	0.17
18H-2, 117	159.2	0.21
18H-3, 93	160.4	0.16
18H-4, 96	162	0.16
18H-4, 96	162	0.20
18H-5, 127	163.8	0.18
18H-6, 148	165.5	0.16
18H-2, 73	158.7	0.15
19H-1, 130	167.3	0.16
19H-3, 145	170.5	0.14
19H-4, 105	171.6	0.17
19H-5, 127	173.3	0.16
19H-6, 100	174.5	0.16
20H-1, 122	176.7	0.15
20H-2, 100	178	0.17
20H-3, 100	179.5	0.14
20H-4, 100	181	0.17
20H-5, 50	182	0.16
20H-6, 90	183.9	0.15
21H-2, 90	187.4	0.17
21H-1, 146	186.5	0.16
21H-3, 147	189.5	0.15
21H-4, 100	190.5	0.14
21H-5, 140	192.4	0.17
21H-5, 92	191.9	0.17
21H-6, 86	193.4	0.17
22H-1, 103	195.5	0.16
22H-2, 100	197	0.15
22H-3, 45	198	0.16
22H-4, 45	199.5	0.15
22H-5, 120	201.7	0.16
22H-6, 120	203.2	0.18
23H-3, 37	207.4	0.27
24H-1, 50	214	0.29
24H-5, 128	220.8	0.41
24H-3, 101	217.5	0.35
24H-7, 33	222.8	0.37
25H-3, 95	227	0.42
25H-1, 98	224	0.17
25H-5, 102	230	0.17
25H-7, 38	232.4	0.18
26H-1, 61	233.1	0.21
26H-3, 112	236.6	0.34
26H-7, 38	241.9	0.26
26H-4, 20	237.2	0.29
27H-1, 47	242.5	0.15
27H-3, 134	246.3	0.41
27H-5, 63	248.6	0.36
27H-7, 30	251.3	0.25
28H-5, 42	257.9	0.18
28H-6, 30	259.3	0.20
28H-6, 52	259.5	0.16
28H-6, 82	259.8	0.17
29H-3, 110	265.1	0.35
29H-3, 133	265.3	0.36
29H-6, 131	269.8	0.34
29H-6, 56	269.1	0.18
29H-7, 38	270.4	0.16
30H-1, 62	271.1	0.31
30H-2, 92	272.9	0.27
30H-3, 85	274.4	0.26
30H-4, 116	276.2	0.25
30H-5, 120	277.7	0.19
30H-6, 100	279	0.21
31H-2, 100	282.5	0.21
31H-4, 100	285.5	0.29
31H-5, 100	287	0.19
31H-6, 60	288.1	0.26
31H-7, 60	289.6	0.20
31H-1, 128	281.3	0.28
31H-3, 61	283.6	0.26
32H-2, 3	291	0.24
32H-2, 78	291.8	0.22
32H-3, 96	293.5	0.20
32H-4, 30	294.3	0.25
32H-4, 106	295.1	0.23
32H-5, 80	296.3	0.21
32H-6, 15	297.2	0.20
32H-6, 118	298.2	0.26
32H-7, 30	297.3	0.20
32H-1, 15	289.7	0.19
33H-2, 38	300.9	0.23
33H-2, 105	301.6	0.30
33H-3, 40	302.4	0.22
33H-3, 118	303.2	0.23
33H-4, 100	304.5	0.25
33H-4, 30	303.8	0.27
33H-5, 36	305.4	0.21
33H-5, 87	305.9	0.32
33H-6, 135	307.9	0.26
33H-6, 40	306.9	0.24
34H-1, 121	309.7	0.19
34H-2, 99	311	0.24
34H-3, 75	312.3	0.22
34H-5, 133	315.8	0.26
34H-6, 114	317.1	0.22
154-925C-		
1H-1, 75	0.75	0.14
1H-2, 75	2.25	0.14
1H-3, 75	3.75	0.14
1H-5, 75	6.75	0.16
2H-2, 82	10.32	0.16
2H-4, 10	12.6	0.15
2H-6, 30	15.8	0.16
3H-2, 43	19.43	0.18
3H-2, 126	20.26	0.18
3H-3, 30	20.8	0.18
3H-4, 25	22.25	0.17
3H-5, 53	24.03	0.17
3H-6, 107	26.07	0.16
4H-4, 55	32.05	0.19
4H-4, 80	32.3	0.19
4H-2, 49	28.99	0.22
4H-6, 99	35.49	0.23
4H-3, 15	30.15	0.26
4H-3, 50	30.5	0.20
4H-3, 142	31.42	0.24
4H-4, 59	32.09	0.19
4H-2, 27	28.77	0.19
4H-2, 143	29.93	0.19
4H-5, 75	33.75	0.18
6H-4, 12	50.62	0.24
6H-2, 37	47.87	0.25
6H-2, 78	48.28	0.20
6H-4, 109	51.59	0.23
6H-4, 48	50.98	0.23
7H-2, 97	57.97	0.20
7H-4, 54	60.54	0.19
7H-5, 92	62.42	0.21
7H-6, 60	63.6	0.20
8H-2, 115	67.65	0.26
8H-4, 12	69.62	0.23
8H-6, 113	73.63	0.23
9H-2, 50	76.5	0.27
9H-4, 79	79.79	0.24
9H-6, 77	82.77	0.25
10H-2, 116	86.66	0.23
10H-6, 47	91.97	0.17
10H-4, 120	89.7	0.19
11H-2, 132	96.32	0.21
11H-4, 85	98.85	0.19
11H-6, 32	101.3	0.22
12H-1, 75	103.8	0.22
12H-3, 75	106.8	0.21
12H-2, 67	105.2	0.18
12H-5, 75	109.8	0.21
12H-4, 90	108.4	0.20
13H-1, 75	113.3	0.21
13H-3, 75	116.3	0.22
13H-4, 75	117.8	0.21
13H-5, 75	119.3	0.19
13H-6, 75	120.8	0.21
14H-1, 75	122.8	0.17
14H-2, 75	124.3	0.17
14H-3, 75	125.8	0.22
14H-4, 75	127.3	0.21
14H-5, 75	128.8	0.21
14H-6, 75	130.3	0.23
15H-1, 100	132.5	0.19
15H-2, 100	134	0.21
15H-3, 104	135.5	0.18
15H-5, 102	138.5	0.18
15H-6, 100	140	0.18
16H-1, 90	141.9	0.20
16H-2, 90	143.4	0.16
16H-3, 100	145	0.19
16H-4, 100	146.5	0.19
16H-5, 100	148	0.18
16H-6, 100	149.5	0.17
17H-1, 100	151.5	0.23
17H-2, 100	153	0.23
17H-3, 100	.5	0.19
17H-4, 100	156	0.22
17H-5, 100	157.5	0.22
17H-6, 100	159	0.20
18H-1, 75	160.8	0.19
18H-2, 75	162.3	0.18
18H-3, 75	163.8	0.19
18H-4, 80	165.3	0.18
18H-5, 75	166.8	0.18
18H-6, 75	168.3	0.21
19H-1, 75	170.3	0.18
19H-2, 75	171.8	0.21
19H-3, 75	173.3	0.21
19H-4, 75	174.8	0.23
19H-5, 75	176.3	0.21
19H-6, 75	177.8	0.20
20H-1, 90	179.9	0.19
20H-2, 90	181.4	0.19
20H-3, 90	182.9	0.23
20H-3, 90	182.9	0.38
20H-4, 90	184.4	0.38
20H-5, 90	185.9	0.34
20H-6, 90	187.4	0.34
21H-1, 90	189.4	0.31
21H-2, 90	190.9	0.35
21H-3, 90	192.4	0.32
21H-4, 90	193.9	0.34
21H-5, 90	195.4	0.32
21H-6, 84	196.8	0.34
22H-1, 100	199	0.32
22H-2, 100	200.5	0.32
22H-3, 100	202	0.35
22H-4, 100	203.5	0.33
22H-5, 100	205	0.31
22H-6, 100	206.5	0.34
23H-1, 64	208.1	0.35
23H-2, 64	209.6	0.32
23H-3, 64	211.1	0.29
23H-4, 64	212.6	0.29
23H-5, 64	214.1	0.31
23H-6, 64	215.6	0.29
24H-1, 24	217.2	0.30
24H-2, 13	218.6	0.30
24H-4, 24	221.7	0.31
24H-6, 111	225.6	0.27
25H-2, 55	228.6	0.29

Table 13 (continued).

Core, section, interval (cm)	Depth (mbsf)	Resistivity (Ωm)
25H-4, 36	231.4	0.29
25H-5, 79	233.3	0.27
25H-1, 43	226.9	0.25
26H-2, 66	238.2	0.33
26H-4, 11	240.6	0.27
26H-6, 95	244.5	0.24
26H-3, 72	239.7	0.28
26H-1, 9	236.1	0.31
25H-3, 5	229.6	0.29
25H-3, 22	229.7	0.28
25H-3, 32	229.8	0.28
25H-3, 44	229.9	0.29
25H-3, 66	230.2	0.26
25H-3, 77	230.3	0.29
25H-3, 120	230.7	0.28
25H-3, 137	230.9	0.28
25H-4, 6	231.1	0.27
25H-4, 18	231.2	0.28
25H-4, 40	231.4	0.28
25H-4, 62	231.6	0.27
25H-4, 79	231.8	0.26
25H-4, 92	231.9	0.27
25H-4, 106	232.1	0.28
25H-4, 121	232.2	0.28
25H-4, 142	232.4	0.26
27H-2, 57	247.6	0.29
27H-6, 26	253.3	0.31
27H-6, 116	254.2	0.28
28H-2, 66	257.2	0.32
28H-4, 97	260.5	0.30
28H-6, 130	263.8	0.29
29H-1, 11	264.6	0.30
29H-2, 73	266.7	0.35
29H-4, 130	270.3	0.30
29H-6, 100	273	0.49
29H-7, 34	273.8	0.65
29H-3, 77	268.3	0.29
29H-5, 42	270.9	0.33
30H-2, 117	276.7	0.32
30H-4, 97	279.5	0.45
30H-6, 115	282.7	0.51
30H-7, 49	283.5	0.68
31H-2, 77	285.8	0.50
31H-4, 87	288.9	0.50
31H-6, 55	291.6	0.41
31H-7, 11	292.6	0.52
32H-1, 80	293.8	0.29
32H-2, 77	295.3	0.36
32H-4, 83	298.3	0.40
32H-6, 72	301.2	0.36
33H-2, 71	304.7	0.39
33H-4, 97	308	0.35
33H-1, 87	303.4	0.35
33H-3, 86	306.4	0.55
33H-6, 95	311	0.52
33H-5, 95	309.5	0.28
34H-1, 60	312.6	0.22
34H-2, 60	314.1	0.43
34H-3, 90	315.9	0.22
34H-4, 96	317.5	0.40
34H-5, 96	319	0.32
34H-6, 96	320.5	0.30
35X-1, 117	322.7	0.39
35X-2, 110	324.1	0.53
35X-3, 110	325.6	0.40
35X-4, 110	327.1	0.44
35X-5, 100	328.5	0.44
35X-6, 8	329.1	0.49
36X-1, 110	332.3	0.55
36X-2, 93	333.6	0.49
36X-3, 93	335.1	0.41
36X-4, 126	337	0.45
36X-5, 114	338.3	0.46
36X-6, 59	339.3	0.49
37X-1, 90	341.7	0.36
37X-2, 90	343.2	0.43
37X-3, 102	344.8	0.54
37X-4, 102	346.3	0.55
37X-5, 102	347.8	0.53
37X-6, 100	349.3	0.56
38X-1, 90	351.3	0.63
38X-2, 90	352.8	0.66
38X-3, 93	354.3	0.55
38X-4, 90	355.8	0.67
38X-5, 90	357.3	0.43
38X-6, 90	358.8	0.52
154-925D-		
1H-4, 80	7.8	0.27
1H-5, 80	9.3	0.19
1H-6, 80	10.8	0.21
2H-1, 80	12.8	0.23
2H-2, 80	14.22	0.17
2H-3, 80	15.72	0.16
2H-4, 80	17.22	0.17
2H-5, 80	18.92	0.21
3H-1, 100	22.5	0.20
3H-2, 100	24	0.20
3H-3, 100	25.5	0.18
3H-4, 100	27	0.17
3H-5, 100	28.5	0.18
3H-6, 100	30.25	0.19
4H-1, 125	32.25	0.25
4H-2, 125	33.75	0.19
4H-3, 125	35.25	0.19
4H-4, 125	36.75	0.18
4H-5, 125	38.25	0.18
4H-6, 125	39.8	0.17
5H-1, 130	41.8	0.32
5H-2, 130	43.3	0.18
5H-3, 130	44.8	0.18
5H-4, 130	46.3	0.18
5H-5, 130	47.8	0.18
5H-6, 130	48.68	0.19
6H-1, 68	50.63	0.25
6H-2, 63	52.18	0.18
6H-3, 68	53.68	0.19
6H-4, 68	55.18	0.17
6H-5, 68	56.68	0.19
6H-6, 68	57.7	0.19
7H-1, 20	59.7	0.33
7H-2, 20	61.2	0.24
7H-3, 20	62.7	0.30
7H-4, 20	64.2	0.21
7H-5, 20	65.7	0.23
7H-6, 20	67.9	0.18
8H-1, 90	69.83	0.27
8H-2, 83	71.4	0.23
8H-3, 90	72.9	0.23
8H-4, 90	74.4	0.20
8H-5, 90	75.9	0.18
8H-6, 90	76.7	0.19
9H-1, 20	78.7	0.37
9H-2, 20	80.2	0.17
9H-3, 20	81.7	0.20
9H-4, 20	83.2	0.18
9H-5, 20	84.7	0.18
9H-6, 20	86.2	0.22
9H-7, 20	87.8	0.21
10H-3, 30	91.3	0.18
10H-4, 30	92.8	0.22
10H-5, 30	94.3	0.22
10H-6, 30	95.8	0.20
10H-7, 30	98.2	0.22
11H-1, 120	98.7	0.25
11H-2, 120	100.2	0.22
11H-3, 120	101.7	0.25
11H-4, 120	103.2	0.21
11H-5, 120	104.7	0.18
11H-6, 120	106.2	0.27
12H-1, 120	108.2	0.24
12H-2, 120	109.7	0.19
12H-3, 120	111.2	0.19
12H-4, 120	112.7	0.18
12H-5, 120	114.2	0.18
12H-6, 123	115.2	0.17
13H-1, 70	117.2	0.22
13H-2, 70	118.7	0.18
13H-3, 70	120.2	0.19
13H-4, 70	121.7	0.20
13H-5, 70	123.2	0.20
13H-6, 70	125.1	0.18
14H-1, 110	127.1	0.20
14H-2, 110	128.6	0.20
14H-3, 110	130.1	0.20
14H-4, 110	131.6	0.20
14H-5, 110	133.1	0.21
14H-6, 110	134.3	0.18
15H-1, 80	136.3	0.19
15H-2, 80	137.8	0.18
15H-3, 80	139.3	0.20
15H-4, 80	140.8	0.21
15H-5, 80	142.3	0.17
15H-6, 75	144.2	0.23
16H-1, 120	146.2	0.20
16H-2, 120	147.7	0.19
16H-3, 120	149.2	0.24
16H-4, 120	150.7	0.22
16H-5, 120	152.2	0.19
16H-6, 120	153.5	0.20
17H-1, 100	155.5	0.20
17H-2, 100	157	0.20
17H-4, 100	160	0.20
17H-5, 100	161.5	0.22
17H-6, 100	163.2	0.22
18H-1, 120	165.2	0.32
18H-2, 120	166.7	0.33
18H-3, 120	168.2	0.35
18H-4, 120	169.7	0.34
18H-5, 120	171.2	0.36
18H-6, 120	172.3	0.35
19H-5, 80	180.3	0.36
19H-6, 80	182.3	0.34
20H-1, 125	184.3	0.32
20H-2, 125	185.8	0.30
20H-3, 125	187.3	0.29
20H-4, 125	188.8	0.29
20H-5, 125	189.8	0.30
21H-1, 80	193.3	0.33
21H-2, 80	194.8	0.28
21H-3, 80	196.3	0.29
21H-4, 80	197.8	0.30
21H-5, 80	199.3	0.33
21H-6, 80	200.3	0.32
22H-1, 30	202.3	0.31
22H-2, 30	203.6	0.32
22H-4, 30	206.6	0.35
22H-5, 30	208.1	0.36
22H-6, 30	210	0.31
23H-1, 70	212.2	0.29
23H-2, 70	213.7	0.29
23H-3, 70	215.2	0.30
23H-4, 70	216.7	0.30
23H-5, 70	218.2	0.28
23H-6, 70	220.3	0.29
24H-1, 125	222.4	0.27
24H-2, 125	223.8	0.27
24H-3, 125	225.3	0.26
24H-4, 125	226.8	0.31
24H-5, 125	228.3	0.31
24H-6, 125	229.5	0.29
25H-1, 100	231.5	0.28
25H-2, 100	233	0.31
25H-3, 100	234.5	0.27
25H-4, 100	236	0.29
25H-5, 100	237.5	0.29
25H-6, 100	238.2	0.26
26H-1, 20	240.2	0.32
26H-2, 20	241.7	0.27
26H-3, 20	243.2	0.32
26H-4, 20	244.7	0.30
26H-5, 20	246.2	0.29
26H-6, 20	248.3	0.31
27H-1, 80	250.3	0.38
27H-2, 80	251.1	0.35
27H-3, 10	253.3	0.37
27H-3, 80	253.3	0.36
27H-4, 80	254.8	0.38
27H-5, 80	256.3	0.38
27H-6, 80	258.4	0.34
28H-1, 140	260.4	0.35
28H-2, 140	261.9	0.31
28H-3, 140	263.4	0.37
28H-4, 140	264.9	0.30
28H-5, 140	266.4	0.32
28H-6, 140	267.6	0.29
29H-1, 105	269.6	0.31
29H-2, 105	271.1	0.34
29H-3, 105	272.6	0.30
29H-4, 105	274.1	0.32
29H-5, 105	275.6	0.34
29H-6, 105	277	0.35
30H-1, 100	279	0.36
30H-2, 100	280.5	0.37
30H-3, 100	282	0.37
30H-4, 100	283.5	0.48
30H-5, 100	285	0.40
30H-6, 100	286.5	0.35
31H-1, 100	288.5	0.39
31H-2, 100	290	0.52
31H-3, 100	291.5	0.44
31H-4, 100	293	0.39
31H-5, 100	294.5	0.39
31H-6, 100	295.9	0.42
32H-2, 90	299.4	0.37
32H-3, 90	300.9	0.44
32H-4, 90	302.4	0.38
32H-5, 90	303.9	0.43
32H-6, 90	305.1	0.39
33H-1, 60	307.1	0.34
33H-2, 60	308.3	0.36
33H-3, 25	309.9	0.37
33H-3, 42	310.1	0.38
33H-3, 60	310.4	0.34
33H-3, 90	309.8	0.40
33H-4, 30	311.6	0.38
33H-5, 60	313.1	0.44
33H-6, 60	314.6	0.37
34H-1, 60	316.6	0.32
34H-2, 60	318.1	0.30
34H-3, 60	319.6	0.25
34H-4, 60	321.1	0.31
34H-5, 60	322.6	0.31
35H-1, 63	326.1	0.30
35H-2, 63	327.6	0.30
35H-3, 63	329.1	0.31
35H-4, 63	330.6	0.24
35H-5, 63	332.1	0.44
35H-6, 63	333.7	0.30
36H-1, 70	335.7	0.27
36H-5, 70	341	0.32
154-925E-		
1H-1, 20	0.2	0.27
1H-2, 20	1.7	0.23
1H-3, 20	3.2	0.22
1H-1, 60	0.6	0.21
1H-4, 60	5.1	0.18
2H-1, 100	8	0.19
2H-2, 100	9.5	0.20
2H-3, 100	11	0.20
2H-4, 100	12.5	0.23
2H-5, 100	14	0.21
3H-6, 60	24.6	0.18
3H-5, 60	23.1	0.20
3H-4, 60	21.6	0.16
3H-3, 60	20.1	0.18
3H-2, 60	18.6	0.17
3H-1, 60	17.1	0.16
5H-1, 110	36.6	0.15
5H-2, 110	38.1	0.17
5H-3, 110	39.6	0.16
5H-4, 110	41.1	0.17
5H-5, 110	42.6	0.16
5H-6, 110	44.1	0.16
6H-1, 95	45.95	0.19
6H-2, 95	47.45	0.17
6H-3, 95	48.95	0.18
6H-4, 95	50.45	0.16

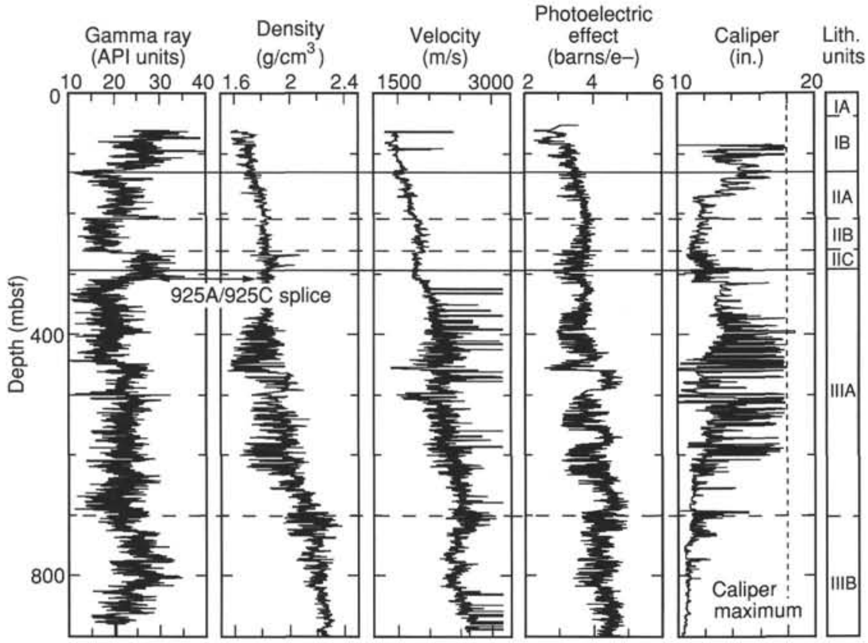

Figure 47. Composite logs from Site 925. Log data from Holes 925A and 925C were spliced at 311.26 mbsf. Note the dramatic increase in borehole diameter variability (washouts) below ~360 mbsf. Lithologic units are shown at right (from "Lithostratigraphy" section, this chapter).

gamma-ray emission, GRAPE density, and P-wave velocity. These records will be valuable as means for correlating core and downhole logging data, and as proxies of sediment lithology. The natural gamma data and the reflectance (which is collected in 31 discrete wavelength bands) contain much more geological information than can be exploited aboard ship.

Even without any sophisticated age model development, the relationship between the visually striking sedimentary cycles and orbital cycles can be demonstrated by spectral analysis (see Fig. 10). Despite the lack of a paleomagnetic record at Site 925, we anticipate that the temporal refinement that will be provided by calibrating the lithologic cycles to orbital cycles will provide unique data on biogenic and lithogenic sedimentary fluxes and the erosional history caused by changes in deep-water circulation and chemistry at the Ceara Rise over the past 40 m.y.

REFERENCES*

Allen, D., Barber, T., Flaum, C., Hemingway, J., Anderson, B., Des Ligneris, S., Everett, B., and Morriss, C., 1988. Advances in high-resolution logging. *Tech. Rev.,* 36:4–15.

Backman, J., and Hermelin, J.O.R., 1986. Morphometry of the Eocene nannofossil *Reticulofenestra umbilicus* lineage and its biochronological consequences. *Palaeogeogr., Palaeclimatol., Palaeoecol.,* 57:103–116.

Bassinot, F.C., Marsters, J.C., Mayer, L.A., and Wilkens, R.H., 1993. Variations of porosity in calcareous sediments from the Ontong Java Plateau. *In* Berger, W.H., Kroenke, L.W., Mayer, L.A., et al., *Proc. ODP, Sci. Results,* 130: College Station, TX (Ocean Drilling Program), 653–661.

Berggren, W.A., Kent, D.V., and Van Couvering, J.A., 1985. The Neogene: Part 2. Neogene geochronology and chronostratigraphy. *In* Snelling, N.J. (Ed.), *The Chronology of the Geological Record.* Geol. Soc. London Mem., 10:211–260.

Berggren, W.A., and Miller, K.G., 1988. Paleogene tropical planktonic foraminiferal biostratigraphy and magnetobiochronology. *Micropaleontology,* 34:362–380.

Bolli, H.M., and Saunders, J.B., 1985. Oligocene to Holocene low latitude planktonic foraminifera. *In* Bolli, H.M., Saunders, J.B., and Perch-Nielsen, K. (Eds.), *Plankton Stratigraphy*: Cambridge (Cambridge Univ. Press), 155–262.

*Abbreviations for names of organizations and publications in ODP reference lists follow the style given in *Chemical Abstracts Service Source Index* (published by American Chemical Society).

Bukry, D., 1973. Low-latitude coccolith biostratigraphic zonation. *In* Edgar, N.T., Saunders, J.B., et al., *Init. Repts. DSDP,* 15: Washington (U.S. Govt. Printing Office), 685–703.

————, 1978. Biostratigraphy of Cenozoic marine sediment by calcareous nannofossils. *Micropaleontology,* 24:44–60.

Chaisson, W.P., in press. Population counts of planktonic foraminifers in the equatorial Pacific: a comparison of Leg 130 and Leg 138. *In* Pisias, N.G., Mayer, L.A., Janecek, T.R., Palmer-Julson, A., and van Andel, T.H. (Eds.), *Proc. ODP, Sci. Results,* 138: College Station, TX (Ocean Drilling Program).

Chaisson, W.P., and Leckie, R.M., 1993. High-resolution Neogene planktonic foraminifer biostratigraphy of Site 806, Ontong Java Plateau (western equatorial Pacific). *In* Berger, W.H., Kroenke, L.W., Mayer, L.A., et al., *Proc. ODP, Sci. Results,* 130: College Station, TX (Ocean Drilling Program), 137–178.

Couture, R., Miller, R.S., and Gieskes, J.M., 1977. Interstitial water and mineralogical studies, Leg 41. *In* Lancelot, Y., Seibold, E., et al., *Init. Repts. DSDP,* 41: Washington (U.S. Govt. Printing Office), 907–914.

deMenocal, P.B., Bristow, J.F., and Stein, R., 1992. Paleoclimatic applications of downhole logs: Pliocene-Pleistocene results from Hole 798B, Sea of Japan. *In* Pisciotto, K.A., Ingle, J.C., Jr., von Breymann, M.T., Barron, J., et al., *Proc. ODP, Sci. Results,* 127/128 (Pt. 1): College Station, TX (Ocean Drilling Program), 393–406.

Gieskes, J.M., 1981. Deep-sea drilling interstitial water studies: implications for chemical alteration of the oceanic crust, layers I and II. *In* Warme, J.E., Douglas, R.G., and Winterer, E.L. (Eds.), *The Deep Sea Drilling Project: A Decade of Progress.* Spec. Publ.—Soc. Econ. Paleontol. Mineral., 32:149–167.

Gieskes, J.M., Elderfield, H., Lawrence, J.R., Johnson, J., Meyers, B., and Campbell, A., 1982. Geochemistry of interstitial waters and sediments, Leg 64, Gulf of California. *In* Curray, J.R., Moore, D.G., et al., *Init. Repts. DSDP,* 64 (Pt. 2): Washington (U.S. Govt. Printing Office), 675–694.

Gradstein, F.M., and Berggren, W.A., 1981. Flysch-type agglutinated foraminifera and the Maestrichtian to Paleogene history of the Labrador and North seas. *Mar. Micropaleontol.,* 6:211–268.

Harris, S., Hagelberg, T., Mix, A., Pisias, N., and Shackleton, N.J., in press. Sediment depths determined by comparisons of GRAPE and logging density data during Leg 138. *In* Pisias, N.G., Mayer, L.A., Janecek, T.R., Palmer-Julson, A., and van Andel, T.H. (Eds.), *Proc. ODP, Sci. Results,* 138: College Station, TX (Ocean Drilling Program).

Herbert, T.D., and Mayer, L.A., 1991. Long climatic time series from sediment physical property measurements. *J. Sediment. Petrol.,* 61:1089–1108.

Keigwin, L.D., Jr., 1982. Neogene planktonic foraminifers from Deep Sea Drilling Project Sites 502 and 503. *In* Prell, W.L., Gardner, J.V., et al., *Init. Repts. DSDP,* 68: Washington (U.S. Govt. Printing Office), 269–288.

Kroenke, L.W., Berger, W.H., Janecek, T.R., et al., 1991. *Proc. ODP, Init. Repts.,* 130: College Station, TX (Ocean Drilling Program).

Ladd, C.C., Foott, R., Ishihara, K., Schlosser, F., and Poulos, H.G., 1977. Stress-deformation and strength characteristics: state-of-the-art report. *Proc. 9th Int. Conf. Soil Mechanics Foundation Engineering,* Tokyo, 2:421–482.

Lee, H.J., 1982. Bulk density and shear strength of several deep-sea calcareous sediments. *In* Demars, K.R., and Chaney, R.C. (Eds.), *Geotechnical Properties, Behavior, and Performance of Calcareous Soils.* ASTM Spec. Tech. Publ., 777:54–78.

MacKillop, A.K., Moran, K., Jarrett, K., Farrell, J., and Murray, D., in press. Consolidation properties of equatorial Pacific sediment and their relationship to stress history and offsets in the Leg 138 composite depth sections. *In* Pisias, N.G., Mayer, L.A., Janecek, T.R., Palmer-Julson, A., and van Andel, T.H. (Eds.), *Proc. ODP, Sci. Results,* 138: College Station, TX (Ocean Drilling Program).

Martin, J.B., Kastner, M., and Elderfield, H., 1991. Lithium: sources in pore fluids of Peru slope sediments and implications for oceanic fluxes. *In* Meyer, A.W., Davies, T.A., and Wise, S.W. (Eds.), *Evolution of Mesozoic and Cenozoic Continental Margins.* Mar. Geol., 102:281–292.

Martini, E., 1971. Standard Tertiary and Quaternary calcareous nannoplankton Zonation. *In* Farinacci, A. (Ed.), *Proc. 2nd Int. Conf. Planktonic Microfossils, Roma:* Rome (Ed. Tecnosci.), 2:739–785.

Mayer, L., Pisias, N., Janecek, T., et al., 1992. *Proc. ODP, Init. Repts.,* 138 (Pts. 1 and 2): College Station, TX (Ocean Drilling Program).

Mayer, L.A., 1979. Deep-sea carbonates: acoustic, physical, and stratigraphic properties. *J. Sediment. Petrol.,* 49:819–836.

Mitchell, J.K., 1976. *Fundamentals of Soil Behavior:* New York (Wiley).

Okada, H., 1990. Quaternary and Paleogene calcareous nannofossils, Leg 115. *In* Duncan, R.A., Backman, J., Peterson, L.C., et al., *Proc. ODP, Sci. Results,* 115: College Station, TX (Ocean Drilling Program), 129–174.

Olafsson, G., 1991. Quantitative calcareous nannofossil biostratigraphy and biochronology of early Miocene through late Miocene sediment from DSDP Hole 608. *Medd. Stockholm Univ. Geol. Geochem.,* 283:1–28.

Olafsson, G., and Villa, G., 1992. Reliability of sphenoliths as zonal markers in Oligocene sediments from the Atlantic and Indian oceans. *In* Proto Decima, F., Monechi, S., and Rio, D. (Eds.), *Proc. Int. Nannoplankton Assoc. Conf., Firenze 1989.* Mem. Sci. Geol., 43:261–275.

Pearson, P.N., in press. Planktonic foraminifer biostratigraphy and the development of pelagic caps on guyots in the Marshall Islands Group. *In* Haggerty, J., Premoli Silva, I., Rack, F., and McNutt, M.K. (Eds.), *Proc. ODP, Sci. Results,* 144: College Station, TX (Ocean Drilling Program).

Perch-Nielsen, K., 1977. Albian to Pleistocene calcareous nannofossils from the western South Atlantic, DSDP Leg 39. *In* Supko, P.R., Perch-Nielsen, K., et al., *Init. Repts. DSDP,* 39: Washington (U.S. Govt. Printing Office), 699–823.

Raffi, I., Backman, J., Rio, D., and Shackleton, N.J., 1993. Plio-Pleistocene nannofossil biostratigraphy and calibration to oxygen isotopes stratigraphies from Deep Sea Drilling Project Site 607 and Ocean Drilling Program Site 677. *Paleoceanography,* 8:387–408.

Raffi, I., and Flores, J.A., in press. Pleistocene through Miocene calcareous nannofossils from eastern equatorial Pacific Ocean (Leg 138). *In* Pisias, N.G., Mayer, L.A., Janecek, T.R., Palmer-Julson, A., and van Andel, T.H. (Eds.), *Proc. ODP, Sci. Results,* 138: College Station, TX (Ocean Drilling Program).

Raffi, I., Rio, D., d'Atri, A., Fornaciari, E., and Rocchetti, S., in press. Quantitative distribution patterns and biomagnetostratigraphy of middle and late Miocene calcareous nannofossils from equatorial Indian and Pacific oceans (Legs 115, 130, and 138). *In* Pisias, N.G., Mayer, L.A., Janecek, T.R., Palmer-Julson, A., and van Andel, T.H. (Eds.), *Proc. ODP, Sci. Results,* 138: College Station, TX (Ocean Drilling Program).

Rea, D.K., Basov, I.A., Janecek, T.R., Palmer-Julson, A., et al., 1993. *Proc. ODP, Init. Repts.,* 145: College Station, TX (Ocean Drilling Program).

Rio, D., Fornaciari, E., and Raffi, I., 1990. Late Oligocene through early Pleistocene calcareous nannofossils from western equatorial Indian Ocean (Leg 115). *In* Duncan, R.A., Backman, J., Peterson, L.C., et al., *Proc. ODP, Sci. Results,* 115: College Station, TX (Ocean Drilling Program), 175–235.

Saito, T., 1976. Geologic significance of coiling direction in the planktonic foraminifera *Pulleniatina. Geology,* 4:305–309.

Schneider, D.A., in press. Paleomagnetism of some Leg 138 sediments: detailing Miocene magnetostratigraphy. *In* Pisias, N.G., Mayer, L.A., Janecek, T.R., Palmer-Julson, A., and van Andel, T.H. (Eds.), *Proc. ODP, Sci. Results,* 138: College Station, TX (Ocean Drilling Program).

Shackleton, N.J., Crowhurst, S., Hagelberg, T., Pisias, N.G., and Schneider, D., in press. A new late Neogene time scale: application to Leg 139 sites. *In* Pisias, N.G., Mayer, L.A., Janecek, T.R., Palmer-Julson, A., and van Andel, T.H. (Eds.), *Proc. ODP, Sci. Results,* 138: College Station, TX (Ocean Drilling Program).

Shipboard Scientific Party, 1989. Site 758. *In* Peirce, J., Weissel, J., et al., *Proc. ODP, Init. Repts.,* 121: College Station, TX (Ocean Drilling Program), 359–453.

Swart, P.K., and Burns, S.J., 1990. Pore-water chemistry and carbonate diagenesis in sediments from Leg 115: Indian Ocean. *In* Duncan, R.A., Backman, J., Peterson, L.C., et al., *Proc. ODP, Sci. Results,* 115: College Station, TX (Ocean Drilling Program), 629–645.

Tjalsma, R.C., and Lohmann, G.P., 1983. Paleocene-Eocene bathyal and abyssal benthic foraminifera from the Atlantic Ocean. *Micropaleontol. Spec. Publ.,* 4.

Valent, P.J., Altschaeffl, A.G., and Lee, H.J., 1982. Geotechnical properties of two calcareous oozes. *In* Demars, K.R., and Chaney, R.C. (Eds.), *Geotechnical Properties, Behavior, and Performance of Calcareous Soils.* ASTM Spec. Tech. Publ., 777:79–96.

van Morkhoven, F.P.C.M., Berggren, W.A., and Edwards, A.S., 1986. Cenozoic cosmopolitan deep-water benthic foraminifera. *Bull. Cent. Rech. Explor.-Prod. Elf-Aquitaine,* Mem. 11.

Weaver, P.P.E., and Raymo, M.E., 1989. Late Miocene to Holocene planktonic foraminifers from the equatorial Atlantic, Leg 108. *In* Ruddiman, W., Sarnthein, M., et al., *Proc. ODP, Sci. Results,* 108: College Station, TX (Ocean Drilling Program), 71–91.

Wei, W., and Wise, S.W., Jr., 1989. Paleogene calcareous nannofossil magnetobiochronology: results from South Atlantic DSDP Site 516. *Mar. Micropaleontol.,* 14:119–152.

Wyllie, M.R.J., Gregory, A.R., and Gardner, L.W., 1956. Elastic wave velocities in heterogeneous and porous media. *Geophysics,* 21:41–70.

Ms 154IR-104

NOTE: For all sites drilled, core-description forms ("barrel sheets") can be found in Section 4 beginning on page 445. Forms containing smear-slide data can be found in Section 5, beginning on page 1087. High-resolution, conventional, and temperature logs; sonic waveforms; and FMS, carbon, GRAPE, index properties, MAGSUS, natural gamma, *P*-wave, and reflectance data are presented on CD-ROM (back pocket) for Site 925.

Table 14. Summary of logging operations at Hole 925C.

11 February 1994
Drillers' TD = 3411.61 mbsf, WD = 3051.5 mbrf, BOP = 3139.8 mbrf (88.33 mbsf).

0600 hr	Last core on deck
0700 hr	Flush hole; pump go devil. BOP at 88.3 mbsf.
1100 hr	RIH with Quad (NGT/DST/DIT/HLDT/CNT-G/LTT)
1330 hr	Begin Quad Pass 1 uplog from 3300 mbrf at 900 ft/hr; WHC on. Raise pipe to 56 mbsf.
1410 hr	End Quad Pass 1 uplog (3300–3108 mbrf; 248.5–56.5 mbsf).
1420 hr	TD at 3403.5 mbrf with tool; WHC on. Begin Quad Pass 2 uplog at 900 ft/hr.
1530 hr	End Pass 2 uplog (3403–3108 mbrf; 351.5–56.5 mbsf).
1730 hr	Quad POOH.
1840 hr	Quad rig down; rig up GHMT.
1900 hr	RIH with GHMT.
2050 hr	Begin GHMT Pass 1 uplog (3350–3245 mbrf; 298.5–193.5 mbsf) at 1800 ft/hr. NRMT not operational.
2115 hr	Begin GHMT Pass 2 uplog (3407–3153 mbrf; 355.5–101.5 mbsf) at 1800 ft/hr. NRMT not operational.
2230 hr	GHMT POOH, rig down; rig up FMS.
2330 hr	RIH with FMS.
0030 hr	Begin FMS Pass 1 uplog (3407–3160 mbrf; 355.5–108.5 mbsf) at 1800 ft/hr.
0100 hr	Begin FMS Pass 2 uplog (3407–3222 mbrf; 355.5–170.5 mbsf) at 1800 ft/hr.
0120 hr	Begin FMS Pass 3 (Main run) uplog (3407–3160 mbrf; 355.5–108.5 mbsf) at 1800 ft/hr.
0230 hr	End of logging operations.

Note: TD = total depth, WD = water depth, BOP = blowout preventer, RIH = run in hole, NGI = natural-gamma spectrometry tool, DST = drill stream test, DIT = dual induction tool, HLDT = slim hole lithodensity logging tool, CNT-G = compensated neutron porosity tool (Schlumberger version G), LTT = temperature logging tool, WHC = wireline heave compensator, POOH = pull out of hole, GHMT = geological high-sensitivity magnetic tool, NRMT = nuclear resonance magnetometer tool, and FMS = Formation MicroScanner.

Table 15. Summary of logging operations at Hole 925A.

17 February 1994
Drillers' TD = 3983.40 mbrf, WD = 3053 mbrf, BOP = 3266.16 mbrf (213.16 mbsf).

0245 hr	Last core on deck, Hole 925A. Begin wiper trip; release bit. Raise pipe to 3266.16 mbrf (213.16 mbsf). Make up cable; rig up Quad.
1100 hr	IH with Quad (NGT/DST/DIT/HLDT/CNT-G/LTT).
1230 hr	Tool hung up on bridge at 3480.5 mbrf (427.5 mbsf).
1305 hr	Begin Quad Pass 1 uplog (3489 to 3285 mbrf; 436 to 232 mbsf) at 900 ft/hr. Raise pipe to 3236 mbrf (183 mbsf). WHC off at 3285 mbrf (232 mbsf). NGT log erratic.
1400 hr	Quad POOH.
1530 hr	Quad rig down; ream and circulate to 450 mbsf; replace NGT tool.
1700 hr	Rig up Quad.
1800 hr	RIH with Quad; lower pipe to 3506.45 mbrf (453.45 mbsf).
1930 hr	Tool hung up on bridge at 3553 mbrf (500 mbsf). Begin Quad Pass 2 uplog (3550-3476 mbrf; 497-423 mbsf).
2005 hr	Quad POOH.
2100 hr	Quad rig down; set up Sidewall Entry Sub.
0345 hr	Rig up Quad.
0430 hr	RIH with Quad.
0700 hr	Begin Quad Pass 2 uplog (3960-3327 mbrf; 907-274 mbsf) at 900 ft/hr.
0800 hr	Stopped at 3752 mbrf (699 mbsf); turned WHC off. WHC on; resume.
0830 hr	Stopped at 3650 mbrf (597 mbsf) to switch pipe over. WHC on; resume.
0850 hr	Stopped at 3590 mbrf (537 mbsf); WHC on.
0910 hr	Resume at 3588 mbrf (535 mbsf).
0930 hr	Tool string hung up on ledge at 3560 mbrf (507 mbsf).
0935 hr	Tool string hung up on another ledge at 3505 mbrf (452 mbsf).
0945 hr	Stop at 3450 mbrf (397 mbsf); WHC erratic, fixed and resume.
1015 hr	Closing caliper at 3360 mbrf (307 mbsf). Stopped and resumed with WHC off. BOP at 3327 mbrf (274 mbsf).
1230 hr	Quad POOH.
1300 hr	Rig down Quad.
1330 hr	Rig up FMS.
1400 hr	RIH with FMS. BOP set to 3703 mbrf (650 mbsf).
1640 hr	Begin FMS Pass 1 uplog (3983-3284 mbrf) (930-231 mbsf) at 1800 ft/hr.
1730 hr	Stop at 3589 mbrf (536 mbsf); resume.
1800 hr	Stop at 3529 mbrf (476 mbsf); resume.
1830 hr	Turn off FMS log at 3284 mbrf (231 mbsf) and continue logging up with GPIT magnetometer channels.
2130 hr	FMS POOH.
2230 hr	Rig down Sidewall Entry Sub; end of logging operations.

Note: See list of abbreviations in note to Table 14.

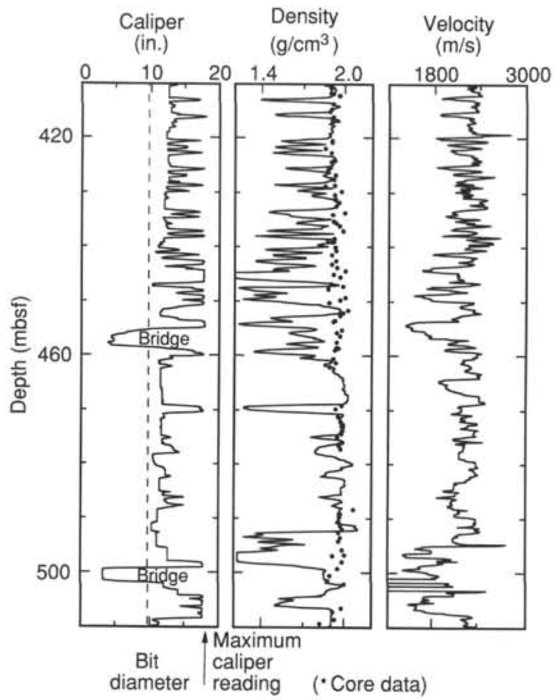

Figure 48. Detail of the caliper, density, and velocity logs from 410 to 510 mbsf in Hole 925A. Note the highly variable caliper measurement, which indicates regular borehole washouts associated with bedding cycles.

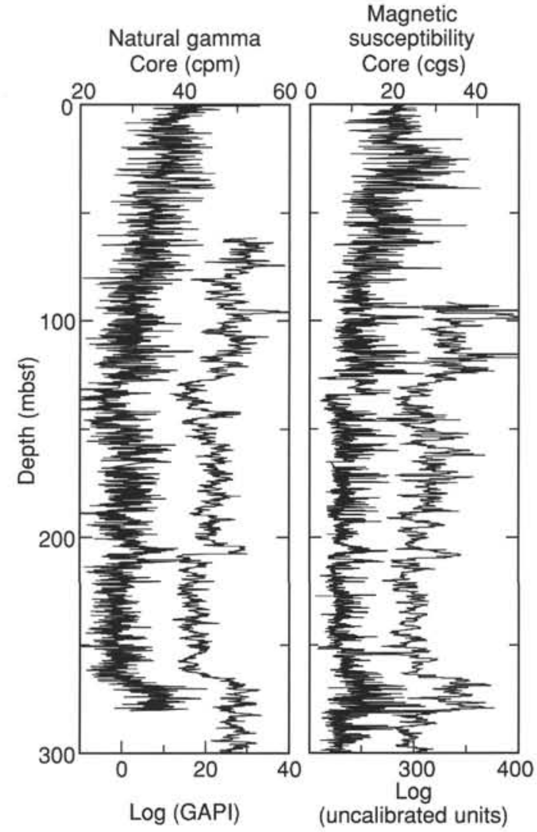

Figure 50. Comparison of core (left) and log (right) measurements of natural gamma activity and magnetic susceptibility for the uppermost 300 mbsf of Hole 925C. Core data are shown without background corrections.

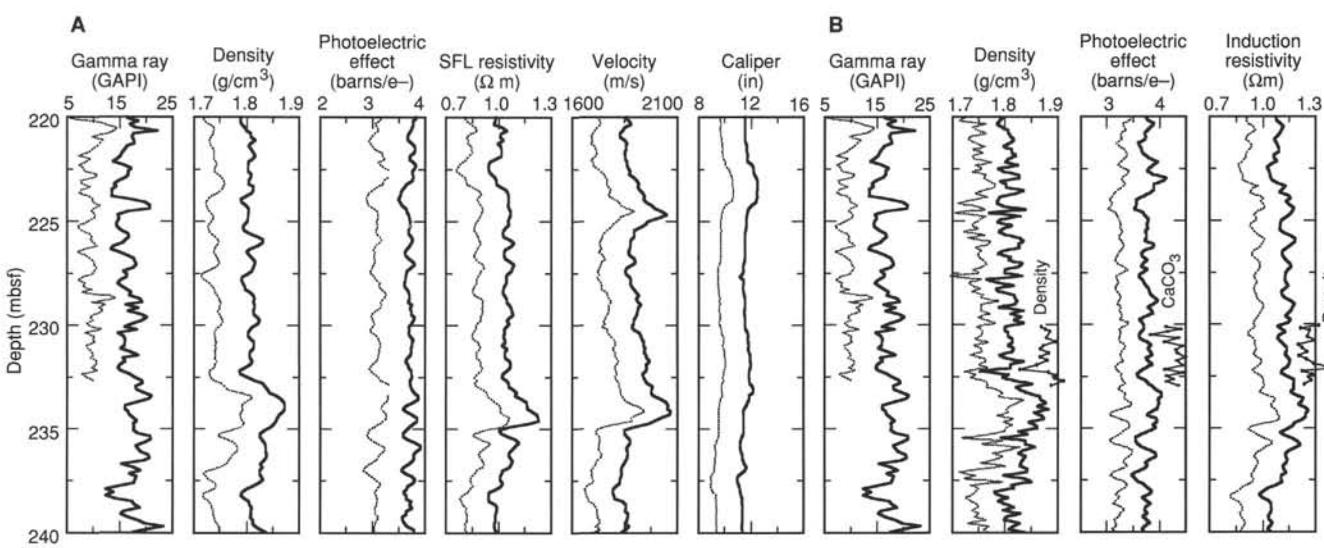

Figure 49. Comparison of standard (**A**) and high-resolution (**B**) log repeatability at Hole 925C. All logs were recorded at 900 ft/hr; repeat runs are offset horizontally for clarity. Standard logs are recorded at 15-cm intervals, whereas the high-resolution logs are recorded at 2.5-cm intervals and undergo real-time enhancement processing during acquisition. Detailed wet-bulk-density, $CaCO_3$, and porosity data from Core 154-925C-28H are shown adjacent to the high-resolution logs; these data are scaled arbitrarily for comparison.

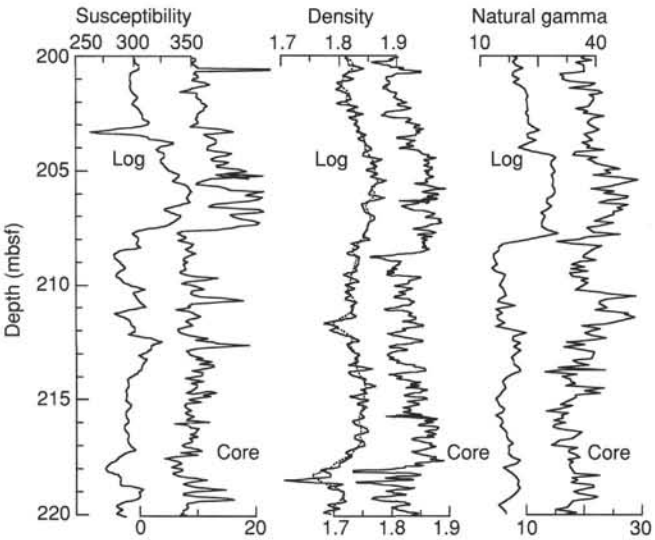

Figure 51. Comparison between core (right) and log (left) measurements of magnetic susceptibility, bulk density, and natural gamma activity for the Hole 925C interval between 200 and 220 mbsf. Note the general similarity between the core and log data sets, as well as the general signal attenuation inherent in the log-derived measurements. Average sedimentation rate for this interval is 2.4 cm/k.y.

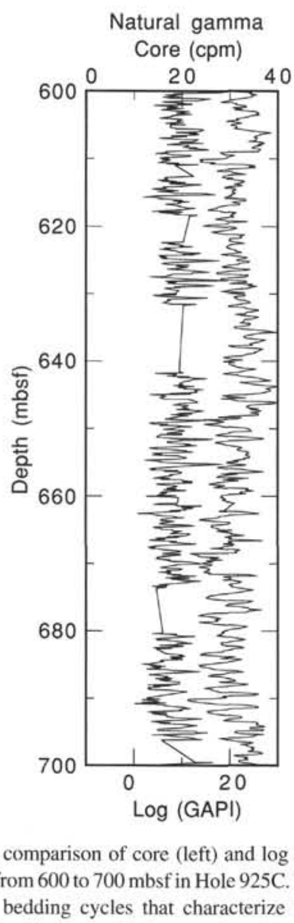

Figure 52. Detailed comparison of core (left) and log (right) natural gamma activity for interval from 600 to 700 mbsf in Hole 925C. Note the log resolution of the 1- to 1.2-m bedding cycles that characterize this interval. Average sedimentation rate for this interval is between 3 and 4 cm/k.y.

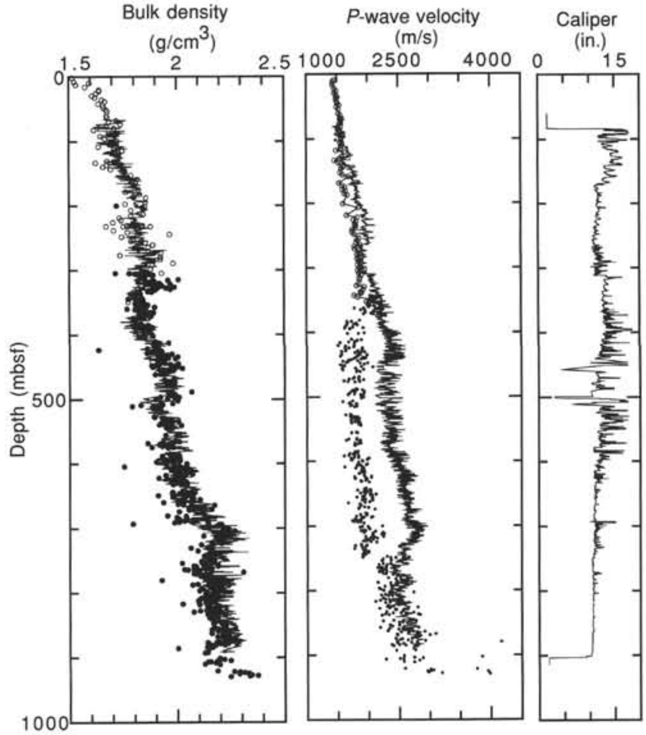

Figure 53. Comparison of core (symbols) and log density and velocity data. Core data have been corrected for elastic rebound.

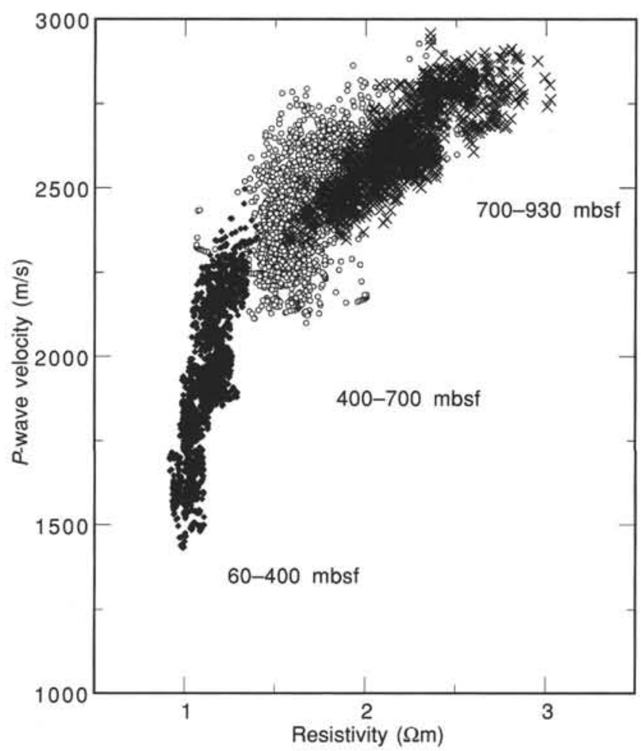

Figure 54. Scatter plot of velocity and resistivity logging data, Site 925.

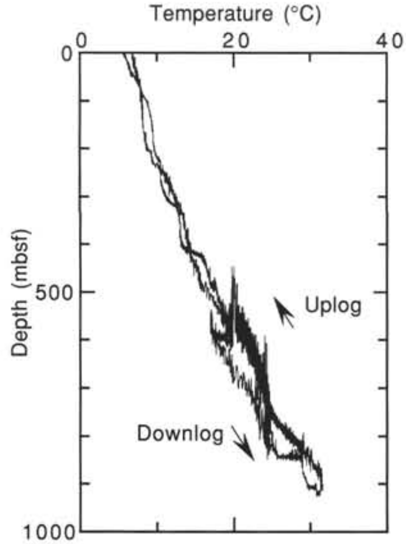

Figure 55. Borehole fluid temperature log from the temperature logging tool. Temperature at total depth was 31.5°C approximately 17 hr after wiper-trip circulation.

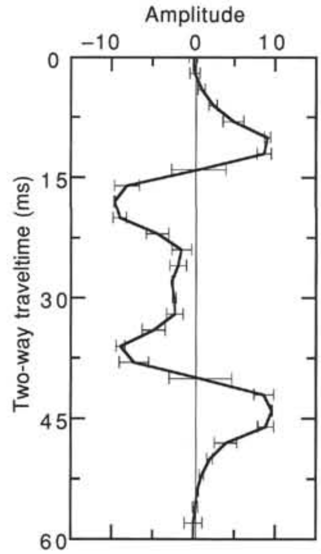

Figure 56. Plot of the seismic source wavelet derived from stacking and averaging the mud-line reflection from 10 shotpoints near Site 925 (Shotpoints 9595–9610). Standard deviation error bars are shown. This signal was used for all Leg 154 synthetic seismogram convolutions.

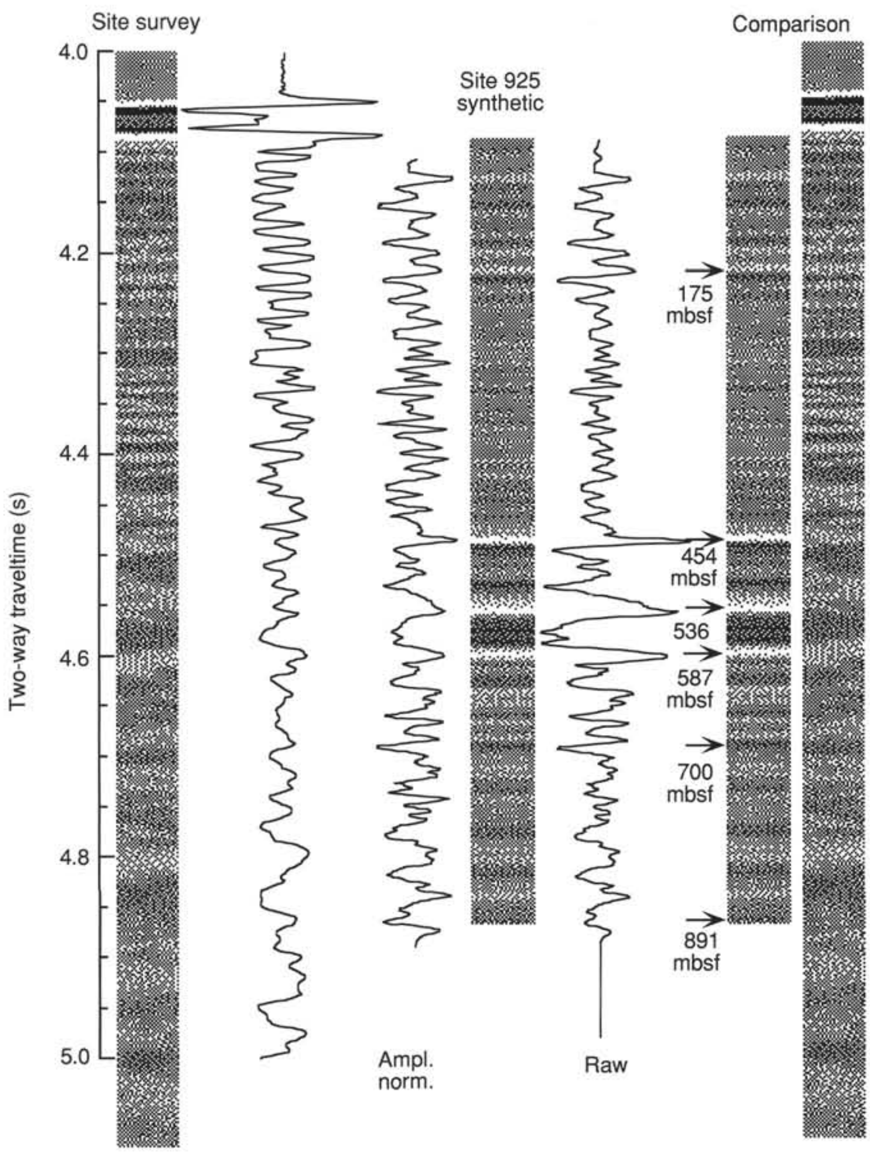

Figure 57. Comparison of synthetic seismogram derived from Site 925 density and velocity logs (filtered to remove bad data caused by borehole washouts) with the seismic line from *Ewing* Cruise 9209, Line 2, Shotpoints 9690–9710. Site 925 is located near Shotpoint 9600 (Mountain and Curry, this volume).

SHORE-BASED LOG PROCESSING

Hole 925A

Bottom felt: 3053 mbrf
Total penetration: 930.4 mbsf
Total core recovered: 490.05 m (52.7%)

Logging Runs

Logging string 1: DIT/SDT/HLDT/CNTG/NGT (3 passes)
Logging string 2: FMS/GPIT/NGT

The wireline heave compensator (WHC) was used to counter moderate ship heave. The WHC was switched off at 240 mbsf during DIT/SDT/HLDT/CNTG/NGT pass 1, at 301.5 mbsf during DIT/SDT/HLDT/CNTG/NGT pass 3, and at 283.5 mbsf during FMS/GPIT/NGT.

Drill Pipe

The following drill-pipe depths are as they appear on the logs after depth shift. As such, there might be a discrepancy with the original depths given by the drillers on board. Possible reasons for depth discrepancies are ship heave, use of wireline heave compensator, and drill-string and/or wireline stretch.

DIT/SDT/HLDT/CNTG/NGT (pass 1): Bottom of drill pipe at ~186 mbsf
DIT/SDT/HLDT/CNTG/NGT (pass 2): Bottom of drill pipe at ~ 452.5 mbsf
DIT/SDT/HLDT/CNTG/NGT (pass 3): Bottom of drill pipe at ~252 mbsf
FMS/GPIT/NGT: Bottom of drill pipe at ~254 mbsf

Processing

Depth shift: The reference run for depth shift was DIT/SDT/HLDT/CNTG/NGT (pass 3). All original logs (including high-resolution logs) have been interactively depth shifted with reference to NGT from DIT/SDT/HLDT/CNTG/NGT, and to the seafloor (–3046.6 m). The amount of depth shift differs from the "bottom felt" depth given by the drillers because it incorporates some additional depth shift applied by the logging scientists during correlation of the logs with the multisensor track (MST) data from core.

Gamma-ray processing: The NGT data from DIT/SDT/HLDT/CNTG/NGT pass 3 have been processed to correct for borehole size and type of drilling fluid. Data from passes 2 and 3 are invalid.

Acoustic data processing: The sonic logs have been processed to eliminate some of the noise and cycle skipping experienced during the recording. Processing was performed on the data recorded in the "long-spacing" (curves LTT1, LTT2, etc.) and "short-spacing" (curves TT1, TT2, etc.) modes during runs 1 and 3. The "short-spacing" mode data from runs 1 and 3 have been merged before being processed. The "long-spacing" mode data have been processed from run 3 and only above 790 m, as one of the curves (LTT3) was very noisy in the lower part of the hole. The reprocessed "long-spacing" mode data look better than the "short-spacing" mode data through most of the hole. The curves resulting from the two different processings have been merged as follows:

187.5–265 mbsf: run 1 (short-spacing mode)
265–750 mbsf: run 3 (long-spacing mode)
750–890 mbsf: run 3 (short-spacing mode)

Merging of data: Runs 1 and 3 were merged as follows:
Resistivity data: Spliced at 350 mbsf
Density data (both standard and high resolution): Spliced at 350 mbsf
Neutron data (both standard and high resolution): Spliced at 350 mbsf
Acoustic data: See **Acoustic data processing** section above.

Quality Control

No valid density data were recorded during DIT/SDT/HLDT/CNTG/NGT pass 2 because the caliper did not open.

No valid gamma-ray data were recorded during DIT/SDT/HLDT/CNTG/NGT passes 1 and 2.

Data such as the neutron and gamma-ray logs recorded through pipe should be used qualitatively only because of the attenuation on the incoming signal.

Hole diameter was recorded by the hydraulic caliper on the HLDT tool (CALI), and the caliper on the FMS string (C1 and C2). The HLDT caliper started closing at about 227 and 291 mbsf during DIT/SDT/HLDT/CNTG/NGT runs 1 and 3 before getting into the pipe. The density data recorded above those depths is extremely noisy, as it could not be corrected for the actual hole diameter; therefore, it is not presented here.

Note: Because of the frequent stops and pulls experienced during recording, the data from the DIT/SDT/HLDT/CNTG/NGT run 3 should be used with caution in the following intervals: 410, 505, 540, 605, and 705 mbsf. In addition, the density data show invalid spikes at 445–450,493–497, and 587 mbsf.

Details of standard shore-based processing procedures are found in the "Explanatory Notes" chapter, this volume. For further information about the logs, please contact:

Cristina Broglia
Phone: 914-365-8343
Fax: 914-365-3182
E-mail: chris@ldeo.columbia.edu

Elizabeth Pratson
Phone: 914-365-8313
Fax: 914-365-3182
E-mail: beth@ldeo.columbia.edu

Hole 925A: Resistivity-Velocity-Natural Gamma Ray Log Summary

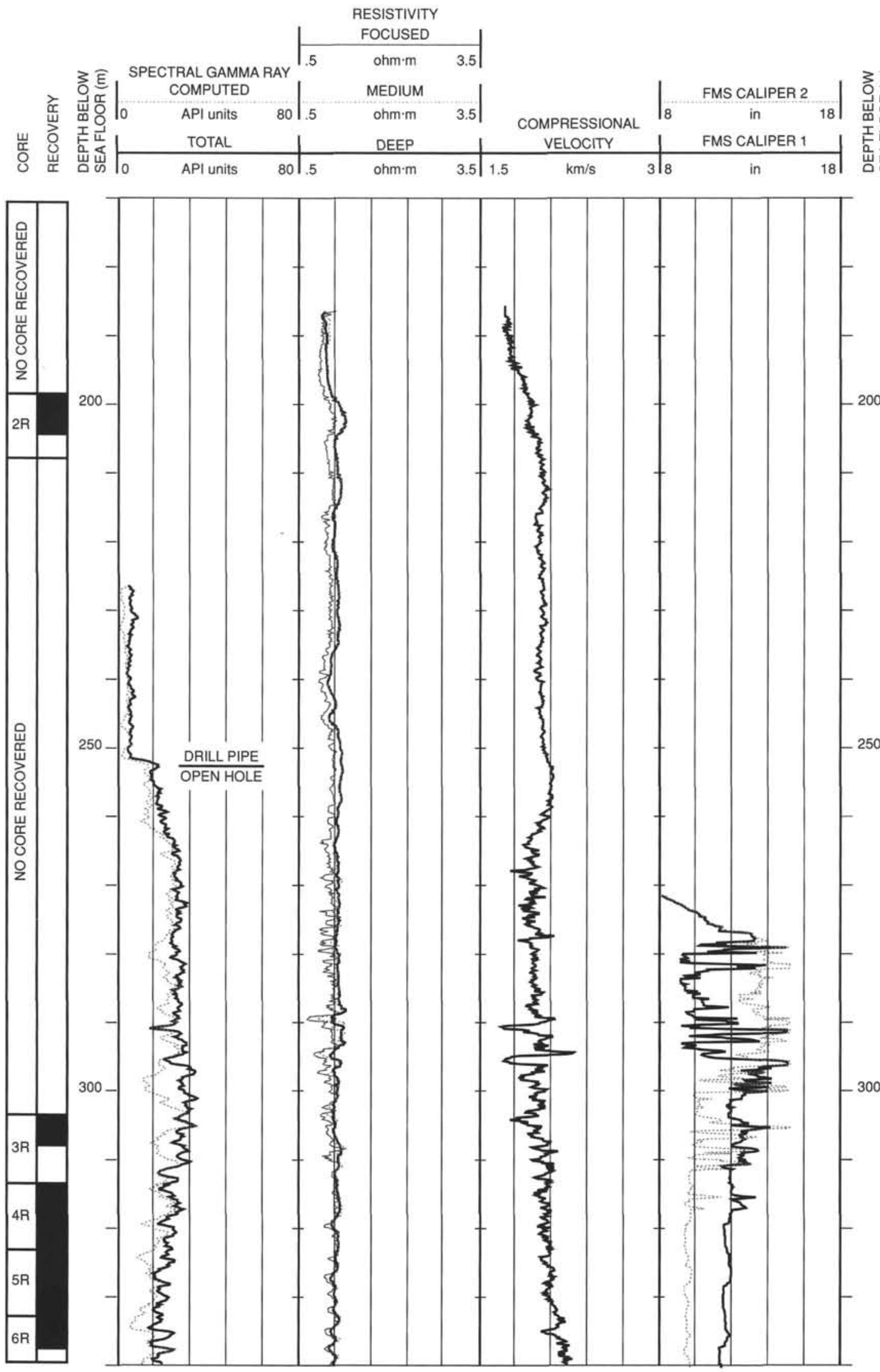

Hole 925A: Resistivity-Velocity-Natural Gamma Ray Log Summary (cont.)

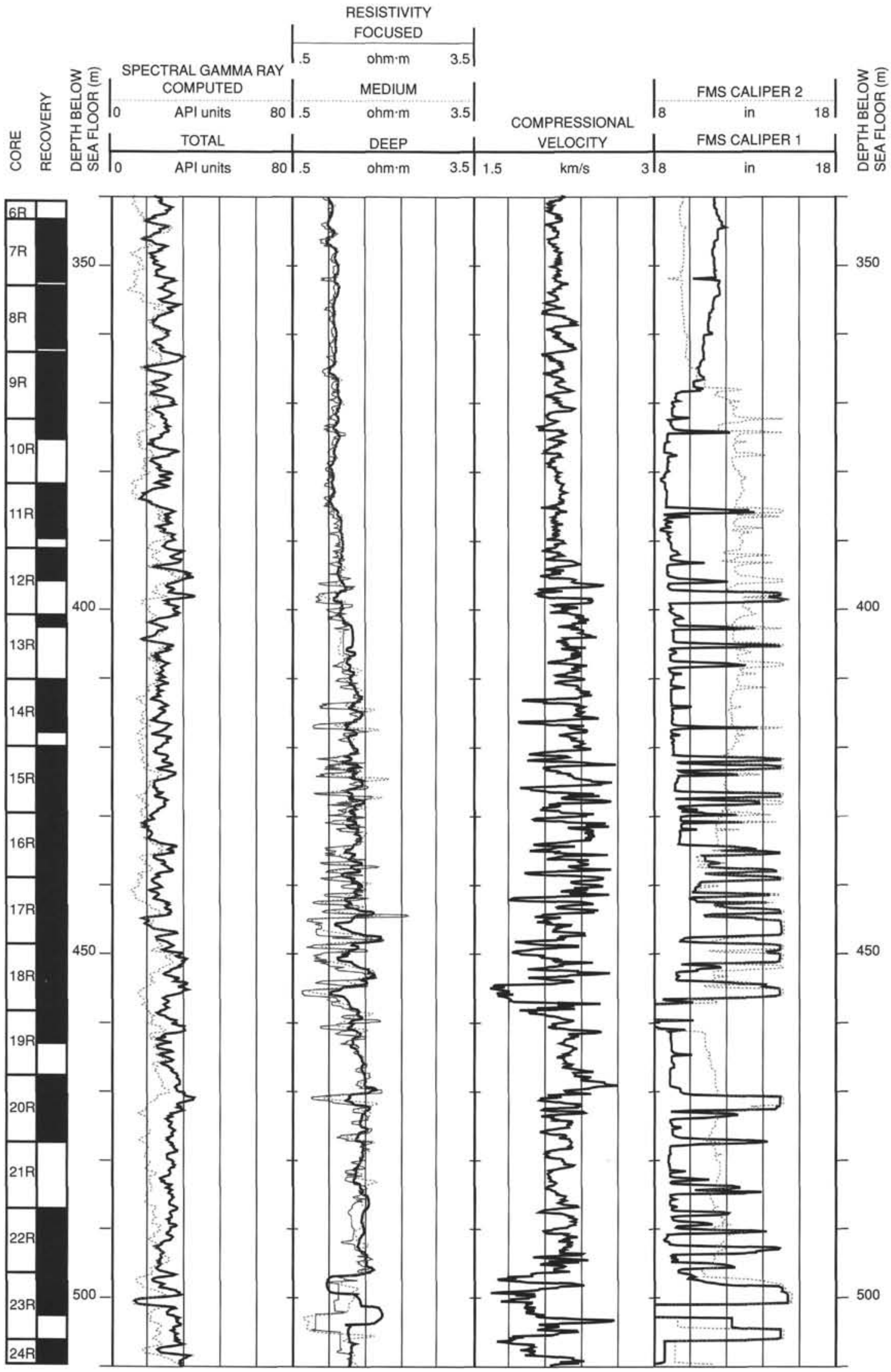

Hole 925A: Resistivity-Velocity-Natural Gamma Ray Log Summary (cont.)

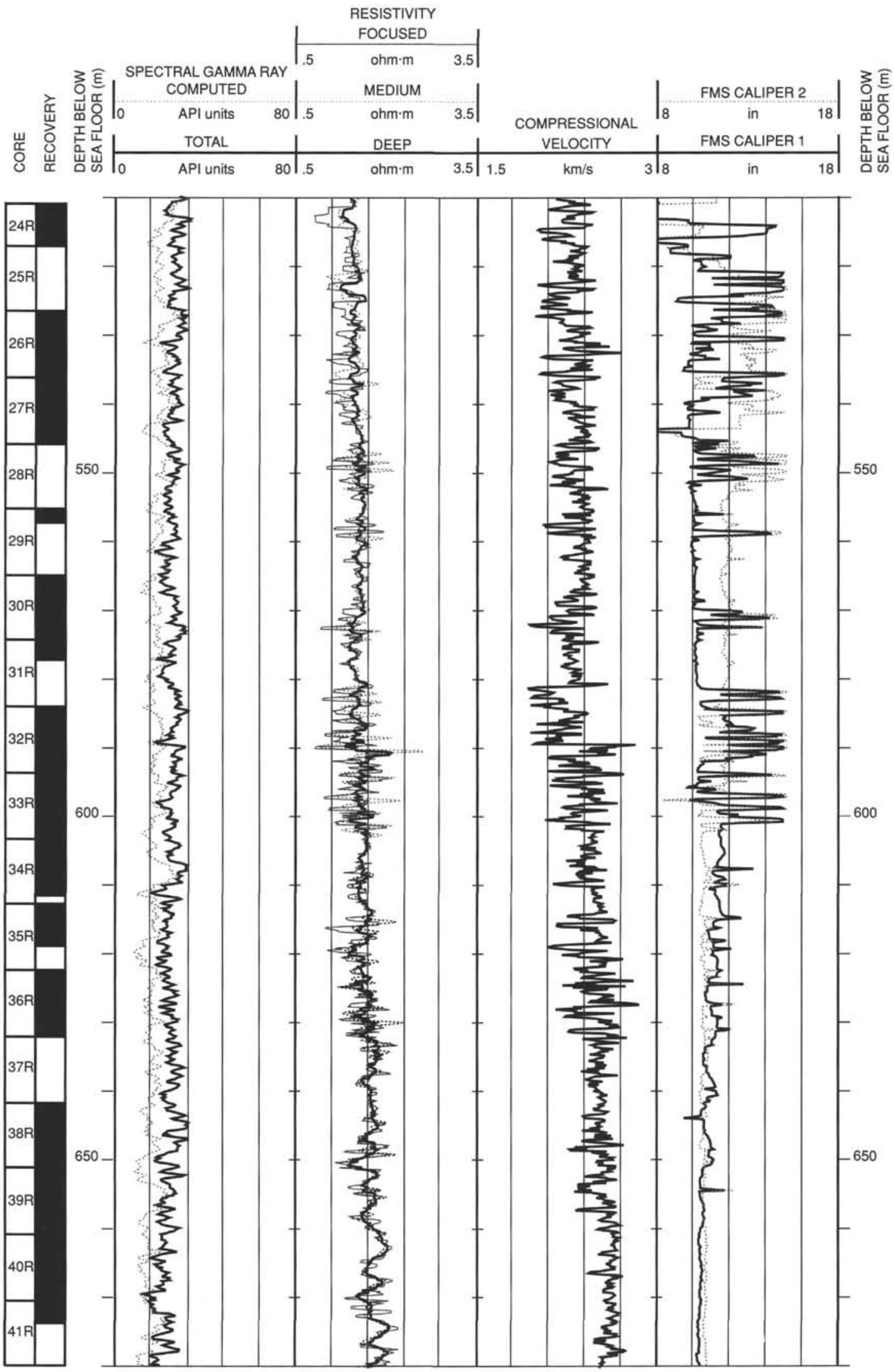

Hole 925A: Resistivity-Velocity-Natural Gamma Ray Log Summary (cont.)

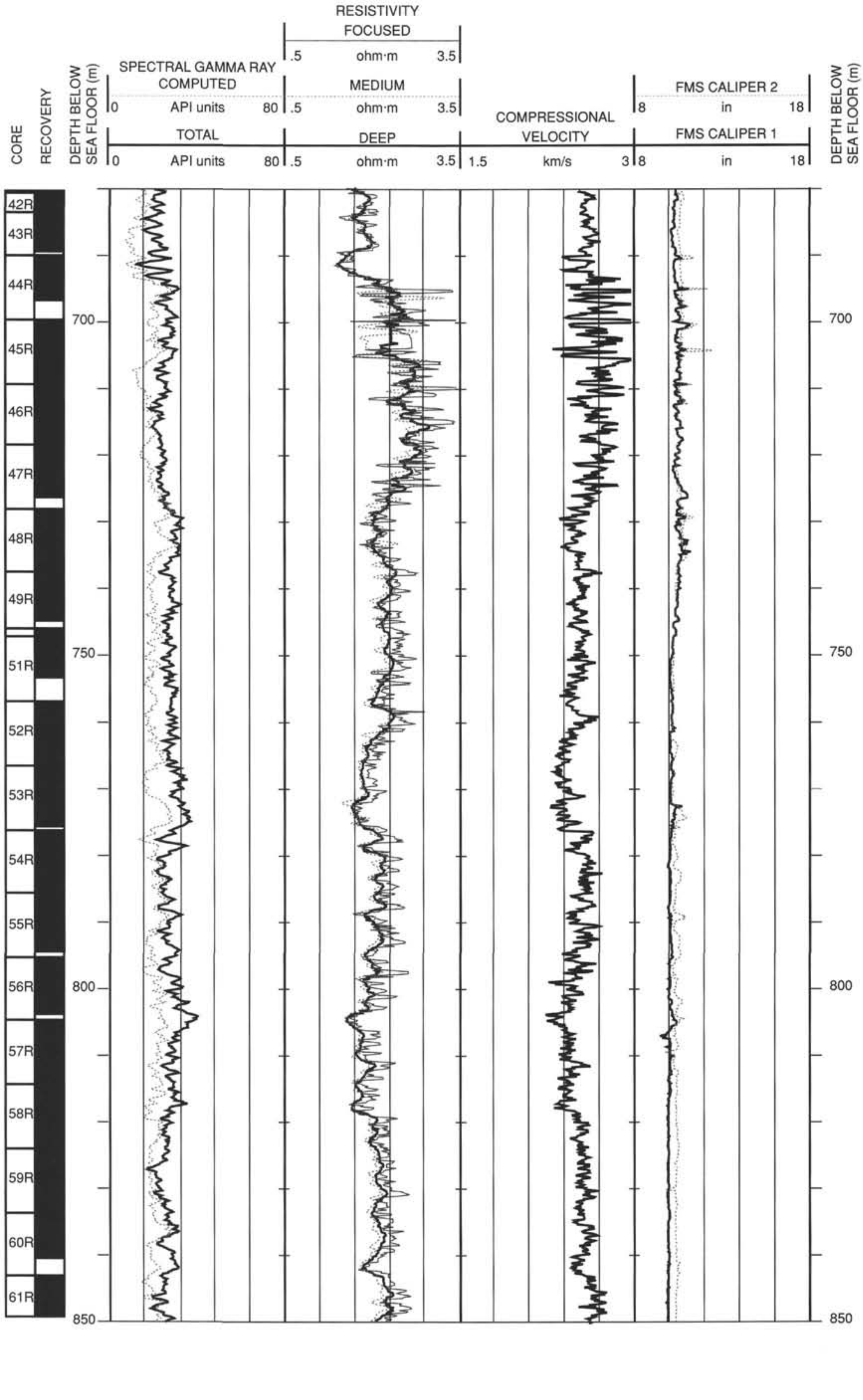

Hole 925A: Resistivity-Velocity-Natural Gamma Ray Log Summary (cont.)

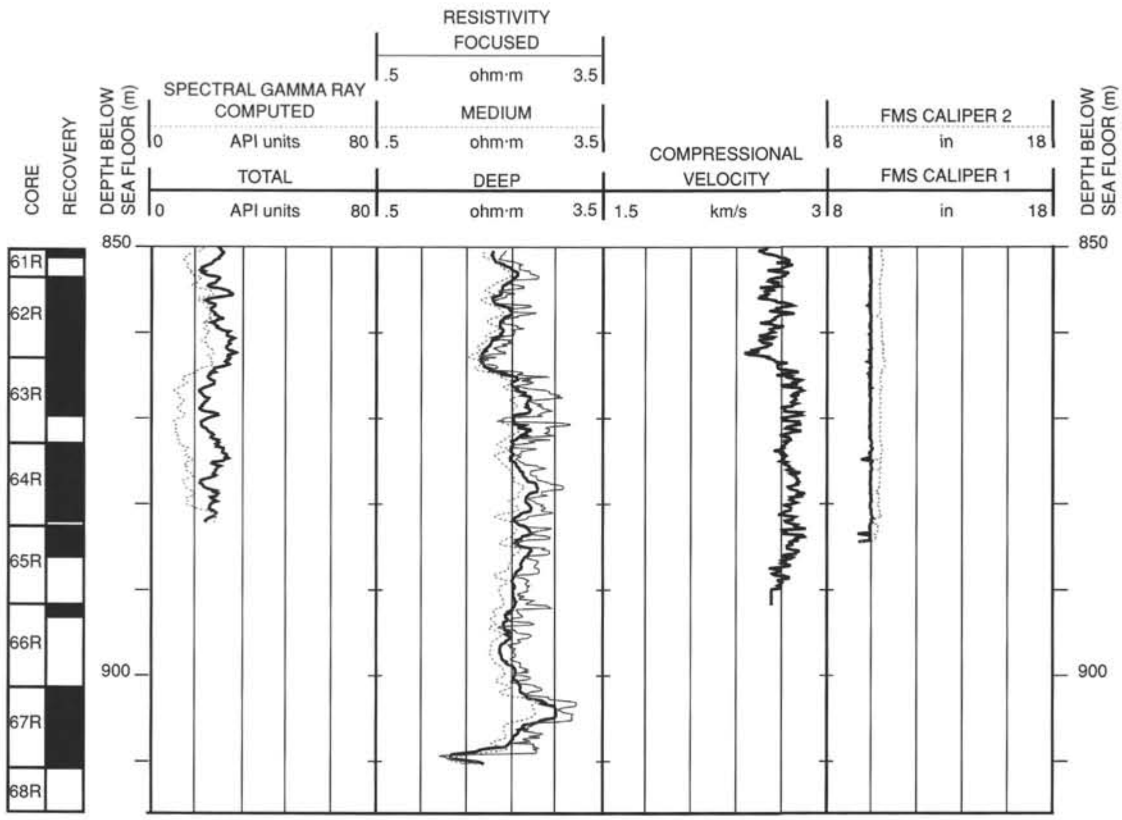

Hole 925A: Density-Natural Gamma Ray Log Summary

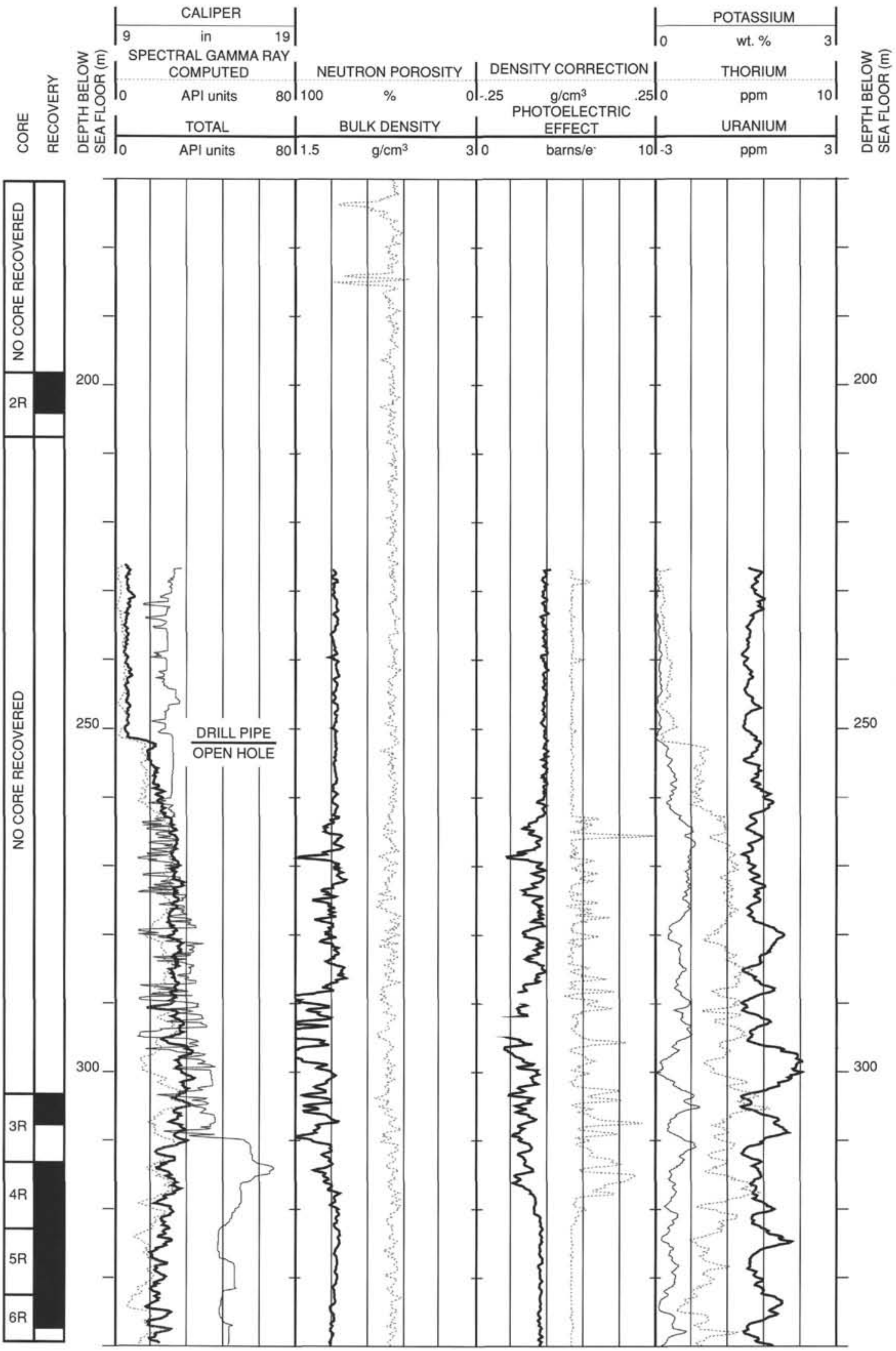

Hole 925A: Density-Natural Gamma Ray Log Summary (cont.)

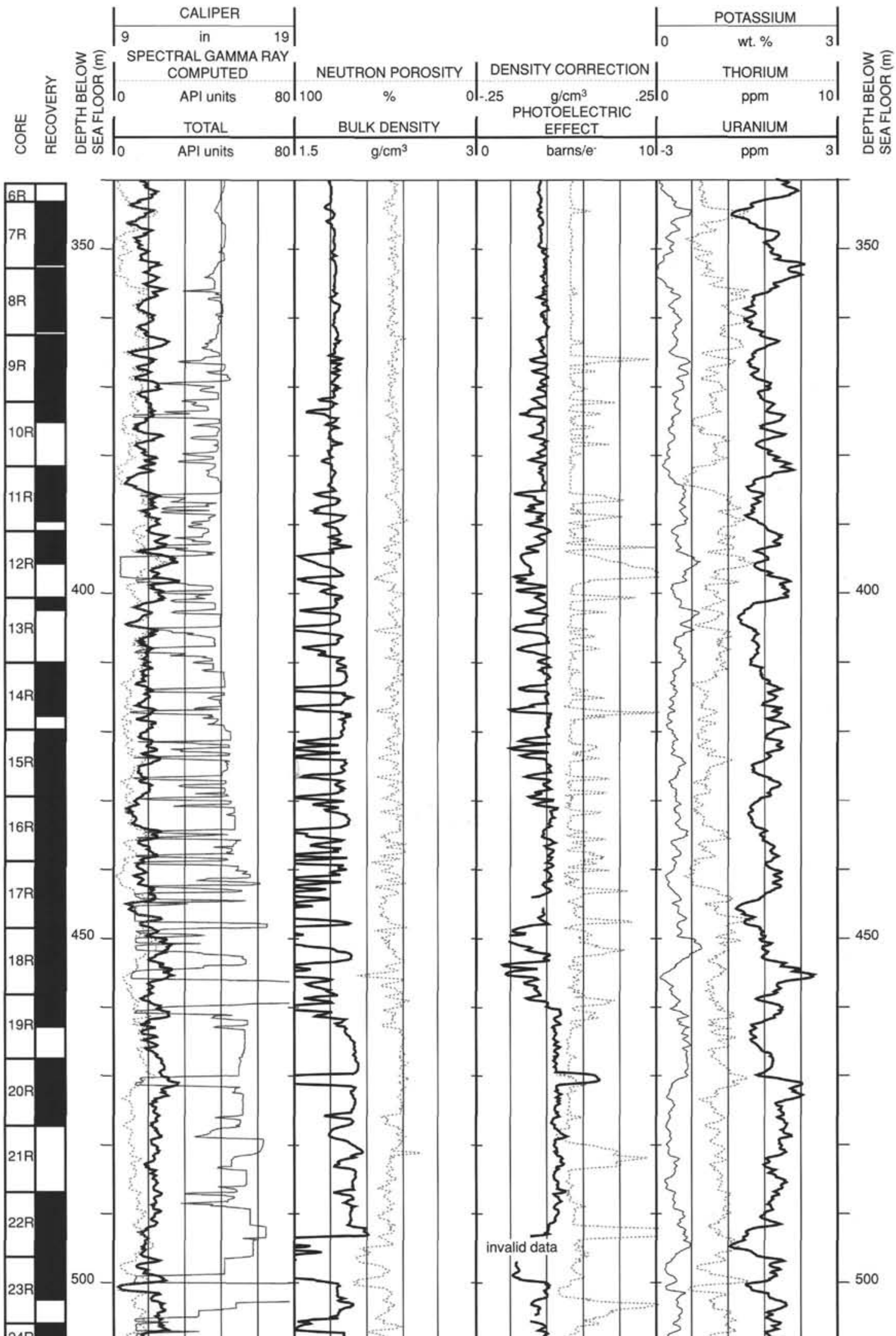

Hole 925A: Density-Natural Gamma Ray Log Summary (cont.)

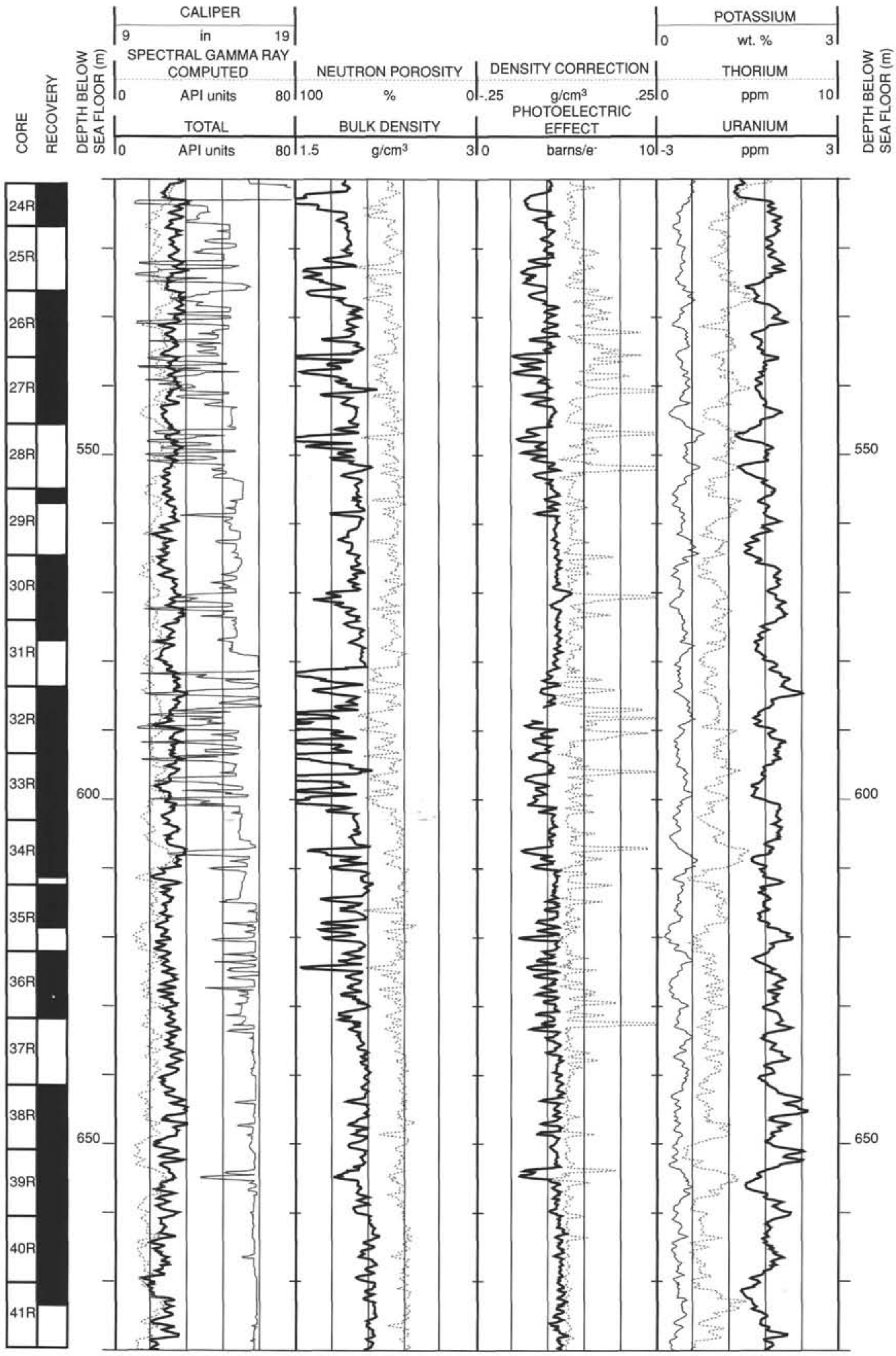

Hole 925A: Density-Natural Gamma Ray Log Summary (cont.)

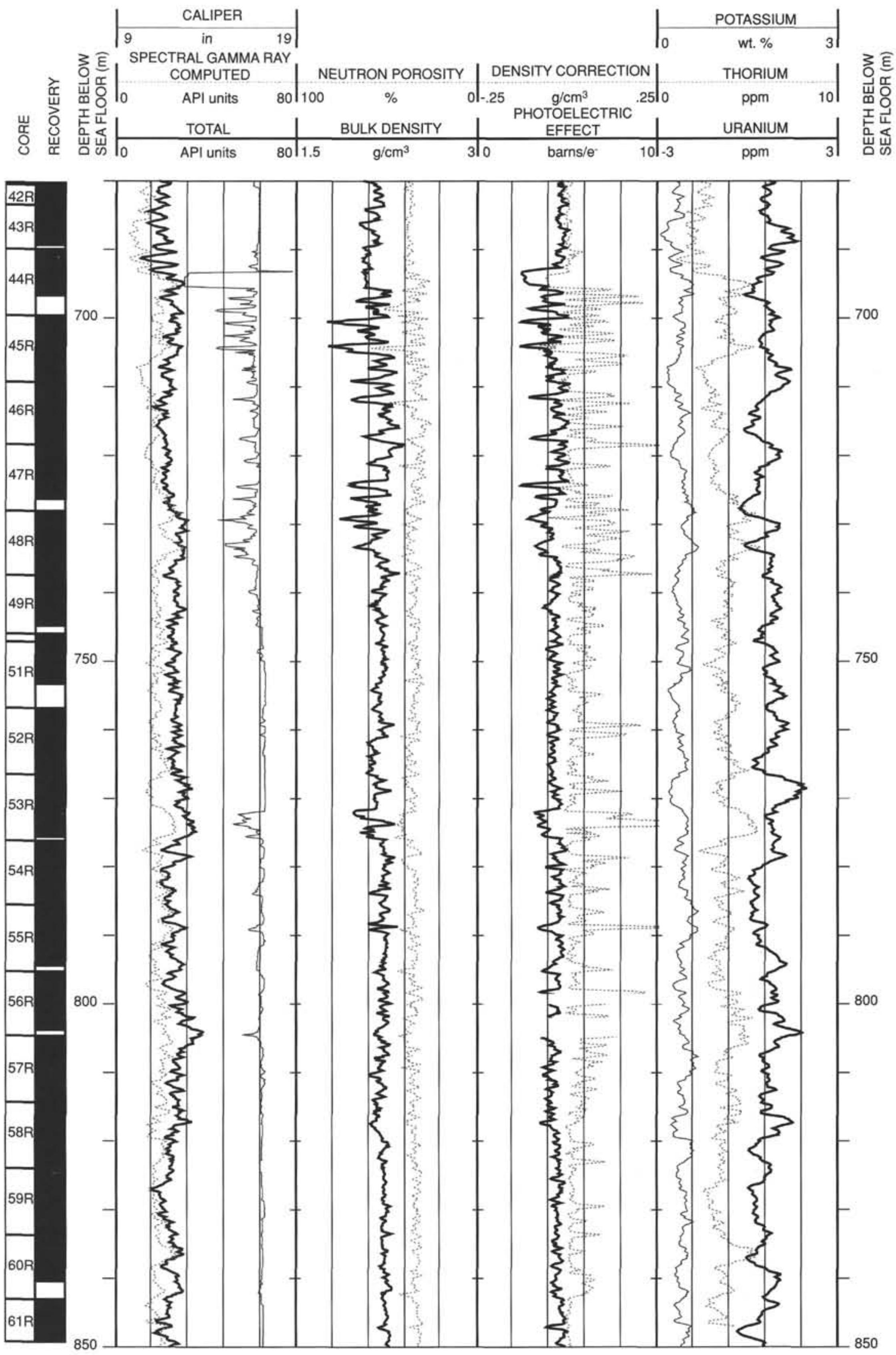

Hole 925A: Density-Natural Gamma Ray Log Summary (cont.)

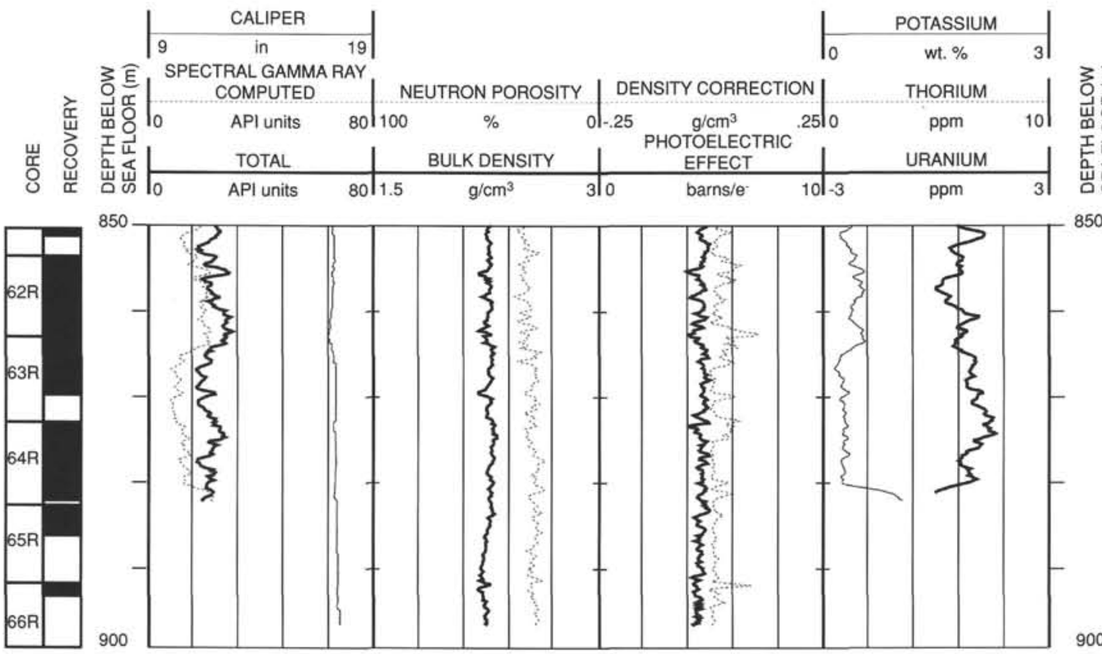

SHORE-BASED LOG PROCESSING

Hole 925C

Bottom felt: 3051.5 mbrf
Total penetration: 360.1 mbsf
Total core recovered: 368.78 m (102.4%)

Logging Runs

Logging string 1: DIT/SDT/HLDT/CNTG/NGT
Logging string 2: FMS/GPIT/NGT (3 passes)

The wireline heave compensator (WHC) was used to counter moderate ship heave. The WHC was switched off at 85 mbsf before entering the pipe.

Drill Pipe

The following drill-pipe depths are as they appear on the logs after differential depth shift (see **Depth shift** section below) and depth shift to the seafloor. As such, there might be a discrepancy with the original depths given by the drillers on board. Possible reasons for depth discrepancies are ship heave, use of wireline heave compensator, and drill-string and/or wireline stretch.

DIT/SDT/HLDT/CNTG/NGT: Bottom of drill pipe at 60 mbsf
FMS/GPIT/NGT: Bottom of drill pipe at 60 mbsf

Processing

Depth shift: The reference run for depth shift was FMS/GPIT/NGT (main pass).

All original logs have been interactively depth shifted with reference to NGT from the FMS/GPIT/NGT run, and to the seafloor (–3049 m). The amount of depth shift differs from the "bottom felt" depth given by the drillers because it incorporates some additional depth shift applied by the logging scientists during correlation of the logs with the multisensor track (MST) data from core.

Gamma-ray processing: The NGT data have been processed to correct for borehole size and type of drilling fluid.

Acoustic data processing: The sonic logs have been processed to eliminate some of the noise and cycle skipping experienced during recording. Processing was performed on the data recorded in the "long-spacing" mode (curves LTT1, LTT2, etc.), as those recorded in the "short-spacing" mode displayed a bad transit time (TT2).

Quality Control

Data such as the neutron and gamma-ray logs recorded through pipe should be used qualitatively only because of the attenuation on the incoming signal.

Hole diameter was recorded by the hydraulic caliper on the HLDT tool (CALI), and the caliper on the FMS string (C1 and C2). The HLDT caliper started closing at about 85 mbsf; therefore, the density data recorded above that depth should be used cautiously as they are not corrected for the actual hole diameter.

Invalid gamma-ray data were recorded at 37 and 55 mbsf during the DIT/SDT/HLDT/CNTG/NGT run.

Details of standard shore-based processing procedures are found in the "Explanatory Notes" chapter, this volume. For further information about the logs, please contact:

Cristina Broglia
Phone: 914-365-8343
Fax: 914-365-3182
E-mail: chris@ldeo.columbia.edu

Elizabeth Pratson
Phone: 914-365-8313
Fax: 914-365-3182
E-mail: beth@ldeo.columbia.edu

Hole 925C: Resistivity-Velocity-Natural Gamma Ray Log Summary

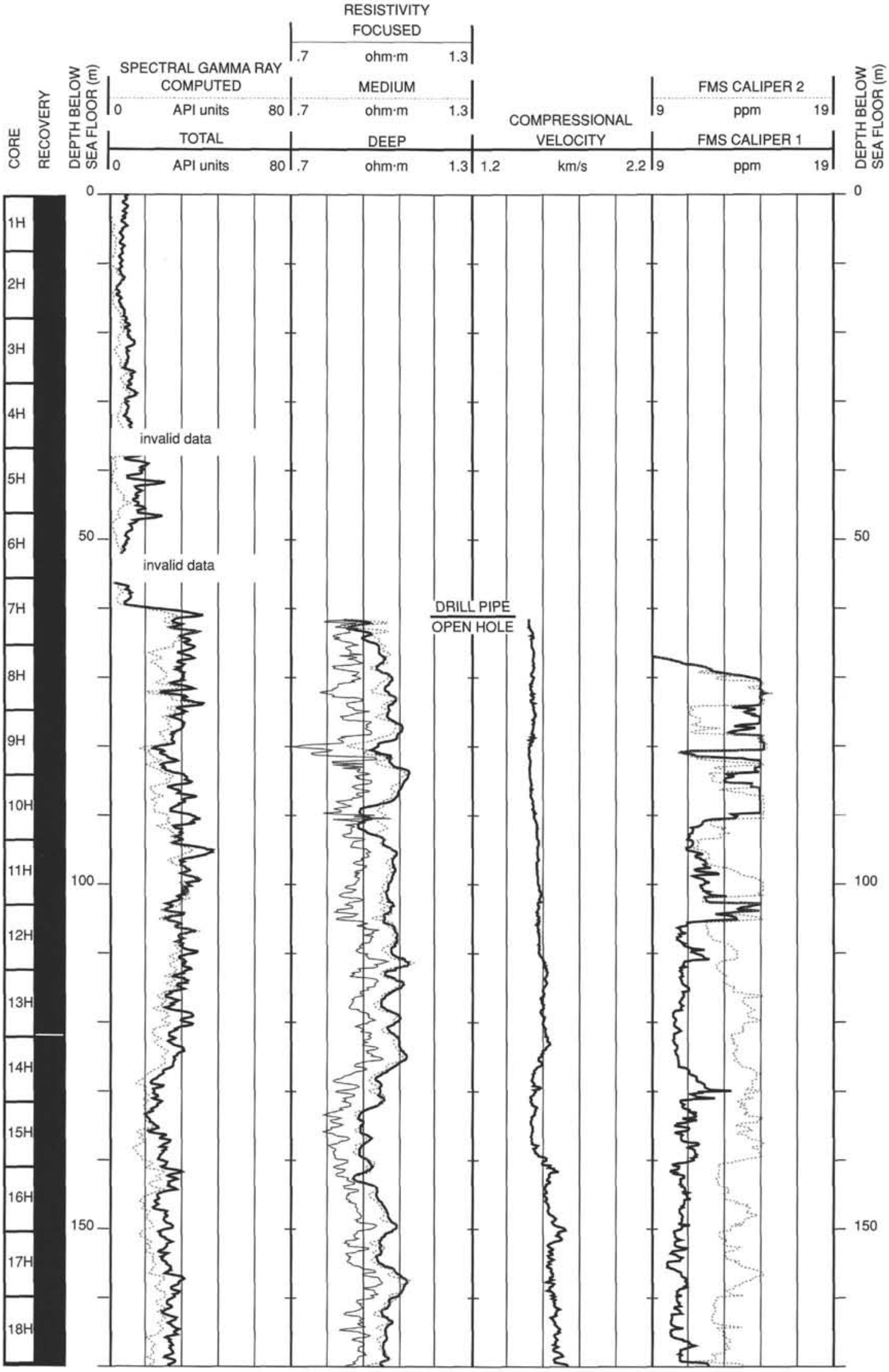

Hole 925C: Resistivity-Velocity-Natural Gamma Ray Log Summary (cont.)

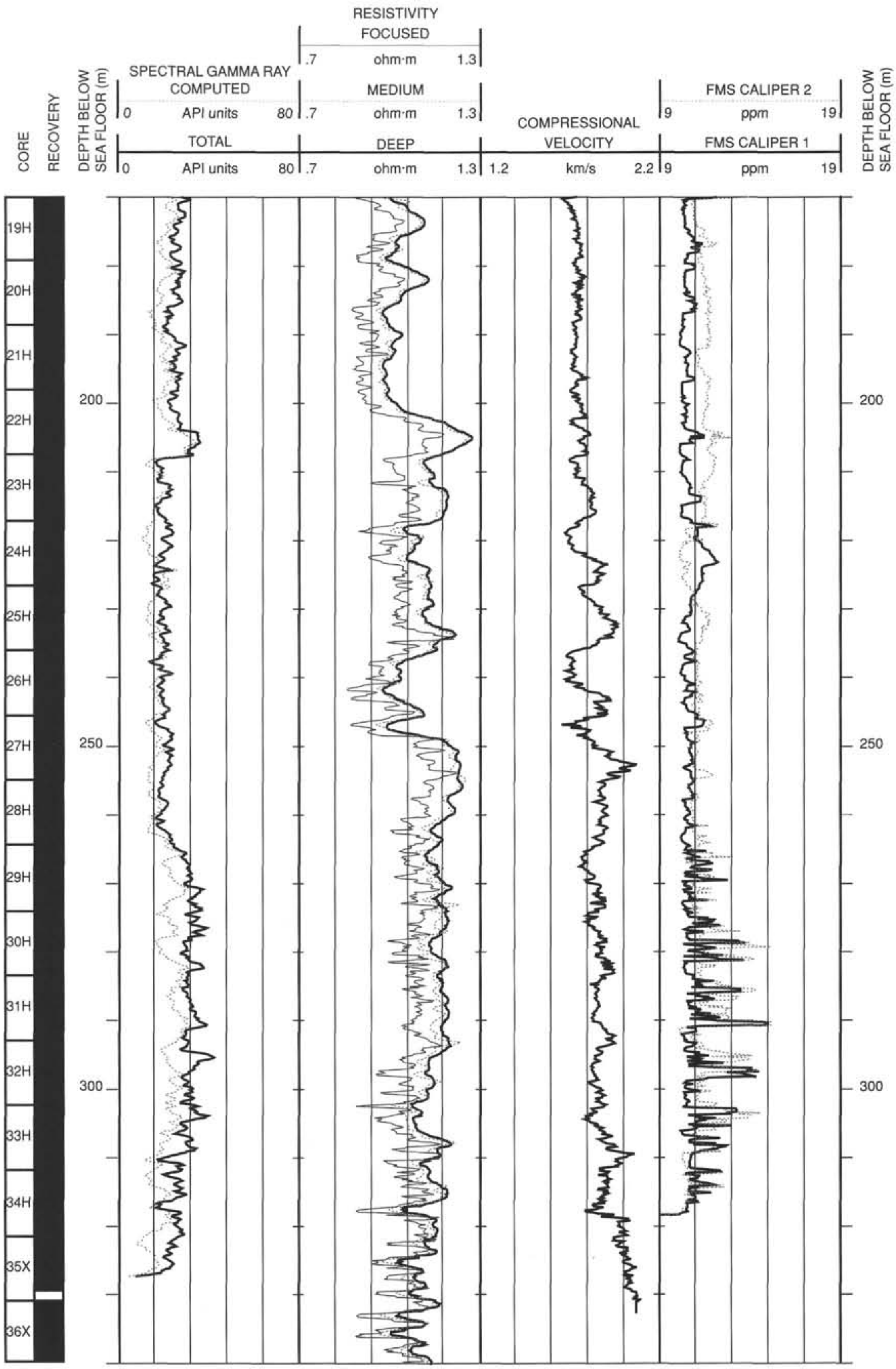

Hole 925C: Resistivity-Velocity-Natural Gamma Ray Log Summary (cont.)

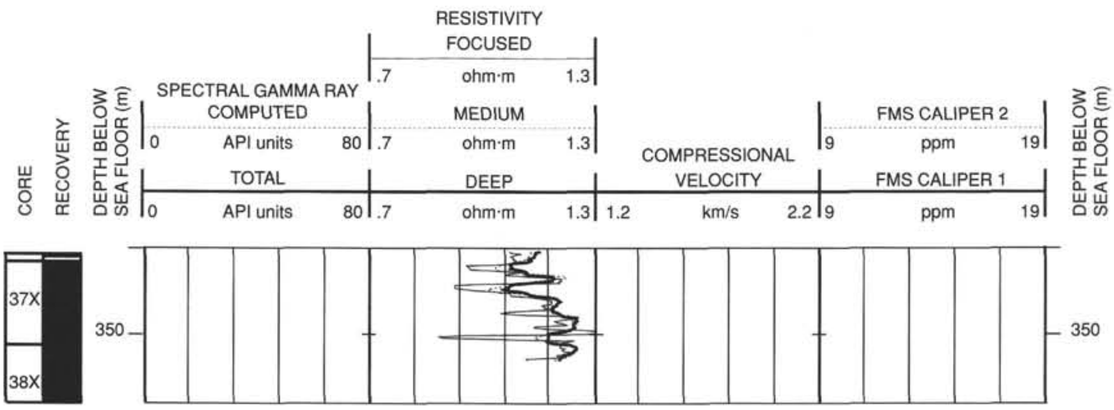

Hole 925C: Density-Porosity-Natural Gamma Ray Log Summary

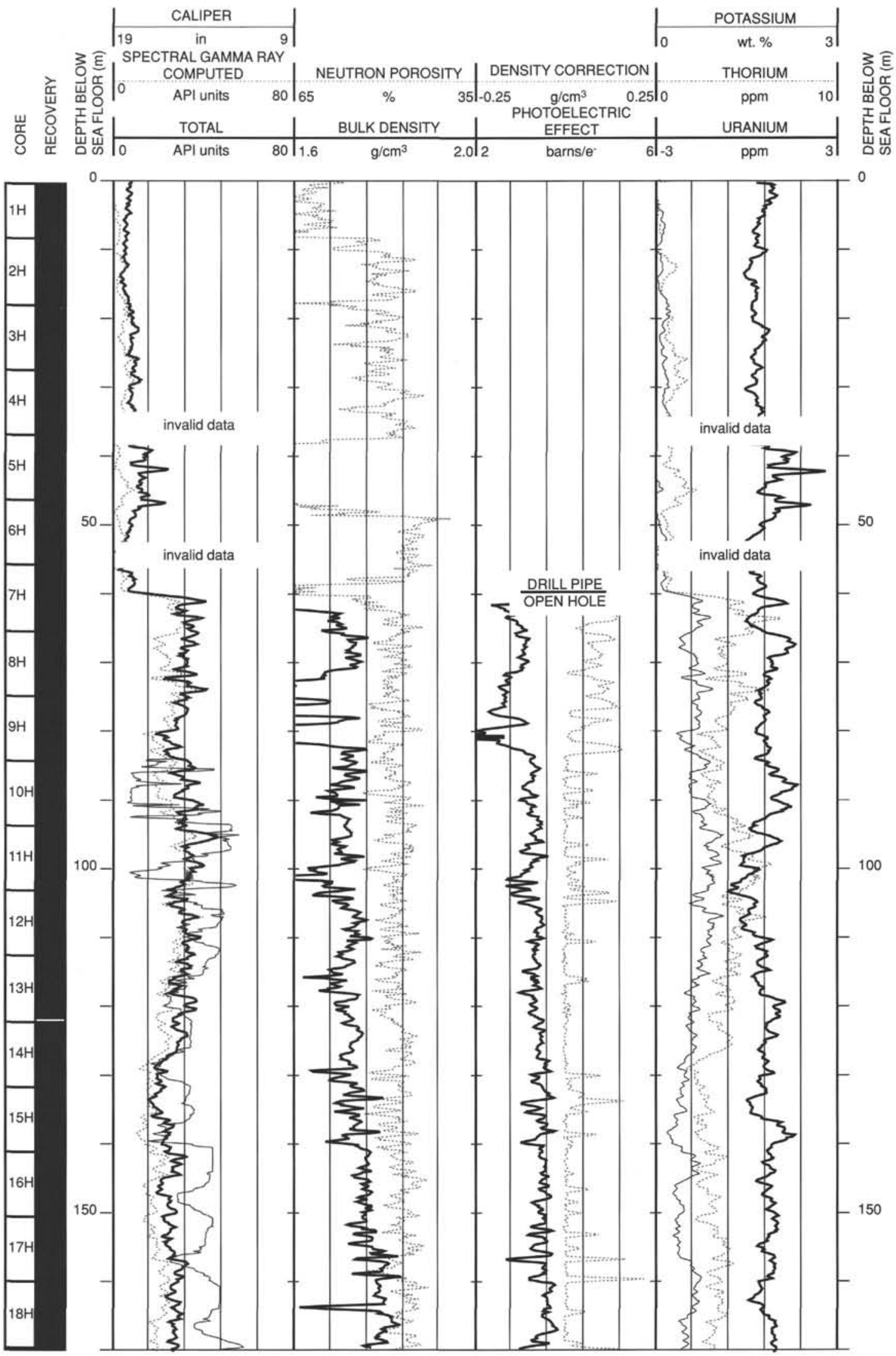

Hole 925C: Density-Porosity-Natural Gamma Ray Log Summary (cont.)

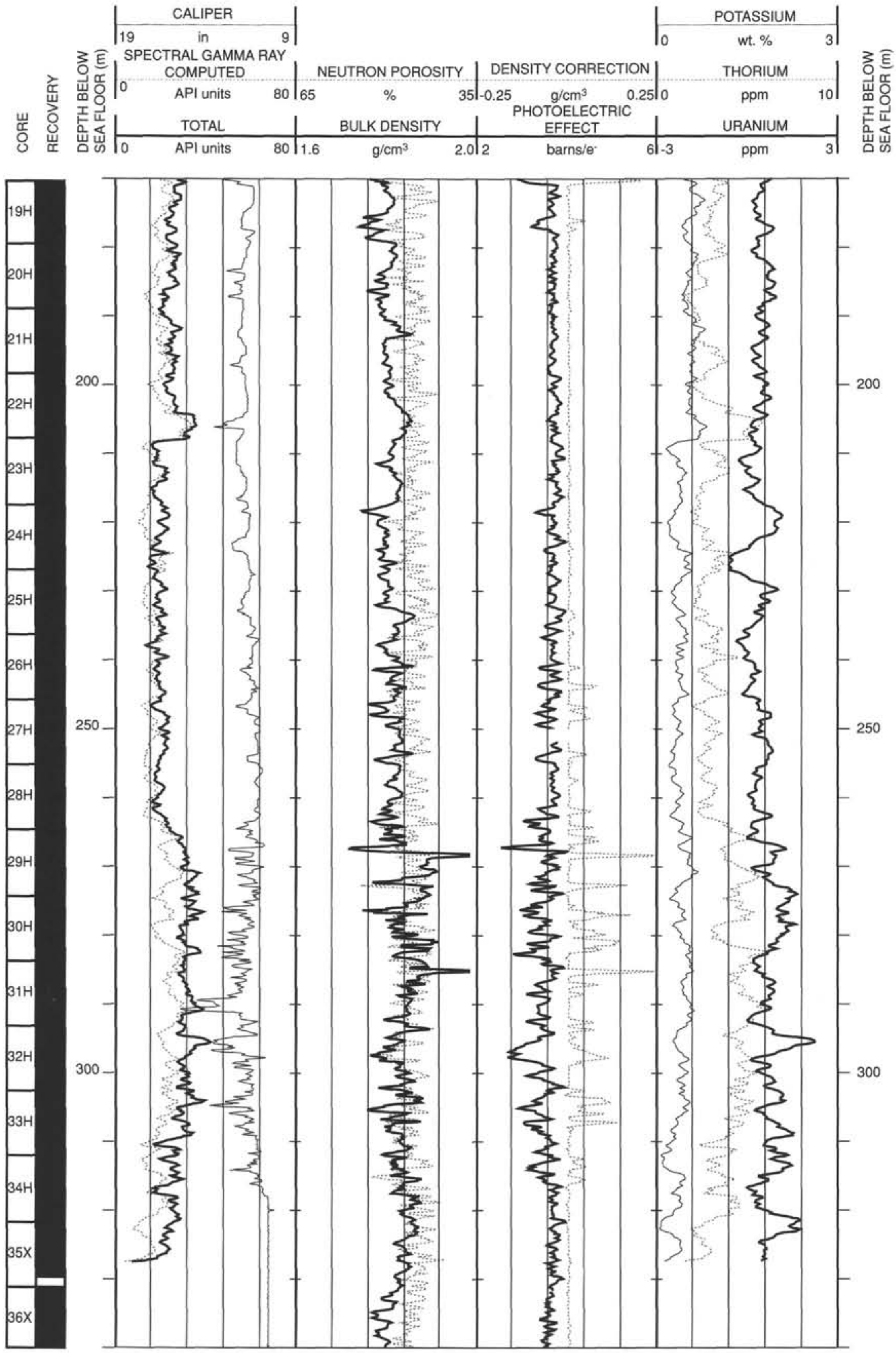

Hole 925C: Density-Porosity-Natural Gamma Ray Log Summary (cont.)